

Date: October 4, 2018

# Workshop on Physics with Neutral Kaon Beam at JLab (KL2016) Mini-Proceedings

1st - 3rd February, 2016 Thomas Jefferson National Accelerator Facility,  
Newport News, VA, U.S.A.

M. Albrow, M. Amaryan, E. Chudakov, P. Degtyarenko, A. Feijoo, C. Fernandez-Ramirez, I.P. Fernando, A. Filippi, J.L. Goity, H. Haberzettl, B.C. Jackson, H. Kamano, C. Keith, M. Kohl, I. Larin, Wei-Hong Liang, V.K. Magas, M. Mai, D.M. Manley, V. Mathieu, F. Myhrer, K. Nakayama, H. Noumi, Y. Oh, H. Ohnishi, E. Oset, M. Pennington, A. Ramos, D. Richards, E. Santopinto, R. Schumacher, A. Szczepaniak, S. Taylor, B. Wojtsekhowski, Ju-Jun Xie, V. Ziegler, and B. Zou

**Editors:** M. Amaryan, E. Chudakov, C. Meyer, M. Pennington, J. Ritman, and I. Strakovsky

## Abstract

The KL2016 Workshop is following the Letter of Intent LoI12–15–001 *Physics Opportunities with Secondary  $K_L^0$  beam at JLab* submitted to PAC43 with the main focus on the physics of excited hyperons produced by the Kaon beam on unpolarized and polarized targets with GlueX setup in Hall D. Such studies will broaden a physics program of hadron spectroscopy extending it to the strange sector. The Workshop was organized to get a feedback from the community to strengthen physics motivation of the LoI and prepare a full proposal.

Further details about the Workshop can be found on the web page of the conference:  
<http://www.jlab.org/conferences/kl2016/index.html> .

We acknowledge the support of The George Washington University, U.S.A., Institute for Kernphysik & Jülich Center for Hadron Physics, Jülich, Germany, Jefferson Science Associates, U.S.A., Old Dominion University, U.S.A., Thomas Jefferson National Accelerator Facility, U.S.A.

PACS numbers: 13.75.Jz, 13.60.Rj, 14.20.Jn, 25.80.Nv.

# Contents

<b>1</b>	<b>Preface and Summary</b>	<b>1</b>
	<i>M. Pennington</i>	
<b>2</b>	<b>Summaries of Talks</b>	<b>5</b>
2.1	Photoproduction of $K^0$ : Early History . . . . .	5
	<i>M. Albrow</i>	
2.2	Overview of Hall D Complex . . . . .	11
	<i>E. Chudakov</i>	
2.3	The $K_L^0$ Beam Facility at JLab . . . . .	13
	<i>M. Amarian</i>	
2.4	Hadron Physics at J-PARC . . . . .	22
	<i>H. Ohnishi</i>	
2.5	Low Energy Kaon Scattering: Present Status and Open Possibilities . . . . .	31
	<i>A. Filippi</i>	
2.6	$K_L^0 p$ Scattering to Two-Body Final States . . . . .	42
	<i>D.M. Manley</i>	
2.7	Excited Hyperons and their Decays . . . . .	49
	<i>F. Myhrer</i>	
2.8	Hadron Physics with High-Momentum Hadron Beams at J-PARC . . . . .	56
	<i>H. Noumi</i>	
2.9	Cascade Production in $\bar{K}^-$ - and Photon-Induced Reactions . . . . .	65
	<i>K. Nakayama, B.C. Jackson, Y. Oh, and H. Haberzettl</i>	
2.10	Predictions for Excited Strange Baryons . . . . .	75
	<i>I.P. Fernando and J.L. Goity</i>	
2.11	The $\bar{K}N \rightarrow K\Xi$ Reaction in a Chiral NLO Model . . . . .	83
	<i>A. Ramos, A. Feijoo, and V.K. Magas</i>	
2.12	Hyperon Studies at JPAC . . . . .	95
	<i>C. Fernández-Ramírez and A. Szczepaniak</i>	

2.13	Spectrum and Quantum Numbers of $\Xi$ Resonances . . . . .	102
	<i>Y. Oh</i>	
2.14	Hyperon Resonance Studies from Charm Baryon Decays at BaBar . . . . .	113
	<i>V. Ziegler</i>	
2.15	Evidence of Some New Hyperon Resonances – to be Checked by KL Beam . . . .	120
	<i>B. Zou</i>	
2.16	Can Spectroscopy with Kaon Beams at JLab Discriminate between Quark Diquark and Three Quark Models ? . . . . .	127
	<i>E. Santopinto</i>	
2.17	Reducing the Ambiguity of the AntiKaon-Nucleon Amplitude Using Modern Ex- perimental Data . . . . .	143
	<i>M. Mai</i>	
2.18	Opportunities in the Hyperon Spectrum with Neutral Kaon Beam . . . . .	152
	<i>V. Mathieu</i>	
2.19	Establishing S = -1 Hyperon Resonances Using Kaon-Induced Meson Productions within Dynamical Coupled-Channels Approach . . . . .	155
	<i>H. Kamano</i>	
2.20	Strangeness Physics at CLAS in the 6 GeV Era . . . . .	163
	<i>R. Schumacher</i>	
2.21	Lattice Studies of Hyperon Spectroscopy . . . . .	170
	<i>D. Richards</i>	
2.22	Formation of the $f_0(980)$ and $a_0(980)$ resonances by $\bar{K}$ Induced Reactions on Protons	178
	<i>E. Oset, Ju-Jun Xie, Wei-Hong Liang</i>	
2.23	TREK @ J-PARC: Beyond the Standard Model with Stopped $K^+$ . . . . .	191
	<i>M. Kohl</i>	
2.24	Simulation Study of $K_L$ Beam: $K_L$ Rates and Background . . . . .	198
	<i>I. Larin</i>	
2.25	$K_L$ Simulation Studies with the GlueX Detector . . . . .	205
	<i>S. Taylor</i>	
2.26	Compact Photon Source Conceptual Design . . . . .	214

	<i>P. Degtyarenko and B. Wojtsekhowski</i>	
2.27	Targets for a Neutral Kaon Beam . . . . .	223
	<i>C. Keith</i>	
<b>3</b>	<b>List of Participants of KL2016 Workshop</b>	<b>228</b>



# 1 Preface and Summary

Michael Pennington

*Thomas Jefferson National Accelerator Facility  
Newport News, VA 23606, U.S.A.*

## 1. Primary Physics with Secondary Beams of $K_L$ 's

Not all of physics can be explored by primary beams of electrons and protons, however much these have taught us over the past 60 years. Electron-positron colliders give access to restricted sets of quantum numbers. From proton-proton collisions we have long learned about all manner of high energy reactions. However, access to excited mesons and baryons has been most universally achieved with pion and kaon secondary beams, and latterly photon beams both virtual and real. Nowadays the wealth of information on polarized photon beams on polarized targets has totally revolutionized baryon spectroscopy, especially in the lightest flavor sector. The measurement of polarization asymmetries has constrained partial wave analyses far beyond anything conceivable with pion beams. Nevertheless, these only give access to the product of photocouplings of each excited baryon and its coupling to the hadron final state, such as  $\pi N$ ,  $\pi\pi N$ ,  $\eta N$ , *etc.* Contemporaneously, in the meson sector, the COMPASS experiment with pion beams on protons at 190 GeV/c, together with heavy flavor decays in  $e^+e^-$  annihilation, have given access to multi-meson final states, like  $2\pi$ ,  $3\pi$ , with greater precision than ever before. This has given hints and suggestions of new resonances, like the  $a_1(1420)$ .

To understand the constituent structure of hadrons requires information on the relationship of each meson and baryon to those with different flavors, but the same  $J^P$  quantum numbers. At its simplest, this is to understand the quark model multiplet structure, where this is appropriate. What is more, so ubiquitous are  $\pi\pi$ ,  $\pi K$ ,  $K\bar{K}$ ,  $\eta\pi$ ,  $\eta K$ , ... final states as the decay products of almost every hadron, that knowledge of the properties of these is critical to every analysis. Unitarity colors and shapes the universality of such final state interactions in each set of quantum numbers. This means that however precise our measurements of  $\gamma N \rightarrow \pi\eta^{(\prime)}N$ , with GlueX for instance, we cannot really determine the fine resonant structure of such a process without some information on  $\pi\eta$  and  $\pi\eta'$  scattering too. Nor can we determine any flavor partners without information on the corresponding  $K\eta^{(\prime)}$  channels. For that secondary kaon beams are essential.

While J-PARC has a whole program of charged strange particle and hypernuclear reactions, photon beams allow unique access to other channels. It was realized long ago that intense photon beams like that about to be delivered to Hall D at JLab, could produce secondary beams. The charged particles can readily be bent away, leaving a neutral particle beam dominated by  $K_L$ : long lived kaons being produced far more copiously than neutrons above 3–4 GeV momentum. Such a facility provides access to a whole range of physics that is the subject of this meeting.

The reactions that can be studied cover the meson spectrum and dynamics, the baryon spectrum and dynamics, and final state interactions that link mesons and baryons together. This includes particularly the channels  $K\pi$ ,  $K\eta$ ,  $K\eta'$  in the meson sector. These explore the very limitations of chiral dynamics: the strange quark's current mass is 30-50 times that of the

average  $u, d$  mass, so corrections from explicit breaking are likely significant. Moreover, are there eight or nine Goldstone bosons? In a world of large  $N_c$ , a nonet of light pseudoscalars is natural, but is the  $N_c = 3$  world close to this or not? At the same time, information on  $KM$  final states, with  $M = \pi, \eta, \eta'$ , is vital in understanding excited meson multiplets. This also provides links to  $J/\psi\pi\pi$  dynamics and its relation to  $\phi\pi\pi$  and  $K^*\bar{K}\pi$  with hidden strangeness. In the baryon sector, while earlier seemingly “missing” states are appearing with  $N^*$ ’s and  $\Delta^*$ ’s, few of the related  $\Sigma^*$ ’s and  $\Xi^*$ ’s are known.

The exact connection of the Constituent Quark Model to QCD is not really understood. Nevertheless calculations in Lattice QCD with heavier than physical pions give a baryon spectrum much like that of the Constituent Quark Model. This is perhaps not surprising since with only single hadron operators, the excited states are almost stable. Though dynamical quarks allow additional  $q\bar{q}$  pairs to be produced, with a heavy pion (and hence heavy  $u, d$  quarks) the Fock space of excited  $N^*$ ’s are dominated by  $qqq$  configurations. Computations including gluonic operators allow hybrid states of  $qqqg$  that are a GeV or so heavier than  $qqq$  configurations with the same  $J^P$ . The spectrum from Lattice QCD can be regarded as the 21st century version of the Constituent Quark Model. However, it is naturally improvable, not just because by lowering the pion mass the phase space for decays increases. This is not sufficient to reproduce experiment. More efficacious is the inclusion of multiparticle scattering states. Hadrons become resonances by coupling to these scattering states. For mesons like the  $\rho$  and  $K^*$ , rather precise calculations have now been made, but for baryons like those in Fig. 1, which are much more computationally intensive, these are still to come.

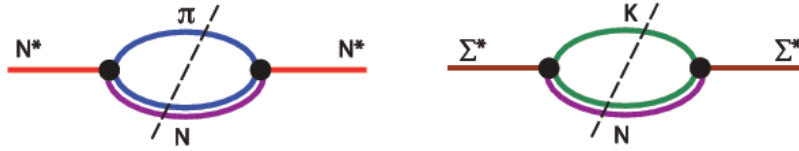


Figure 1: The propagator of an unstable particle is affected by the coupling to hadronic intermediate states. The imaginary part of these contributions (signified by the dashed line that places the intermediate state particles on-shell) gives the resulting resonance a width, as well as changing the real part of its mass function.

Scattering states do not just allow decays and give the states a width, but these in turn shift the masses of the resonances, particularly when the decays are  $S$ -wave. For their strange partners, with fewer open channels, the shifts may be less, as illustrated in Fig. 2. Thus one might expect the strange, doubly strange and even more the triply strange baryons to be closest to where our new Lattice version of the Constituent Quark Model may predict, while the  $N^*$ ’s and  $\Delta^*$ ’s may be shifted significantly.

Indeed in some cases they may be indistinguishable from the continuum, in others conventional and hybrid baryons may have distinct decay patterns. So where the  $\Sigma^*$ ’s,  $\Lambda^*$ ’s and  $\Xi^*$ ’s are that partner the Roper,  $N^*(1440)$  with  $J^P = (1/2)^+$ , may teach us about how this dynamics works. It is likely much of this same dynamics with its interplay of both col-

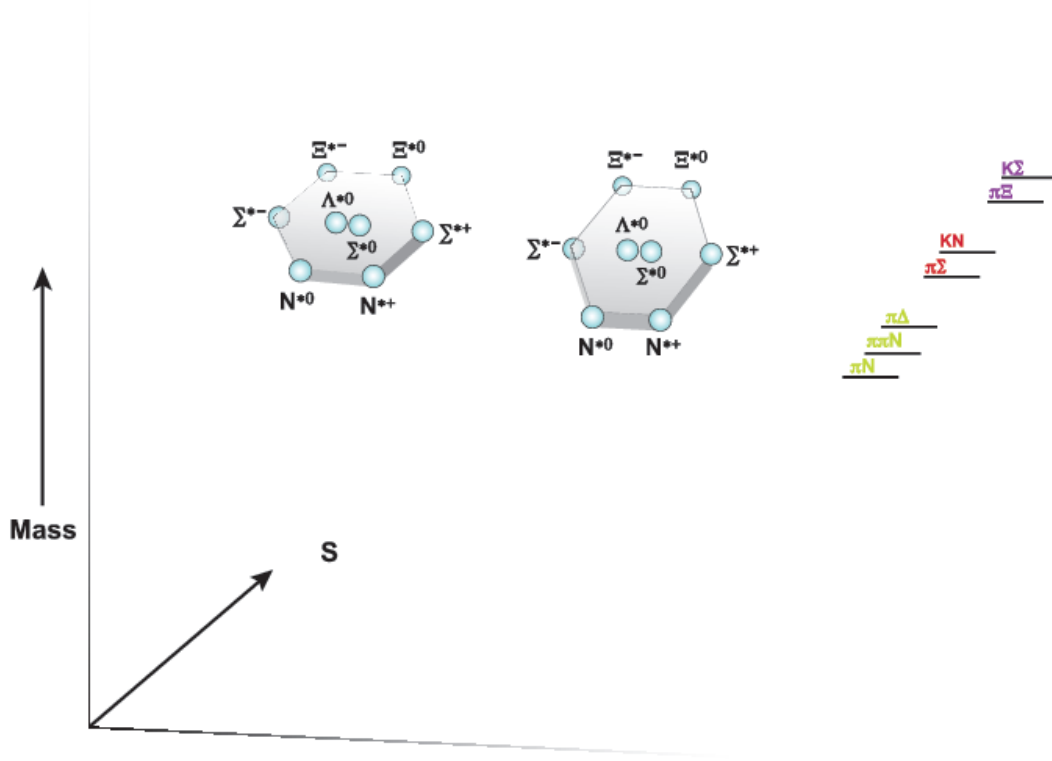


Figure 2: An example of a flavor octet of excited baryons. The multiplet on the left is that expected for stable states in the Constituent Quark Model with the strange quark having a 150 MeV heavier mass than the  $u, d$  quarks. The coupling to nearby hadronic channels, indicated on the right, through graphs like that in Fig. 1, affects the mass of the unstable states. This might leave the  $\Xi^{*-}$ 's least disturbed, while significantly shifting the masses of the less strange members of the multiplet.

ored (quark and gluon) and color singlet degrees of freedom underlies the appearance of the  $X, Y, Z$ , and  $P_c$  states. Indeed such interplay is integral to generating their very existence. Strange baryon studies enabled by  $K_L$  beams may provide unique insights into this newly exposed world.

Since the primary focus of the GlueX experiment is to study the photoproduction of mesons, it is unrealistic to expect its replacement by a secondary beam of  $K_L$ 's before a few years of photon data-taking. Indeed, there would be little point until the DIRC bars, and even a RICH for kaon identification, are in place. Then while the GlueX analysis is concentrating on gluonic excitations with millions of events on many channels, from which to extract physics, perhaps an opportunity arises to show that a secondary  $K_L$  beam can provide unique data on the very strange baryons. A short program that successfully identifies  $\Xi^{*-}$ 's and  $\Omega^{*-}$ 's not just as bumps in cross-sections, but with quantum numbers determined from their decays, may spur the demand for longer running and make the  $K_L$  beam a facility for hadron physics

unique in the world.

A long march starts with the first stride: this is the step taken by this workshop. The second step is to plan for the minimal Be target, sweeping magnet and pair spectrometer required for a feasibility run. As always this requires a lead time of several years. Consequently whether to proceed, to even this limited stage within the Hall D schedule, demands a timely decision.

## **2. Acknowledgements**

This material is based upon work supported by the U.S. Department of Energy, Office of Science, Office of Nuclear Physics under contract DE-AC05-06OR23177.

## 2 Summaries of Talks

### 2.1 Photoproduction of $K^0$ : Early History

Michael Albrow

*Fermi National Accelerator Laboratory*

*P.O.Box 500, Wilson St.*

*Batavia, IL 60510, U.S.A.*

#### Abstract

I discuss the first measurements of photoproduction of neutral Kaons in the 1960's, and early experiments on  $K^0$  decays and interactions carried out with such beams.

#### 1. Motivation for $K^0$ Photoproduction

In July 1964 Christenson, Cronin, Fitch and Turlay announced [1] the observation of the long-lived  $K^0$  decaying to two pions, which was the discovery of CP-violation. It was already realised that  $K_0 - \bar{K}^0$  physics was extremely interesting [2], with particles and their antiparticles being distinct under strong interactions, but able to mix through weak interactions to form short-lived and long-lived states, now called  $K_S^0$  and  $K_L^0$ . That was the year I started my postgraduate studies at Manchester University. Prof. Paul Murphy led the group from 1965, and the nearby Daresbury Nuclear Physics Laboratory (DNPL) was constructing a 5 GeV electron synchrotron, NINA (Northern Institutes National Accelerator). This would be a local laboratory for the northern universities to balance the Rutherford Laboratory's NIMROD 7 GeV proton accelerator in southern England. The possibility that a useful  $K^0$  beam could be made at an electron synchrotron by photoproduction was being considered, and a 1965 prediction for SLAC by Drell and Jacob [3] was optimistic. They expected the dominant mechanism to be virtual  $K^*$ -exchange in the  $t$ -channel,  $\gamma + K^* \rightarrow K$ , with a cross section, peaking at  $\theta \sim 2^\circ$ , at least  $20 \mu\text{b/sr}$ , for 15 BeV (now GeV !) photons. We now know that  $K^*$ -exchange is not the dominant process.

In 1965, the Manchester Group decided to measure  $K^0$  photoproduction at NINA with a view to using the beam for decay measurements.

#### 2. First Observations

While our Manchester experiment was being carried out the first "observation" of photo-produced  $K^0$  was published [4] by the Cambridge Bubble Chamber Group; after scanning 865,000 (sic !) hydrogen bubble chamber photographs they found about 50 examples of  $K^0 \rightarrow \pi^+\pi^-$ . Of these, 35 were classified as  $\Lambda^0 K^0 \pi^+$  events, and a few were possibly photoproduction of  $\phi \rightarrow K_S^0 K_L^0$ , but the evidence for that was "weak". This was followed by an experiment [5] in 1967, using a multi-gap optical spark chamber, still taking photographs but now with the ability to trigger on a neutral particle entering the fiducial volume (with a veto counter) and a pair of charged particles in a scintillation counter hodoscope behind. As in our Manchester experiment, a  $K_S^0$ -regenerator was placed in front of the decay volume. There was no magnetic field, but coplanar V's were selected, and assuming  $K^0 \rightarrow \pi^+\pi^-$

the Kaon momentum is known from kinematics. The Cambridge Electron Accelerator produced 5.5 GeV electrons, and the  $K^0$  were produced in Al- and Be-targets at polar angles from  $0^\circ$  -  $10^\circ$ . Since an intermediate photon beam was not used, the flux is a combination of electro- and photo-production in the targets. With about 400 events, they reported a yield of  $1.3 \times 10^{-5}$   $K^0$ /electron for  $1.0 < p_K < 5.5$  GeV/c at  $3.5^\circ$ . The spectrum peaks at 2 GeV/c, which they interpreted as due to  $\phi$ -photoproduction and decay, incorrectly as it turns out. Absence of  $K^0$  with momenta closer to the beam momentum gave an upper limit on the two-body processes:  $\gamma + p \rightarrow K^0 + \Sigma^+$ ,  $\gamma + n \rightarrow K^0 + \Sigma^0$ , and  $\gamma + n \rightarrow K^0 + \Lambda^0$ . Schivell *et al.* said it was [5]: *an extremely clean beam which appears quite free of neutrons*, although they did not elucidate. Of course for most “decay” experiments neutron background is unimportant, but for scattering and interaction experiments it can be serious.

A major hydrogen bubble chamber study [6] (1.7 million pictures !) using a bremsstrahlung beam up to  $E_\gamma = 5.8$  GeV at DESY reported a few  $\gamma + p \rightarrow K^0 + \Sigma^+$  events with  $\sigma = 0.68 \pm 0.48$   $\mu\text{b}$ , with a considerably larger cross section for  $\gamma + p \rightarrow \Lambda^0 + K^0 + \pi^+ (+\pi^0 \dots)$ . So  $K^0$  photoproduction at these energies is usually accompanied by pions.

### 3. The Manchester Experiment at NINA (Daresbury, UK)

A key innovation of the Manchester experiment was to use “automatic” (electronic) spark chambers, to progress beyond the prevalent scanning and measuring of bubble chamber or optical spark chamber pictures. We built small prototypes of three types: (a) sonic, with three microphones around the edge of the spark gap, and timing the sound of the sparks, (b) magnetostrictive, with one electrode consisting of wires crossing a magnetostrictive ribbon, and (c) ferrite core memory, in which each wire of an electrode plane was threaded through a  $\sim 1$  mm diameter ferrite core. The spark current-pulse flipped the magnetisation of the core, inducing a pulse on a “read” wire connected to the data acquisition, before being reset by a pulse on a third wire. (So our core memory board had about 1 mm<sup>3</sup>/bit; compare with memory density today, 50 years later !) The ferrite core technique was chosen for the experiment, and we made 12 planes, each  $70 \times 121$  cm. I believe that was the largest system of electronic spark chambers in operation in 1968. <sup>1</sup> But that was the very year that Charpak invented the multi-wire proportional chamber that superseded spark chambers, with a steady high voltage, no sparks, more gentle discharges, and high rate capability.

The method of measuring the  $K^0$  flux after a 40 m flight path, where there are only  $K_L^0$  left ( $c\tau(K_L^0) = 15.34$  m), was to insert a  $K_S^0$  regenerator made of 14 cm of iron. Because  $K^0$  and  $\bar{K}^0$  have different strong interactions and are differently attenuated in the iron, a  $K_S^0$  component appears, and since  $c\tau(K_S^0) = 2.684$  cm they conveniently decay in a short fiducial region, 69.2% of the time to  $\pi^+\pi^-$ . With two tracks to be detected from the  $K_S^0$  decays we needed to resolve the  $x, y$ -ambiguity (if only two coordinates had been measured), so the chambers immediately following the decay region were in  $u, v, x$  triplets, with wires at  $60^\circ$ . The sides ratio  $70/121 = \tan(30^\circ)$  was conveniently chosen so the inclined  $u$ - and  $v$ -wire planes were parallel to the diagonals, and the wires emerged at the top and bottom with exactly twice the spacing of the  $x$ -wires. The sum of the coordinates  $u + v + x$  is a constant for a real track, simplifying analysis on our PDP8 computer (programmed with punched paper tape !).

---

<sup>1</sup>With the lights off, we could see through the wires the pions making tracks of sparks; that was exciting !

The main improvements over the previous experiments [4,5] were the first use of “electronic” wire chambers (no more scanning and measuring photographs !), using a bremsstrahlung photon beam (from a  $0.1 X_0$  tungsten target), using a 60 cm hydrogen target [7] as well as nuclear targets (Be, Al, Cu) [8], and using a magnet to measure the momentum of at least one pion. The acceptances and efficiencies were calculated with Monte Carlo simulations. After fitting to  $K_S^0 \rightarrow \pi^+\pi^-$ , the reconstructed  $K_S^0$  lifetime showed that the sample had no background. The yields showed a strong increase with  $E_\gamma$ , see Fig. 1(a), rising from threshold to  $d\sigma/d\Omega = 15 \pm 3 \mu\text{b}/\text{sr}/\text{e.q.}^2$  on hydrogen for  $p_K > 1.5 \text{ GeV}/c$  at  $\theta = 3^\circ$ . The momentum spectra of the  $K^0$  peak at low values,  $\sim 1.5 \text{ GeV}/c$ ; two-body reactions (see above) do not dominate. The yield is significantly less than that predicted by Drell and Jacob, implying a  $K^*K\gamma$  coupling much smaller than they expected. Photoproduced  $\phi \rightarrow K\bar{K}$  can only account for a small fraction of the data; the total cross section for  $\gamma \rightarrow \phi$  being small ( $\sim 0.4 \mu\text{b}$ ).

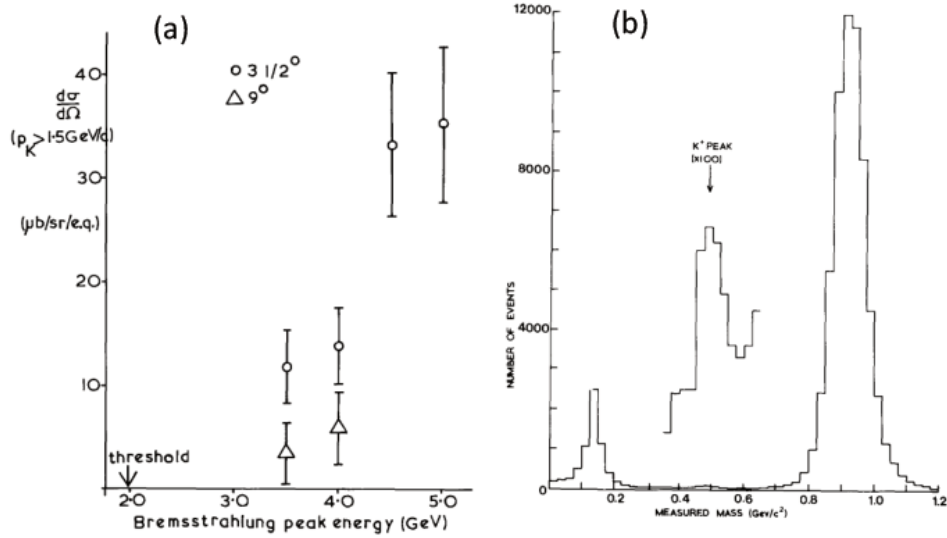


Figure 1: (a)  $K^0$  yields [8] from hydrogen, above  $1.5 \text{ GeV}/c$ , as a function of the peak bremsstrahlung energy; (b) Mass spectrum of charged particles [9] from time-of-flight of the beam particle ( $K^0$  or  $n$ ) plus final charged particle ( $K^+$  or  $p$ ), knowing the momentum of the latter. Note the  $\pi^+$  background.

The data with nuclear targets ( $0.45 X_0$  of Be, Al, and Cu) required corrections for the absorption of the photon beam in the target and of the  $K^0$  leaving it. The photoproduction cross section “per nucleon” shows a very small  $A$ -dependence :  $d\sigma/d\Omega \propto A^{1.09 \pm 0.03}$  (this is after subtracting the few % contribution from coherent  $\phi$ -photoproduction). The residual

<sup>2</sup>e.q., means “equivalent quantum”, a measure of the photon flux using a quantameter.

small rise could result from another coherent process, or from a difference in the production of neutrons and protons. Quoting Ref. [8] *It seems probable that most of the  $K_L^0$  yield is produced in association with pions in multiparticle production events. This would account for the large yield of low momentum  $K_L^0$  mesons.*

#### 4. $K_L^0$ Decays

Having established a photoproduced  $K^0$  beam, the  $K_S^0$ -regenerator was removed to measure  $K_L^0$  3-body decays. (The CP-violating  $K_L^0 \rightarrow \pi^+\pi^-\pi^0$  decay has a probability  $\sim 2 \times 10^{-3}$  and was not on our menu.) At the time these studies were “state of the art”. An excellent review of the contemporary theory is given in Ref. [10].

##### (a) $K_L^0 \rightarrow \pi^+\pi^-\pi^0$

Our first decay measurement [11] was the  $\pi^+\pi^-\pi^0$  mode  $K_{3\pi}$ , which has a branching fraction  $BF = 12.5\%$  [12]. The  $\pi^0$  was not detected, and the  $K_{3\pi}$  mode was distinguished from the  $\pi^\pm\mu^\mp\nu$  mode using kinematics. In a particular reference frame (the Astier [13] frame) the kinetic energy of the  $K_L^0$  is positive for the  $3\pi$  mode, but it is mostly negative for the semileptonic modes [11]. From 660,000 triggers 70,000 two-track decays in the fiducial region were selected, of which 29,000 were classified as  $K_L^0 \rightarrow \pi^+\pi^-\pi^0$ , with 17% semileptonic background. The main thrust of the analysis was to study the decay matrix element using the distribution of decays over the triangular “Dalitz plot”. (The energies of the three pions in their c.m. frame have to add up to  $M(K)$ , and the normals to the sides of an equilateral triangle have to add up to a constant. So each event can be plotted as a point on  $60^\circ$ -triangular graph paper.)

Reconstructing the  $K_L^0$  momentum from the two pions involves a quadratic ambiguity, which has to be considered in the analysis. The results can be presented in the form of the  $\pi^0$  kinetic energy,  $T_0$ , spectrum, for which Weinberg had proposed [14] a general form with linear, quadratic, cubic, *etc.* terms. Including a cubic term improved the, basically linear, fit.

##### (b) $K_L^0 \rightarrow \pi^\pm\ell^\mp\nu$

Studies were made of both the muon decay [15]  $K_{\mu 3}$  ( $BF = 27\%$ ) and the electron decay [16]  $K_{e 3}$  ( $BF = 40.6\%$ ). This was a decade before the discovery of the real  $W$ , but the term “strangeness-changing hadronic vector current” described in V – A theory was the current language. The  $K^0$  emits a highly off-shell (!)  $W$  with 4-momentum-squared  $q^2 = (p_K - p_\pi)^2$  (4-vectors), that couples to  $e\nu$  or  $\mu\nu$ . The aim is to investigate the structure of this weak current; one writes down “form factors”  $f_+(q^2)$  and  $f_-(q^2)$  that can be determined by fitting the Dalitz plot of the decays. Scalar and/or tensor exchanges could show up in these distributions, so it was a test of the V – A theory.

For the  $K_{\mu 3}$  measurements an iron absorber and a scintillation counter hodoscope were added behind the spark chambers. The distribution of 9,066 events over the Dalitz plot was measured, after correcting for acceptance and efficiencies using  $10^5$  Monte Carlo-generated events. I will not discuss the fits using form factor parametrisations, except that the  $f_+$  form factor, which should depend only on  $q^2$ , shows a clear linear increase from  $q^2/m(\pi)^2 = 1.5$  to 5.0. In contrast the  $f_-$  form factor is negative and did not show significant  $q^2$ -dependence. Limits were put on scalar and tensor couplings.



The  $K_{e3}$  decays were distinguished by kinematics and the absence of a muon penetrating the Pb + Fe wall; this still left 13%  $K_{\mu3}$  background (there was no electromagnetic calorimeter). The  $f_+(q^2)$  distribution is similar to that for  $K_{\mu3}$ , but  $f_-$  is suppressed by the kinematic factor  $(m_e/m_K)^2$ . Again the data did not show any evidence for scalar or tensor couplings, but the sensitivity was not very high:  $f_S < 0.19 f_+(0)$  and  $f_T < 1.0 f_+(0)$  separately, assuming no destructive interference between them.

## 5. $K_L^0$ Interactions: $K^0 + p \rightarrow K^+ + n$

Although photoproduced  $K^0$  beams are not neutron-free, at least in the conditions of our DNPL experiment, the  $n : K^0$  ratio is much less than in proton-produced beams, and the Manchester-DNPL group took advantage of that [9] to measure  $K^0 + p \rightarrow K^+ + n$  from 0.6 to 1.5 GeV/c. The quark-model was still relatively new, and while the known baryons could all be accommodated as  $\{qqq\}$ , a baryon with positive strangeness, then called  $Z^*$ , would have to be  $\{qqqq\bar{q}\}$ , a “pentaquark”, although that name came much later ( $\sim 1987$ ). A  $K^+p$  state or resonance, having  $B = +1$  and  $S = +1$  would have to be  $\{uuud\bar{s}\}$  and a  $K^+n$  state  $\{uudd\bar{s}\}$ , these were called “exotics”. (I had left the Manchester group by this time, but had looked for a  $Z^*$  in  $K^+p$  elastic scattering (pure  $I = 1$ ) with a polarized target [17] at CERN.) The reactions  $K^+ + n \rightarrow K^+ + n$  and  $K^+ + n \rightarrow K^0 + p$  required deuterium targets; they have isospin amplitudes  $\frac{1}{2}(f_1 + f_0)$  and  $\frac{1}{2}(f_1 - f_0)$ , respectively. The inverse reaction  $K^0 + p \rightarrow K^+ + n$  avoids the neutron target complication, but has a neutron in the final state. This was detected in a large scintillator block, but there would be a large background from the reaction  $n + p \rightarrow p + n$ . One must distinguish  $K^0 \rightarrow K^+$  from  $n \rightarrow p$ , knowing the momentum of the outgoing charged track but not its identity. The trick used was to measure the time-of-flight over the 21 m of the beam particle “plus” the 5m of the charged particle, using the RF of the synchrotron (0.5 ns bunch every 4.908 ns) picked up in a cavity on the circulating beam. See Fig. 1(b). For our experiment, the bunch spacing in NINA was doubled, since 5 ns caused ambiguities. The dominant (by a factor  $\sim 200$ )  $n + p \rightarrow p + n$  events could be used to calibrate the neutron counter timing. The  $K^0 + p \rightarrow K^+ + n$  cross sections  $d\sigma/d\Omega(p, \cos \theta)$  are presented, fit to Legendre polynomials and partial and total cross sections derived. For details, see Ref. [9], but the last sentence is: *The evidence for a  $Z_0^*$  state must therefore be considered slender.* Nevertheless, some 40 years later (now), an experiment could certainly be done with much higher statistics and resolution and less background. Pentaquarks are now in fashion. An exercise for this Workshop.

One last remark or suggestion. The  $K_L^0$  beam is  $(K^0 - \bar{K}^0)/\sqrt{2}$ , while a  $K_S^0$  is  $(K^0 + \bar{K}^0)/\sqrt{2}$ . Normally  $K^0$  strong interactions are studied in a (pure)  $K_L^0$  beam. If the interaction target can be placed very close to the  $K^0$  production target, before the  $K_S^0$  have decayed, the strong interactions will have a different mixture of  $K^0$  and  $\bar{K}^0$ . By subtraction one can in principle study the  $I = 0$  and  $I = 1$  amplitudes separately. Alternatively one can study the interactions close behind a regenerator when the beam is a mixture of  $K_S^0$  and  $K_L^0$ , and by varying the distance between the regenerator and the target one can vary the mix in a known fashion.

## 6. Acknowledgments

I thank Paul Murphy (my professor 1965-1969) and Fred Loebinger for “the good old days”.

And I thank the organizers, especially Igor Strakovsky, and JLab for the opportunity to (reminisce and) participate in this Workshop. This work is supported by the US DOE.

## References

- [1] J.H. Christenson, J.W. Cronin, V.L. Fitch, and R. Turlay, Phys. Rev. Lett. **13**, 138 (1964).
- [2] See, *e.g.*, P.K. Kabir, *The CP Puzzle* (Academic Press, 1968).
- [3] S.D. Drell and M. Jacob, Phys. Rev. **138**, B1312 (1965).
- [4] Cambridge Bubble Chamber Group, Phys. Rev. **156**, 1426 (1967).
- [5] J.F. Schivell *et al.*, Phys. Rev. Lett. **19**, 1349 (1967).
- [6] R. Erbe *et al.* (Aachen-Berlin-Bonn-Hamburg-Munich Collaboration), Phys. Rev. **188**, 2060 (1969).
- [7] M.G. Albrow *et al.*, Phys. Lett. **29B**, 54 (1969).
- [8] M.G. Albrow *et al.*, Nucl. Phys. B **23**, 509 (1970).
- [9] J.C.M. Armitage *et al.*, Nucl. Phys. B **123**, 11 (1977).
- [10] L.M. Chounet, J.-M. Gaillard and M.K. Gaillard, Phys. Rep. **4**, 199 (1972).
- [11] M.G. Albrow *et al.*, Phys. Lett. **33B** 516 (1970).
- [12] K.A. Olive *et al.* (Particle Data Group), Chin. Phys. C **38**, 090001 (2014).
- [13] A. Astier *et al.*, Int. Conf. on Elementary Particles, Aix-en-Provence (1961) p. 227 (in French).
- [14] S. Weinberg, Phys. Rev. Lett. **17**, 153 (1966).
- [15] M.G. Albrow *et al.*, Nucl. Phys. B **44**, 1 (1972).
- [16] M.G. Albrow *et al.*, Nucl. Phys. B **58**, 22 (1973).
- [17] M.G. Albrow *et al.*, Nucl. Phys. B **30**, 273 (1971).

## 2.2 Overview of Hall D Complex

Eugene Chudakov

*Thomas Jefferson National Accelerator Facility*

*Newport News, VA 23606, U.S.A.*

1. Hall D is a new experimental hall at Jefferson Lab, designed for experiments with a photon beam. The primary motivation for Hall D is the GlueX experiment [1, 2], dedicated to meson spectroscopy. The Hall D complex consists of:
  - An electron beam line used to extract the 5.5-pass electrons from the accelerator into the Tagger Hall. The designed beam energy is  $E_e = 12$  GeV.
  - The Tagger Hall, where the electron beam passes through a thin radiator ( $\sim 0.01\%$  R.L.) and is deflected into the beam dump. The electrons that lost  $>30\%$  of their energy in the radiator are detected with scintillator hodoscopes providing a  $\sim 0.1\%$  energy resolution for the tagged photons. Aligned diamond radiators allow to produce linearly polarized photons via the Coherent Bremsstrahlung. The beam dump is limited to 60 kW (5  $\mu$ A at 12 GeV).
  - The Collimator Cave contains a collimator for the photon beam and dipole magnets downstream in order to remove charged particles. The 3.4 mm diameter collimator, located about 75 m downstream of the radiator, selects the central cone of the photon beam increasing its average linear polarization, up to  $\sim 40\%$  in the coherent peak at 9 GeV.
  - Hall D contains several elements of the photon beam line, and the main spectrometer. A Pair Spectrometer consists of a thin converter, a dipole magnet, and a two-arm detector used to measure the energy spectrum of the photon beam. The main spectrometer is based on a 2-T superconducting solenoid, 4 m long and 1.85 m bore diameter. The liquid hydrogen target is located in the front part of the solenoid. The charged tracks are detected with a set of drift chambers; photons are detected with two electromagnetic calorimeters. There are also scintillator hodoscopes for triggering and time-of-flight measurements. The spectrometer is nearly hermetic in an angular range of  $1^\circ < \theta < 120^\circ$ . The momentum resolution is  $\sigma_p/p \sim 1 - 3\%$  depending on the polar angle  $\theta$ . The energy resolution of the electromagnetic calorimeters is about 7% at 1 GeV.

The main spectrometer is designed for photon beam rates below 100 MHz in the coherent peak. Such a rate can be provided by a 2.2  $\mu$ A beam on a 0.02 mm = 0.0125% R.L. diamond crystal. The 1-st stage of GlueX is planned to run at a lower rate of 10 MHz.

Hall D and the GlueX experiment had 3 commissioning runs in 2014–2016. By April 2016, all the systems have been commissioned at some level and most of them have reached the specifications. Preliminary results of the 2014–2015 commissioning have been reported [3]. In addition to the GlueX experiment, two other experiments (both using Primakoff-type reactions) have been approved by the Program Advisory Committee (PAC). In total, about 500 days of effective running have been approved by the PAC.

## 2. Acknowledgments

This material is based upon work supported by the U.S. Department of Energy, Office of Science, Office of Nuclear Physics under contract DE-AC05-06OR23177.

## References

- [1] M. Dugger *et al.* (GlueX Collaboration), arXiv:1210.4508.
- [2] A. AlekSejevs *et al.* (GlueX Collaboration), arXiv:1305.1523.
- [3] H.A. Ghoul *et al.* (GlueX Collaboration), in *16th International Conference on Hadron Spectroscopy* (Hadron 2015) Newport News, Virginia, USA, September, 2015; arXiv:1512.03699.

## 2.3 The $K_L^0$ Beam Facility at JLab

Moskov Amaryan

*Department of Physics*

*Old Dominion University*

*Norfolk, VA 23529, U.S.A.*

### Abstract

Following a Letter of Intent submitted to PAC43 at JLab in this talk we discuss the possibility to create a secondary  $K_L^0$  beam in Hall D to be used with GlueX detector for spectroscopy of excited hyperons.

### 1. Introduction

Our current understanding of strong interactions is embedded in Quantum Chromodynamics (QCD). However, QCD being a basic theory, extremely successful in explaining the plethora of experimental data in the perturbative regime, faces significant challenges to describe the properties of hadrons in non-perturbative regime. Constituent Quark Model (CQM) is surprisingly successful in explaining spectra of hadrons, especially in the ground state; however, CQM appears to be too naive to describe properties of excited states. It is natural that excited states are not simply explained with spatial excitations of constituent quarks, but it is an effective representation revealing complicated interactions of quarks and gluons inside. Hadron spectroscopy aims to provide a comprehensive description of hadron structure based on quark and gluon degrees of freedom. Despite many successes in observing hundreds of meson and baryon states experimentally we haven't succeeded to either observe or rule out existence of glueballs, hybrids and multi quark systems; although it is tempting to explain recently observed X, Y, Z [1] states as first evidences of tetraquarks as well as recently observed heavy baryon states at LHCb [2] as charmed pentaquarks.

An extensive experimental program is developed to search for hybrids in the GlueX experiment at JLab. Over the last decade, significant progress in our understanding of baryons made of light ( $u, d$ ) quarks have been made in CLAS at JLab. However, systematic studies of excited hyperons are very much lacking with only decades old very scarce data filling the world database in many channels. In this experiment we propose to fill this gap and study spectra of excited hyperons using the modern CEBAF facility with the aim to use proposed secondary  $K_L^0$  beam with physics target of the GlueX experiment in Hall D. The goal is to study  $K_L - p$  and  $K_L - d$  interactions and do the baryon spectroscopy for the strange baryon sector.

Unlike in the cases with pion or photon beams, Kaon beams are crucial to provide the data needed to identify and characterize the properties of hyperon resonances.

Our current experimental knowledge of strange resonances is far worse than our knowledge of  $N$  and  $\Delta$  resonances; however, within the quark model, they are no less fundamental. Clearly there is a need to learn about baryon resonances in the "strange sector" to have a complete understanding of three-quark bound states.

The masses and widths of the lowest mass baryons were determined with Kaon-beam experiments in the 1970s [1]. First determination of pole positions, for instance for  $\Lambda(1520)$ , were

obtained only recently from analysis of Hall A measurement at JLab [3]. An intense Kaon beam would open a window of opportunity not only to locate missing resonances, but also to establish properties including decay channels systematically for higher excited states.

A comprehensive review of physics opportunities with meson beams is presented in a recent paper [4]. Importance of baryon spectroscopy in strangeness sector was discussed in Ref. [5].

## 2. Reactions that Could be Studied with $K_L^0$ Beam

More details about this chapter could be found in a talk by Mark Manley at this workshop.

### (a) Elastic and charge-exchange reactions

$$K_L^0 p \rightarrow K_S^0 p \quad (1)$$

$$K_L^0 p \rightarrow K^+ n \quad (2)$$

### (b) Two-body reactions producing $S = -1$ hyperons

$$K_L^0 p \rightarrow \pi^+ \Lambda \quad (3)$$

$$K_L^0 p \rightarrow \pi^+ \Sigma^0 \quad (4)$$

### (c) Three-body reactions producing $S = -1$ hyperons

$$K_L^0 p \rightarrow \pi^+ \pi^0 \Lambda \quad (5)$$

$$K_L^0 p \rightarrow \pi^+ \pi^0 \Sigma^0 \quad (6)$$

$$K_L^0 p \rightarrow \pi^0 \pi^0 \Sigma^+ \quad (7)$$

$$K_L^0 p \rightarrow \pi^+ \pi^- \Sigma^+ \quad (8)$$

$$K_L^0 p \rightarrow \pi^+ \pi^- \Sigma^- \quad (9)$$

### (d) Two- and three-body reactions producing $S = -2$ hyperons

$$K_L^0 p \rightarrow K^+ \Xi^0 \quad (10)$$

$$K_L^0 p \rightarrow \pi^+ K^+ \Xi^- \quad (11)$$

$$K_L^0 p \rightarrow K^+ \Xi^{0*} \quad (12)$$

$$K_L^0 p \rightarrow \pi^+ K^+ \Xi^{-*} \quad (13)$$

### (e) Three-body reactions producing $S = -3$ hyperons

$$K_L^0 p \rightarrow K^+ K^+ \Omega^- \quad (14)$$

$$K_L^0 p \rightarrow K^+ K^+ \Omega^{-*} \quad (15)$$

Reactions 10–15 will be discussed in more details below.

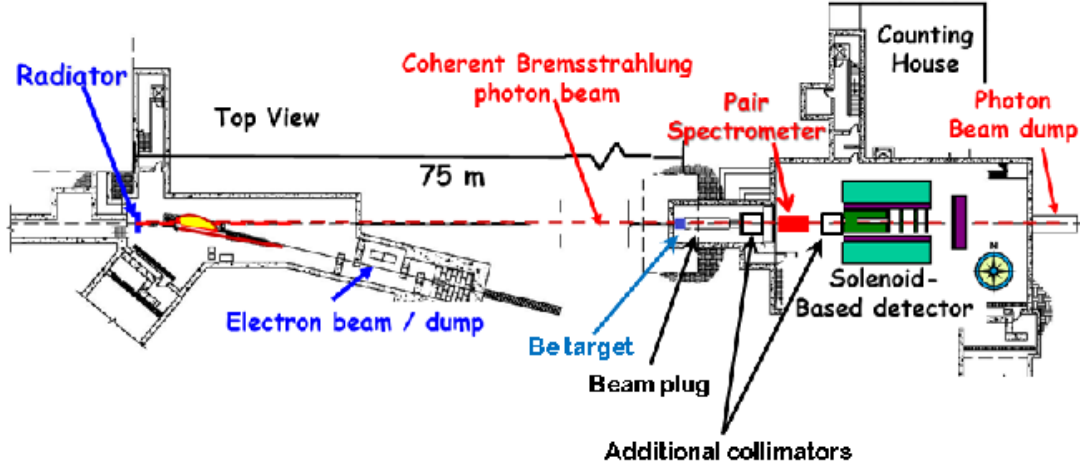


Figure 1: Schematic view of Hall D beamline. See a text for explanation.

### 3. The $K_L^0$ Beam in Hall D

In this Section, we describe photo-production of secondary  $K_L^0$  beam in Hall D. There are few points that need to be decided. To produce intensive photon beam one needs to increase radiation length of the radiator up to 10% radiation length. In a first scenario  $E_e = 12$  GeV, electrons produced at CEBAF will scatter in a radiator in the tagger vault, generating intensive beam of bremsstrahlung photons. This may will then require removal of all tagger counters and electronics and very careful design of radiation shielding, which is very hard to optimize and design. In a second scenario one may use Compact Photon Source design (for more details see a talk by Pavel Degtiarenko at this workshop) installed after the tagger magnet, which will produce bremsstrahlung photons and dump electron beam inside the source shielding the radiation inside. At the second stage, bremsstrahlung photons interact with Be target placed on a distance 16 m upstream of liquid hydrogen ( $LH_2$ ) target of GlueX experiment in Hall D producing  $K_L^0$  beam. To stop photons a 30 radiation length lead absorber will be installed in the beamline followed by a sweeping magnet to deflect the flow of charged particles. The flux of  $K_L$  on  $LH_2$  target of GlueX experiment in Hall D will be measured with pair spectrometer upstream the target. Details of this part of the beamline (for a details see a talk by Ilya Larin at this workshop). Momenta of  $K_L$  particles will be measured using the time-of-flight between RF signal of CEBAF and start counters surrounding  $LH_2$  target. Schematic view of beamline is presented in Fig. 1. The bremsstrahlung photons, created by electrons at a distance about 75 m upstream, hit the Be target and produce  $K_L^0$  mesons along

with neutrons and charged particles. The lead absorber of  $\sim 30$  radiation length is installed to absorb photons exiting Be target. The sweeping magnet deflects any remaining charged particles (leptons or hadrons) remaining after the absorber. The pair spectrometer will monitor the flux of  $K_L^0$  through the decay rate of Kaons at given distance about 10 m from Be target. The beam flux could also be monitored by installing nuclear foil in front of pair spectrometer to measure a rate of  $K_S^0$  due to regeneration process  $K_L + p \rightarrow K_S + p$  as it was done at NINA (for details see a talk by Michael Albrow at this workshop).

Here, we outline experimental conditions and simulated flux of  $K_L^0$  based on GEANT4 and known cross sections of underlying subprocesses [6–8].

- An electron beam with energy  $E_e = 12$  GeV and current  $I_e = 5 \mu A$  (maximum possible, limited by the Hall D beam dump).
- A thickness of radiator 5 % radiation length.
- Primary Be target with  $R = 4$  cm,  $L = 40$  cm.
- $LH_2$  target with  $R = 2$  cm,  $L = 30$  cm.
- Distance between Be and  $LH_2$  targets 24 m.

The expected flux of  $K_L^0$  mesons integrated in the range of momenta  $P = 0.3 - 10$  GeV/ $c$  will be  $\approx 2 \times 10^3$   $K_L^0$ /sec on the physics target of the GlueX setup.

In a more aggressive scenario with

- A thickness of radiator 10%.
- Be target with a length  $L = 60$  cm.
- $LH_2$  target with  $R = 3$  cm.

The expected flux of  $K_L^0$  mesons integrated over the same momentum range will increase to  $\approx 10^4$   $K_L^0$ /sec.

In addition to these requirements it will require lower repetition rate of electron beam with  $\sim 40$  ns spacing between bunches to have enough time to measure time-of-flight of the beam momenta and to avoid an overlap of events produced from alternating pulses. Lower repetition rate was already successfully used by G0 experiment in Hall C at JLab [9].

The radiation length of the radiator needs further studies in order to estimate the level of radiation and required shielding in the tagger region. During this experiment all photon beam tagging detector systems and electronics will be removed.

The final flux of  $K_L^0$  is presented with 10% radiator, corresponding to maximal rate .

In the production of a beam of neutral Kaons, an important factor is the rate of neutrons as background. As it is well known, the ratio  $R = N_n/N_{K_L^0}$  is on the order  $10^3$  from primary proton beams [10], the same ratio with primary electromagnetic interactions is much lower. This is illustrated in Fig. 2, which presents the rate of Kaons and neutrons as a function of the momentum, which resembles similar behavior as it was measured at SLAC [11].



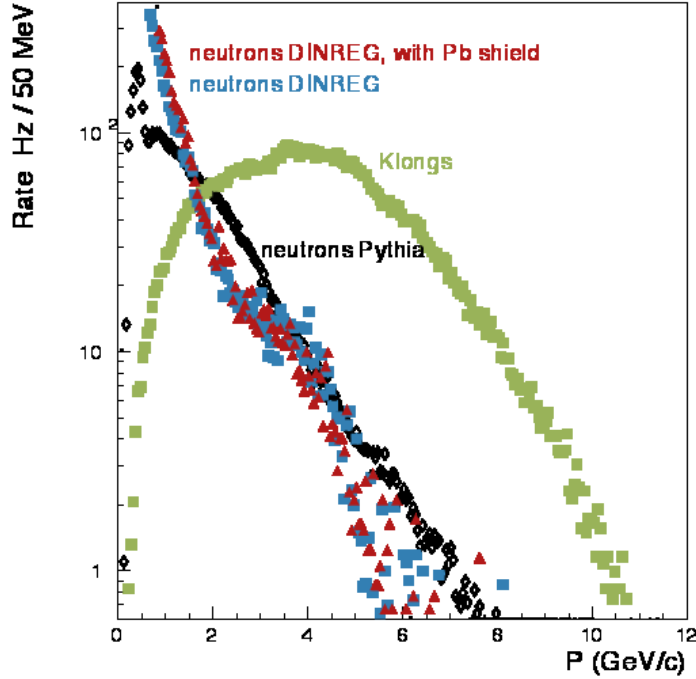


Figure 2: The rate of neutrons (open symbols) and  $K_L^0$  (full squares) on  $LH_2$  target of Hall D as a function of their momenta simulated with different MC generators with  $10^4 K_L^0/\text{sec}$ .

Shielding of the low energy neutrons in the collimator cave and flux of neutrons has been estimated to be affordable, however detailed simulations are under way to show the level of radiation along the beamline.

The response of GlueX setup, reconstruction efficiency and resolution are presented in a talk by Simon Taylor at this workshop.

#### 4. Expected Rates

In this Section, we discuss expected rates of events for some selected reactions. The production of  $\Xi$  hyperons has been measured only with charged Kaons with very low statistical precision and never with primary  $K_L^0$  beam. In Fig. 3 panel a) shows existing data for the octet ground state  $\Xi$ 's with theoretical model predictions for  $W$  (the reaction center of mass energy) distribution, panel b) shows the same model prediction [12] presented with expected experimental points and statistical error for 10 days of running with our proposed setup with a beam intensity  $2 \times 10^3 K_L/\text{sec}$  using missing mass of  $K^+$  in the reaction  $K_L^0 + p \rightarrow K^+ \Xi^0$  without detection of any of decay products of  $\Xi^0$  (for more details on this topic see a talk by Kanzo Nakayama at this workshop).

The physics of excited hyperons is not well explored, remaining essentially at the pioneering stages of '70s-'80s. This is especially true for  $\Xi^*(S = -2)$  and  $\Omega^*(S = -3)$  hyperons. For example, the  $SU(3)$  flavor symmetry allows as many  $S = -2$  baryon resonances, as

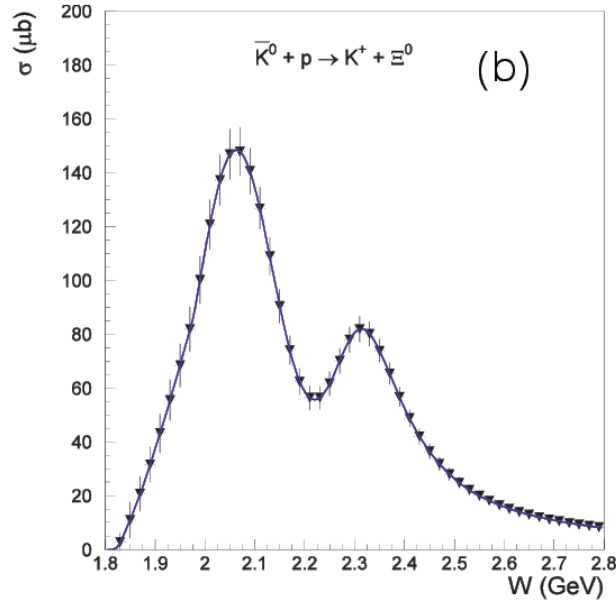
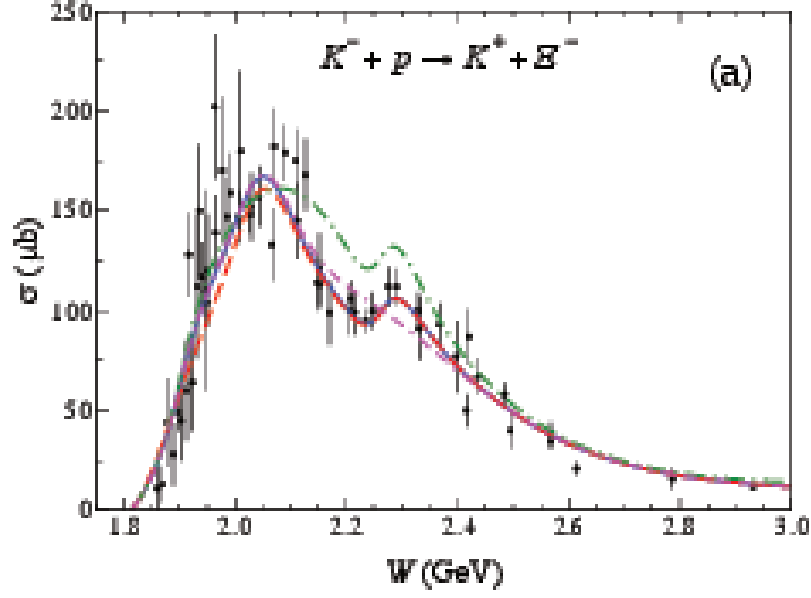


Figure 3: a) Cross section for existing world data on  $K^- + p \rightarrow K^+ \Xi^-$  reaction with model predictions from [12]; b) expected statistical precision for the reaction  $K_L^0 + p \rightarrow K^+ \Xi^0$  in 10 days of running with a beam intensity  $2 \times 10^3 K_L/\text{sec}$  overlaid on theoretical prediction [12].

there are  $N$  and  $\Delta$  resonances combined ( $\approx 27$ ); however, until now only three [ground state  $\Xi(1382)1/2^+$ ,  $\Xi(1538)3/2^+$ , and  $\Xi(1820)3/2^-$ ] have their quantum numbers assigned and

few more states have been observed [1]. The status of  $\Xi$  baryons is summarized in a table presented in Fig. 4 together with quark model predicted states [13].

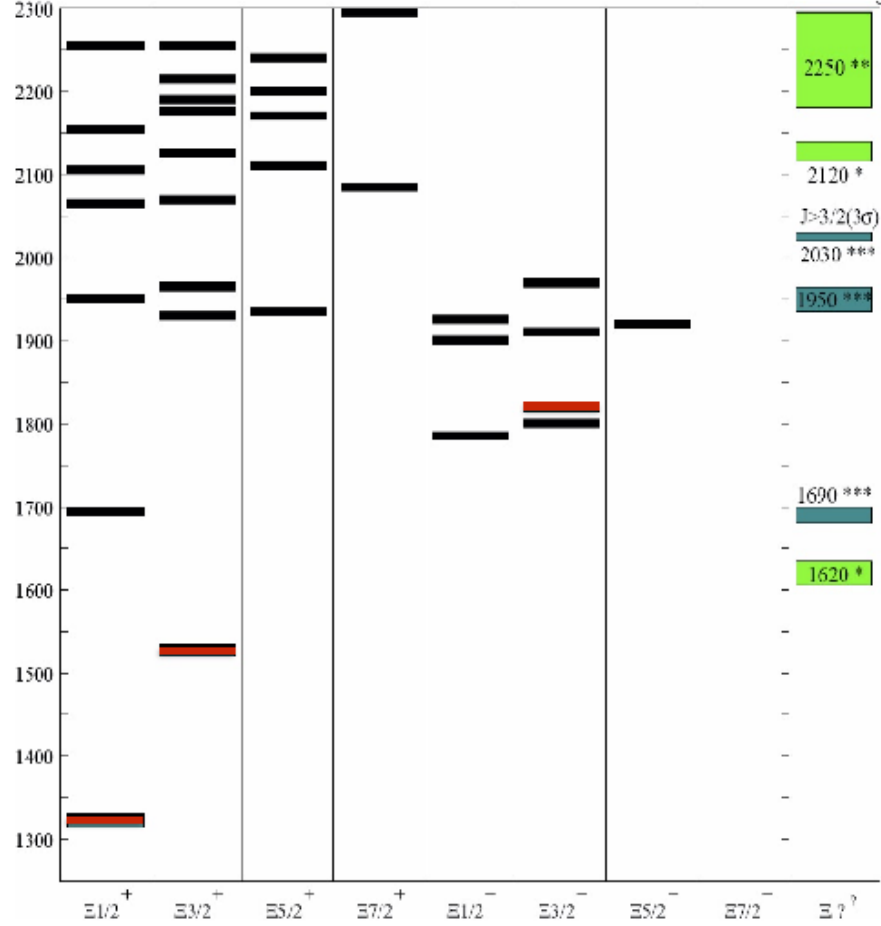


Figure 4: Black bars: Predicted  $\Xi$  spectrum based on the quark model calculation [13]. Colored bars: Observed states. The two ground octet and decuplet states together with  $\Xi(1820)$  in the column  $J^P = 3/2^-$  are shown in red color. Other observed states with unidentified spin-parity are plotted in the rightest column.

Historically the  $\Xi^*$  states were intensively searched for mainly in bubble chamber experiments using the  $K^-p$  reaction in '60s-'70s. The cross section was estimated to be on the order of  $1-10 \mu b$  at the beam momenta up to  $10 \text{ GeV}/c$ . In '80s-'90s, the mass or width of ground and some of excited states were measured with a spectrometer in the CERN hyperon beam experiment. Few experiments have studied cascade baryons with the missing mass technique. In 1983, the production of  $\Xi^*$  resonances up to  $2.5 \text{ GeV}$  were reported from  $p(K^-, K^+)$  reaction from the measurement of the missing mass of  $K^+$  [14]. The ex-

perimental situation with  $\Omega^{*-}$ 's is even worse than the  $\Xi^*$  case, there are very few data for excited states. The main reason for such a scarce dataset in multi strange hyperon domain is mainly due to very low cross section in indirect production with pion or, in particular, - photon beams. Currently only ground state  $\Omega^-$  quantum numbers are identified. Recently significant progress is made in lattice QCD calculations of excited baryon states [15, 16] which poses a challenge to experiments to map out all predicted states (for more details see a talk by David Richards at this workshop). The advantage of baryons containing one or more strange quarks for lattice calculations is that then number of open decay channels is in general smaller than for baryons comprising only the light  $u$  and  $d$  quarks. Moreover, lattice calculations show that there are many states with strong gluonic content in positive parity sector for all baryons. The reason why hybrid baryons have not attracted the same attention as hybrid mesons is mainly due to the fact that they lack manifest "exotic" character. Although it is difficult to distinguish hybrid baryon states, there is significant theoretical insight to be gained from studying spectra of excited baryons, particularly in a framework that can simultaneously calculate properties of hybrid mesons. Therefore this program will be very much complementary to the GlueX physics program of hybrid mesons.

The proposed experiment with a beam intensity  $10^4 K_L/\text{sec}$  will result in about  $2 \times 10^5 \Xi^{*}$ 's and  $4 \times 10^3 \Omega^{*}$ 's per month.

A similar program for  $KN$  scattering is under development at J-PARC with charged Kaon beams [17]. The current maximum momentum of secondary beamline of 2 GeV/c is available at the K1.8 beamline. The beam momentum of 2 GeV/c corresponds to  $\sqrt{s}=2.2$  GeV in the  $K^-p$  reaction which is not enough to generate even the first excited  $\Xi^*$  state predicted in the quark model. However, there are plans to create high energy beamline in the momentum range 5 – 15 GeV/c to be used with the spectrometer commonly used with the J-PARC E50 experiment which will lead to expected yield of  $(3 - 4) \times 10^5 \Xi^{*}$ 's and  $10^3 \Omega^{*}$ 's per month.

Statistical power of proposed experiment with  $K_L$  beam at JLab will be of the same order as that in J-PARC with charged Kaon beam.

An experimental program with Kaon beams will be much richer and allow to perform a complete experiment using polarized target and measuring recoil polarization of hyperons. This studies are under way to find an optimal solution for GlueX setup.

## 5. Summary

In summary, we intend to create high intensity  $K_L$  beam using photoproduction processes from a secondary Be target. A flux as high as  $10^4 K_L/\text{sec}$  could be achieved. Momenta of  $K_L$  beam particles will be measured with time of flight. The flux of Kaon beam will be measured through partial detection of  $\pi^+\pi^-$  decay products from their decay to  $\pi^+\pi^-\pi^0$  by exploiting similar procedure used by LASS experiment at SLAC [11]. Besides using unpolarized  $LH_2$  target currently installed in GlueX experiment additional studies are needed to find the optimal choice of polarized targets. This proposal will allow to measure  $KN$  scattering with different final states including production of strange and multi strange baryons with unprecedented statistical precision to test QCD in non perturbative domain. It has a potential to distinguish between different quark models and test lattice QCD predictions for excited baryon states with strong hybrid content.

## 6. Acknowledgments

This work is supported, in part, by the U.S. Department of Energy, Office of Science, Office of Nuclear Physics, under Award Number DE-FG02-96ER40960.

## References

- [1] K.A. Olive *et al.* (Particle Data Group), *Chin. Phys. C* **38**, 090001 (2014).
- [2] R. Aaij *et al.* (LHCb Collaboration), *Phys. Rev. Lett.* **115**, 072001 (2015).
- [3] Y. Qiang, Ya.I. Azimov, I.I. Strakovsky, W.J. Briscoe, H. Gao, D.W. Higinbotham, and V.V. Nelyubin, *Phys. Lett. B* **694**, 123 (2011).
- [4] W.J. Briscoe, M. Döring, H. Haberzettl, D.M. Manley, M. Naruki, I.I. Strakovsky, and E.S. Swanson, *Eur. Phys. J. A* **51**, 129 (2015).
- [5] U. Al-Binni *et al.*, *Project X: Physics Opportunities*, in *Community Summer Study 2013: Snowmass on the Mississippi* (CSS2013), Minneapolis, MN, USA, July–August, 2013, edited by A.S. Kronfeld and R.S. Tschirhart.
- [6] H. Seraydaryan *et al.* (CLAS Collaboration), *Phys. Rev. C* **89**, 055206 (2014).
- [7] A.I. Titov and T.-S.H. Lee, *Phys. Rev. C* **67**, 065205 (2003).
- [8] G. McClellan *et al.*, *Phys. Rev. Lett.* **26**, 1593 (1971).
- [9] D. Androic *et al.* (G0 Collaboration), *Nucl. Instrum. Meth. A* **646**, 59 (2011).
- [10] W.E. Cleland *et al.*, *Phys. Rev. D* **12**, 1247 (1975).
- [11] G.W. Brandenburg *et al.*, *Phys. Rev. D* **7**, 708 (1973).
- [12] B.C. Jackson, Y. Oh, H. Haberzettl, and K. Nakayama, *Phys. Rev. C* **91**, 065208 (2015).
- [13] K.-T. Chao, N. Isgur, and G. Karl, *Phys. Rev. D* **23**, 155 (1981).
- [14] C.M. Jenkins *et al.*, *Phys. Rev. Lett.* **51**, 951 (1983).
- [15] R.G. Edwards, N. Mathur, D.G. Richards, and S.J. Wallace (Hadron Spectrum Collaboration), *Phys. Rev. D* **87**, 054506 (2013).
- [16] G.P. Engel, C.B. Lang, D. Mohler, and A. Schfer (BGR Collaboration), *Phys. Rev. D* **87**, 074504 (2013).
- [17] H. Takahashi, *Proceedings of the 11th International Conference on Hypernuclear and Strange Particle Physics* (HYP 2012), *Nucl. Phys. A* **914**, 553 (2013).

## 2.4 Hadron Physics at J-PARC

Hiroaki Ohnishi

*RIKEN, Nishina Center*

*2-1 Hirosawa*

*Wako, Saitama 351-0198, Japan &*

*Research Center for Nuclear Physics (RCNP)*

*Osaka University, Osaka*

*567-0047, Japan*

### Abstract

One of the main goals for the hadron physics is to understand the effective degrees of freedom (EDoF) in hadron and reveal their interactions. Spectroscopy of ground and excited states of baryons will give us hints to understand the EDoF of hadron. In addition, testing properties of known mesons/baryons, such as masses and decay widths, inside nuclear matter, will give us unique information on the interaction between EDoF and QCD vacuum.

In this paper, I will discuss the goal of the hadron physics and summarize experimental programs performed and planned at J-PARC. Finally, I will briefly discuss a future project at J-PARC, which is now under discussion.

### 1. Introduction

The strong interaction between elementary particles has been described very well by the quantum chromo dynamics (QCD). The missing element of a standard model of elementary particles, *i.e.*, the Higgs boson, has been discovered at CERN/LHC in 2012. Therefore the theory of known elementary particles, including the strong interaction, is now completed. There are many varieties of matter created by QCD, such as hadrons, nuclei and very high-density nuclear matter, such as neutron stars. Those type of matter must be interpreted by the QCD. However, due to the complexity of the QCD theory, it is very difficult to solve all problems and to understand the connection between elementary particles like quarks and gluons and hadrons or extremely high-density matter. It should be noted that not even the first step, how the hadrons and their excited states are created, is clearly understood. Therefore, not only more experimental efforts to understand hadron phenomena, but also strong theoretical supports for the hadron/nuclear physics are still mandatory to understand the matter created by QCD.

Some of the goals of hadron physics could be summarized as in the following two questions. First, how the hadrons are created via QCD? In other words, what are the effective degrees of freedom to describe hadron and excited hadrons? Second, hadrons are understood as excitations of QCD vacuum. Therefore, a change of vacuum condition should affect directly to the properties of hadron, such as mass and width. Thus, we need to know how hadron properties change when environmental condition changed, *i.e.*, vacuum inside nuclear matter.

In normal conditions, the world consists only from light quarks, *i.e.*,  $u$  and  $d$  quarks. However, inside the compressed QCD matter, creation of hadrons with strangeness is expected, theoretically. For such condition, hadrons with strangeness cannot be ignored to understand high-density matter. For example, anti-Kaon in nucleus is a hot subject in the hadron physics,

which may give us hints toward physics in high-density nuclear matter. On the other hand, baryons with strangeness themselves are also a very important subject. According to the quark model, color magnetic interaction between constituent quarks can be expressed as follows.

$$V_{CMI} \sim \frac{\alpha_s}{m_i m_j} (\lambda_i \cdot \lambda_j) (\vec{\sigma}_i \cdot \vec{\sigma}_j), \quad (1)$$

where,  $m$ ,  $\lambda$  and  $\vec{\sigma}$  are mass, color and spin of constituent quarks, respectively. The equation tells us that if we choose heavy quarks as constituents for hadrons, color-magnetic interaction between a light quark and heavy quark is going to be zero.

Therefore, the interaction between light quarks will be dominant. In the case of baryons, strong correlation between di-quark will be realized. Hints for this type of correlation are expected to appear in the excited baryon spectra/decay pattern of hadron. Since the strange quark mass is heavier than  $u$  and  $d$  are, we may expect signal for such di-quark correlation in the  $S=-1$  baryon system. In addition,  $S=-2$  baryon can be treated as an analogy of baryon with two heavy quarks. It should be noted that baryon with two heavy quarks, such as  $\Xi_{cc}$  for example, have not been observed. Therefore,  $S=-2$  baryon spectroscopy will be a unique doorway to understand the structure of baryons with heavy quarks, in other words, the investigation will give us an insight to the effective degrees of freedom to describe hadrons. Therefore, hadron with strangeness, *i.e.*, baryon with strangeness ( $\Lambda/\Xi/\Omega$ ) and/or Kaon, will be a key ingredient to understand the questions mentioned above.

## 2. J-PARC

The Japan Proton accelerator Research Complex (J-PARC) is one of the key machines to perform hadron physics. Proton beam accelerated up to 30 GeV by J-PARC Main Ring Synchrotron (MR) is delivered to Hadron experimental facility (HD) and shoot onto the production target, which is made by gold, to produce secondary hadron beams, such as  $\pi^\pm$ ,  $K^\pm$  and  $p, \bar{p}$ . Typical beam intensity of the primary proton beam is  $4.8 \times 10^{13}$  proton per spill (pps), where the spill length is 2 seconds with a 5.52 seconds repetition cycle. Inside HD, four beamlines are designed, two (K1.8, K1.8BR) are in operation and two (K1.1 and High-p) are under construction. The typical beam intensities for secondary particle for each beam lines are summarized in Table 2. As one can see, particle separated beams can be available up to 2 GeV/ $c$  and unseparated beam is available up to 20 GeV/ $c$ . In addition, a primary proton beam is also available for the experiment. A more detailed description can be found elsewhere [1].

## 3. Hadron Physics Performed at J-PARC

### (a) Search for Penta-Quark Baryon

Only color singlet state can exist as hadrons. This is a conclusion from QCD. Therefore, hadrons which have 5 quarks ( $qqqq\bar{q}$ ) are not forbidden by QCD. Thus, many experimental challenges have been performed to search for such exotic states. Strong evidence have been reported from photo-production experiment [2], however, also many negative results are reported (mainly from hadro-production) [3–6]. At J-PARC hadro-production of penta-quark state using high intensity pion beam is performed, by ( $\pi, K$ )

Table 1: J-PARC Beam line specifications.

beamline	particle	momentum range	typical beam intensity (40 kW MR operation)
K1.8BR	$\pi^\pm, K^\pm$ and $p, \bar{p}$ (separated)	$< 1.1 \text{ GeV}/c$	$1.5 \times 10^5 \text{ K}^-/\text{spill@ } 1 \text{ GeV}/c$
K1.8	$\pi^\pm, K^\pm$ and $p, \bar{p}$ (separated)	$< 2.0 \text{ GeV}/c$	$5.0 \times 10^5 \text{ K}^-/\text{spill@ } 2 \text{ GeV}/c$
K1.1	$\pi^\pm, K^\pm$ and $p, \bar{p}$ (separated)	$< 1.1 \text{ GeV}/c$	$1.5 \times 10^5 \text{ K}^-/\text{spill@ } 1 \text{ GeV}/c$
High-p	$\pi^\pm, K^\pm$ and $p, \bar{p}$ (unseparated)	up to $20 \text{ GeV}/c$	$> \sim 10^7 \pi^-/\text{spill@ } 20 \text{ GeV}/c$ $> \sim 10^6 \text{ K}^-/\text{spill@ } 7 \text{ GeV}/c$
	primary proton	30 GeV	$\sim 10^{11} \text{ proton / spill}$

reaction on hydrogen target [7, 8]. No signal has been observed so far. To date, still the conclusion has not been reached concerning whether a penta-quark state exists or not.

#### (b) Search for Kaonic Nucleus

Because strong attractive force exists between anti-Kaon and nucleon, the existence of the strongly bound Kaonic-nuclear state has been discussed for a long time. It is interesting to note that, theoretically, the inside of the Kaonic nucleus could turn into high density, much higher than normal nuclear matter density. Therefore, the study of Kaonic nucleus will give us some insight on QCD at high-density matter. There are many experiments to search for such exotic state, which have been performed to date, however, still not strong conclusion is made. Two new experiments have been performed at J-PARC. Both experiments are focussing on the lightest Kaonic nuclear cluster, *i.e.*,  $K^-pp$  state. One is the E27 experiment, which aims to search for  $K^-pp$  cluster via  $(\pi, K)$  reaction. The result shows some indication for the deeply bound  $K^-pp$  bound state [9]. The other experiment is the E15 experiment, which aims to search for the  $K^-pp$  bound state via  ${}^3\text{He}(K^-, n)$  reaction. The first results from the E15 experiment shows [10] no clear signal found in deeply bound region, but an interesting events enhancement has been observed near the  $K^-pp$  threshold region. Recently, the E15 experiment reported new results on exclusive analysis on  ${}^3\text{He}(K^-, \Lambda p)n$  reaction [11]. The result is shown in Figure 1. Figure 1(a) shows a scatter plot for the invariant mass of  $\Lambda p$  versus neutrons emitted angle in the center of mass frame. Figure 1(b) and (c) are the projection of the plot to the axes. Expected contributions are also plotted as histogram in Figure 1(b). A clear enhancement with respect to the expected contributions are seen just below the  $\bar{K}NN$  threshold. It is interesting to note that as shown in Figure 1(c), a clear event concentration at  $\cos(\theta_{CM}) \sim 0$ , where slowly moving  $\bar{K}$  produced is seen. This will be a necessary condition to form  $\bar{K}NN$  bound state. However, due to the small statistics, it is still hard to conclude whether  $\bar{K}NN$  bound states are produced or not.

Because both experiments try to produce  $K^-pp$  cluster by different production mechanisms further detailed studies are still needed to conclude whether  $K^-pp$  cluster really exists or not, and to know its properties.

#### (c) Mesons in Nuclei

Chiral symmetry in QCD vacuum is spontaneously broken. It is now understood that



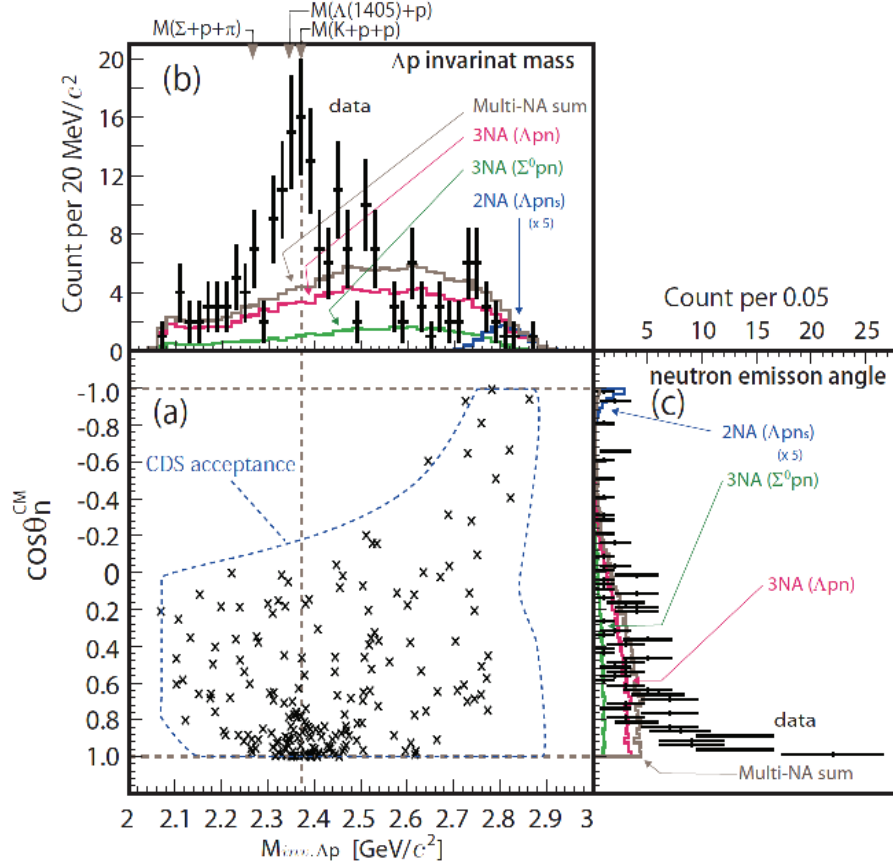


Figure 1: Results recently published by the J-PARC E15 Collaboration [11].

mass of the hadrons is generated dynamically by the broken symmetry. However, the chiral symmetry will be partially restored in high-density matter such as inside nuclei. This information can be checked through the measurement of the mass of mesons or search for the meson nuclear bound state. Because vector mesons have relatively long lifetime, therefore three experiments have been proposed to study the vector mesons in nuclear matter: E16 [12], E26 [13], and E29 [14].

The E16 experiment is aiming to measure the line shape of vector mesons via measuring  $V \rightarrow e^+e^-$  decay inside a nucleus. The experiment is planned to be performed using the 30 GeV primary proton beam at the high momentum beam line.

The E26 experiment is planned to search for  $\omega$  meson nuclear bound state. To maximize the formation probability of  $\omega$  meson nucleus, slowly moving  $\omega$  mesons are selectively produced via  $(\pi, n)$  reaction using the 2 GeV/c pion beam at K1.8 beamline. Signal of  $\omega$  mesic nucleus is identified via missing mass spectroscopy of forward going neutron.

The E29 experiment is focusing on the  $\phi$  meson nuclear bound state. Very exotic elementary reaction channel,  $\bar{p}p \rightarrow \phi\phi$ , has been chosen to produce slowly moving  $\phi$  meson. The experiment is planning to use the 1.1 GeV/c  $\bar{p}$  beam at K1.8BR beamline. The signal is identified via missing mass analysis using the forward going  $\phi$  meson, together with the  $K^+$  and  $\Lambda$  from the target as final state particles, to ensure the double

strangeness pairs are produced.

**(d) S=-2 and S=-3 Baryon Spectroscopy**

To understand the effective degree of freedom to describe hadrons, in other words, what are the DoF to control the excited baryon spectra, it is very important to identify the complete spectra of S=-2 and/or S=-3 baryons. However, according to the PDG, only a small number of S=-2 baryons are established. In case of  $\Omega$  baryon, only ground state is known. High intensity Kaon beam will improve the situation drastically. It should be noted that in case of nucleon resonances, the widths are very broad, typically more than  $\sim 270$  MeV, thus it is hard to identify the states easily. However, the trend of baryon with strangeness shows widths which are much narrower than of nuclear resonances, it is about  $\sim 40$  MeV. Therefore, we have a chance to identify those excited multi-strangeness baryon clearly. The experiment to identify  $\Xi$  baryons are in preparation at High-p beam line where high momentum  $K^-$  beam will be available. The missing mass spectroscopy via  $(K^-, K^+)$  or  $(K^-, K^+\pi^+)$  is planed to establish and search for the  $\Xi$  baryons [15]. The experiment is expected to pin down the  $\Xi$  baryon spectra up to the baryons with mass  $\sim 3$  GeV/ $c^2$ .

**(e) Future projects: Hadron Hall Extension**

To extend the physics cases reachable at J-PARC, an extension of the HD facility is under discussion. It is true that high momentum  $K^-$  is already available at High-p beamline. However, the intensity of the beam is rather low, which limits the reach of the excited  $\Xi$  search. Moreover, excited state for  $\Omega$  baryon are not possible at High-p beamline, because the expected cross section is very small (sub  $\mu b$ ). In addition, at High-p beamline, only a cocktail beam of  $\pi^-$ ,  $K^-$  and  $\bar{p}$  is available, but most of it are pions. Therefore, experiments will be facing serious problems of pion interactions, which is indeed the main background for Kaon interaction studies. Therefore, high intensity and particle separated beamline is very important to enhance the physics opportunities at J-PARC.

Figure 2 shows a conceptual design for the extended hadron hall. For this extension, we will construct three new charged particle beamlines for hadron/nuclear physics and one new  $K_0$  beam line to search the  $K_L^0 \rightarrow \pi^0 \nu \bar{\nu}$  decay. which has great sensitivity to the beyond the standard model. Here, we will concentrate on the K10 beamline, where high intensity and high momentum  $K^-$  and  $\bar{p}$  beam will be available. Figure 3 shows the expected beam intensities at K10 for  $K^-$  and  $\bar{p}$ . As one can see in Figure 3, the expected beam intensities will be  $10^7$  per spill at 4 to 6 GeV/ $c$   $K^-$  and  $10^7$  per spill for 10 GeV/ $c$   $\bar{p}$ . Utilizing those beam particles, we are planing to perform  $\Omega$  baryon spectroscopy which will be possible at J-PARC once the hadron hall extension is realized. Moreover, recent lattice QCD calculation shows that tha interaction between  $\Omega$  baryon and nucleon is attractive. If this is true,  $\Omega$  baryon and nucleon may form  $\Omega$ -N bound state. Therefore the experiment to search for the  $\Omega$ -N bound state may be very important.

In addition, high intensity  $\bar{p}$  beam will open new opportunity to investigate charmed meson properties in nucleus (nuclear matter). Since long time, the interaction between D meson and nucleon is believed to be attractive, based on the many theoretical predictions [16–18]. However, recent QCD sum rule calculation shows it is repulsive, in

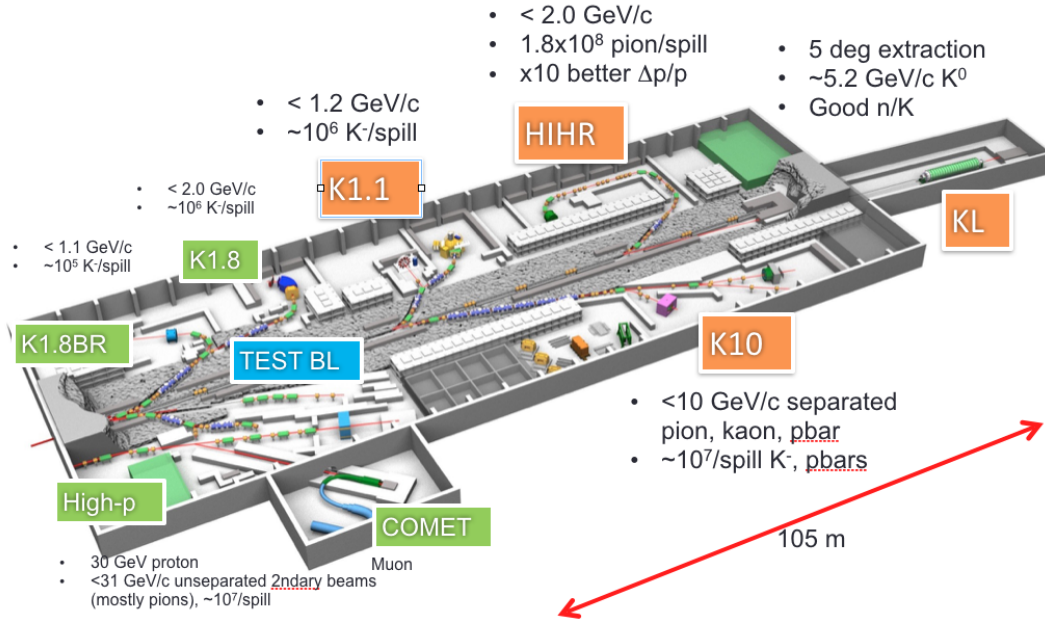


Figure 2: Conceptual design for extended Hadron Hall.

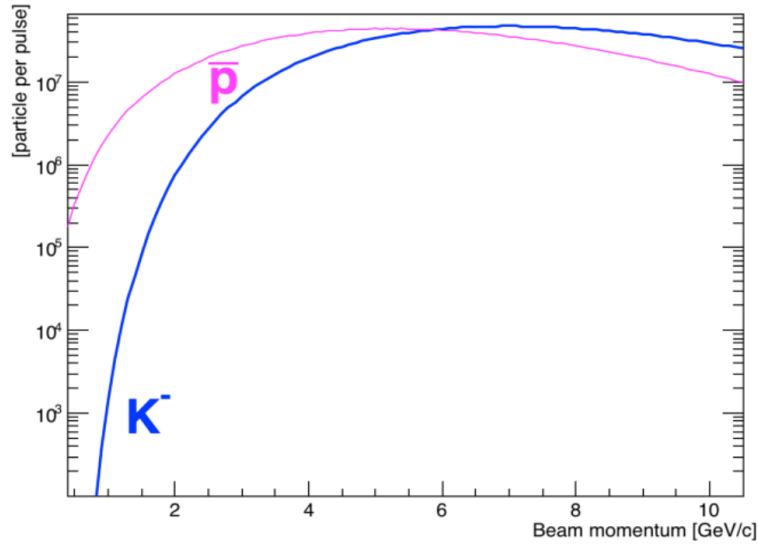


Figure 3: Expected beams intensities at K10 beamline.

other words, D meson is getting heavier in nuclear matter [19, 20]. Because no experiment was performed to investigate the D meson and nucleon interaction, no concrete information is available experimentally.

Therefore, the D meson properties in nuclear matter is one of the interesting subject to date. At K10, we plan to perform the experiment to measure  $\bar{D}D$  production with  $\bar{p}$  beam on proton and on nuclei, which will give us a hints for the  $DN$  interaction. It is interesting to note that recently many exotic hadrons are reported by collider exper-

iments, such as Belle, BaBar, LHCb, BES *etc.* Those measurements provide insight into the structure of hadrons, which can be summarize as follows.

- i. Charmonium spectra can be describe very well by the model of constituent quarks acting as effective degree of freedom to describe charmonium, *i.e.*, constituent quark model.
- ii. Many exotic hadrons are also discovered. It is interesting that those exotic hadrons exist only above the  $D\bar{D}$  production threshold.

Those phenomena indicates that the production cross section of  $D\bar{D}$  near the production threshold might be sensitive whether such exotic states are really produced or not. Figure 4 shows conceptual design for the spectrometer we are planing to install K10 beamline. The detector consists of large volume solenoid detector surrounding the target together with forward dipole spectrometer.

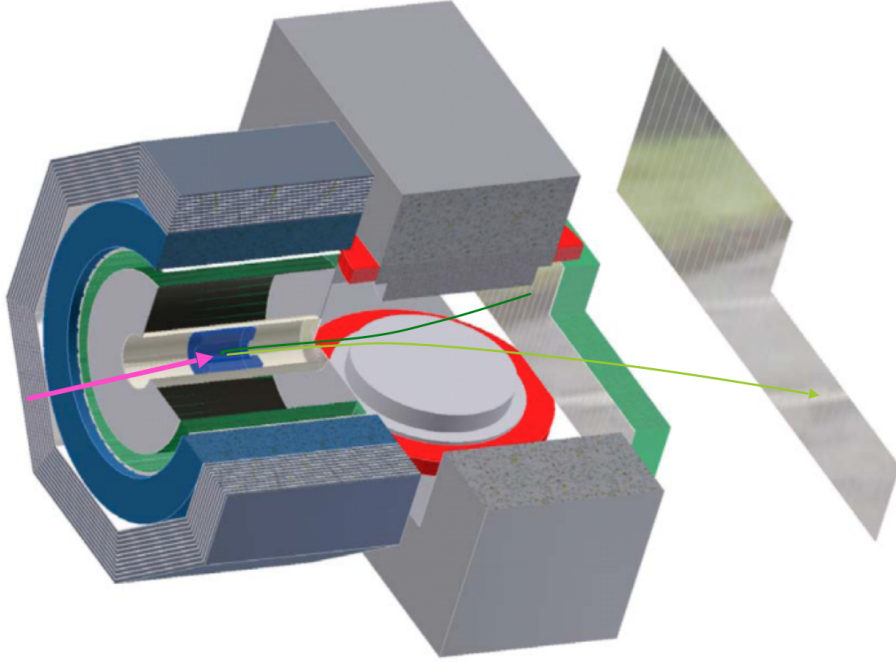


Figure 4: Conceptual design for Detector at K10.

#### 4. Summary

In this paper, physics programs currently performed at J-PARC are reviewed. Baryon spectroscopy and mesons in nucleus using high intensity pion and Kaons beams are main topics for experimental programs at the current J-PARC hadron hall. Many new results are coming out.

At present, investigation for  $\bar{K}N$  interaction is performed using high intensity low momentum  $K^-$ . Recently available new data from E15 shows strong hint about  $\bar{K}NN$  cluster. However, to make strong conclusion, we need to wait the completion of the analysis with large data sample. Data have already been taken and data analysis is under the way.

A new project at J-PARC, *i.e.*, Hadron hall extension, was introduced. Three separated charged secondary beamlines will be constructed. In particular high intensity and high momentum particle separated beamline(K10) is very important for the hadron physics. High momentum Kaons beam at K10 will allow to perform multi-strangeness baryons spectroscopy. Moreover, the high intensity anti-proton beam will open the door to a new physics subject, *i.e.*, charmed mesons in nuclei.

## References

- [1] Prog. Theor. Exp. Phys. (2012) 02B011.
- [2] T. Nakano *et al.*, Phys. Rev. C **79**, 025210 (2009).
- [3] M.J. Longo *et al.*, Phys. Rev. D **70**, 111101(R) (2004).
- [4] I. Abt *et al.*, Phys. Rev. Lett. **93**, 212003 (2004).
- [5] S. Schael *et al.*, Phys. Lett. B **599**, 1 (2004).
- [6] J.Z. Bai *et al.*, Phys. Rev. D **70**, 012004 (2004).
- [7] K. Shirotori *et al.*, Phys. Rev. Lett. **109**, 132002 (2012).
- [8] M. Moritsu *et al.*, Phys. Rev. C **90**, 035205 (2014).
- [9] Y. Ichikawa *et al.*, Prog. Theor. Exp. Phys. (2015) 021D01.
- [10] T. Hashimoto *et al.*, Prog. Theor. Exp. Phys. (2015) 061D01.
- [11] Y. Sada *et al.*, arXiv:1601.06876 .
- [12] S. Yokkaichi *et al.*, J-PARC E16 proposal,  
[http://j-parc.jp/researcher/Hadron/en/pac\\_0606/pdf/p16-Yokkaichi\\$2.pdf](http://j-parc.jp/researcher/Hadron/en/pac_0606/pdf/p16-Yokkaichi$2.pdf) .
- [13] K. Ozawa *et al.*, J-PARC E26 proposal,  
[http://j-parc.jp/researcher/Hadron/en/pac\\_0903/pdf/Ozawa.pdf](http://j-parc.jp/researcher/Hadron/en/pac_0903/pdf/Ozawa.pdf) .
- [14] H. Ohnishi *et al.*, J-PARC E29 proposal,  
[http://j-parc.jp/researcher/Hadron/en/pac\\_0907/pdf/Ohnishi.pdf](http://j-parc.jp/researcher/Hadron/en/pac_0907/pdf/Ohnishi.pdf) .
- [15] M. Naruki and K. Shirotori, Letter of Intent,  
[http://j-parc.jp/researcher/Hadron/en/pac\\_1405/pdf/LoI\\_2014-4.pdf](http://j-parc.jp/researcher/Hadron/en/pac_1405/pdf/LoI_2014-4.pdf) .
- [16] A. Sibirtsev, K. Tsushima, and A.W. Thomas, Eur. Phys. J. A **6**, 351 (1999).
- [17] A. Mishra and A. Mazumdar, Phys. Rev. C **79**, 024908 (2009).

- [18] A. Hayashigaki, Phys. Lett. B **487**, 96 (2000).
- [19] T. Hilger, R. Thomas, and B. Kämpfer, Phys. Rev. C **79**, 025202 (2009)
- [20] K. Suzuki, P. Gubler, and M. Oka, arXiv:1511.04513 [hep-ph].

## 2.5 Low Energy Kaon Scattering: Present Status and Open Possibilities

Alessandra Filippi

*I.N.F.N. Sezione di Torino*

*Torino 10125, Italy*

### Abstract

An overview of the experimental results on low energy scattering of charged and neutral Kaons is given. Emphasis is put on the still missing information, which could be essential to provide a thorough description of the  $\bar{K}N$  interaction close to threshold as well as below it, and that could be achieved by exploiting the unique features of a high intensity  $K_L^0$  beam.

### 1. Neutral Kaon Scattering: Properties and Cross Sections Measurements at Low Energies

The low energy cross section data for the interaction of charged Kaons with protons or neutrons (in deuterium targets) are rather few and imprecise. Below 350 MeV/c incident momentum only old measurements exist, which date back to the Eighties and earlier years, and were performed in bubble chamber experiments or with emulsions [1]. This low energy region could still be fruitfully explored by the DAΦNE machine in Frascati, and proposals were put forward some years ago in this respect [2].

For neutral Kaons the situation is even worse. Few data exist down to 130 MeV/c with a statistical accuracy limited to 10-20% for the  $K_L^0 p$  scattering, and a little better for  $K_L^0 d$  [3]. The trend of low momentum  $K_L^0 p$  total cross section, from Ref. [3], is reported in Fig. 1: a typical total cross section at low momenta for  $K_L^0$  induced scattering on protons is around 70 mb, and twice as large on deuterons.

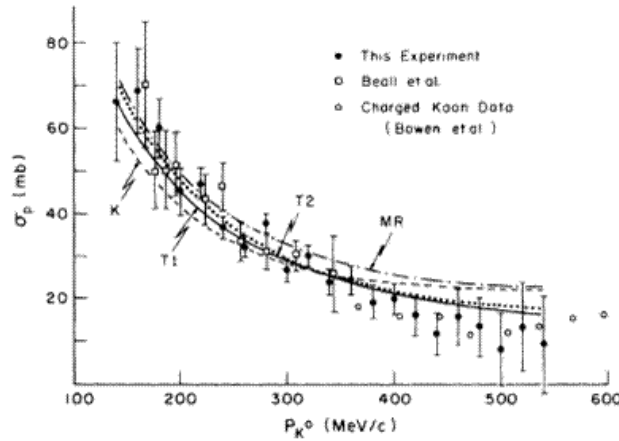


Figure 1: Total  $K_L^0 p$  cross section. From Ref. [3]. The superimposed curves are the trends expected on the basis of different solutions for the  $K^-p$  scattering lengths (see text).

It is useful to recall that neutral Kaons behave as two different kinds of particles depending on the interaction they are subject to. The weakly interacting particles,  $CP$ -eigenstates  $K_S^0$

and  $K_L^0$ , are linear combinations (of almost equal strength, at the precision level of scattering measurements) of the strangeness eigenstates,  $K^0$  and  $\bar{K}^0$ . These are the relevant particles for evaluating the effect of the strong interaction in the scattering. According to the strangeness of the meson, however, its behavior as hadronic probe is largely different.

The Kaons with strangeness  $S = +1$ , *i.e.*,  $K^+$  and  $K^0$ , have just a mild interaction with the medium. The cross sections are small, of the order of 10 mb, and are dominated by the elastic channel with a small contribution from Charge Exchange. The relevance of these scattering processes is mainly related to the possible formation of exotic pentaquark systems ( $q^4\bar{q}$ ), that however have never been observed so far (anyway, if ever existing, these states are not likely to show up at low energies). In the  $K^+p$  scattering a sizeable contribution, almost as large as the one due to strong interaction, comes from the electromagnetic interaction, relevant especially at small angles [4]. The  $K^+p$  system is a pure isospin  $I = 1$  state, and its  $S$ -wave scattering length, which will be described in more detail in Sec. 2.5.1.a, has been determined with good ( $\sim 1\%$ ) precision.

On the other hand, Kaons with strangeness  $S = -1$  are strongly absorbed. The interaction cross sections are larger than 50 mb, and several baryonic resonances (formerly known as  $Y^*$ ), both with isospin 0 and 1, may be excited even below threshold. The  $\bar{K}N$  system is therefore strongly coupled, via these resonances, to several channels, like  $\Lambda\pi$ ,  $\Sigma\pi$ ,  $Y\eta$ ,  $Y\pi\pi$  *etc.* The different behavior of the two  $K_L^0$  components implies that the interaction of such a beam with dense matter basically kills the  $\bar{K}^0$  amplitude, which is almost completely absorbed. However, if the interaction of  $K_L^0$  occurs on protons, final states are produced resulting from both  $K^0$  and  $\bar{K}^0$  interactions with different amplitudes: from their interference one might extract information on the relative sign of the  $K^0N$  and  $\bar{K}^0N$  potentials. While the  $K^0p$  system is a mixture of  $I = 0$  and  $I = 1$  amplitudes, the  $\bar{K}^0p$  is in pure  $I = 1$ : the information the latter can provide is complementary to what can be obtained by the study of  $K^+p$ , but without any Coulomb interaction. Moreover, the final states which can be produced in a  $\bar{K}^0p$  scattering are the charge conjugate of those reachable in a  $K^-n$  interaction; therefore, they carry the same information but don't require the use of deuterium as a target, which inevitably introduces three-body interactions between the target and the projectile that need to be properly taken into account.

It is also worthwhile to notice that on the basis of charge symmetry one can assume that  $\sigma_{tot}(K^0p) = \sigma_{tot}(K^+n)$  and  $\sigma_{tot}(\bar{K}^0p) = \sigma_{tot}(K^-n)$ . These equalities were proved to be valid at least to the precision level of old bubble chamber experiments, and were often used to indirectly assess unmeasured cross sections [5].

The existence of resonant states prevents the use of perturbative theories to describe the  $\bar{K}N$  interaction close to threshold. To this purpose, non-perturbative chiral based coupled channel approaches are usually applied, adapting the models to all the available experimental observations, including, besides elastic and inelastic cross sections, also measurements of hadronic branching ratios close to threshold, resonances lineshapes, and inputs from Kaonic atom levels shifts due to strong interaction and their widths. Several models have been elaborated in the years to reproduce the  $K^-N$  experimental data [6]; more new inputs would of course be welcome not only to improve the data description, but also to provide a more reliable prediction of the below-threshold behavior, that is relevant for the study of sub-threshold



baryonic resonances and the possible existence of multinucleon-antiKaon aggregates, as will be discussed in Sec. 2.5.2.a.

(a) **Low energy scattering parameterizations**

An old fashioned simple but useful way to describe the low energy interaction of particles is to parametrize the scattering cross sections in terms of *S*-wave *scattering lengths* [7]. Assuming the reaction energy to be low enough to allow only the *S*-wave to be involved, and the “zero-effective range” approximation to be applicable, the scattering length  $A = a + ib$ , that in general is a complex number, can be used to describe univoquely the phase-shift in each channel of given isospin and strangeness through the relationship  $\cot \delta = 1/kA$ , where  $\delta$  is the phase-shift and  $k$  the projectile wave number. In a definite isospin-strangeness channel, the scattering cross section may then be expressed by the general formula:

$$\sigma = \frac{a^2 + b^2 + b/k}{k^2 a^2 + (1 + kb)^2}. \quad (2)$$

The efforts of the first experiments measuring  $K^-$  scattering was mainly to extract the real and imaginary part of the scattering lengths for the two isospin sources from the available cross sections [8]. Due to the lack of data and the loose constraints provided, however, these assessments were far from being precise and several equally good solutions were often found, with large ambiguities which survived until recently, when precise measurements of Kaonic atom levels were performed and could be used as precise additional inputs.

The *S*-wave  $K_L^0 p$  scattering cross sections may be expressed, in zero-range approximation, through four parameters: the isospin  $I=0$  and  $I=1$  real scattering lengths  $a_0$  and  $a_1$  for the  $S = +1$  channels, and the complex (absorptive)  $\bar{A} = \bar{a}_1 + \bar{b}_1$  scattering length for the  $S = -1$ ,  $I = 1$  channel [9]. By means of these parameters the low-energy cross sections have the following simple expressions:

**total cross section**

$$\sigma_{tot} = 2\pi \left[ \frac{1}{2} \frac{a_0^2}{1 + k^2 a_0^2} + \frac{1}{2} \frac{a_1^2}{1 + k^2 a_1^2} + \frac{\bar{a}_1^2 + \bar{b}_1^2 + \bar{b}_1/k}{k^2 \bar{a}_1^2 + (1 + k\bar{b}_1)^2} \right];$$

**elastic cross section**

$$\sigma(K_L^0 p \rightarrow K_L^0 p) = \pi \left| \frac{1}{2} \frac{a_0}{1 - ika_0} + \frac{1}{2} \frac{a_1}{1 - ika_1} + \frac{\bar{a}_1 + i\bar{b}_1}{k^2 \bar{a}_1^2 + (1 + k\bar{b}_1)^2} \right|^2;$$

**regeneration cross section**

$$\sigma(K_L^0 p \rightarrow K_S^0 p) = \pi \left| \frac{1}{2} \frac{a_0}{1 - ika_0} + \frac{1}{2} \frac{a_1}{1 - ika_1} - \frac{\bar{a}_1 + i\bar{b}_1}{k^2 \bar{a}_1^2 + (1 + k\bar{b}_1)^2} \right|^2;$$

**one nucleon absorption cross section**

$$\sigma(K_L^0 p \rightarrow Y\pi) = \frac{2\pi}{k} \frac{\bar{b}_1}{k^2(\bar{a}_1^2 + \bar{b}_1^2) + 2k\bar{b}_1 + 1}.$$

In the following a short account of the existing measurements of the above cross sections at low momenta will be given.

i.  $K_L^0 p \rightarrow K_S^0 p$  **regeneration cross section**

The main purpose of the first measurements of the regeneration cross sections [10] was the investigation of the features of the  $Y_1^*$  resonances (in particular, the  $\Sigma(1385)$ ), and the search for the possible existence of exotic  $I = 0$ ,  $S = +1$   $Z^*$  states. The amplitude may be written by the sum of the  $I = 0$  and  $I = 1$   $K^0 N$  terms, and the  $I = 1$   $\bar{K}^0 N$  one:  $T = \frac{1}{4}(Z_0 + Z_1) - \frac{1}{2}Y_1$ ; the resulting cross section derives from the interference between the  $S = -1$  and  $S = 1$  amplitudes. Regeneration cross sections were measured down to 300 MeV/c [11], and at the lowest momenta they amount to about 5 mb. Fig. 2 reports the available experimental data with, superimposed, a few parameterizations deduced from different solutions for the  $K^- n$  scattering length value (via the application of the charge symmetry assumption). The differential cross sections exhibit moreover a marked backward peaked trend as a function of the  $K_S^0$  emission angle in the reaction center of mass [12].

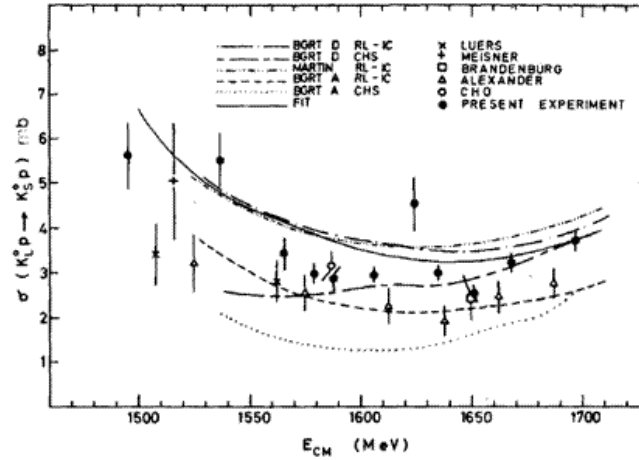


Figure 2: Low momentum  $K_L^0$  regeneration cross section, from Ref. [10].

ii. **Inelastic Cross Sections and Hyperon Production Yields**

The relevant reactions for the  $K_L^0$  induced production of baryonic resonances at low energies are  $K_L^0 p \rightarrow \Lambda \pi^+$ ,  $\Sigma^0 \pi^+$  and  $K_L^0 p \rightarrow \Lambda \pi^+ \pi^0$ . An assessment of the ratio of regeneration to elastic yields,  $R = \frac{\sigma(K_S^0 p)}{\sigma(\Lambda \pi^+) + 2\sigma(\Sigma^0 \pi^+)}$ , was used by early experiments [13, 14] to discriminate among the expected trends, as a function of  $K_L^0$  momentum, from different sets of solutions for the  $K^- p$  scattering length. As shown in Fig. 3 (left), none of the trends expected for  $R$  on the basis of different solution sets could reproduce in a satisfactory way the observed yields. Figures 3 center and right show, respectively, the inelastic cross sections for the reactions  $K_L^0 p \rightarrow \Lambda \pi^+$  (about 5 mb at 300 MeV/c) and  $K_L^0 p \rightarrow \Sigma^0 \pi^+$  ( $\sim 3$  mb). The  $K_L^0 p \rightarrow \Lambda \pi^+ \pi^0$  channel is less relevant ( $< 1$  mb) [15], and is mainly dominated by the  $\Sigma^0(1385)$  production.

## 2. Low Energy $\bar{K}N$ Dynamics: Open Problems

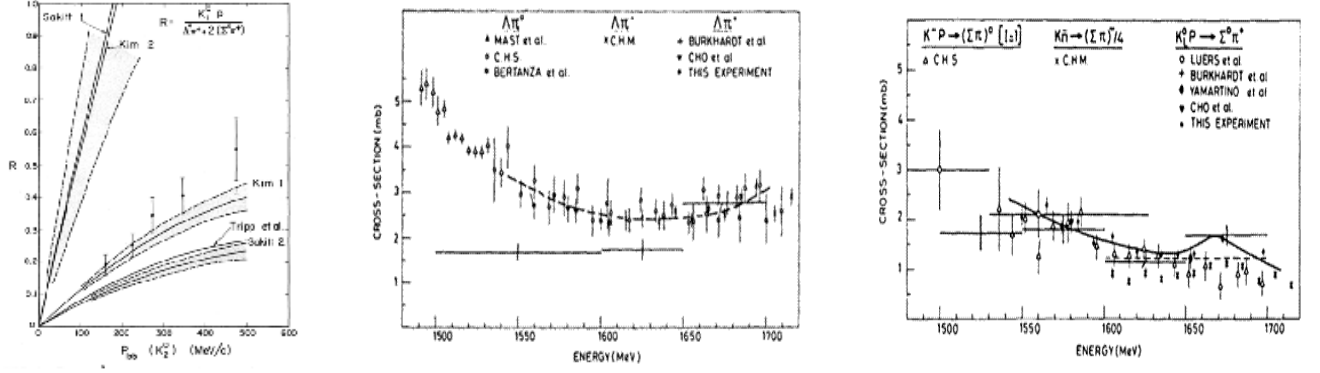


Figure 3: Left: ratio, as a function of  $K_L^0$  momentum, of the yields for regeneration to inelastic scattering. The lines represent the expected trends on the basis of different solutions chosen for the  $K^-p$  scattering length, from Ref. [13]. Center:  $K_L^0 p \rightarrow \Lambda\pi^+$  cross section; Right:  $K_L^0 p \rightarrow \Sigma^0\pi^+$  cross section. When existing, the data are compared to cross section measurements in the charge conjugated channels. The last two pictures are from Ref. [15].

The  $\bar{K}N$  interaction still presents some obscure aspects which only few more accurate data will be able to shed light on. The basic fact is the strong attractiveness of the interaction close to threshold and even below it, that manifests itself with the existence of a baryonic quasi-bound  $\bar{K}N$  state, the  $\Lambda(1405)$ , embedded in the  $\pi\Sigma$  continuum. This means that a strong coupled-channel dynamics between  $\bar{K}N$  and  $\Sigma\pi$  exists; to reproduce this behaviour a below-threshold extrapolation of the trend of the  $\bar{K}N$  amplitude based on observed data must be exploited. However, the relatively scarce precision of the presently available experimental data close to threshold has severe drawbacks on the accuracy of the sub-threshold extrapolations. For this reason, new experimental inputs would certainly be welcome, especially if characterized by fixed quantum numbers (like the Coulomb free  $I = 1$   $K_L^0 p$  interaction).

Several chiral inspired coupled-channels models have been elaborated over the years [6]. The most recent ones [16] are able to reproduce satisfactorily most of the existing data through global fits, especially since when the newest measurement of the Kaonic hydrogen  $1S$  level performed by the SIDDARTHA Collaboration [17] was included in the data set. We recall that the energy shift  $\Delta E$  and width  $\Gamma$  of the  $1S$  Kaonic hydrogen line are directly related to the  $a(K^-p)$  scattering length value through the Trueman-Deser formula (including second order isospin corrections):  $\Delta E - i\Gamma/2 = -2\alpha^3\mu_T^2 a(K^-p) [1 + 2\alpha\mu_T(1 - \log \alpha)a(K^-p)]$ , where  $\alpha$  is the strong coupling constant, and  $\mu_T$  the reduced mass of the  $K^-p$  system. The new measurement performed by the SIDDARTHA Collaboration fixes the inconsistencies emerging from the previous experiments on Kaonic hydrogen, and is fully compatible with all the existing scattering data. Unfortunately, the experiment was not sensitive enough to perform also a measurement of the  $1S$  Kaonic deuterium level, that could allow the determination of the  $K^-n$  scattering length; however, an upgrade was proposed to this purpose and is foreseen to run at DAΦNE in the near future.

The Kaonic hydrogen new measurement is very useful to provide much more stringent constraints for the determination of the scattering lengths in the two different isospin chan-

nels [18]. Calculations have been performed also to assess the extent of the  $K^-n$  (fixed  $I = 1$ ) scattering length [19], but the evaluation is still rather imprecise due to the large uncertainty of the experimental inputs (especially of the scattering data in the  $\Lambda\pi$  channel). As shown in Ref. [20] the  $I = 1$   $\bar{K}N$  interaction is expected to be weaker as compared to the  $I = 0$  source; therefore, data from Kaonic deuterium or from  $K_{LP}^0$  scattering would be useful in this respect.

(a) **Subthreshold behavior: the  $\Lambda(1405)$  case and the case for possible nuclear-Kaonic aggregates**

The measurement of the Kaonic hydrogen  $\Delta E$  and  $\Gamma$  provides a single experimental point to constrain the behavior of the below-threshold real and imaginary part of the  $K^-p$  elastic scattering amplitude, as shown in Fig. 4 from Ref. [21]. This result is just one typical snapshot of the outcomes of several equivalent high-quality below-threshold extrapolations:  $\text{Re}(a(K^-p)) = -0.65 \pm 0.10$  fm, and  $\text{Im}(a(K^-p)) = 0.81 \pm 0.15$  fm. In spite of the uncertainty of the prediction, represented by the grey band around the best fit result, basically all models agree on the existence of the  $\Lambda(1405)$  resonance, to be interpreted as a  $I = 0$   $\bar{K}N$  system bound by 27 MeV. This resonance is dynamically generated by the interplay of two poles in the second Riemann sheet, one at higher mass ( $1424 - i26$  MeV) coupled to the  $\bar{K}N$  channel, and the second at a lower mass value ( $1381 - i81$  MeV) dominated by the  $\Sigma\pi$  coupling [19].

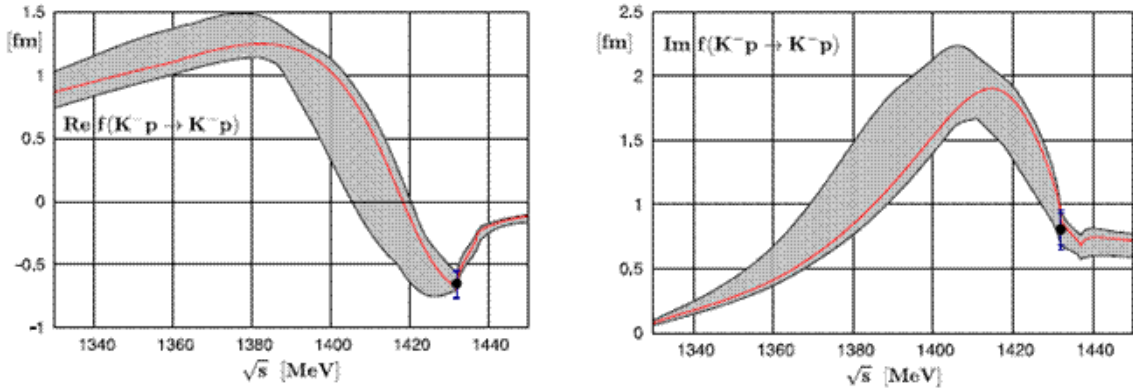


Figure 4: Solutions for the real and imaginary part of the  $K^-p$  elastic scattering amplitude, based on the chiral inspired model of Ref. [19]. The best fit to the experimental data is represented by the continuous line, while the grey area shows the uncertainty of the model, determined by the precision of the available experimental data used for the fit. The two data points correspond to the assessment of the real and imaginary parts of the  $K^-p$  scattering length derived from the experimental measurement of the Kaonic hydrogen  $1S$  level by the SIDDARTHA Collaboration.

From the experimental point of view the observations of the  $\Lambda(1405)$  were often hindered by the existence, in the same mass region, of the  $\Sigma(1385)$  baryon, which shares with the  $\Lambda(1405)$  the charged  $\Sigma\pi$  decay mode. The decays in charged  $\Sigma\pi$  pairs were

studied by early experiments on deuterium targets [22]. The first observations were confirmed, with higher statistics, by second generation experiments which were also able to measure the  $\Sigma^0\pi^0$  decay channel, which is mostly important as it is only allowed for the decay of the  $\Lambda(1405)$ , but is prevented to  $\Sigma(1385)$ . The latter, on the other hand, may only decay to  $\Lambda\pi^0$  (channel excluded for  $\Lambda(1405)$ ). The most complete data-set collected so far defining the  $\Lambda(1405)$  lineshape comes from the CLAS experiment, based on photo- and electroproduction of the  $\Sigma\pi$  final states [23]. The best fit of the data suggests the lineshapes of the three charge combinations of the  $\Sigma\pi$  invariant mass systems to be reproduced by introducing a dominant  $I = 0$  contribution (at  $m = 1338 \pm 10 \text{ MeV}/c^2$ , with  $\Gamma = 85 \pm 10 \text{ MeV}$ ), plus two  $I = 1$  amplitudes, one of which is most probably related to the  $\Sigma(1385)$  broad resonance ( $m = 1394 \pm 40 \text{ MeV}/c^2$ ,  $\Gamma = 149 \pm 40 \text{ MeV}$ ), while the second, narrower and at higher mass ( $m = 1412 \pm 10 \text{ MeV}/c^2$ ,  $\Gamma = 52 \pm 10 \text{ MeV}$ ), has a still uncertain nature. Its necessity, to provide a good description of the data, has been remarked by theoretical models [24]; for its interpretation, the possibility that it might be due to a new, exotic pentaquark baryonic state [25] is still open.

Related to the existence of the  $\Lambda(1405)$  is the case of the so-called (anti)Kaon-nuclear clusters. Following the hypothesis suggested by Akaishi and Yamazaki in 2002 [26], the  $\Lambda(1405)$  could be the founding block based on which more complex aggregates, composed by an anti-Kaon deeply bound to two or more nucleons, could exist. Even though the existence of such states is not ruled out in most of the chiral inspired models elaborated so far [27], very few of them agree on their observability as narrow states mainly decaying via the non mesonic channel ( $\Sigma\pi$  and  $\Lambda\pi$  being prevented by their strong binding and by isospin conservation). Most of the models, in fact, foresee for the  $\bar{K}N$  potential rather shallow wells, so a mild binding. In the initial formulation, on the contrary, these states are expected to be narrow, bound by more than 100 MeV and forming very compact systems, with a density more than three times as large as compared to ordinary nuclear matter. The medium in which their formation could more likely occur is also a controversial point: while according to the starting hypothesis the observation in light targets could be easier, other calculations [28] indicate that heavy targets should be preferred. If this were the case, however, probably large Final State Interaction effects would spoil completely their observability as narrow states.

From the experimental point of view, the situation is still rather confused and a few observations claimed so far [29] still need a sound confirmation. For the latest findings of this search using a  $^3\text{He}$  target (E15 experiment running at J-PARC) the reader may refer to Ref. [30].

The search for such states has been performed so far only relative to the  $K^-NN(N)$  systems; no measurement were ever attempted with neutral Kaon beams. Therefore, provided a  $^3\text{He}$  or  $^4\text{He}$  (or even heavier) target could be exploited, the search for such states could represent a completely new field of investigation to be pursued with  $K_L^0$  as projectiles (again, free from Coulomb interactions and related to the binding properties of  $I = 1 \bar{K}N$  systems only).

### 3. Possible Measurements with $K_L^0$ Beams and Experimental Reach

With a liquid hydrogen/deuterium target, the following reactions could be measured at low momenta, to improve the present knowledge on the scattering cross sections:

**elastic scattering**  $K_L^0 p \rightarrow K_L^0 p$ ,  $K_L^0 d \rightarrow K_L^0 d$  (coherent),  $K_L^0 d \rightarrow K_L^0 np$  (quasi-elastic scattering on  $n$ );

**inelastic scattering on protons with  $Y$  formation**  $K_L^0 p \rightarrow \Lambda\pi^+$ ,  $\Sigma^0\pi^+$ ,  $\Sigma^+\pi^0$ ,  $\Lambda\pi^+\pi^0$ ;

**inelastic scattering on deuterons for below-threshold  $Y$  resonances production**  $K_L^0 d \rightarrow \Lambda(1405)N$ ;

**charge exchange reactions**  $K_L^0 p \rightarrow K^+ n$ ;

**regeneration reaction**  $K_L^0 p \rightarrow K_S^0 p$ .

One or two measurements of low momentum cross sections below 350 MeV/ $c$  at the 10% precision level would be highly desirable to complement the experimental data set on which close-to-threshold  $\bar{K}N$  interaction studies are based. Differential information, for instance as a function of the emission angle, could be fruitfully explored as well.

A few experimental possibly critical drawbacks have however to be taken into account. Among them:

- (a) The  $K_L^0$  beam intensity at low momentum. As shown by experiments exploiting the  $K_L^0$  production by means of photoproduction on a Be target,  $K_L^0$ 's are produced with a continuum momentum spectrum [31,32]. The low momentum portion is roughly some  $10^{-3}$  of the total integrated  $K_L^0$  momentum spectrum, for a maximum photon energy of around 10 GeV [32], close to that foreseen for the 12 GeV CEBAF machine. This could still allow to have a fair number of low momentum  $K_L^0$  (some Hz), provided they can be effectively discriminated from neutrons even at these low energies;
- (b) The capability of detecting low momentum particles in the final state. The momentum resolution is not a crucial problem in a few body reaction, but the curling of low momentum particles in a high intensity magnetic field could prevent them from reaching the position sensitive detectors and therefore impair the observation of the mentioned reactions. A careful study on how to increase the apparatus acceptance to low momentum particles would most likely be required in the planning of such measurements.

A tentative yield evaluation, with some optimistic but reasonable detection efficiencies (assuming that all the emitted particles enter the apparatus acceptance), indicates that for an elastic cross section measurement with a precision at the level of 10% some hours of data taking could be enough, while a few days at most would be required for the less frequent inelastic channels.

#### (a) Hypernuclei formation studies

A completely new research field, that could be explored with a  $K_L^0$  beam and for which no experimental result exist so far, is the production of hypernuclei in  $\bar{K}^0$  induced reactions. The spectroscopy of the formation pion, in reactions on  $^AZ$  nuclei like  $^AZ(\bar{K}^0, \pi^+)_{\Lambda}^A(Z-1)$  or  $^AZ(\bar{K}^0, \pi^0)_{\Lambda}^AZ$ , requires a very high momentum resolution (on

the order of a few per mil), which, however, is probably out of scope for an apparatus conceived for hadron spectroscopy like GlueX. This information might be of unprecedented value for the investigation of the so-called Charge Symmetry Breaking effect, which consists in a sizeable difference between the binding energies of the ground states of mirror hypernuclei. So far, the effect has been observed in light mirror hypernuclei pairs (like  ${}^4_{\Lambda}\text{He}$  vs  ${}^3_{\Lambda}\text{H}$ ), and is supposed to be due to a strong  $\Lambda\Sigma$  mixing [33]. While in this case the binding energies differ of about 250 KeV, for heavier ( $P$ -shell) hypernuclei the difference is expected to decrease. Studies of mirror light hypernuclei production would be welcome to investigate this interesting effect in deeper detail.

#### 4. Conclusions

With a beam of low momentum  $K_L^0$  new tools to improve the knowledge of the  $\bar{K}N$  interaction, never exploited so far, could be available. It is important to recall that with a  $K_L^0$  beam the isospin  $I = 1$  source of the  $\bar{K}N$  amplitude may be selected: its features are largely unknown as, with charged Kaons, this information may only be pursued using deuterium as a target, which involves a complicated treatment due to the inherent few-body interaction. Moreover, the  $K_L^0 p$  interaction is free from any Coulomb-related effect.

Data on  $K_L^0 p$  scattering might improve the present knowledge of  $I = 1$  scattering length, providing complementary information to the already planned measurements of Kaonic deuterium. An extension of the charged Kaon scattering database to neutral Kaon induced reactions would be important to improve the precision of  $\bar{K}N$  models especially regarding their below-threshold extrapolations, that are crucial to improve the understanding of some still critical subjects, like the nature of the  $\Lambda(1405)$  as a true baryonic resonance.

With targets heavier than deuterium, the study of more complex systems like Kaon-nuclear bound states or hypernuclei produced in  $K_L^0$  induced reactions could potentially be feasible, and thoroughly yet unexplored research topics could be opened.

## References

- [1] K.A. Olive *et al.* (Particle Data Group), Chin. Phys. C **38**, 090001 (2014):  
[http://pdg.lbl.gov/2015/hadronic-xsections/rpp2014-kplusp\\_kplused\\_kplusn\\_plots.pdf](http://pdg.lbl.gov/2015/hadronic-xsections/rpp2014-kplusp_kplused_kplusn_plots.pdf) .
- [2] L. Bosisio *et al.*, *Interacting Kaons On Nucleons (IKON)*, Letter of Intent presented at I.N.F.N. Frascati National Laboratories, Apr. 2010.
- [3] W. Cleland *et al.*, Phys. Rev. D **12**, 1247 (1975).
- [4] S. Eidelman *et al.*, Phys. Lett. B **592**, 1 (2004);  
T. Bowen *et al.*, Phys. Rev. D **2**, 2599 (1970);  
T. Bowen *et al.*, Phys. Rev. D **7**, 22 (1973);  
S. Goldhaber *et al.*, Phys. Rev. Lett. **9**, 135 (1962);  
J.S. Hyslop *et al.*, Phys. Rev. D **46**, 961 (1992).
- [5] P. Darriulat *et al.*, Phys. Lett. B **33**, 433 (1970).

- [6] B. Borasoy, N. Nibler, and W. Weise, Phys. Rev. Lett. **96**, 199201 (1996);  
N. Kaiser, T. Waas, and W. Weise, Nucl. Phys. A **612**, 297 (1997);  
E. Oset and A. Ramos, Nucl. Phys. A **635**, 99 (1998);  
U.-G. Meißner, U. Raha, and A. Rusetsky, Eur. Phys. J. C **35**, 349 (2004);  
B. Borasoy, U.-G. Meißner, and N. Nibler, Phys. Rev. C **74**, 055201 (2006).
- [7] R.H. Dalitz and S.F. Tuan, Ann. Phys. **3**, 307 (1960).  
M.H. Ross and G.L. Shaw, Ann. Phys. **9**, 391 (1960).
- [8] J.K. Kim, Phys. Rev. Lett. **21**, 29 (1965);  
W. Kittel *et al.*, Phys. Lett. **21**, 349 (1966);  
J. Ciborowski *et al.*, J. Phys. G **8**, 13 (1982);  
M. Sakitt *et al.*, Phys. Rev. **139**, 719 (1965);  
W.E. Humphrey and R.R. Ross, Phys. Rev. **127**, 1305 (1962).
- [9] N.N. Biswas, Phys. Rev. **118**, 866 (1960);  
R.A. Donald *et al.*, Phys. Lett. **22**, 711 (1968);  
G.A. Sayer *et al.*, Phys. Rev. **169**, 169 (1968).
- [10] G. Alexander *et al.*, Phys. Lett. B **55**, 484 (1975).
- [11] A. Bigi *et al.*, Nucl. Phys. B **110**, 25 (1976).
- [12] Y. Cho *et al.*, Phys. Lett. B **60**, 293 (1976).
- [13] J. Kadyk *et al.*, Phys. Rev. Lett. **17**, 599 (1966).
- [14] D. Luers *et al.*, Phys. Rev. Lett. **7**, 255 (1961).
- [15] W. Cameron *et al.* (BEGPR Collaboration), Nucl. Phys. B **132**, 189 (1978).
- [16] M. Mai, *these Proceedings*;  
M. Mai and U.-G. Meißner, Eur. Phys. J. A **51**, 30 (2015).
- [17] M. Bazzi *et al.* (SIDDARTHA Collaboration), Phys. Lett. B **704**, 113 (2011).
- [18] M. Döring and U.-G. Meißner, Phys. Lett. B **704**, 663 (2011).
- [19] Y. Ikeda *et al.*, Nucl. Phys. A **881**, 98 (2012).
- [20] A. Cieply *et al.*, Phys. Rev. C **84**, 045206 (2011).
- [21] Y. Ikeda, T. Hyodo, and W. Weise, Phys. Lett. B **704**, 63 (2011).
- [22] O. Braun *et al.*, Nucl. Phys **124**, 45 (1977);  
D. Cline *et al.*, Phys. Rev. Lett. **20**, 452 (1968);  
D. Eastwood *et al.*, Phys. Rev. D **3**, 2603 (1971);  
D.P. Goyal *et al.*, Phys. Rev. D **18**, 948 (1978);  
R.J. Hemingway *et al.*, Nucl. Phys. B **253**, 742 (1985).



- [23] K. Moriya *et al.* (CLAS Collaboration), Phys. Rev. C **87**, 035206 (2013);  
R. Schumacher, *these Proceedings*.
- [24] L. Roca and E. Oset, Phys. Rev. C **88**, 055206 (2011).
- [25] B.S. Zou, Nucl. Phys. A **835**, 199 (2010).
- [26] Y. Akaishi and T. Yamazaki, Phys. Rev. C **65**, 044005 (2002);  
T. Yamazaki and Y. Akaishi, Nucl. Phys. B **535**, 70 (2002).
- [27] W. Weise and H. Härtle, Nucl. Phys. B **535**, 70 (2002);  
N.V. Shevchenko *et al.*, Phys. Rev. Lett. **98**, 082301 (2007);  
A. Ramos and E. Oset, Nucl. Phys. B **71**, 153 (2000).
- [28] J. Mareš, Nucl. Phys. A **804**, 296 (2008);  
J. Mareš *et al.*, Nucl. Phys. A **770**, 84 (2006).
- [29] M. Agnello *et al.* (FINUDA Collaboration), Phys. Rev. Lett. **94**, 212203 (2005);  
M. Agnello *et al.* (FINUDA Collaboration), Phys. Lett. B **654**, 80 (2007);  
G. Bendiscioli *et al.*, Eur. Phys. J. A **40**, 11 (2009);  
T. Yamazaki *et al.*, Phys. Rev. Lett. **104**, 132502 (2010);  
G. Agakashiev *et al.* (HADES Collaboration), Phys. Lett. B **742**, 242 (2015).
- [30] T. Ohnishi, *these Proceedings*.
- [31] D.G. Cassel *et al.*, Phys. Lett. B **34**, 223 (1971);  
J.F. Schivell *et al.*, Phys. Rev. Lett. **19**, 1349 (1967);  
M.G. Albrow *et al.*, Nucl. Phys. B **23**, 509 (1970).
- [32] G.W. Brandeburg *et al.*, Phys. Rev. D **7**, 708 (1973).
- [33] A. Gal, Phys. Lett. B **744**, 352 (2015).

## 2.6 $K_L^0 p$ Scattering to Two-Body Final States

D. Mark Manley

*Department of Physics*

*Kent State University*

*Kent, OH 44242 U.S.A.*

### Abstract

Our main interest in creating a high-quality secondary  $K_L^0$  beam is to investigate hyperon spectroscopy through both formation and production processes. Here we review what can be learned by studying hyperon formation processes using  $K_L^0 p$  scattering going to two-body final states.

### 1. Introduction and Formalism

The mean lifetime of the  $K^-$  is 12.38 ns ( $c\tau = 3.7$  m) whereas the mean lifetime of the  $K_L^0$  is 51.16 ns ( $c\tau = 15.3$  m) [1]. For this reason, it is much easier to perform measurements of  $K_L^0 p$  scattering at low beam energies compared with  $K^- p$  scattering. Here, we summarize some of the physics issues involved with such processes. The differential cross section and polarization for  $K_L^0 p$  scattering are given by

$$\frac{d\sigma}{d\Omega} = \lambda^2(|f|^2 + |g|^2), \quad (1)$$

$$P \frac{d\sigma}{d\Omega} = 2\lambda^2 \text{Im}(fg^*), \quad (2)$$

where  $\lambda = \hbar/k$ , with  $k$  the magnitude of c.m. momentum for the incoming meson. Here  $f = f(W, \theta)$  and  $g = g(W, \theta)$  are the usual spin-nonflip and spin-flip amplitudes at c.m. energy  $W$  and meson c.m. scattering angle  $\theta$ . In terms of partial waves,  $f$  and  $g$  can be expanded as

$$f(W, \theta) = \sum_{l=0}^{\infty} [(l+1)T_{l+} + lT_{l-}] P_l(\cos \theta), \quad (3)$$

$$g(W, \theta) = \sum_{l=1}^{\infty} [T_{l+} - T_{l-}] P_l^1(\cos \theta), \quad (4)$$

where  $l$  is the initial orbital angular momentum,  $P_l(\cos \theta)$  is a Legendre polynomial, and  $P_l^1(\cos \theta) = \sin \theta \times dP_l(\cos \theta)/d(\cos \theta)$  is an associated Legendre function. The total angular momentum for the amplitude  $T_{l+}$  is  $J = l + \frac{1}{2}$ , while that for the amplitude  $T_{l-}$  is  $J = l - \frac{1}{2}$ . For hadronic scattering reactions, we may ignore small CP-violating terms and write

$$K_L^0 = \frac{1}{\sqrt{2}}(K^0 - \overline{K}^0), \quad (5)$$

$$K_S^0 = \frac{1}{\sqrt{2}}(K^0 + \overline{K}^0). \quad (6)$$

We may generally have both  $I = 0$  and  $I = 1$  amplitudes for  $KN$  and  $\bar{K}N$  scattering, so that the amplitudes  $T_{l\pm}$  can be expanded in terms of isospin amplitudes as

$$T_{l\pm} = C_0 T_{l\pm}^0 + C_1 T_{l\pm}^1, \quad (7)$$

where  $T_{l\pm}^I$  are partial-wave amplitudes with isospin  $I$  and total angular momentum  $J = l \pm \frac{1}{2}$ , with  $C_I$  the appropriate isospin Clebsch-Gordon coefficients.

## 2. $KN$ and $\bar{K}N$ Final States

The amplitudes for reactions leading to  $KN$  and  $\bar{K}N$  final states are

$$T(K^-p \rightarrow K^-p) = \frac{1}{2}T^1(\bar{K}N \rightarrow \bar{K}N) + \frac{1}{2}T^0(\bar{K}N \rightarrow \bar{K}N), \quad (8)$$

$$T(K^-p \rightarrow \bar{K}^0n) = \frac{1}{2}T^1(\bar{K}N \rightarrow \bar{K}N) - \frac{1}{2}T^0(\bar{K}N \rightarrow \bar{K}N), \quad (9)$$

$$T(K^+p \rightarrow K^+p) = T^1(KN \rightarrow KN), \quad (10)$$

$$T(K^+n \rightarrow K^+n) = \frac{1}{2}T^1(KN \rightarrow KN) + \frac{1}{2}T^0(KN \rightarrow KN), \quad (11)$$

$$T(K_L^0p \rightarrow K_S^0p) = \frac{1}{2} \left( \frac{1}{2}T^1(KN \rightarrow KN) + \frac{1}{2}T^0(KN \rightarrow KN) \right) - \frac{1}{2}T^1(\bar{K}N \rightarrow \bar{K}N), \quad (12)$$

$$T(K_L^0p \rightarrow K_L^0p) = \frac{1}{2} \left( \frac{1}{2}T^1(KN \rightarrow KN) + \frac{1}{2}T^0(KN \rightarrow KN) \right) + \frac{1}{2}T^1(\bar{K}N \rightarrow \bar{K}N), \quad (13)$$

$$T(K_L^0p \rightarrow K^+n) = \frac{1}{\sqrt{2}} \left( \frac{1}{2}T^1(KN \rightarrow KN) - \frac{1}{2}T^0(KN \rightarrow KN) \right) - \frac{1}{2}T^1(\bar{K}N \rightarrow \bar{K}N). \quad (14)$$

No differential cross section data are available for  $K_L^0p \rightarrow K_L^0p$  below  $W \sim 2948$  MeV. A fair amount of data are available for the reaction,  $K^+n \rightarrow K^0p$ , measured on a deuterium target. Figure 1 shows a sample of available differential cross section data for  $K_L^0p \rightarrow K_S^0p$  compared with predictions determined from our previous partial-wave analysis of  $\bar{K}N \rightarrow \bar{K}N$  data [2, 3], combined with  $KN \rightarrow KN$  amplitudes from the SAID website [4]. The predictions at lower and higher energies tend to agree less well with the data.

## 3. $\pi\Lambda$ Final States

The amplitudes for reactions leading to  $\pi\Lambda$  final states are

$$T(K^-p \rightarrow \pi^0\Lambda) = \frac{1}{\sqrt{2}}T^1(\bar{K}N \rightarrow \pi\Lambda), \quad (15)$$

$$T(K_L^0p \rightarrow \pi^+\Lambda) = -\frac{1}{\sqrt{2}}T^1(\bar{K}N \rightarrow \pi\Lambda). \quad (16)$$

The  $K^-p \rightarrow \pi^0\Lambda$  and  $K_L^0p \rightarrow \pi^+\Lambda$  amplitudes imply that observables for these reactions measured at the same energy should be the same except for small differences due to

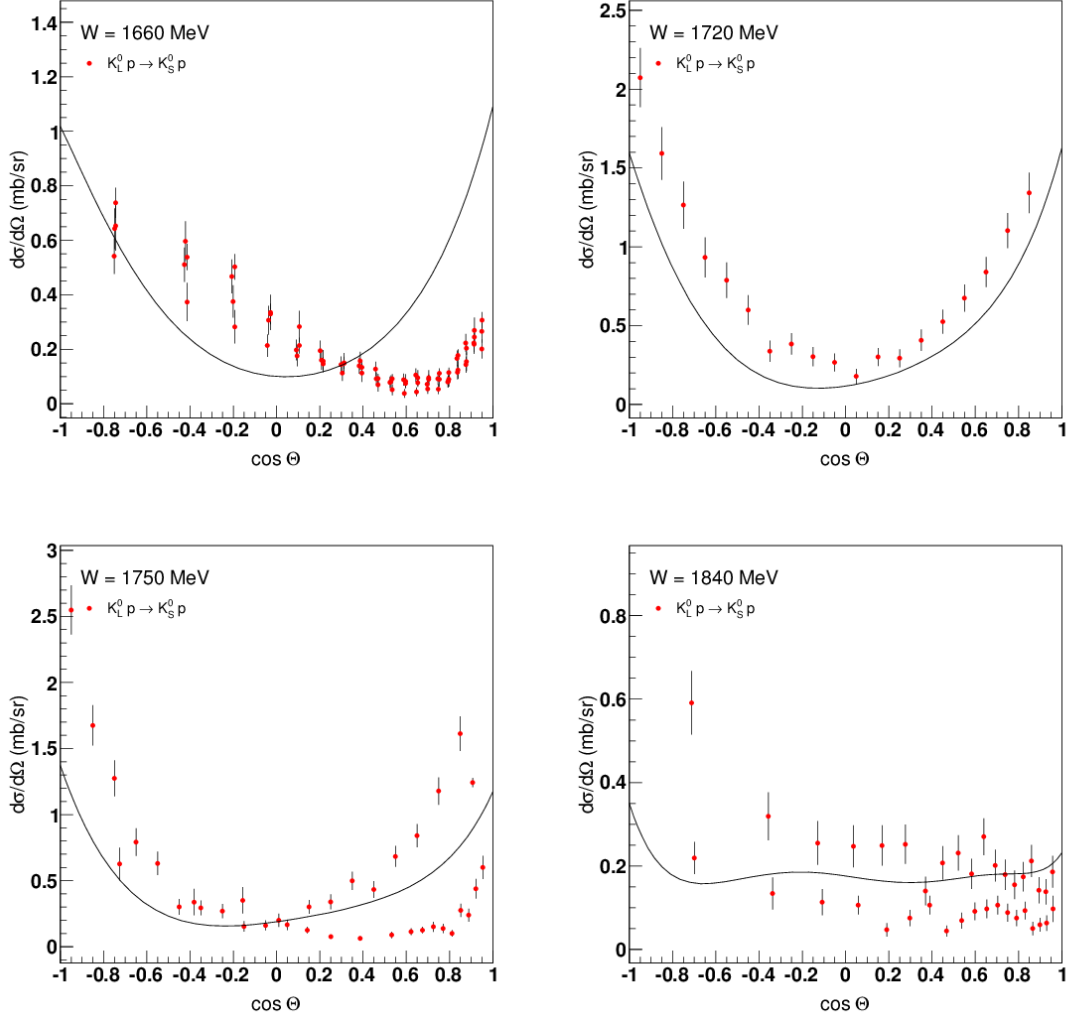


Figure 1: Selected differential cross section data for  $K_L^0 p \rightarrow K_S^0 p$  at 1660 MeV, 1720 MeV, 1750 MeV, and 1840 MeV. The curves are predictions using amplitudes from our previous partial-wave analysis of  $\bar{K}N \rightarrow \bar{K}N$  data [2, 3], combined with  $KN \rightarrow KN$  amplitudes from the SAID website [4].

the isospin-violating mass differences in the hadrons. No differential cross section data for  $K^- p \rightarrow \pi^0 \Lambda$  are available at c.m. energies  $W < 1540$  MeV, although data for  $K_L^0 p \rightarrow \pi^+ \Lambda$  are available at such energies. At 1540 MeV and higher energies, differential cross section and polarization data for the two reactions are in fair agreement, as shown in Figs. 2 and 3.

#### 4. $\pi\Sigma$ Final States

The amplitudes for reactions leading to  $\pi\Sigma$  final states are

$$T(K^- p \rightarrow \pi^- \Sigma^+) = -\frac{1}{2}T^1(\bar{K}N \rightarrow \pi\Sigma) - \frac{1}{\sqrt{6}}T^0(\bar{K}N \rightarrow \pi\Sigma), \quad (17)$$

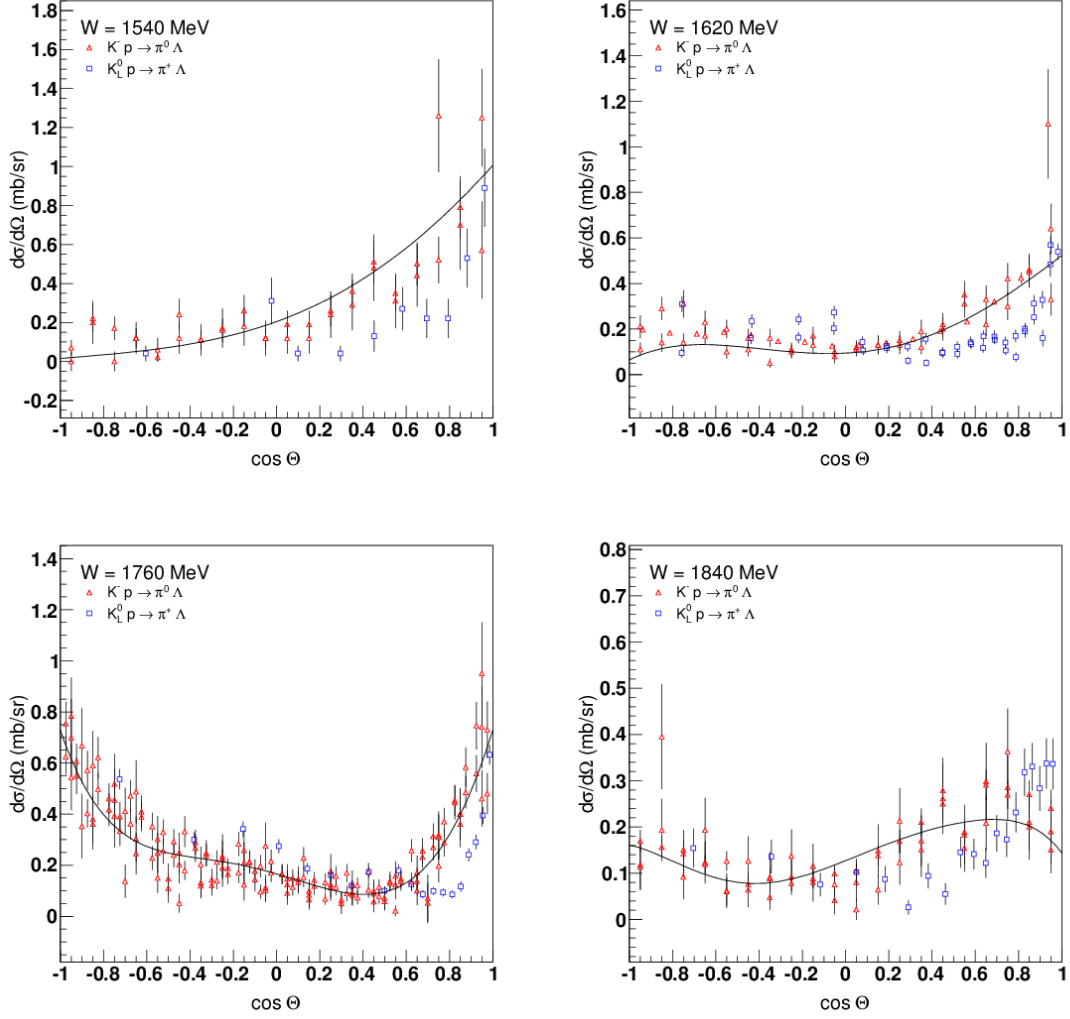


Figure 2: Comparison of selected differential cross section data for  $K^-p \rightarrow \pi^0\Lambda$  and  $K_L^0p \rightarrow \pi^+\Lambda$  at 1540 MeV, 1620 MeV, 1760 MeV, and 1840 MeV. The curves are from our previous partial-wave analysis of  $K^-p \rightarrow \pi^0\Lambda$  data [2, 3].

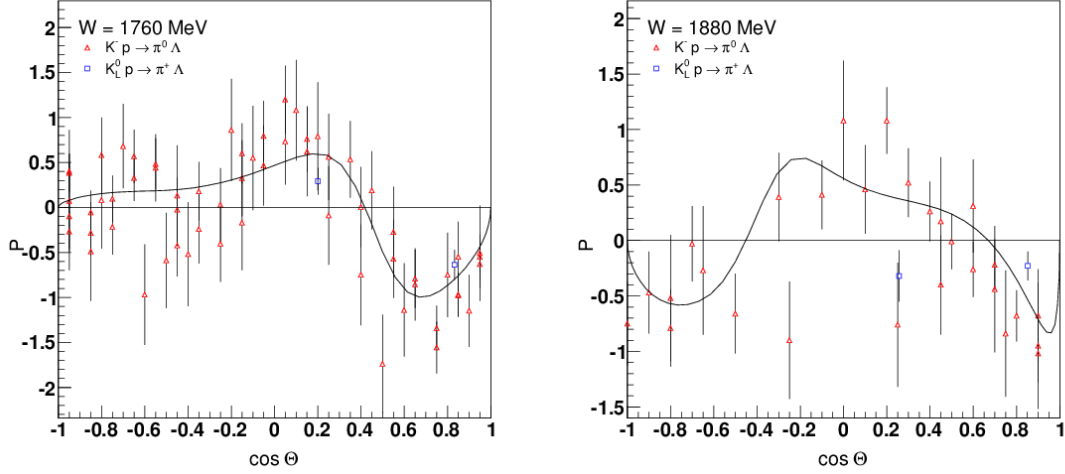


Figure 3: Comparison of selected polarization data for  $K^-p \rightarrow \pi^0\Lambda$  and  $K_L^0p \rightarrow \pi^+\Lambda$  at 1760 MeV and 1880 MeV. The curves are from our previous partial-wave analysis of  $K^-p \rightarrow \pi^0\Lambda$  data [2, 3].

$$T(K^-p \rightarrow \pi^+\Sigma^-) = \frac{1}{2}T^1(\bar{K}N \rightarrow \pi\Sigma) - \frac{1}{\sqrt{6}}T^0(\bar{K}N \rightarrow \pi\Sigma), \quad (18)$$

$$T(K^-p \rightarrow \pi^0\Sigma^0) = \frac{1}{\sqrt{6}}T^0(\bar{K}N \rightarrow \pi\Sigma), \quad (19)$$

$$T(K_L^0p \rightarrow \pi^+\Sigma^0) = -\frac{1}{2}T^1(\bar{K}N \rightarrow \pi\Sigma), \quad (20)$$

$$T(K_L^0p \rightarrow \pi^0\Sigma^+) = \frac{1}{2}T^1(\bar{K}N \rightarrow \pi\Sigma). \quad (21)$$

Figure 4 shows a comparison of differential cross section data for  $K^-p$  and  $K_L^0p$  reactions leading to  $\pi\Sigma$  final states at  $W = 1660$  MeV (or  $P_{\text{lab}} = 716$  MeV/c). The curves are based on energy-dependent isospin amplitudes from our previous partial-wave analysis [2, 3]. No differential cross section data are available for  $K_L^0p \rightarrow \pi^0\Sigma^+$ . As this example shows, the quality of the  $K_L^0p$  data is comparable to that for the  $K^-p$  data. It would therefore be advantageous to combine the  $K_L^0p$  data in a new coupled-channel partial-wave analysis with available  $K^-p$  data. Note that the reactions  $K_L^0p \rightarrow \pi^+\Sigma^0$  and  $K_L^0p \rightarrow \pi^0\Sigma^+$  are isospin selective (only  $I = 1$  amplitudes are involved) whereas the reactions  $K^-p \rightarrow \pi^-\Sigma^+$  and  $K^-p \rightarrow \pi^+\Sigma^-$  are not. New measurements with a  $K_L^0$  beam would amplitudes for  $K^-p$  scattering to  $\pi\Sigma$  final states.

## 5. $K\Xi$ Final States

The amplitudes for reactions leading to  $K\Xi$  final states are

$$T(K^-p \rightarrow K^0\Xi^0) = \frac{1}{2}T^1(\bar{K}N \rightarrow K\Xi) + \frac{1}{2}T^0(\bar{K}N \rightarrow K\Xi), \quad (22)$$

$$T(K^-p \rightarrow K^+\Xi^-) = \frac{1}{2}T^1(\bar{K}N \rightarrow K\Xi) - \frac{1}{2}T^0(\bar{K}N \rightarrow K\Xi), \quad (23)$$

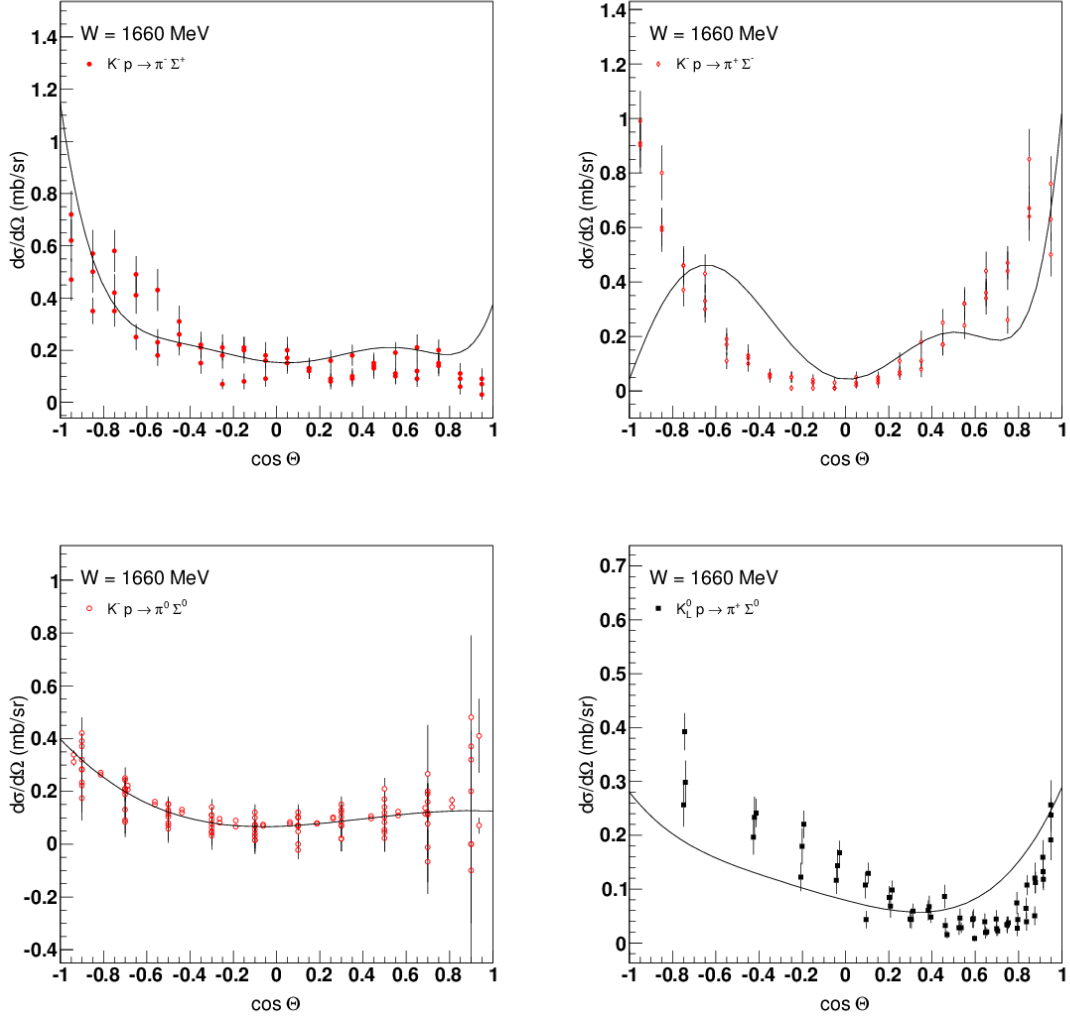


Figure 4: Comparison of selected differential cross section data for  $K^-p \rightarrow \pi^- \Sigma^+$ ,  $K^-p \rightarrow \pi^+ \Sigma^-$ ,  $K^-p \rightarrow \pi^0 \Sigma^0$ , and  $K_L^0 p \rightarrow \pi^+ \Sigma^0$  at 1660 MeV. The curves are from our previous partial-wave analysis of  $K^-p \rightarrow \pi \Sigma$  data [2, 3].

$$T(K_L^0 p \rightarrow K^+ \Xi^0) = -\frac{1}{\sqrt{2}} T^1(\bar{K} N \rightarrow K \Xi). \quad (24)$$

The threshold for  $K^- p$  and  $K_L^0 p$  reactions leading to  $K \Xi$  final states is fairly high ( $W_{\text{thresh}} = 1816$  MeV). There are no differential cross section data available for  $K_L^0 p \rightarrow K^+ \Xi^0$  and very few (none recent) for  $K^- p \rightarrow K^0 \Xi^0$  or  $K^- p \rightarrow K^+ \Xi^-$ . Measurements for these reactions would be very helpful, especially for comparing with predictions from dynamical coupled-channel (DCC) models. The *Review of Particle Physics* [1] lists only two states with branching fractions (BF) to  $K \Xi$ , namely,  $\Lambda(2100)_{\frac{7}{2}}^-$  (BF < 3%) and  $\Sigma(2030)_{\frac{7}{2}}^+$  (BF < 2%).

## 6. Summary

In summary, precise new data for  $K_L^0 p$  scattering with good kinematic coverage could significantly improve our knowledge of  $\Lambda^*$  and  $\Sigma^*$  resonances. Although not the focus of this talk, a  $K_L^0$  beam facility would also be advantageous for studying  $\Xi^*$  and  $\Omega^*$  states via production processes. Polarization data are very important to measure in addition to differential cross sections to help remove ambiguities in partial-wave analyses. Unfortunately, the current data base for  $K_L^0 p$  scattering includes very few polarization data. As noted here, several  $K_L^0 p$  reactions are isospin-1 selective, which would provide a useful constraint for a combined partial-wave analysis of  $K_L^0 p$  and  $K^- p$  reactions. Finally, the long lifetime of the  $K_L^0$  compared with the  $K^-$  would allow a larger beam flux on target, which would allow  $K_L^0 p$  measurements to be made at lower energies than easily measurable with  $K^-$  beams.

## 7. Acknowledgments

The author thanks Dr. Igor Strakovsky for providing the data files used in this work, and Brian Hunt for providing all the figures. This material is based upon work supported by the U.S. Department of Energy, Office of Science, Office of Medium Energy Nuclear Physics, under Award No. DE-SC0014323.

## References

- [1] K.A. Olive *et al.* (Particle Data Group), *Chin. Phys. C* **38**, 090001 (2014).
- [2] H. Zhang, J. Tulpan, M. Shrestha, and D.M. Manley, *Phys. Rev. C* **88**, 035204 (2013).
- [3] H. Zhang, J. Tulpan, M. Shrestha, and D.M. Manley, *Phys. Rev. C* **88**, 035205 (2013).
- [4] The George Washington University INS Data Analysis Center (SAID); <http://gwdac.phys.gwu.edu> .



## 2.7 Excited Hyperons and their Decays

Fred Myhrer

*Department of Physics and Astronomy*

*University of South Carolina*

*Columbia, SC 29208, U.S.A.*

### Abstract

There are several missing states in the mass spectrum of the first excited negative parity  $\Lambda^*$  and  $\Sigma^*$  states. To gain further understanding of QCD quark confinement and how QCD should be implemented in quark models, it is desirable to establish if these missing states exist, and to measure more accurately the decay properties of the hyperon states

### 1. Introduction

The QCD theory describes the forces among the quarks, and perturbative QCD has successfully explained asymptotic freedom and high four-momentum hadronic processes. At high energies QCD predicts the existence of quark-jets and the gluon-jets which were observed as predicted [1, 2]. This means that high energy quarks radiate gluons, which hadronize producing a jet of gluon quantum numbers. At low energy the large strong QCD coupling constant requires an effective theory or a model approach to explain the structure of baryons. The quark model organizes the many observed colorless meson and baryon states, and the model provides some insights of the structure of these states. The quark model was extended to also predict the existence of multi-quark (exotic) mesons and baryons including *glueballs*, *e.g.*,  $QQ\bar{Q}\bar{Q}$ ,  $QQQQ\bar{Q}$ ,  $Q\bar{Q}$ glue, where  $Q$  and *glue* are both treated as building blocks. The question is if such states exist. Have we taken the quark and gluon building blocks scenario too literary? We need further guidance from what QCD would allow. At present the QCD confinement of light quarks is not understood. According to the quark model there are several states among the first excited hyperon states which are missing or are not established. Do QCD require that these missing states should exist, or does QCD require further model restrictions not implemented in today's quark models? Many of the quark model predicted  $N^*$  and  $\Delta^*$  states, made of the very light  $u$  and  $d$  quarks, have been extensively studied. These states will not be discussed in this paper. Instead, I will concentrate only on the first excited hyperon, negative parity  $\Lambda^*$  and  $\Sigma^*$  states and make some observation on what we could learn about QCD through the use of quark model evaluations. In order to answer the questions above, it is imperative that we experimentally can establish the first excited hyperon mass spectrum of  $\Lambda^*$  and  $\Sigma^*$ . We know that most excited baryon states have large decay widths. The decay branching ratios can give us further information about the structure of these states. In this presentation I will first present a few general quark model arguments, which will be used in the discussion to follow.

### 2. The Quark Models

Due to the very slow experimental progress on strange baryon spectroscopy during the last decades, there are several of the first negative parity excited hyperon states which have not been established. Some of the  $\Sigma^*$  states have at most one star in the Particle Data Tables

rating [3]. One possible question to ponder is: Does QCD contain dynamical features, which are not considered by present day quark models and would imply that these states should be absent? The  $\Lambda^*$  and  $\Sigma^*$  states have one “heavy”  $s$ -quark and two very light quarks. Could this extra feature of having one heavy quark give us some extra insight into QCD beyond what  $N^*$  and  $\Delta^*$  states can provide? These observations and arguments would then be used to gain a better understanding of the  $\Xi^*$  and  $\Omega^*$  states.

The quarks interact via gluon exchanges, which couple the quark spins, very similar to what happens to pion- and rho-meson exchanges between nucleons in a nucleus. Analogous to the three-nucleon states,  $^3H$  and  $^3He$ , we should therefore expect the three valence quark baryon ground states to have a three-quark spatial wave function which contains a mixture of S, S' and D quark states. The effective pseudo-scalar meson cloud surrounding the quark core of the baryons will contribute to this spatial mixture of states. As will be presented these spatial admixtures affect strongly some excited hyperon decays. Much of this talk is based on the extensive work of the non-relativistic quark model (NRQM) by Nathan Isgur and Gabriel Karl and their coworkers [4].

#### (a) Quark Model Assumptions

The generic non-relativistic baryon wave function has the following structure

$$\Psi = \Psi_{color} \Psi_{flavor} \Psi_{spin} \Psi_{space} . \quad (1)$$

We assume that isospin is a good symmetry, *i.e.*, the masses of the  $u$  and  $d$  quarks are equal:  $m_u = m_d = m_q$ . However, the  $SU_F(3)$  is a broken symmetry since the  $s$  quark has a mass  $m_s > m_q$ . For this reason, we will adopt the  $uds$  basis when the baryon wave functions are evaluated. [Please note that in the (cloudy or MIT) bag model the masses of the  $u$  and  $d$  quarks are zero.]

In bag models the effective quark masses are generated by the confinement condition, which presumably reflects the very soft gluon exchanges between the three quarks. The other usual quark model assumptions are the following:

- All hadrons are  $SU(3)$ -color singlets, *i.e.*,  $\Psi_{color}$  is a totally anti-symmetric wave function under the interchange of any two quarks.
- Confinement of quarks is universal and is the same for all quark flavors. It is presumed to be a Lorentz scalar condition.
- The Pauli principle tells us that two identical quarks must have a totally anti-symmetric wave function. Since  $\Psi_{color}$  is anti-symmetric the product of the other components in Eq.(1) must be symmetric under the interchange of any two quarks.
- The non-relativistic quarks interact via an effective one-gluon-exchange, a la De Rujula *et al.* [5]. This effective gluon exchange generates a spin-spin interaction among the quarks and makes the *decuplet* baryons heavier than the *octet* baryons.

The non-relativistic effective one-gluon-exchange (OGE) between quarks  $i$  and  $j$  is:

$$H_{hyp}^{ij} = A_{ij} \left\{ \frac{8\pi}{3} \vec{S}_i \cdot \vec{S}_j \delta^3(\vec{r}_{ij}) + \frac{1}{r_{ij}^3} \left( \frac{3(\vec{S}_i \cdot \vec{r}_{ij})(\vec{S}_j \cdot \vec{r}_{ij})}{r_{ij}^2} - \vec{S}_i \cdot \vec{S}_j \right) \right\} ,$$

where  $A_{ij}$  is a constant which depends on the quark masses [5]. As can be inferred from this expression, the spin-spin and the tensor quark-quark interactions are closely related, and the tensor component will produce a spatial D-state quark wave function. Note that this non-relativistic reduction of the effective OGE quark-quark interaction neglects the spin-orbit force. Isgur and Karl argue that the spin-orbit force should be small. In bag models ( $m_q = 0$  MeV), the quark P-state with  $j=3/2$  has a lower energy than  $j=1/2$ , *i.e.*, the bag models' Lorentz-scalar confinement condition introduces a spin-orbit splitting of the quark states. Fortunately, the relativistic OGE introduces an effective spin-orbit force of opposite sign. In cloudy bag model calculations these two spin-orbit contributions basically cancel, and what remains are the spin-spin and tensor interactions due to OGE and the pseudo-scalar meson (pion, Kaon) cloud surrounding the quark core, see for example Refs. [6, 7]. The spin-spin and tensor interactions strongly affect the decay rates of  $\Lambda^*$  and  $\Sigma^*$  states to  $\bar{K}N$  and  $\pi\Sigma$ .

**(b) A Decay Rate Observation**

As mentioned we adopt the  $uds$  basis and not the  $SU_F(3)$  flavor basis in order to construct the baryon wave functions. The spatial wave function of three quarks is given by the two relative coordinates between the three quarks (ignoring the center of mass motion):

$$\vec{\rho} = (\vec{r}_1 - \vec{r}_2) / \sqrt{2}, \quad (2)$$

$$\vec{\lambda} = (\vec{r}_1 + \vec{r}_2 - 2\vec{r}_3) / \sqrt{6}. \quad (3)$$

Here quarks 1 and 2 are the  $u$  and  $d$  quarks, and quark 3 is the heavy  $s$ -quark. The corresponding reduced masses are  $m_\rho = m_q$  and  $m_\lambda = 3m_q m_s / (2m_q + m_s)$ . In an NRQM, the spatial confinement of the quarks is simulated by an harmonic oscillator potential. The harmonic oscillator confinement potential with a given flavor independent spring constant gives a difference in  $\rho$  and  $\lambda$  oscillator frequencies,  $\omega_\rho$  and  $\omega_\lambda$  due to the difference in the two reduced quark masses [4],

$$\omega_\rho - \omega_\lambda = \omega_\rho \left[ 1 - \left( \frac{2(m_q/m_s) + 1}{3} \right)^{1/2} \right] > 0, \quad (4)$$

where the frequency  $\omega_\rho$  is the one relevant for the nucleon ground state.

The mass splitting between the  $\Lambda^*(5/2^-)$  and the  $\Sigma^*(5/2^-)$  states, shown in Fig. 1, can easily be understood. In essence, the masses of these two  $J^P = 5/2^-$  states differ mainly due to confinement and  $SU_F(3)$  breaking since  $m_q < m_s$ . The detailed explanation goes as follows: The quarks in these excited hyperons have an orbital angular momentum  $L = 1$ . Both  $J^P = 5/2^-$  states have totally symmetric spin wave functions since the total spin of the quarks must be  $S = 3/2$ . Furthermore, since  $\Lambda^*(1830)$  is an iso-singlet, due to the Pauli principle, it must have a  $\vec{\rho}$ -dependent spatial wave function, which is anti-symmetric under the interchange of quarks 1 and 2, as seen in Eq.(4). On the other hand,  $\Sigma^*(1775)$ , is an iso-triplet, and since  $\vec{\lambda}$  is symmetric under the interchange ( $1 \leftrightarrow 2$ ), Eq.(3),  $\Sigma^*(1775)$  must have a  $\vec{\lambda}$ -dependent spatial wave function. In

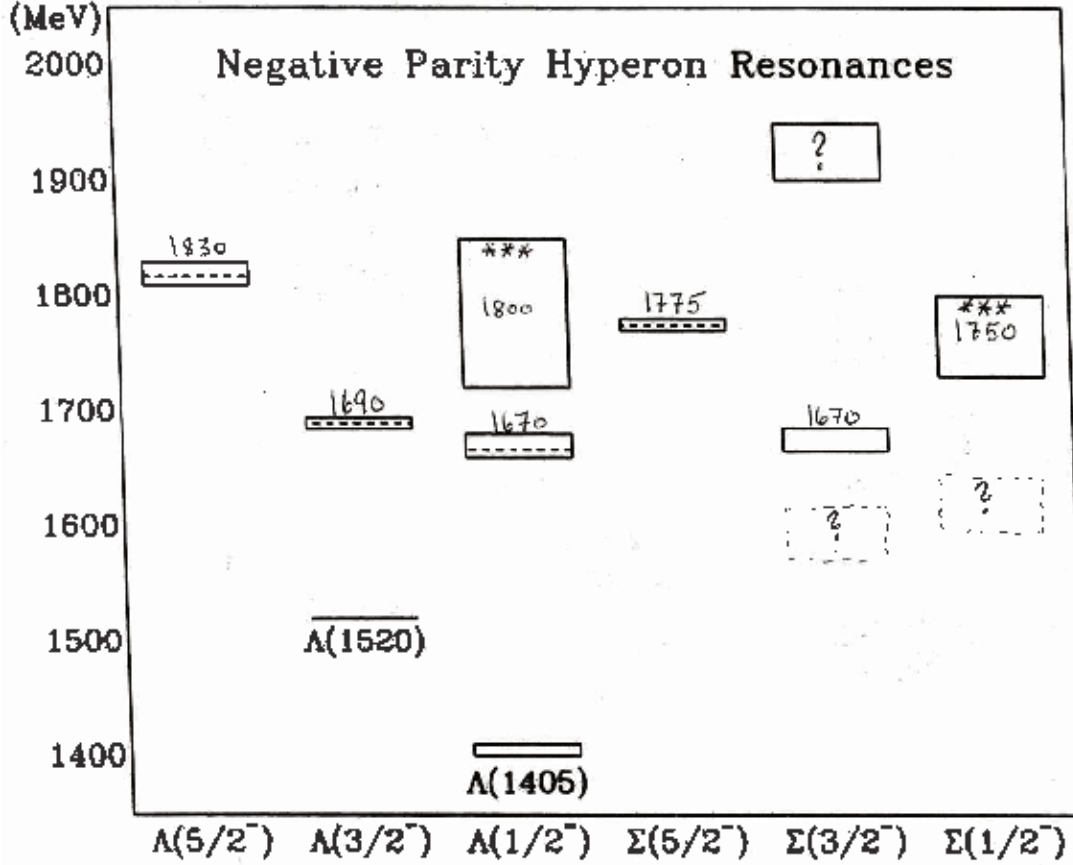


Figure 1: The confirmed mass spectrum of the first excited negative parity  $\Lambda^*$  and  $\Sigma^*$  states where we have included the three-star states [3]. The height of the squares illustrate the mass uncertainties of the “established” states. The squares with the question marks are states which are controversial. According to quark models there are two completely missing three-quark states in this figure.

other words  $\Lambda^*(1830)$  contains the energy  $\hbar\omega_\rho$  whereas  $\Sigma^*(1775)$  has  $\hbar\omega_\lambda$ , and their mass difference is  $\hbar(\omega_\rho - \omega_\lambda) \approx 75$  MeV, which will be modified by  $H_{hyp}$  [4].

This difference in the spatial decomposition of the two  $J^P = 5/2^-$  states’ wave functions has the following decay implications:  $\Lambda^*(1830)$  couples weakly to  $\bar{K}N$  since the nucleon spatial wave function is symmetric under the interchange  $1 \leftrightarrow 2$ , whereas  $\Sigma^*(1775)$  couples easily to  $\bar{K}N$  for the same reason. When modifications due to  $H_{hyp}$  is included, the difference in the two observed decays widths are easily explained [4], as will be detailed in the next subsection. This example illustrates the close relations between the internal structure of the initial and final baryon and the magnitude of the corresponding decay width. With more precise experimental data one looks forward to be able to make similar arguments for mass differences and decay branching ratios for the other excited hyperon states.

### (c) Spatial Wave Function and the Decay Widths

As emphasized by Isgur and Karl even the ground state baryons have a complicated spatial wave function due to  $H_{hyp}$  as mentioned earlier. For example, in their NRQM the nucleon state has the following structure:

$$|N\rangle \simeq 0.90|^2S_S\rangle - 0.34|^2S'_S\rangle - 0.27|^2S_M\rangle - 0.06|^2D_M\rangle, \quad (5)$$

where  $|S'\rangle$  and  $|D\rangle$  are the excited S- and D- quark states of the harmonic oscillator. The subscripts  $S$  and  $M$  denote symmetric and mixed symmetry spatial states, respectively. Similarly, Isgur and Karl find the  $\Lambda(1116)$  state to be:

$$|\Lambda\rangle \simeq 0.93|^2S_S\rangle - 0.30|^2S'_S\rangle - 0.20|^2S_M\rangle - 0.03|^4D_M\rangle - 0.05|1,^2S_M\rangle. \quad (6)$$

Given present day experimental accuracies of the masses and decay branching ratios determinations, Isgur and Karl assume that the D-state components of the states have no practical consequences and can be neglected. The expressions in Eqs. (5) and (6) tell us that the ground state baryons are not pure symmetric  $|^2S_S\rangle$  states. They contain spatially mixed symmetry states, and the  $|^2S'_S\rangle$  and  $|^2S_M\rangle$  components of the ground state baryon octet will modify (sometimes strongly) the excited baryon to ground states decay widths. For example, by including the mixed symmetric component  $|^2S_M\rangle$  of the nucleon state, one finds the ratio of decay amplitudes [4]:

$$\frac{A(\Lambda^*(1830) \rightarrow \bar{K}N)}{A(\Sigma^*(1775) \rightarrow \bar{K}N)} \simeq -0.28. \quad (7)$$

The excited  $\Lambda^*$  and  $\Sigma^*$  states have similar mixed spatial states, again due to  $H_{hyp}$  and also due to the pseudo-scalar meson cloud surrounding the quark core in cloudy bag models. These mixed states will further affect the relative decay branching ratios of the excited hyperon states.

### (d) Electromagnetic Decays of the $\Lambda^*$ and $\Sigma^*$ states

In the first excited states, one quark is in a  $P$ -state relative to the two others which are in a relative  $S$ -state. In an electromagnetic decay to the ground state the  $P$ -state quark couples to the photon (or in strong decays to the outgoing meson, *e.g.*,  $\pi$ ,  $\bar{K}$  or  $\eta$ ). For example, the  $\Lambda^*(1520)$  state is a well established state and has the following decomposition in terms of  $SU_F(3)$  multiplets:

$$|\Lambda^*(1520)\rangle \simeq a|^2\mathbf{1}\rangle + b|^4\mathbf{8}\rangle + c|^2\mathbf{8}\rangle. \quad (8)$$

Different quark models give different values for the  $a$ ,  $b$  and  $c$  coefficients. Using the harmonic oscillator of the NRQM of Isgur and Karl find  $a = 0.92$ ,  $b = -0.04$ , and  $c = 0.39$  [4], which results in the following values for two electromagnetic widths  $\Gamma[\Lambda(1520) \rightarrow \Lambda\gamma] = 96$  keV and  $\Gamma[\Lambda(1520) \rightarrow \Sigma^0\gamma] = 74$  keV [8]. A cloudy bag model calculation produces the values  $a = 0.95$ ,  $b = -0.09$  and  $c = 0.30$ . The decay widths in the cloudy bag model, where the emitted photon also couple to the meson cloud, are  $\Gamma[\Lambda(1520) \rightarrow \Lambda\gamma] = 32$  keV,  $\Gamma[\Lambda(1520) \rightarrow \Sigma^0\gamma] = 49$  keV [7].

In Table 1, we compare several different quark model calculations of the decay rate  $\Gamma_\gamma$  for  $\Lambda(1520) \rightarrow \Lambda(1116) + \gamma$ . As can be read off from the Table 1, this rate is not only

Table 1: The evaluation of  $\Gamma_\gamma$  by several quark model calculations are given. The references to the various models can be found in [10]. The columns give the coefficients  $a$ ,  $b$  and  $c$  of the  $\Lambda(1520)$  wave functions, Eq.(8), found in the various publications as well as the structure of the ground state wave function  $\Lambda(1116)$  used in the different calculations. The “dash” means that values of the coefficients or the  $\Lambda(1116)$  state cannot be ascertained.

Models	a	b	c	$\Lambda(1116)$	$\Gamma_\gamma$ (keV)
NRQM	0.91	0.01	0.40	$ ^2S_S >$	96
NRQM (SU(6)–basis)	0.91	0.01	0.40	–	98
$\chi$ QM	0.91	0.01	-0.40	$ ^2S_S >$	85
$\chi$ QM	0.91	0.01	-0.40	mixed	134
NRQM (uds–basis)	–	–	–	mixed	154
MIT bag	0.86	0.34	-0.37	–	46
Cloudy bag	0.95	0.09	-0.29	$ ^2S_S >$	32
RCQM	0.91	0.01	0.40	mixed	215
Bonn–CQM	–	–	–	–	258

sensitive to the coefficients  $a$ ,  $b$ , and  $c$  in Eq.(8), but also to the  $\Lambda(1116)$  configuration mixing, which may change  $\Gamma_\gamma$  by 50% or more. The decay width  $\Gamma_\gamma$  is very difficult to measure and it is not very well determined [9]. The evaluations of  $\Gamma_\gamma$  in quark models where  $SU_F(3)$  is broken are very involved and it is desirable to have a more precise experimental determination of  $\Gamma_\gamma$  before one revisits such a calculation.

(e) **A short note on  $\Lambda(1405)$**

A question within quark models, which has not been resolved satisfactory, is: Why is  $\Lambda(1405)$  about 100 MeV below  $\Lambda(1520)$  in mass? If we assume that the  $\Lambda^*$  states are mainly three-quark states, quark models have serious problems generating this large observed spin-orbit-like mass splitting. Could a strong coupling of the lowest three-quark state with  $J^P = \frac{1}{2}^-$  to the meson-baryon decay channels (beyond how this is presently treated in cloudy bag models) explain this mass-splitting? Historically, Dalitz and Tuan [11] proposed that  $\Lambda(1405)$  is a  $K^-p$  bound state, *i.e.*, could  $\Lambda(1405)$  be like a quark molecule?. Could it have a large multi-quark (pentaquark) state component? A very readable recent paper on the arXiv by Molina and Döring [12] discusses the possible pole structure of  $\Lambda(1405)$ . This paper contains an overview of many theoretical publications, including lattice evaluations, regarding possible structure of  $\Lambda(1405)$ . Apart from recent measurements of the  $K^-p$  atom [13], most data on this subject are old. We urgently need better data to settle the numerous theoretical discussions regarding  $\Lambda(1405)$ .

### 3. Summary and Outlook

It is imperative that we can experimentally establish the mass spectrum of the lowest excited negative parity  $\Lambda^*$  and  $\Sigma^*$  states in order to enhance our understanding of how QCD operates

among the three “light” quarks,  $u$ ,  $d$  and  $s$ , and generates the masses and decay widths of the hyperons. The JLab proposed  $K_L^0$  beam scattering off a hydrogen target can access  $\Sigma^*$  states and could firmly establish some of the missing  $\Sigma^*$  states in Fig. 1. In order to explore the  $\Lambda^*$  states, the reaction  $\gamma + p \rightarrow K^+ \Lambda^*$  looks more promising. The  $\Sigma^*$  states decay to  $\bar{K}N$  or  $\pi\Sigma$  or possibly both, as well as  $\pi\Lambda$  according to theory estimates. Measurements of the branching ratios of these decays will further enhance our understanding of these states. At the moment our understanding of light quark confinement in QCD is very rudimentary. The suggested measurements would contribute to a clarification of this aspect of QCD.

#### 4. Acknowledgments

This work is supported in part by funds provided by the National Science Foundation, Grant No. PHY-1068305.

## References

- [1] P. Hoyer, P. Osland, H.G. Sander, T.F. Walsh, and P.M. Zerwas, Nucl. Phys. B **161**, 349 (1979).
- [2] J.R. Ellis and I. Karliner, Nucl. Phys. B **148**, 141 (1979).
- [3] K.A. Olive *et al.* (Particle Data Group), Chin. Phys. C **38**, 090001 (2014).
- [4] N. Isgur and G. Karl, Phys. Rev. Lett. **41**, 1269 (1978); Phys. Lett. B **74**, 353 (1978); Phys. Rev. D **18**, 4187 (1978); R. Koniuk and N. Isgur, Phys. Rev. D **21**, 1868 (1980).
- [5] A. De Rujula, H. Georgi, and S.L. Glashow, Phys. Rev. D **12**, 147 (1975).
- [6] F. Myhrer and J. Wroldsen, Rev. Mod. Phys. **60**, 629 (1988).
- [7] Y. Umino and F. Myhrer, Nucl. Phys. A **529**, 713 (1991), *ibid.* **554**, 593 (1993).
- [8] J.W. Darewych, M. Horbatsch, and R. Koniuk, Phys. Rev. D **28**, 1125 (1983).
- [9] S. Taylor *et al.*, Phys. Rev. C **71**, 054609 (2005); Yu.M. Antipov *et al.*, Phys. Lett. B **604**, 22 (2004); T.S. Mast *et al.*, Phys. Rev. Lett. **21**, 1715 (1968).
- [10] F. Myhrer, Phys. Rev. C **74**, 065202 (2006).
- [11] R.H. Dalitz and S.F. Tuan, Ann. Phys. **10**, 307 (1960).
- [12] R. Molina and M. Döring, arXiv:1512.05831 (2015).
- [13] M. Bazzi *et al.* (SIDDHARTA Collaboration), Phys. Lett. B **704**, 113 (2011).

## 2.8 Hadron Physics with High-Momentum Hadron Beams at J-PARC

Hiroyuki Noumi

*Research Center for Nuclear Physics (RCNP)*

*Osaka University*

*Osaka, 567-0047, Japan*

### Abstract

Baryon spectroscopy with heavy flavors provides unique opportunities to study internal motions of ingredients in baryons, from which we can learn the effective degrees of freedom to describe hadrons. We proposed an experiment on charmed baryon spectroscopy via the  $(\pi^-, D^{*-})$  reaction at the J-PARC high-momentum beam line. Mass spectrum from the ground state to highly-excited states of the excitation energy up to more than 1 GeV will be observed by means of a missing mass technique. Production cross sections and decay branching ratios of these states will be measured. It is worthy to compare how nature of baryons with different flavors changes. In particular, double-strangeness baryons,  $\Xi$ , are of interest. A neutral Kaon beam at JLab is unique to produce  $\Xi$  baryons. Hadron beams at J-PARC play complimentary roles to the neutral Kaon beam at JLab.

### 1. Baryon Spectroscopy with Heavy Flavors

“How hadrons are formed from quarks ?” is a fundamental question in hadron physics. We know that the quantum chromo-dynamics (QCD) is a fundamental theory to describe dynamics of quarks and gluons. However, it is still very hard to describe hadrons by solving the QCD equation in low energy because of its non-perturbative nature of the strong interaction, where the coupling constant becomes very large when the energy scale is close to the scale parameter  $\Lambda_{\text{QCD}}$ . Quarks drastically change their nature below  $\Lambda_{\text{QCD}}$ . Then, constituent quarks as effective degree of freedom to describe hadrons seem to work rather well. Actually, the constituent quark model well describes properties of hadrons in the ground state, such as masses, spin-flavor classifications, magnetic moment of octet baryons, and so on. However, it sometimes fails in excited states. In particular, not only recent reports on so-called exotic hadrons, such as  $X$ ,  $Y$ ,  $Z$ , and pentaquark states in heavy sector but also a long-standing puzzle in  $\Lambda(1405)$  indicate that we need a new aspect in describing hadrons. Internal correlations among ingredients of hadrons such as diquarks and hadron clusters are expected to play an important role. Since they are confined in a hadron, hadron spectroscopy to look into more details of internal structure or motions of the composites in hadrons is necessary.

Since the color magnetic interaction between quarks is proportional to the inverse of the quark mass, spin-dependent interactions to a heavy quark vanish in the heavy quark mass limit. In the heavy quark mass limit, a heavy quark spin and the spin of the other system become good quantum numbers. This is the so-called heavy quark symmetry of QCD. Let us consider a baryon with a heavy quark. A relative motion between two light quarks ( $\rho$  mode) and a collective motion of the light quark pair ( $\lambda$  mode) are separated in excited states, as illustrated in Fig. 1. This is known as the so-called isotope shift. These states are further split due to spin-dependent interactions between quarks [1]. The spin-correlation between



light quarks becomes stronger than those to a light quark and a heavy quark due to the heavy quark spin symmetry. Internal structure of the baryon with a heavy quark is characterized by the two light-quark (diquark) correlation. Nature of these baryons is reflected in mass, decay width (branching ratio), and production rate.

Therefore, we proposed an experimental study of charmed baryons via the  $(\pi^-, D^{*-})$  reaction on hydrogen [2] at the J-PARC high-momentum beam line. In the reaction, we reconstruct charmed baryons by means of missing mass technique. An excitation spectrum of charmed baryon states can be measured independent of their decay final states. We could also identify decay modes with detecting a decay particle together with scattered  $D^{*-}$  and identifying a daughter particle in a missing mass. A branching ratio (partial decay width) of the decay mode can be obtained rather easily. Branching ratios provide information on diquark motions of excited charmed baryons, as described later. This is an advantage of the missing mass method.

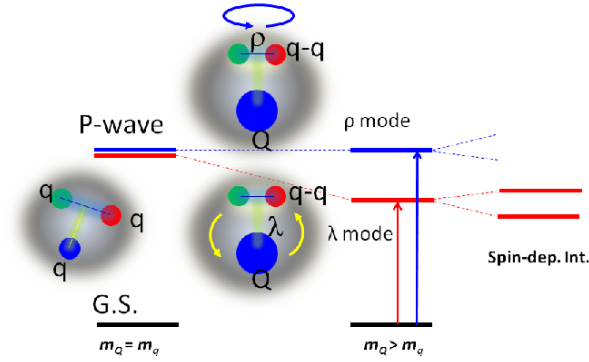


Figure 1: Schematic level structure of excited baryons with a heavy quark.

## 2. Beam Line

A new beam line, called high-momentum beam line, is being constructed in the Hadron Experimental Facility of the Japan Proton Accelerator Research Complex (J-PARC). It is branched from the slow extraction primary beam line in the switch yard. A small fraction of the primary beam is transported to the experimental area, located about 130 m downstream from the branch point, for the E16 experiment which aims at measuring spectral changes of vector mesons in nuclei [3].

The high-momentum beam line can deliver secondary beams if we install a production target at the branching point. The layout of the beam line magnets are arranged so as to transport secondary beams up to 20 GeV/c, as shown in Fig. 2. The beam line is carefully designed to realize a dispersive beam at the dispersive focal point, where a momentum and a horizontal position of the secondary particles are strongly correlated. Fig. 3-top demonstrates the correlation calculated by the DECAY TURTLE [4]. We place 3 sextupole magnets to reduce second order aberrations and to sharpen the correlation. The calculation tells that a momentum resolution of 0.12% is expected by measuring a beam position with a spatial resolution

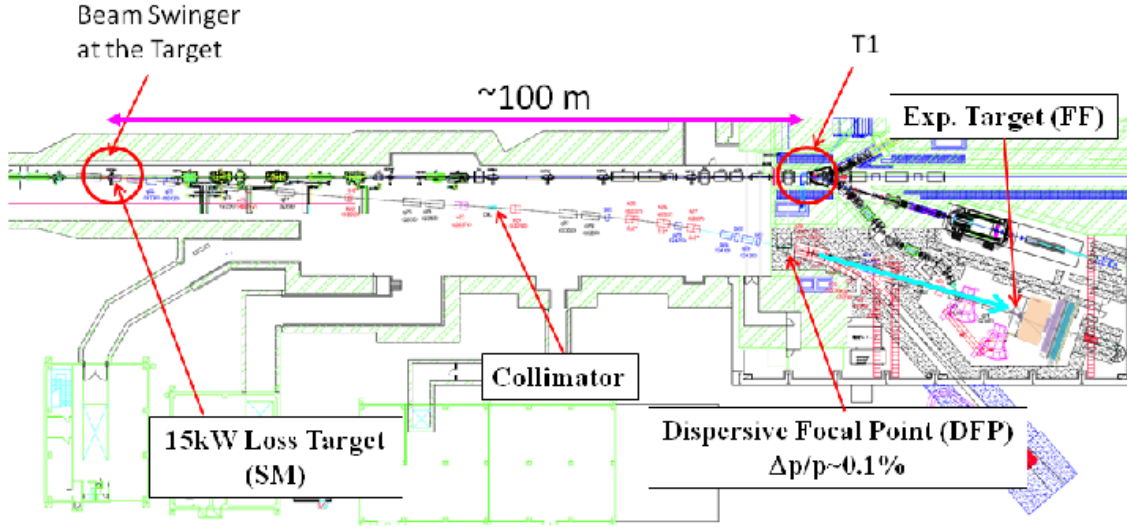


Figure 2: High-momentum beam line at the J-PARC Hadron Experimental Facility.

of 1 mm, as illustrated in Fig. 3-bottom. The momentum resolution is mostly determined by a beam size at the production target (actually, its image at the dispersive focal point). We assume the beam size of 1 mm in  $\sigma$  in the horizontal direction at the production target.

The beam line length and acceptance are 133 m and 1.5 msr·%. We estimated intensities of secondary particles by the so-called Sanford-Wang formula [5], assuming that a 6-cm thick platinum target is irradiated by a 30-GeV proton beam of 30 kW (15-kW beam loss at the target), as shown in Fig. 4. Here, a production angle for negative and positive particles are assumed to be 0 degree and 3.9 degrees. We expect that the negative pion beam intensity is more than  $10^7$  per second at 20 GeV/c.

### 3. Spectrometer

An incident pion momentum will be measured at a resolution as good as  $\sim 0.1\%$  in the high-momentum beam line. We designed a spectrometer system to reconstruct scattered  $D^{*-}$  from its decay chain of  $D^{*-} \rightarrow \bar{D}^0 \pi^-$ ,  $\bar{D}^0 \rightarrow K^+ \pi^-$ , as shown in Fig. 5. The spectrometer is based on a single dipole magnet with a circular pole of 2.1 m in diameter and a gap of 1 m. A rigidity of the magnet is 2.3 Tm. A typical momentum resolution is expected to be  $\sim 0.5\%$  at 5 GeV/c. A liquid hydrogen target of 57 cm in length (4 g/cm<sup>2</sup> in thickness) will be placed close to the entrance face of the magnet. Fiber trackers with 1 mm scintillating fiber will be placed just after the target. A set of drift chambers will be placed surrounding the pole and after the magnet to detect scattered particles with lower and higher momenta, respectively. A ring image Cherenkov counter (RICH) with dual radiators of aerogel with a reflection index of 1.04 and a C<sub>4</sub>F<sub>10</sub> gas with an index of 1.00137 will be used for identifying pion, Kaon, and proton in a wide momentum range from 2 to 16 GeV/c [6]. Time of flight counters will be placed to identify scattered particles with lower momenta. The spectrometer

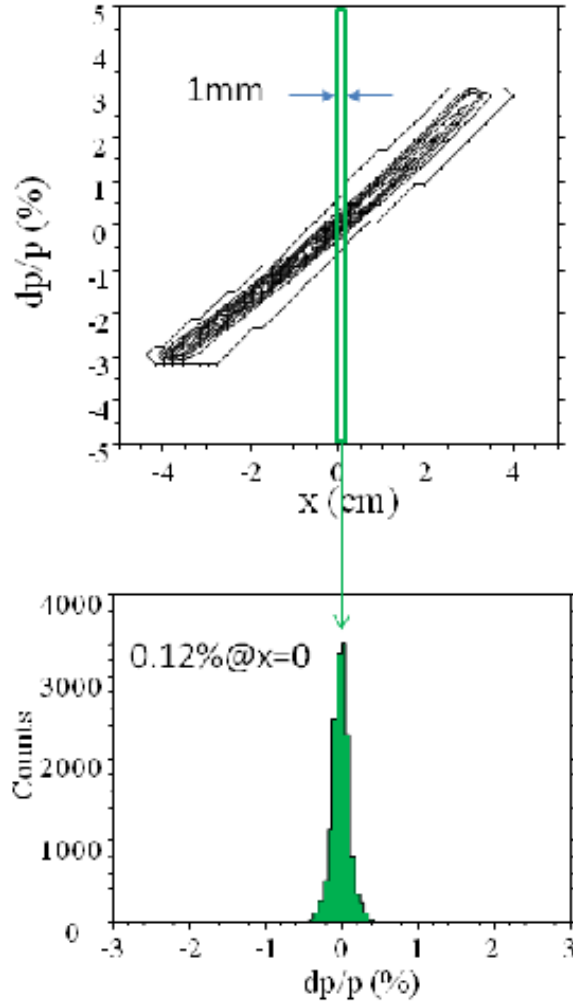


Figure 3: Top: correlation between beam momentum and position at the dispersive focal point. Bottom: momentum distribution within a 1-mm space in horizontal at the beam center.

covers about 60 % of solid angle for scattered  $D^{*-}$  and about 80 % for decay pions from produced charmed baryons.

Identifying two charmed mesons from the decay final state,  $K^+\pi^-\pi^-$ , we could reduce huge background events of  $K^+\pi^-\pi^-$  productions by a factor of  $\sim 10^6$ . Expected charmed baryon spectrum is demonstrated by a Monte Carlo simulation in Fig. 2. Here, the states reported by the Particle Data Group [7] are taken into account. One sees that a series of charmed baryons from the ground state to highly excited states with higher spins are clearly observed.

We found that the production cross sections of the excited states relative to that of the ground state do not go down. This is an important feature of the  $(\pi^-, D^{*-})$  reaction. We estimated the production rates of the excited charmed baryons in the framework of a  $D^*$  exchange in the  $t$ -channel at a very forward scattering angle [8]. Employing harmonic oscillator wave

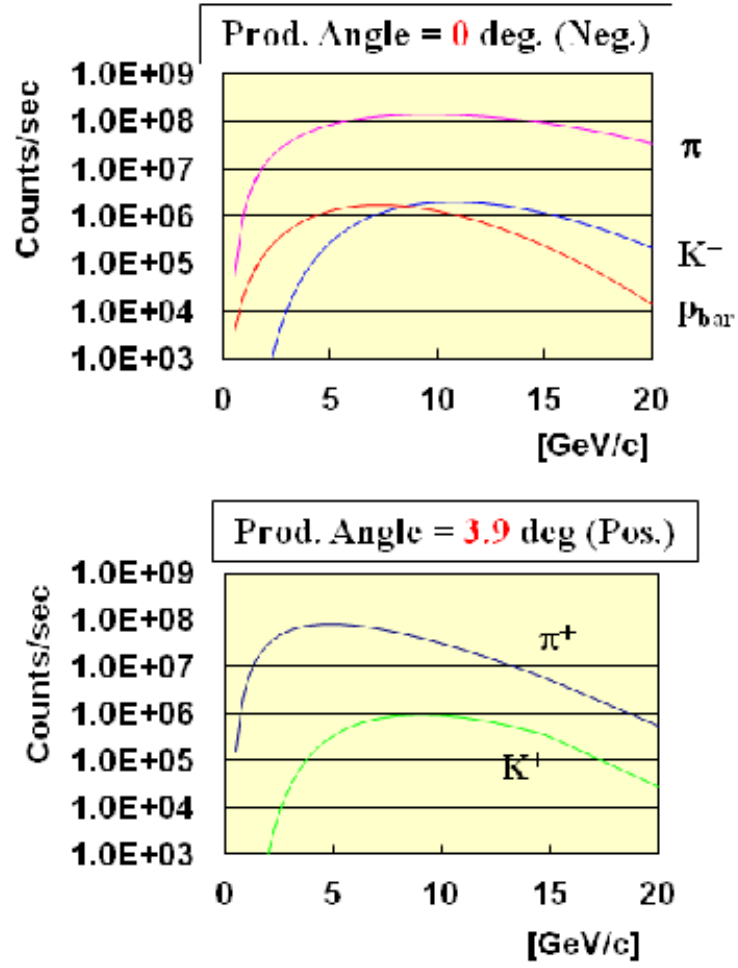


Figure 4: Intensities of secondary beams calculated by Sanform-Wang's formula [5]. See text for assumed conditions.

functions of constituent quarks in the initial and final baryons, we estimate that the production rate,  $R$ , is expressed as

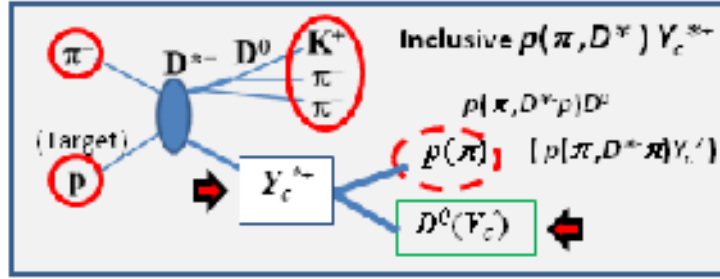


Figure 5: Top: reaction scheme to identify charmed baryons and their decays by means of a missing mass technique. Bottom: designed spectrometer layout.

where  $\phi_i$  and  $\phi_f$  represent initial and final states of baryons. An effective momentum transfer  $q_{eff}$ , taking a recoil effect of the residual  $ud$  diquark, is as large as  $1.4 \text{ GeV}/c$  in the  $p(\pi^-, D^{*-})$  reaction at the pion beam momentum of  $20 \text{ GeV}/c$ . An oscillator parameter  $A$  is taken to be  $\sim 0.4 \text{ GeV}$ , which corresponds to the inverse of a typical baryon size. In this reaction, a  $u$  quark in a proton is converted to a  $c$  quark in the final charmed baryon in the reaction. The  $ud$  diquark behaves as a spectator. Thus, this reaction well populates  $\lambda$ -mode excited states, where an angular momentum  $L$  is introduced between a  $c$  quark and a diquark. Due to a large factor of  $(q_{eff}/A)$ , an absolute value of the production cross section is reduced very much. On the other hand, the ratio of  $R$  for an excited state with  $L$  to that for the ground state ( $L = 0$ ) is  $\sim (q_{eff}/A)^L$ , which does not go down even for  $L > 0$ . The  $(\pi^-, D^{*-})$  reaction is suitable to populate higher spin states.

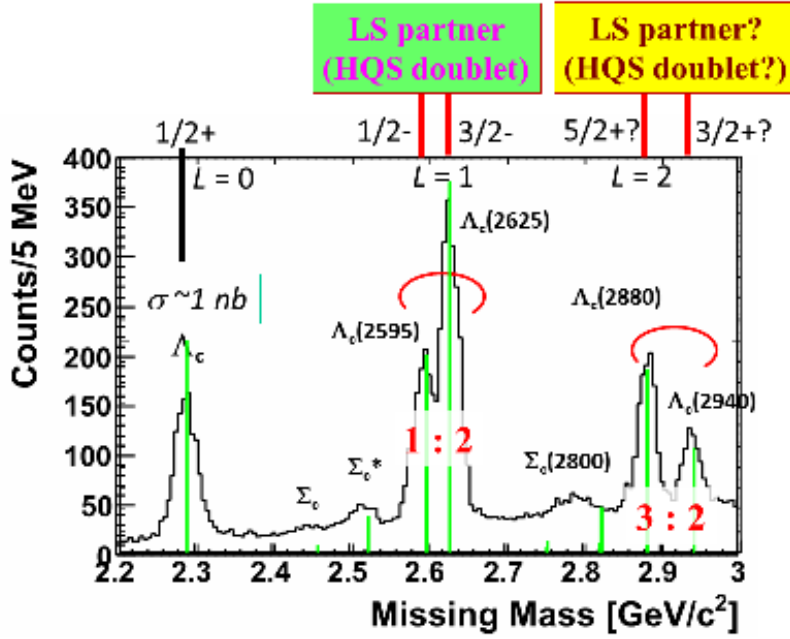


Figure 6: Expected missing mass spectrum in the  $(\pi^-, D^{*-})$  reaction on hydrogen.

The  $\lambda$ -mode  $\Lambda_c$  baryons with  $L > 0$  has two spin states coupled to  $L \pm 1/2$ . These states are LS partners. Therefore, we find that the production ratio of the two states should be  $L:L+1$ . Reversely, we can determine the spin-parity of the  $\lambda$ -mode  $\Lambda_c$  baryons by measuring the cross sections.

So far, a production cross section of  $\Lambda_c$  in the  $p(\pi^-, D^{*-})$  reaction has not been measured. Only upper limit, 7 nb, was reported in 1985 [9]. We estimate the production cross section to be a few nano barn at incident pion momentum of 20 GeV/c [10] by employing a framework of reggeon exchange model, which describes binary peripheral reactions well at high energy. We expect to observe 1000 events of the ground state  $\Lambda_c$  production for 100 days.

Decay branching ratios carry information on internal structure of a baryon. The ratio of decay into a heavy meson and a light baryon to that into a light meson and a heavy baryon is of particular interesting. The former is expected to be dominant, if it is energetically allowed, in  $\lambda$ -mode excited baryon, which is an orbital excitation between a heavy quark and a light diquark. The situation is to be opposite in  $\rho$ -mode. One can find a suggestion in the case of  $\Lambda(1520)$ , which is a P-wave hyperon with spin-parity of  $3/2^-$ . In  $\Lambda(1520)$  dominantly decays into a Kaon and a nucleon, while a Q-value in the decay is smaller than that in the decay into a pion and a  $\Sigma$  hyperon. The  $\Lambda(1520)$  hyperon can be classified as a  $\lambda$ -mode hyperon although  $\rho/\lambda$  mode classification has yet to be established in any baryon excited states. Systematic measurements of decay branching ratios for the excited charmed baryons are of particular importance.

#### 4. Baryon Spectroscopy with Different Flavors

The above-mentioned discussion on internal structure of baryons with a single heavy quark can be extended to baryons with double heavy quarks. In the case of double heavy-quark baryons, the order of the excitation energy for  $\lambda$  and  $\rho$  modes interchanges. Here, the  $\lambda$  mode is a motion of the light quark to the heavy-quark pair, and the  $\rho$  mode is a relative motion between two heavy quarks. One expects that a  $\lambda$  mode excited state favors a decay into a light meson and a double heavy-quark baryon. A  $\rho$  mode state may dominantly decay into a single-heavy meson and a single-heavy baryon.

A several states of cascade hyperons  $\Xi$  are listed [7]. Little is known about their spin-parities and decay branching ratios. The  $(\bar{K}, K^+)$  reaction is one of promising reactions to produce cascade hyperons. Since the  $(\bar{K}, K^+)$  reaction has no single-meson exchange process in  $t$  channel,  $\Xi$  productions at backward angles are expected to play a principal role.  $\rho$ -mode  $\Xi$  hyperons may be populated well through  $u$ -channel process. It is quite worthy to measure production rates and decay branching ratios of  $\Xi$  hyperons.

#### 5. Concluding Remark

- Masses, decay branching ratios, and production rates of baryons with heavy flavors provide information on internal motions of ingredients, such as diquark correlation.
- We proposed an experiment on charmed baryon spectroscopy via the  $(\pi^-, D^{*-})$  reaction at the J-PARC high-momentum beam line. We will measure a mass spectrum of charmed baryons from the ground state to highly excited states in an excitation energy range of more than 1 GeV by means of a missing mass technique. Production cross sections and decay branching ratios of produced charmed baryons will be measured.
- The present argument on baryon spectroscopy with a charm quark should be extended to those with different flavors. In particular,  $\Xi$  baryons are of interest as double-heavy quark system that can be accessible in experiment. Neutral Kaon beam at JLab is unique in hadron spectroscopy and plays a complimentary role to the J-PARC. Constructive collaboration to integrate efforts to realize hadron spectroscopy with hadron beams in JLab and J-PARC is desired.

## References

- [1] T. Yoshida, E. Hiyama, A. Hosaka, M. Oka, and K. Sadato, Phys. Rev. D **92**, 114029 (2015).
- [2] H. Noumi *et al.*, *Charmed Baryon Spectroscopy via the  $(\pi^-, D^{*-})$  reaction*, J-PARC P50 Proposal, 2012:  
[http://www.j-parc.jp/researcher/Hadron/en/Proposal\\_e.html#1301](http://www.j-parc.jp/researcher/Hadron/en/Proposal_e.html#1301)
- [3] S. Yokkaichi *et al.*, *Electron pair spectrometer at the J-PARC 50-GeV PS to explore the chiral symmetry in QCD*, J-PARC E16 Proposal, 2006:  
[http://www.j-parc.jp/researcher/Hadron/en/Proposal\\_e.html\#0606](http://www.j-parc.jp/researcher/Hadron/en/Proposal_e.html\#0606)

- [4] Urs Rohrer, *Compendium of Transport Enhancements*,  
[http://aea.web.psi.ch/Urs\\_Rohrer/MyWeb/trancomp.htm](http://aea.web.psi.ch/Urs_Rohrer/MyWeb/trancomp.htm) .
- [5] J.R. Sanford and C.L. Wang, BNL 11279 and BNL 11479, (1967); C.L. Wang, Phys. Rev. Lett. **25**, 1068 (1970).
- [6] T. Yamaga *et al.*, Nucl. Instr. Meth. A **776**, 36 (2014).
- [7] K.A. Olive *et al.* (Particle Data Group), Chin. Phys. C **38**, 090001 (2014).
- [8] S.H. Kim, A. Hosaka, H.C. Kim, H. Noumi, and K. Shirotori, Prog. Theor. Exp. Phys. **103D01** (2014).
- [9] J.H. Christensen *et al.*, Phys. Rev. Lett. **55**, 154 (1985).
- [10] S.H. Kim, A. Hosaka, H.C. Kim, and H. Noumi, Phys. Rev. D **92**, 094021 (2015).



## 2.9 Cascade Production in $\bar{K}$ - and Photon-Induced Reactions

Kanzo Nakayama and B.C. Jackson

*Department of Physics and Astronomy  
University of Georgia  
Athens, GA 30602, U.S.A.*

Yongseok Oh

*Department of Physics  
Kyungpook National University  
Daegu 702-701, Korea &  
Institute for Nuclear Studies and Department of Physics  
The George Washington University  
Washington, DC 20052, U.S.A.*

Helmut Haberzettl

*Institute for Nuclear Studies and Department of Physics  
The George Washington University  
Washington, DC 20052, U.S.A.*

### Abstract

The  $\bar{K} + N \rightarrow K + \Xi$  and  $\gamma + N \rightarrow K + K + \Xi$  reactions are investigated in a combined analysis within an effective Lagrangian approach to learn about the basic features of these reactions. Such a study should help construct more complete reaction models within a full coupled-channels approach to extract relevant physics information from forthcoming experimental data in the multi-strange particle physics programs at modern experimental facilities including J-PARC and JLab. Among the above-threshold three- and four-star  $S = -1$  resonances considered in this work, a minimum of three resonances, namely  $\Sigma(2030)7/2^+$ ,  $\Sigma(2265)5/2^-$ , and  $\Lambda(1890)3/2^+$ , are found to be required to reproduce the available data in the considered  $\bar{K}$ - and photon-induced reactions. Among them, the  $\Sigma(2030)7/2^+$  resonance is shown to play a clear and important role in both reactions.

### 1. Introduction

One of the major interests in baryon spectroscopy in the strangeness sector is the possibility to learn about the properties of the so-called multi-strangeness baryons, *i.e.*, baryons with strangeness quantum number  $S < -1$ . Although the multi-strangeness baryons have played an important role in the development of our understanding of strong interactions, and thus should be an integral part of any baryon spectroscopy program, the current knowledge of these baryons is still extremely limited. In fact, the SU(3) flavor symmetry allows as many  $S = -2$  baryon resonances, called  $\Xi$ , as there are  $N$  and  $\Delta$  resonances combined ( $\sim 27$ ); however, until now, only eleven  $\Xi$  baryons have been discovered [1]. Among them, only three [ground state  $\Xi(1318)1/2^+$ ,  $\Xi(1538)3/2^+$ , and  $\Xi(1820)3/2^-$ ] have their quantum numbers assigned. This situation is mainly due to the fact that multi-strangeness particle productions have relatively low yields. For example, if there are no strange particles in the initial

state,  $\Xi$  is produced only indirectly and the yield is only of the order of nb in the photoproduction reaction [2], whereas the yield is of the order of  $\mu\text{b}$  [3] in the hadronic  $\bar{K}$ -induced reaction, where the  $\Xi$  is produced directly because of the presence of an  $S = -1$   $\bar{K}$  meson in the initial state. The production rates for  $\Omega$  baryons with  $S = -3$  are much lower [4]. The initiative to having a  $K_L$  beam at the Thomas Jefferson National Accelerator Facility (JLab) in particular to study, among other things, multi-strangeness baryon spectroscopy is, therefore, extremely valuable.

The study of multi-strangeness baryons has started to attract renewed interests recently. Indeed, the CLAS Collaboration at JLab plans to initiate a  $\Xi$  spectroscopy program through the photoproduction reaction using the upgraded 12-GeV machine, and measure exclusive  $\Omega$  photoproduction for the first time [5]. Some data for the production of the  $\Xi$  ground state, obtained from the 6-GeV machine, are already available [2]. J-PARC is going to study the  $\Xi$  baryons via the  $\bar{K} + N \rightarrow K + \Xi$  process (which is the reaction of choice for producing  $\Xi$ ) [6, 7] in connection to its program proposal for obtaining information on  $\Xi$  hypernuclei spectroscopy. It also plans to study the  $\pi + N \rightarrow K + K + \Xi$  reaction as well as  $\Omega$  production. At the FAIR facility of GSI, the reaction  $\bar{p} + p \rightarrow \bar{\Xi} + \Xi$  will be studied by the PANDA Collaboration [8].

In the present work, we concentrate on the production of  $S = -2$   $\Xi$ , in particular, on the production reaction processes of the ground state  $\Xi$ :

$$\bar{K} + N \rightarrow K + \Xi, \quad (1)$$

$$\gamma + N \rightarrow K + K + \Xi. \quad (2)$$

The  $\bar{K}$ -induced reaction (1) has been studied experimentally mainly throughout the 60's which was followed by several measurements made in the 70's and 80's. The existing data are rather limited and suffer from large uncertainties. There exist only very few early attempts to understand this reaction. Recent calculations are reported by Sharov *et al.* [9] and by Shyam *et al.* [10]. Although the analyses of both works are based on very similar effective Lagrangian approaches, the number of  $S = -1$  hyperon resonances included as intermediate states are different. While in Ref. [9] only the  $\Sigma(1385)$  and  $\Lambda(1520)$  were considered in addition to the above-threshold  $\Sigma(2030)$  and  $\Sigma(2250)$  resonances, in Ref. [10] eight of the 3- and 4-star  $\Lambda$  and  $\Sigma$  resonances with masses up to 2.0 GeV have been considered. While the authors of Ref. [9] pointed out the significance of the above-threshold resonances, the authors of Ref. [10] have found the dominance of the sub-threshold  $\Lambda(1520)$  resonance. Reaction (2) has been also considered by Magas *et al.* [11] within the coupled-channels Unitarized Chiral Perturbation approach when determining the parameters of the next-to-leading-order interactions. The authors of Ref. [11] have added the  $\Sigma(2030)$  and  $\Sigma(2250)$  resonances into their calculation to improve the fit quality to the total cross section data. Also the Argonne-Osaka group [12, 13] reported applying their Dynamical Coupled Channels (DCC) approach to  $\bar{K}$ -induced two-body reactions for center-of-momentum energies up to  $W = 2.1$  GeV. Some of the model-independent aspects of the reaction (1) have been studied recently by the present authors [14, 15].

We note here that the proper identification of resonances and the reliable extraction of their parameters require detailed knowledge of the analytic structures of the scattering amplitude

that, to date, can only be obtained through a full coupled-channel treatment, such as that of Refs. [12, 13]. However, because the currently available data in the  $K\Xi$  channel are scarce and of low quality, they do not provide sufficient constraints for the model parameters to permit an in-depth analysis of that channel. In this context, we mention that a coupled-channel partial-wave analysis of  $\bar{K}$ -induced reactions up to  $W = 2.1$  GeV has also been performed recently by the Kent State University group [16, 17] which includes seven reaction channels, but not the  $K\Xi$  channel.

The available experimental data for the photon-induced reaction (2) are also very scarce. In fact, the only data available for this reaction in the resonance energy region are those from JLab [2] using the 6-GeV machine. Specifically, the total cross sections, both the  $K$  and  $\Xi$  angular distributions and the  $KK$  and  $K\Xi$  invariant mass distributions are available. Theoretical studies of this reaction are scarce, too. To date, the work of Refs. [18, 19] is the only one that analyzes the JLab data of Ref. [2].

One of the purposes of the present work is to search for a clearer evidence of the  $S = -1$  hyperon resonances in reactions (1) and (2). However, we emphasize that our main interest here lies not so much in the accurate extraction of  $S = -1$  hyperon resonance parameters, but in an exploratory study to learn about the pertinent reaction mechanisms and, in particular, to identify the resonances that come out to be most relevant for the description of the existing  $\Xi$  production data. In fact, with the exception of the  $\Sigma(2250)$  resonance, whose mass was adjusted slightly to better reproduce the observed bump structure in the total cross section in the charged  $\Xi$  production, the masses and widths of the resonances incorporated here are taken from other sources. Only the product of the coupling constants and the cutoff parameters in the corresponding form factors are adjusted in the present work.

## 2. Formalism

In the present work, we perform an analysis of the existing data based on a relativistic effective Lagrangian approach that includes a phenomenological contact amplitude which accounts for the rescattering contributions and/or unknown (short-range) dynamics that have not been included explicitly into the model. For photoproduction, local gauge invariance as dictated by the appropriate generalized Ward-Takahashi identity is strictly enforced [20]. Figures 1 and 2 display the Feynman diagrams considered in the present work for the  $\bar{K}$ - and photon-induced reactions, (1) and (2), respectively. Further details of the model can be found in Ref. [21] for reaction (1) and, in Refs. [18, 19], for reaction (2). While the tree-level model used here is not very sophisticated, it captures the essential aspects of the processes in question. As such, the use of a simplified and flexible model is particularly well suited for a situation, such as for the reactions (1) and (2), where scarce and/or poor data prevent a more detailed and complete treatment. The present study is our first step toward building a more complete reaction model capable of reliably extracting the properties of hyperons from the forthcoming experimental data, in addition to providing some guidance for planning future experiments.

## 3. Results

We now turn to a selected set of results of the present work which treats the reactions (1) and (2) consistent with each other. It should be mentioned that, although similar, the results

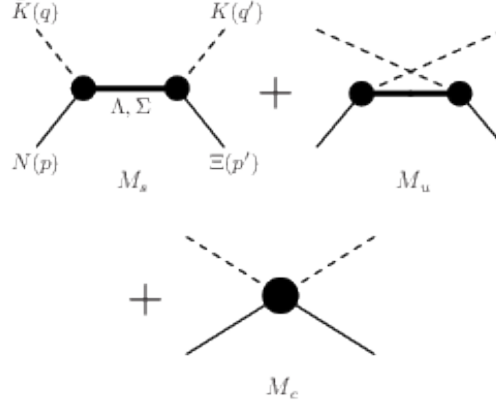


Figure 1: Diagrams describing the amplitude for reaction (1) in the present calculation. The labeling of the external legs of the  $s$ -channel diagram,  $M_s$ , follows the reaction equation (2); the labels apply correspondingly also to the external legs of the  $u$ -channel diagram,  $M_u$ , and the contact term  $M_c$ . The intermediate hyperon exchanges,  $\Lambda$  and  $\Sigma$ , indicated for  $M_s$  also appear in  $M_u$ . The details of the formalism, including the contact amplitude,  $M_c$ , are given in Ref. [21].

we show here differ from those shown in Refs. [18, 19, 21], for the model parameters have been readjusted to reproduce the available data for both reactions considered simultaneously. As far as the  $S = -1$  hyperon contributions are concerned, our analysis reveals that a minimum of three above-the-threshold resonances, namely the  $\Sigma(2030)7/2^+$ ,  $\Sigma(2250)5/2^-$  and  $\Lambda(1890)3/2^+$  resonances, in addition to the  $\Sigma(1385)3/2^+$  and the ground states  $\Lambda(1116)$  and  $\Sigma(1193)$ , suffice to reproduce all the available data in both the  $\bar{K} + N \rightarrow K + \Xi$  and  $\gamma + N \rightarrow K + K + \Xi$  reactions.

#### (a) $\bar{K} + N \rightarrow K + \Xi$ Reaction

In Fig. 3, we illustrate the amount of the above-threshold resonance contributions of the present model to the total cross sections in reaction (1). We do this by comparing the full results (blue solid curves) to the result found by switching off one resonance at a time. We see in Fig. 3(a) that the largest effect of  $\Sigma(2030)$  on the cross sections is in the range of  $W \sim 2.0$  to  $2.4$  GeV. This resonance is clearly needed in our model to reproduce the data. It also affects the recoil polarization as will be discussed later. We note that the present model yields the product of the branching ratios  $\text{Br}(\Sigma(2030) \rightarrow KN) \times \text{Br}(\Sigma(2030) \rightarrow K\Xi) \approx 15.6\%$  which may be contrasted with the corresponding values of  $\approx 16.1\%$  (model A) and  $\approx 20.4\%$  (model B) extracted in Ref. [13] within a DCC approach.<sup>1</sup> The  $\Lambda(1890)$  affects the total cross section in the range of  $W \sim 1.9$  to  $2.1$  GeV, and the  $\Sigma(2250)5/2^-$  contributes around  $W \sim 2.2$  GeV, where it is needed to reproduce the observed bump structure. A more accurate data set is clearly needed for a more definitive answer about the roles of the  $\Lambda(1890)$  and  $\Sigma(2250)$  resonances. Figure 3(b), for the neutral  $\Xi^0$  production, also shows a similar feature observed in the  $\Xi^-$  case for the  $\Sigma(2030)$  resonance. Here, the influence of the

<sup>1</sup>Note that only the product of the  $KYN$  and  $KY\Xi$  coupling constants ( $Y = \Lambda, \Sigma$  resonances) is sensitive to the data in the present model.

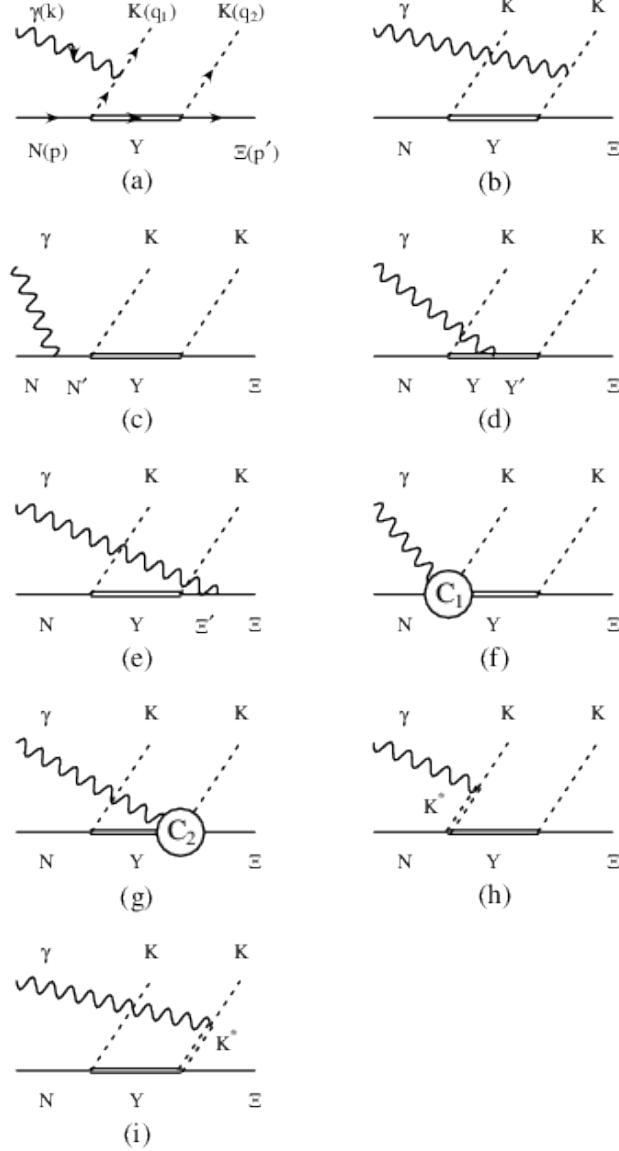


Figure 2: Diagrams contributing to the reaction mechanism of reaction (2). The intermediate baryon states are denoted as  $N'$  for the nucleon and  $\Delta$  resonances,  $Y, Y'$  for the  $\Lambda$  and  $\Sigma$  resonances, and  $\Xi'$  for  $\Xi(1318)$  and  $\Xi(1530)$ . The intermediate mesons in the  $t$ -channel are  $K$  [(a) and (b)] and  $K^*$  [(h) and (i)]. The diagrams (f) and (g) contain the generalized contact currents that maintain gauge invariance of the total amplitude. Diagrams corresponding to (a)–(i) with  $K(q_1) \leftrightarrow K(q_2)$  are also understood. The details of the formalism, including the contact amplitude,  $M_c$ , are discussed in Refs. [18, 19].

$\Sigma(2250)5/2^-$  is smaller and that of the  $\Lambda(1890)$  is hardly seen. Recall that there is no  $u$ -channel  $\Lambda$  contribution in the neutral  $\Xi^0$  production.

A peculiar feature of the  $K^- + p \rightarrow K^+ + \Xi^-$  process is that it is dominated by the  $P$  and  $D$  partial-waves (not shown here). In particular, the  $P$ -wave dominates the total

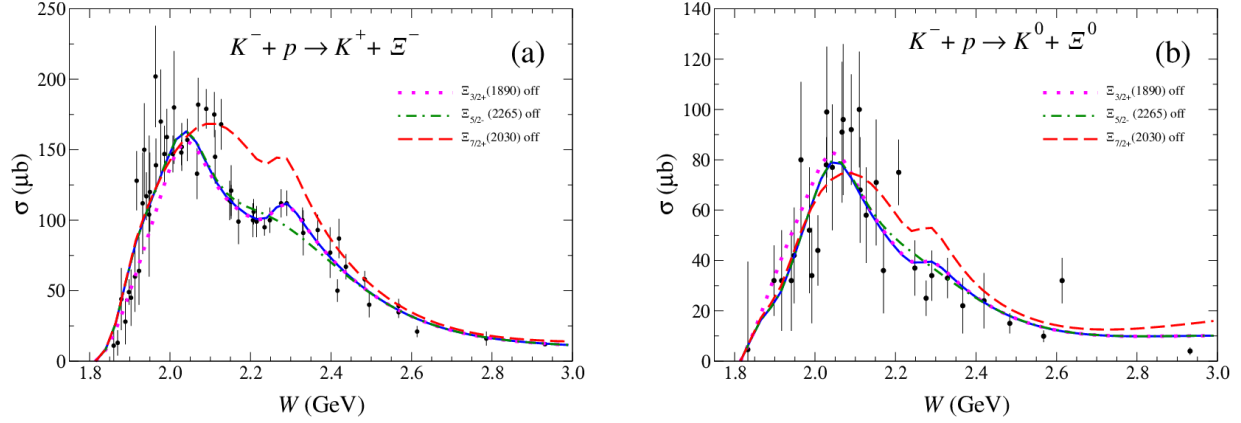


Figure 3: Total cross section results with individual resonances switched off (a) for  $K^- + p \rightarrow K^+ + \Xi^-$  and (b) for  $K^- + p \rightarrow K^0 + \Xi^0$ . The blue solid lines represent the full result. The red dashed lines, which almost coincide with the blue lines represent the result with  $\Lambda(1890)$  switched off. The green dash-dotted lines represent the result with  $\Sigma(2030)$  switched off and the magenta dash-dash-dotted lines represent the result with  $\Sigma(2250)5/2^-$  switched off. The data are the digitized version from Ref. [9].

cross section even down to energies very close to threshold. This is also corroborated by the DCC calculation of Ref. [12]. The experimental total cross section data ( $\sigma$ ) divided by the magnitude of the relative three-momentum in the final state ( $p'$ ),  $\sigma/p'$ , as a function of  $p'^2$ , reveal essentially a linear dependence near threshold, a model-independent indication of the  $P$ -wave contribution.

The results for the recoil polarization asymmetry multiplied by the cross section are shown in Fig. 4. Overall, we reproduce the data reasonably well. We also find that the results shown at  $W = 2.11$  GeV are still significantly affected by the  $\Sigma(2030)$ . This corroborates the findings of Ref. [9]. An interesting observation here is that, although small, the measured recoil polarization asymmetry is finite and non-vanishing. This offers an opportunity to measure the parity of the ground state  $\Xi$  which has never been measured — its positive parity as assigned by the Particle Data Group stems from quark-model predictions [1]. The reflection symmetry in the reaction plane implies that the target and recoil polarization asymmetries,  $T$  and  $P$ , respectively, in reaction (1) are related to each other by [14]

$$T = \pi_{\Xi} P, \quad (3)$$

where  $\pi_{\Xi}$  stands for the parity of the  $\Xi$  hyperon.

We also show in Fig. 5 our prediction for the total cross section in the  $K_L + p \rightarrow K^+ + \Xi^0$  reaction. Unlike the other reaction channels considered above, this channel serves as a total isospin  $I = 1$  filter, for no contribution of  $I = 0$  is present. However, we note that the isoscalar  $\Lambda$  hyperons still contribute to this reaction via the  $u$ -channel process.

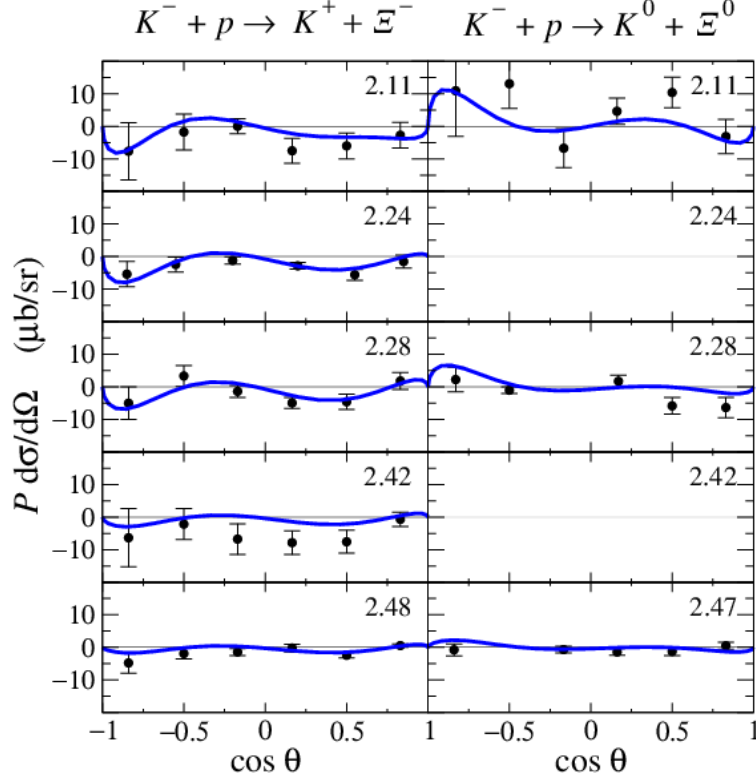


Figure 4: The recoil asymmetry multiplied by the cross section,  $P \frac{d\sigma}{d\Omega}$ , for both the  $K^- + p \rightarrow K^+ + \Xi^-$  and  $K^- + p \rightarrow K^0 + \Xi^0$  reactions. The blue solid lines represent the full results of the current model. Data are the digitized version from Ref. [9].

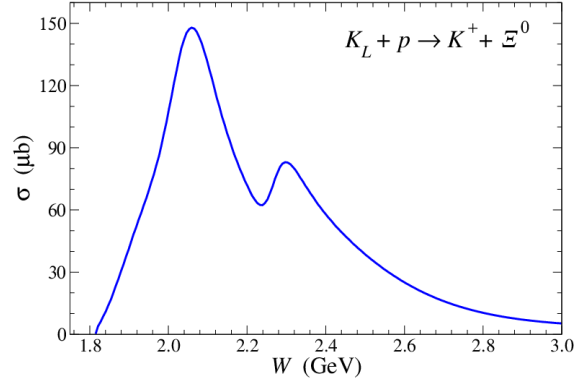


Figure 5: Prediction for the total cross section in the  $K_L + p \rightarrow K^+ + \Xi^0$  reaction.

(b)  $\gamma + N \rightarrow K + K + \Xi$  Reaction

Figures 6(a),(b) display the  $K^+$  and  $\Xi^-$  angular distributions, respectively, in the center-of-mass frame for the reaction  $\gamma + p \rightarrow K^+ + K^+ + \Xi^-$ . Overall, the data are reproduced very well. The same figures also show the results when the  $t$ -channel  $K$ -exchange current diagrams [cf. Fig. 2(a),(b)] involving the  $S = -1$  hyperon resonances are switched

off. We see that they are crucial in providing the observed behavior of the measured angular distributions.

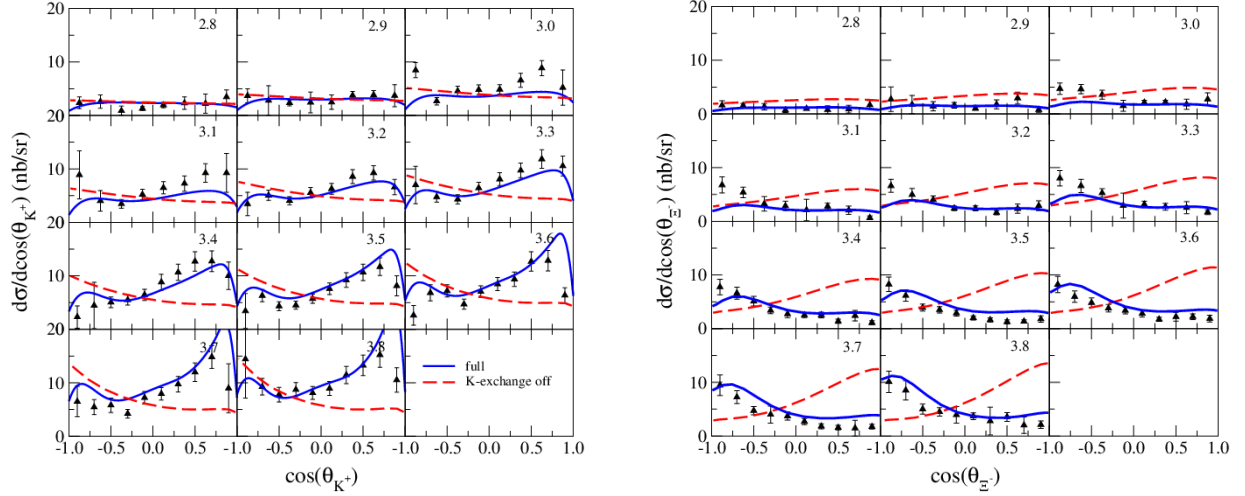


Figure 6: Differential cross sections for the reaction  $\gamma + p \rightarrow K^+ + K^+ + \Xi^-$  in the center-of-mass frame of the system. Left panel:  $K^+$  angular distribution. Right panel:  $\Xi^-$  angular distribution. The blue solid lines represent the full result. The red dashed lines represent the result with the  $t$ -channel  $K$ -exchange currents [cf. Fig. 2(a) and (b)] switched off. The number in the upper right corner in each graph denotes the incident photon energy in units of GeV in the laboratory frame. The data are from Ref. [2].

The results for the  $K^+\Xi^-$  invariant mass distributions are shown in Fig. 7. It reveals the important role of the  $\Sigma(2030)$  and  $\Lambda(1890)$  resonances in reproducing the experimental data. We found that the  $\Sigma(2250)$  resonance has a minor effect here.

#### 4. Conclusion

In this work we have presented a combined analysis of the  $\bar{K} + N \rightarrow K + \Xi$  and  $\gamma + N \rightarrow K + K + \Xi$  reactions within an effective Lagrangian approach. All the currently available data, in both the  $K^- + p \rightarrow K^+ + \Xi^-$  and  $K^- + p \rightarrow K^0 + \Xi^0$  processes, are well reproduced by the present model overall, and some of the basic features of the ground state  $\Xi$  production in these reaction processes have been understood.

The above-threshold resonances  $\Lambda(1890)$ ,  $\Sigma(2030)$ , and  $\Sigma(2250)$  are required to achieve a good fit quality of the  $K^-$ -induced reaction data. Among them, the  $\Sigma(2030)$  resonance is the most critical one. This resonance affects not only the cross sections but also the recoil asymmetry. More accurate data are required before a more definitive answer can be provided for the role of the  $\Lambda(1890)$  and  $\Sigma(2250)$  resonances. In this regard, the multi-strangeness hyperon production programs using an intense anti-Kaon beam at J-PARC and JLab are of particular relevance in providing the much needed higher-precision data for the  $\bar{K}$ -induced reaction. While it may perhaps not be entirely clear which role any particular resonance plays for the  $K^- + N \rightarrow K + \Xi$  reaction, the present and other calculations based on different approaches [9–13] seem to agree that some  $S = -1$  hyperon resonances are required to



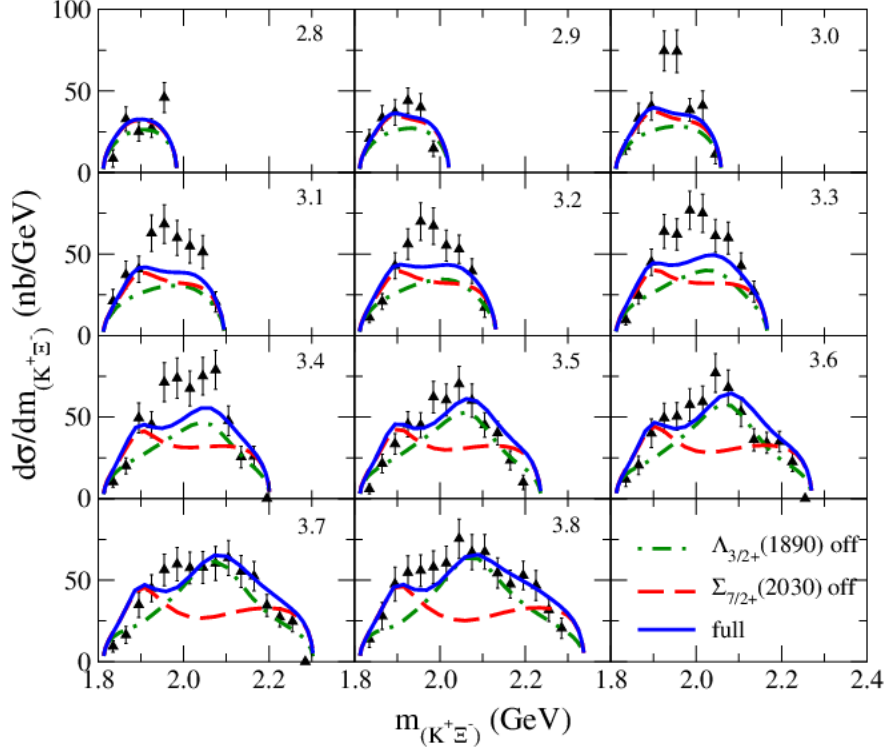


Figure 7:  $K^+\Xi^-$  invariant mass distribution for the reaction  $\gamma + p \rightarrow K^+ + K^+ + \Xi^-$ . The blue solid lines represent the full result. The red dashed lines represent the result with  $\Sigma(2030)$  switched off. The green dash-dotted lines represent the result with  $\Lambda(1890)$  switched off. The number in the upper right corner in each graph denotes the incident photon energy in units of GeV in the laboratory frame. The data are from Ref. [2].

reproduce the existing data. To pin down the role of a particular resonance among them requires more precise and complete data, in addition to more detailed theoretical models such as that of Refs. [12, 13]. In any case, both the  $\bar{K}$ - and photon-induced reactions studied in the present work are very well suited for studying  $S = -1$  hyperon resonances in the  $\sim 2$  GeV region.

We also found that the  $\Lambda(1890)$  and  $\Sigma(2030)$  resonances play an important role in the photon-induced reaction. In particular, they are required to bring the calculated  $K^+\Xi^-$  invariant mass distributions in agreement with the corresponding measurements.

Finally, the present work is our first step toward building a more complete reaction theory to help analyze the data and extract the properties of  $\Xi$  resonances in future experimental efforts in  $\Xi$  baryon spectroscopy. This is a complementary work to that of a model-independent analysis performed recently in Ref. [15] and will also help in analyzing the data to understand the production mechanisms of  $\Xi$  baryons.

## 5. Acknowledgments

This work was partially supported by the National Research Foundation of Korea (Grant No. NRF-2011-220-C00011) and the FFE-COSY (Grant No. 41788390).

## References

- [1] K.A. Olive *et al.* (Particle Data Group), Chin. Phys. C **38**, 090001 (2014).
- [2] L. Guo *et al.* (CLAS Collaboration), Phys. Rev. C **76**, 025208 (2007).
- [3] V. Flaminio, W.G. Moorhead, D.R.O. Morrison, and N. Rivoire (High-Energy Reactions Analysis Group), CERN Report No. CERN-HERA-83-02, 1983.
- [4] H.-Y. Ryu, A. Hosaka, H. Haberzettl, H.-C. Kim, K. Nakayama, and Y. Oh, PoS **Hadron2013**, 140 (2013).
- [5] *Photoproduction of the very strangest baryons on the proton target in CLAS12*, Spokespersons: M. Dugger, J. Goetz, L. Guo, E. Pasyuk, I.I. Strakovsky, D.P. Watts, and V. Ziegler (The Very Strange Collaboration with CLAS Collaboration), JLab Proposal E12-11-005a, Newport News, VA, USA, 2013.
- [6] H. Ohnishi, *Hadron Physics with  $K^-$  at J-PARC, Physics with Neutral Kaon Beam at JLab Workshop* (KL2016), February 1-3, 2016, Thomas Jefferson National Accelerator Facility, Newport News, VA.
- [7] H. Noumi, *Hadron Physics with High-momentum Hadron Beams at J-PARC, Physics with Neutral Kaon Beam at JLab Workshop* (KL2016), February 1-3, 2016, Thomas Jefferson National Accelerator Facility, Newport News, VA.
- [8] W. Erni *et al.* (The  $\overline{\text{PANDA}}$  Collaboration), *Physics performance report for  $\overline{\text{PANDA}}$ : Strong interaction studies with antiprotons*, arXiv:0903.3905.
- [9] D.A. Sharov, V.L. Korotkikh, and D.E. Lanskovy, Eur. Phys. J. A **47**, 109 (2011).
- [10] R. Shyam, O. Scholten, and A. W. Thomas, Phys. Rev. C **84**, 042201 (2011).
- [11] V.K. Magas, A. Feijoo, and A. Ramos, AIP Conf. Proc. **1606**, 208 (2014).
- [12] H. Kamano, S. X. Nakamura, T.-S.H. Lee, and T. Sato, Phys. Rev. C **90**, 065204 (2014).
- [13] H. Kamano, S.X. Nakamura, T.-S.H. Lee, and T. Sato, Phys. Rev. C **92**, 025205 (2015).
- [14] K. Nakayama, Y. Oh, and H. Haberzettl, Phys. Rev. C **85**, 042201(R) (2012).
- [15] B. Jackson, Y. Oh, H. Haberzettl, and K. Nakayama, Phys. Rev. C **89**, 025206 (2014).
- [16] H. Zhang, J. Tulpan, M. Shrestha, and D. M. Manley, Phys. Rev. C **88**, 035204 (2013).
- [17] H. Zhang, J. Tulpan, M. Shrestha, and D. M. Manley, Phys. Rev. C **88**, 035205 (2013).
- [18] K. Nakayama, Y. Oh, and H. Haberzettl, Phys. Rev. C **74**, 035205 (2006).
- [19] J.K.S. Man, Y. Oh, and K. Nakayama, Phys. Rev. C **83**, 055201 (2011).
- [20] H. Haberzettl, K. Nakayama, and S. Krewald, Phys. Rev. C **74**, 045202 (2006).
- [21] B. Jackson, Y. Oh, H. Haberzettl, and K. Nakayama, Phys. Rev. C **91**, 065208 (2015).

## 2.10 Predictions for Excited Strange Baryons

Ishara P. Fernando and José L. Goity

*Department of Physics*

*Hampton University*

*Hampton, VA 23668, U.S.A. &*

*Thomas Jefferson National Accelerator Facility*

*Newport News, VA 23606, U.S.A.*

### Abstract

An assessment is made of predictions for excited hyperon masses which follow from flavor symmetry and consistency with a  $1/N_c$  expansion of QCD. Such predictions are based on presently established baryonic resonances. Low lying hyperon resonances which do not seem to fit into the proposed scheme are discussed.

### 1. Introduction

The present status of excited hadrons is apparently incomplete. This is so for mesons and especially for baryons. There is an incompleteness problem known as “missing baryon resonances”, which is defined by the smaller multiplicity of the experimentally extracted resonances vis-à-vis the predictions of quark models and emphasized by recent studies of the baryon spectrum in lattice QCD (LQCD). While this may turn out to be a lesser problem, because quark models are after all not QCD and LQCD calculations have been done at relatively large quark masses and do not fully include the coupled channels affecting the baryon resonances, there is another missing resonance problem associated with flavor: the missing excited hyperons. According to approximate  $SU(3)$  symmetry we would have the following relations between numbers of states (if excited baryons would only fill 1, 8 and 10 of  $SU(3)$ , and ignoring isospin):  $\#\Sigma = \#\Xi = \#N + \#\Delta$  (PDG [1]: 26 : 12 : 49),  $\#\Omega = \#\Delta$  (PDG: 4:22), and  $\#\Lambda = \#N + \#\text{singlets}$  (PDG: 18:29). An obvious question, is whether missing hyperons are only an experimental issue related to limited data, and thus improvable with future experimental efforts, or, in some cases, due to the breaking of  $SU(3)$  symmetry which in those cases may be too large. The latter situation would be most likely the case for dynamically generated excited baryons with more non-strange resonances than strange ones generated in that way, a situation which however does not seem to occur at least for the lower excited baryons, where, as mentioned later, there are more hyperons than non-strange baryons identifiable with such possible dynamically generated states. Here we critically analyze that question anchoring the discussion in two expansions of QCD, namely the expansions in the light quark masses and in  $1/N_c$ . They connect QCD to the baryons by the approximate symmetries they imply, namely  $SU(3) \times SU(3)$  and spin-flavor  $SU(6)$  [2], respectively. In both cases, the breaking of the symmetries is implemented by an expansion in quark masses and in  $1/N_c$ . Having a well defined framework leads in particular to relations that allow for predictions, *e.g.*, among the masses of the resonances. Testing those relations, when possible, represents an important insight into the actual validity of the framework, and ultimately into QCD itself.

The case of the ground state 8 and 10 baryons is a powerful indicator. Looking at the masses,

one has the Gürsey-Radicati mass formula with the explicit expansion in  $1/N_c$ :

$$M_B = N_c m_0 + \frac{C_{HF}}{N_c} (\vec{S}^2 - \frac{3}{4} N_c) - c_8 m_8 \mathcal{S} - c'_8 m_8 S^i G^{i8} + \mathcal{O}(1/N_c^2; m_8/N_c), \quad (1)$$

where  $\vec{S}$  is the spin operator,  $\mathcal{S}$  is the strangeness and  $G^{ia}$  are the spin-flavor generators of  $SU(6)$  (identified at leading order in  $1/N_c$  with the axial vector currents), and  $m_8 = m_s - m_{u,d}$  is the octet component of the quark masses. The Gell-Mann-Okubo (GMO) and equal spacing relations (ESR) are satisfied up to deviations  $\mathcal{O}(m_8^2/N_c)$  plus terms non-analytic in the quark masses. In addition there is one relation involving simultaneously 8 and 10 baryons that tests  $SU(6)$ , namely (mass of baryon indicated by its name):

$$\Sigma^* - \Sigma = \Xi^* - \Xi + \mathcal{O}(1/N_c^2) \quad 212 \text{ MeV vs } 195 \text{ MeV}, \quad (2)$$

which is satisfied within the expected level of accuracy.

Another test of  $SU(6)$  symmetry is provided by the axial couplings, namely [3]:

$$g_A^{NN} = g_A^{N\Delta} = g_A^{\Delta\Delta}$$

$$Exp : 1.27 : 1.24 : -$$

$$LQCD : 1.17 : 1.07 : 0.98,$$

where the deviations are  $\mathcal{O}(1/N_c^2)$  or 10%.

If we look at the excited baryons, we find that there is only one  $SU(3)$  multiplet that can be empirically identified (disregarding the  $SU(3)$  singlet  $\Lambda_s$ ), namely one of the  $J^P = 1/2^-$  8:  $N(1532)$ ,  $\Lambda(1676)$ ,  $\Sigma(1667)$ ,  $\Xi(1815)$ , which satisfies remarkably well the GMO relation, namely  $-19 \pm 26$  MeV. As shown later, a number of other relations implied by broken  $SU(6)$  symmetry can be derived, some of which can be tested with the listed PDG states.

## 2. Excited Baryons and $SU(6) \times O(3)$

In principle, the S-matrix in the  $SU(3)$  and large  $N_c$  limits should display the exact  $SU(6)$  symmetry of baryons, and one should be able to study all the corresponding observables via an expansion in quark masses and  $1/N_c$  if the breaking of  $SU(6)$  is sufficiently small. In particular, it should be possible to expand the resonance parameters such as pole mass and width, or the Breit-Wigner resonance mass, as well as partial decay widths, *etc.* The framework for implementing such an expansion for excited baryons is based on expanding around an  $SU(6) \times O(3)$  symmetry limit [4]. That framework allows for the derivation of mass formulas for the baryons belonging to a given  $SU(6) \times O(3)$  multiplet–(for issues of mixing of different multiplets see [5]). The importance of these formulas is that they lead to mass relations, and thus to possible predictions. Mass formulas accurate to first order in the quark masses and  $\mathcal{O}(1/N_c)$  have been derived for the  $[56, \ell^P = 0^+, 2^+]$  [6, 7] and for the  $[70, \ell^P = 1^-, 2^+]$  [8–10]. We briefly discuss those results, as they represent the best illustration of the predictivity issues we are discussing. Identifying the baryons in a given irrep of  $SU(6) \times O(3)$  by  $(R, \ell; J, R_3 Y I)$ , the mass formula has the general form:

$$M_B(R, \ell; J, R_3 Y I) = N_c m_0(R, \ell) + \delta M(R, \ell; J, R_3 Y I), \quad (3)$$

where  $\delta M$  provides all the symmetry breaking effects expanded to the given order, and it is constructed in terms of a basis of composite operators built with products of the generators of the symmetry group [4] and ordered in powers of  $m_8$  and  $1/N_c$ . The key observation is that we know how to build such a basis in a systematic way thanks to the fact that we know how to count in  $1/N_c$  at the baryon level [2, 4].

(a) **The  $[56, 2^+]$  Baryons**

As the first illustration, we discuss the  $[56, 2^+]$  baryons, where at  $\mathcal{O}(1/N_c)$  and  $\mathcal{O}(m_8)$  there are only three  $SU(3)$  singlet and three  $SU(3)$  breaking mass operators leaving a total of 14 mass relations [7], and 12 unknown hyperon masses can be predicted from the presently known states in the multiplet [1]. Table 2a shows the mass relations, where some can be tested by the known PDG Breit-Wigner masses. In all cases in this report the fits have been carried out by including PDG states rated with at least three stars.

Table 1:  $[56, 2^+]$  mass relations, include the GMO relations for the two octets and the two ESR for each of the four decuplets.

Relation	Test (MeV)
$\Delta_{5/2} - \Delta_{3/2} = N_{5/2} - N_{3/2}$	$-40 \pm 43$ vs $-17 \pm 51$
$\frac{5}{7}(\Delta_{7/2} - \Delta_{5/2}) = N_{5/2} - N_{3/2}$	$39 \pm 19$ vs $-17 \pm 51$
$\frac{4}{3}(\Delta_{7/2} - \Delta_{1/2}) = N_{5/2} - N_{3/2}$	$18 \pm 9$ vs $-17 \pm 51$
$\frac{4}{15}(\Lambda_{3/2} - N_{3/2}) + \frac{11}{15}(\Lambda_{5/2} - N_{5/2}) = \frac{1}{2}(\Sigma_{5/2} - \Lambda_{5/2}) + \Sigma_{7/2} - \Delta_{7/2}$	$148 \pm 17$ vs $132 \pm 16$
$\Lambda_{5/2} - \Lambda_{3/2} + 3(\Sigma_{5/2} - \Sigma_{3/2}) = 4(N_{5/2} - N_{3/2})$	— —
$\Lambda_{5/2} - \Lambda_{3/2} + \Sigma_{5/2} - \Sigma_{3/2} = 2(\Sigma'_{5/2} - \Sigma'_{3/2})$	— —
$7 \Sigma'_{3/2} + 5 \Sigma_{7/2} = 12 \Sigma'_{5/2}$	— —
$4 \Sigma_{1/2} + \Sigma_{7/2} = 5 \Sigma'_{3/2}$	— —
<b>8s:</b> $2(N_J + \Xi_J) = 3 \Lambda_J + \Sigma_J$	— —
<b>10s:</b> $\Sigma_J - \Delta_J = \Xi_J - \Sigma_J = \Omega_J - \Xi_J$	— —

The masses of all the missing states can be predicted, and they are shown in the case of  $\Lambda$ ,  $\Sigma$  and  $\Xi$  hyperons in Fig. 1.

(b) **The  $[70, 1^-]$  Baryons**

In a similar way one can analyze the 70-plet baryons, in particular the lightest  $[70, 1^-]$  [8, 9]. Here also mass relations can be derived: there are 32 isospin multiplets in the  $[70, 1^-]$ , and the basis of mass operators involves a total of 15 operators, leaving 17 mass relations, of which 11 are GMO and ESR, and the rest are relations that test spin-flavor symmetry. As mentioned earlier, one GMO relation can be tested with the known PDG states. The masses of all missing states can be predicted, as shown in Fig. 1 for the hyperons. The  $[70, 1^-]$  is interesting because there is state mixing, primarily driven by the breaking of the spin-symmetry, but also by  $SU(3)$  breaking. The two mixings involving the pairs of nucleons with  $J=1/2$  and  $3/2$  can be unambiguously determined by including the analysis in the same framework of the decays as mentioned later.

### 3. Mass Predictions and Observations

The predictions for yet unobserved or unidentified hyperons can be seen in Fig. 1. Starting with the  $\Lambda$ s, there is a prediction for a  $3/2^-$  with a mass of 1865 MeV which does not match any PDG listed state: this should therefore be a significant prediction. It should be noted that the  $\Lambda(1405)$ , which being a singlet of  $SU(3)$  can only be constrained in the present framework by the spin-flavor symmetry, can be described in the framework without having to introduce unnatural size coefficients in the mass formula [8, 9]. This of course does not exclude that there is an important role of the  $\Sigma\pi$  and  $NK$  coupled channels in its structure [11, 12]. The  $1/2^+$   $\Lambda(1810)$  is interesting: it is too light to be described within any spin-flavor multiplet, but it sits close to the  $K\Xi$  threshold: is it a  $K\Xi$  resonance or a threshold effect? The higher mass  $\Lambda$ s should belong to other multiplets not considered here.

For the  $\Sigma$ s, the situation becomes quite interesting. There are seven PDG states with undetermined  $J^P$ . Of those, four have masses between 1450 and 1750 MeV. The two lowest lying ones are very difficult to explain: they do not fit into any flavor multiplet as they are way too light. A similar issue but less definite occurs with the next two states. The one star  $3/2^-$  state at 1570 MeV does not seem to fit into a multiplet, and it is about 50 MeV above the  $\pi\Sigma^*$  threshold: it seems therefore to be a difficult state to explain. Among the  $1/2^+$  states, the heavier mass corresponds to the  $\Sigma$  in the decuplet, and the PDG shows two states below it which cannot be matched. The lower one may be related to the  $\eta\Sigma$  threshold, which could explain it, but the upper one is puzzling. In the case of the negative parity states there are three clear predictions as shown in the Fig. 1.

Finally, for the  $\Xi$ s, in which the  $K_L$  beam could play a very important role as a discovery tool, we have a large number of predictions and also possible identifications with PDG states with yet undetermined  $J^P$ . As in the case of the  $\Sigma$ s, there are several PDG listed states which are too light to belong onto identifiable multiplets. For further discussion on the  $\Xi(1620)$  and  $\Xi(1690)$  see [13, 14].

The mentioned lower excited  $\Sigma$ s and  $\Xi$ s quoted in the PDG cannot be assigned to any  $SU(3)$  multiplet because no non-strange partners sufficiently light to fit into such multiplets exist. It is interesting to observe that they are close to thresholds (50 MeV or less), and thus they are likely closely related to those thresholds. While there is one three star state, ( $\Xi(1690)$ ), the rest are one or two star states. Neither quark models nor the LQCD calculations show those states. This can be understood if meson-baryon dynamics is the relevant physics (dynamically generated resonances or threshold effects), which is not captured in either of those approaches. More sophisticated LQCD calculations than the ones performed so far will be needed to find such effects. Those calculations are based on the Lüscher approach to extract hadronic interactions from finite volume effects on energy levels, which in the case of baryons are still in their early stages [15].

For dynamically generated states, which turn out to lie close to thresholds, one expects the effects of  $SU(3)$  symmetry breaking to be magnified, and thus  $SU(3)$  may cease to be a useful predictive tool. This is well known in the case of the scalar mesons, where the lightest  $0^+$  states cannot be accommodated into an octet with a GMO relation being approximately satisfied<sup>1</sup>. It should be emphasized that even in the large  $N_c$  limit one should expect non-trivial

---

<sup>1</sup>Let us remind the reader that for the vector mesons, once one factors in the ideal  $\omega - \phi$  mixing, the GMO relation

meson-baryon dynamics and therefore possible dynamically generated states. This contrasts with mesons, where the meson-meson interaction tends to vanish at large  $N_c$ , and thus the formation of tetra-quark states should eventually become impossible. Thus in baryons, dynamically generated states which cannot be assigned to an  $SU(3)$  multiplet are not excluded by the  $1/N_c$  expansion.

#### 4. Other Possible Predictions: Decays

For states which can be assigned to spin-flavor multiplets, one can expect that other observables beyond the masses will be constrained by symmetry. One case in point are the two-body strong decay partial widths. It is possible to derive relations between the partial decay widths, and in principle also derive predictions. As illustration, we mention here the  $[70, 1^-]$  decays [16]. The partial decay widths play an important role in determining the mixing angles between the two pairs of nucleon states with  $J = 1/2$  and  $3/2$ . Various relations, written in terms of reduced partial decay widths (*i.e.*, by conveniently removing phase space and centrifugal barrier factors [16]) can be tested. Two relations valid at LO in the  $1/N_c$  expansion permit for a determination of the mixing  $\theta_{J=1/2}$  via S-wave decays:

$$\frac{\tilde{\Gamma}(N(1535) \rightarrow N\pi) - \tilde{\Gamma}(N(1650) \rightarrow N\pi)}{\tilde{\Gamma}(N(1535) \rightarrow N\pi) + \tilde{\Gamma}(N(1650) \rightarrow N\pi)} = \frac{1}{5}(3 \cos(2\theta_{1/2}) - 4 \sin(2\theta_{1/2})),$$

$$\frac{\tilde{\Gamma}(N(1535) \rightarrow N\eta) - \tilde{\Gamma}(N(1650) \rightarrow N\eta)}{\tilde{\Gamma}(N(1535) \rightarrow N\eta) + \tilde{\Gamma}(N(1650) \rightarrow N\eta)} = 2 \sin(2\theta_{1/2}), \quad (4)$$

which give respectively:  $\theta_{1/2} = 0.46 \pm 0.10$  or  $1.76 \pm 0.10$  and  $\theta_{1/2} = 0.51 \pm 0.27$ . The global fit in Ref. [17] gives  $\theta_{1/2} \sim 0.40 \pm 0.20$ . Other relations that can be tested are the following ones:

$$\text{S-wave : } \frac{\tilde{\Gamma}(N(1535) \rightarrow N\pi) + \tilde{\Gamma}(N(1650) \rightarrow N\pi)}{\tilde{\Gamma}(\Delta(1620))} = 1; \quad \text{PDG: } 1.64 \pm 0.85,$$

$$\frac{\tilde{\Gamma}(\Delta(1620) \rightarrow N\pi)}{\tilde{\Gamma}(\Delta(1700) \rightarrow \Delta\pi)} = 0.1; \quad \text{PDG: } 0.29 \pm 0.15,$$

$$\text{D-wave : } \frac{2\tilde{\Gamma}(\Delta(1620) \rightarrow \Delta\pi) + \tilde{\Gamma}(\Delta(1700) \rightarrow \Delta\pi)}{15\tilde{\Gamma}(\Delta(1620) \rightarrow N\pi) + 32\tilde{\Gamma}(\Delta(1700) \rightarrow N\pi)} = 1; \quad \text{PDG: } 0.71 \pm 0.30,$$

$$\frac{\tilde{\Gamma}(N(1535) \rightarrow \Delta\pi) + \tilde{\Gamma}(N(1650) \rightarrow \Delta\pi) + 11\tilde{\Gamma}(\Delta(1700) \rightarrow \Delta\pi)}{132\tilde{\Gamma}(\Delta(1700) \rightarrow N\pi) + 90\tilde{\Gamma}(N(1675) \rightarrow N\pi)} = 1; \quad \text{PDG: } 0.78 \pm 0.33,$$

which are to first approximation remarkably well satisfied.

A complete analysis of the  $[70, 1^-]$  decays involving the hyperons can be found in Ref. [16]. The results there could be of course extended to predict the partial decay widths of the yet unseen hyperons in the  $[70, 1^-]$ .

---

is satisfied to a very good approximation.

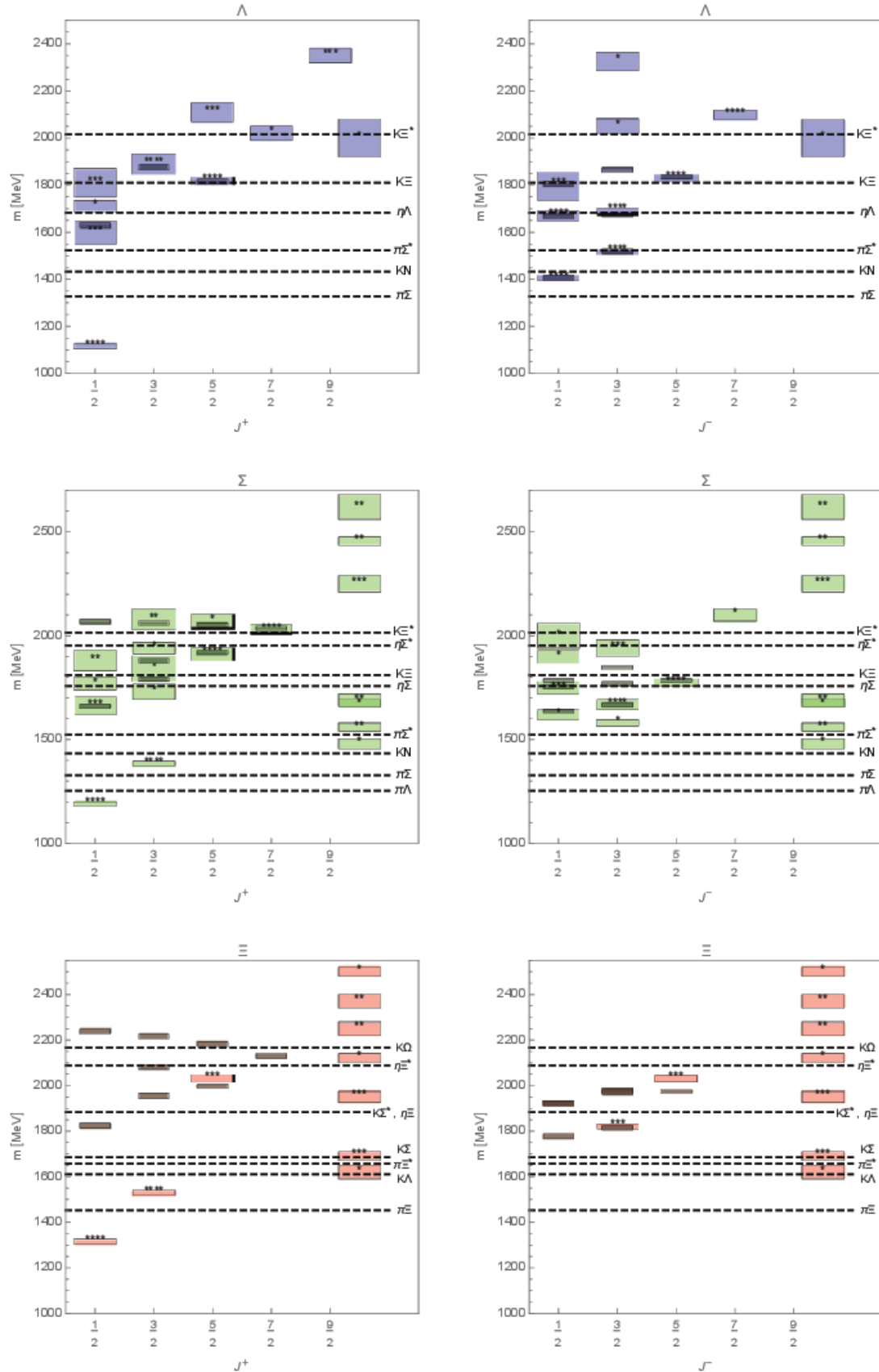


Figure 1: Excited hyperon masses. In color the PDG masses with their star ratings. In dark the results of the fits to the PDG states and the predictions. The dashed lines indicate the relevant thresholds corresponding to a pseudoscalar meson and a low lying 8 or 10 baryon. The masses on the extreme right of the figures are those whose  $J^P$  quantum numbers are not established by the PDG.



## 5. Tests with Lattice QCD Results

Calculations of the baryon spectrum in LQCD represent an important new source of information which can be used to test models as well as the approach discussed here. The advantage is that complete multiplets have been extracted from the calculations, and thus one can test the different mass relations. The disadvantage is that the calculations so far have been carried out at un-physically large quark masses, where apparently QCD dynamics shows resemblance with quark models, and where the framework does not allow to fully describe meson-baryon dynamics. Thanks to the large pions masses the lower lying excited states become relatively narrow, and one expects that the latter issue will not be so important. The LQCD results can be studied in the  $SU(3)$  symmetry breaking and  $1/N_c$  expansions, providing new tests. This was done in Ref. [18], where states obtained in LQCD [19, 20] corresponding to the multiplets discussed above were analyzed. Throughout it is observed that the mass relations are satisfied as expected. The LQCD reported errors on the baryon masses are in the range of 10 to 50 MeV, which is slightly larger than the expected NLO corrections in the mass formulas, and thus give a weaker test of the relations than one would wish. Further study is still necessary to confront our approach with the higher excited states determined in the LQCD calculations.

An open issue in the LQCD calculations is the study of possible dynamically generated states mentioned earlier, in particular the discussed hyperons. This would provide a powerful means for determining the existence of such states and also for answering the questions on symmetry breaking that arise in those cases.

## 6. Comments

A  $K_L$  beam in Hall D at Jefferson Lab would open unique opportunities for the study of excited hyperons, in particular  $\Xi$ s, of which much is still to be learned. Discerning the multiplet structures of excited baryons remains an open experimental issue which would be impacted by that development. The coincidence and interplay with the progress of LQCD studies of excited baryons seems to be particularly auspicious for gaining the much needed understanding of excited baryons.

## 7. Acknowledgments

This work was supported in part by DOE Contract No. DE-AC05-06OR23177 under which JSA operates the Thomas Jefferson National Accelerator Facility and by the National Science Foundation through grant PHY-1307413.

# References

- [1] K.A. Olive *et al.* (Particle Data Group), Chin. Phys. C **38**, 090001 (2014).
- [2] R. Dashen, E. Jenkins, and A.V. Manohar, Phys. Rev. D **51**, 3697 (1995).
- [3] A. Calle Cordon and J.L. Goity, PoS **CD12**, 062 (2013).
- [4] J.L. Goity, Phys. Lett. B **414**, 140 (1997).

- [5] J.L. Goity, *Yad. Fiz.* **68**, 655 (2005); [hep-ph/0405304].
- [6] C.E. Carlson and C.D. Carone, *Phys. Lett. B* **484**, 260 (2000).
- [7] J.L. Goity, C. Schat and N.N. Scoccola, *Phys. Lett. B* **564**, 83 (2003).
- [8] C.L. Schat, J.L. Goity and N.N. Scoccola, *Phys. Rev. Lett.* **88**, 102002 (2002).
- [9] C.L. Schat, J.L. Goity and N.N. Scoccola, *Phys. Rev. D* **66**, 114014 (2002).
- [10] N. Matagne and Fl. Stancu, *Phys. Rev. D* **87**, 076012 (2013).
- [11] C. Fernandez-Ramirez, I.V. Danilkin, D.M. Manley, V. Mathieu, and A.P. Szczepaniak, *Phys. Rev. D* **93**, 034029 (2016).
- [12] R. Molina and M. Döring, arXiv:1512.05831 [hep-lat].
- [13] Y. Oh, *these Proceedings*.
- [14] V. Ziegler, *these Proceedings*.
- [15] C.B. Lang and V. Verduci, *Phys. Rev. D* **87**, 054502 (2013).
- [16] C. Jayalath, J.L. Goity, E. Gonzalez de Urreta, and N.N. Scoccola, *Phys. Rev. D* **84**, 074012 (2011).
- [17] E. Gonzalez de Urreta, J.L. Goity, and N.N. Scoccola, *Phys. Rev. D* **89**, 034024 (2014).
- [18] I.P. Fernando and J.L. Goity, *Phys. Rev. D* **91**, 036005 (2015).
- [19] R.G. Edwards, J.J. Dudek, D.G. Richards, and S.J. Wallace, *Phys. Rev. D* **84**, 074508 (2011).
- [20] R.G. Edwards, N. Mathur, D.G. Richards, and S.J. Wallace (Hadron Spectrum Collaboration), *Phys. Rev. D* **87**, 054506 (2013).

## 2.11 The $\bar{K}N \rightarrow K\Xi$ Reaction in a Chiral NLO Model

Angels Ramos, A. Feijoo and V.K. Magas

*Departament d'Estructura i Constituents de la Matèria and Institut de Ciències del Cosmos  
Universitat de Barcelona*

*Martí Franquès 1*

*Barcelona E08028, Spain*

### Abstract

We present a model for the meson-baryon interaction in s-wave in the strangeness  $S=-1$  sector, based on a chiral  $SU(3)$  Lagrangian up to next-to-leading order (NLO) and implementing unitarization in coupled channels. A particular attention has been paid to fitting our model to the  $K^-p \rightarrow K^+\Xi^-$ ,  $K^0\Xi^0$  cross section data, since these processes are particularly sensitive to the NLO terms. Our model also includes the additional effect of high spin resonances believed to be important in the  $\sim 2$  GeV energy region under study. We present predictions for the cross section of the  $K_L^0 p \rightarrow K^+\Xi^0$  reaction that could be measured with the proposed Secondary  $K_L^0$  beam at Jlab. This process is particularly helpful for determining the properties of the meson-baryon interaction in  $S = -1$ , due to its isospin  $I = 1$  filter character.

### 1. Introduction

The description of low energy hadron reactions employing  $SU(3)$  Chiral Perturbation Theory ( $\chi$ PT), which is based on an effective Lagrangian which respects the symmetries of QCD, has been very successful but the theory fails to describe hadron dynamics in the vicinity of resonances. Unitarized Chiral Perturbation Theory ( $U\chi$ PT), which combines chiral dynamics with unitarization techniques in coupled channels, has shown to be a very powerful tool that permits extending the validity of  $\chi$ PT to higher energies and to describe the physics around the so called dynamically generated resonances (see [1] and references therein). A clear example of the success of  $U\chi$ PT is the description of the  $\Lambda(1405)$  resonance, located only 27 MeV below the  $\bar{K}N$  threshold, that emerges from coupled-channel meson-baryon re-scattering in the  $S = -1$  sector. In fact, the dynamical origin of the  $\Lambda(1405)$  resonance was already hindered more than 50 years ago [2], an idea that was reformulated later in terms of the chiral unitary theory in coupled channels [3]. This success stimulated a lot of activity in the community, which analyzed the effects of including a complete basis of meson-baryon channels, differences in the regularization of the equations, s- and u-channel Born terms in the Lagrangian, next-to-leading (NLO) contributions, *etc.* ... [4–12]. The various developed models could reproduce the  $\bar{K}N$  scattering data very satisfactorily and all these efforts culminated in establishing the  $\Lambda(1405)$  as a superposition of two poles of the scattering amplitude [6, 9, 13].

This topic experienced a renewed interest in the last few years, after the availability of a more precise measurement of the energy shift and width of the  $1s$  state in Kaonic hydrogen by the SIDDHARTA Collaboration [14] at DAΦNE. The CLAS Collaboration at JLab has also recently provided mass distributions of  $\Sigma^+\pi^-$ ,  $\Sigma^-\pi^+$ , and  $\Sigma^0\pi^0$  states in the region of the  $\Lambda(1405)$  [15], as well as differential cross sections [16] and a direct determination of the expected spin-parity  $J^\pi = 1/2^-$  of the  $\Lambda(1405)$  [17]. Invariant  $\pi\Sigma$  mass distributions

from  $pp$  scattering experiments have recently been measured by the COSY Collaboration at Jülich [18] and by the HADES Collaboration at GSI [19]. In parallel with the increased experimental activity, the theoretical models have been revisited [20–25] and analyses of the new reactions, aiming at pinning down the properties of the  $\Lambda(1405)$  better, have been performed [26–28].

In this contribution, we present a study of the  $S = -1$  meson-baryon interaction focused on providing well constrained values of the low-energy constants of the NLO chiral Lagrangian [25]. We employ data in the strong sector, including elastic and inelastic cross section data ( $K^-p \rightarrow K^-p$ ,  $\bar{K}^0n$ ,  $\pi^\pm\Sigma^\mp$ ,  $\pi^0\Sigma^0$ ,  $\pi^0\Lambda$ ) and the precise SIDDHARTA value of the energy shift and width of Kaonic hydrogen, as done by the recent works, but, in addition, we also constrain the parameters of our model to reproduce the  $K\Xi$  production data via the reactions  $K^-p \rightarrow K^+\Xi^-$ ,  $K^0\Xi^0$ . The motivation is that the lowest-order Lagrangian does not contribute directly to these reactions, which then become especially sensitive to the NLO terms. The model is also supplemented by explicit resonant terms, which are unavoidable at CM energies of around 2 GeV characteristic of  $K\Xi$  production, as proposed by several resonance-based models that have investigated the photoproduction of  $\Xi$  particles off the proton [29, 30] or via the strong reactions  $K^-p \rightarrow K^+\Xi^-$ ,  $K^0\Xi^0$  [31–33], as in this contribution.

## 2. Formalism

The lagrangian implementing the interactions between mesons and baryons at lowest order reads

$$\begin{aligned}\mathcal{L}_{\phi B}^{(1)} = & i\langle\bar{B}\gamma_\mu[D^\mu, B]\rangle - M_0\langle\bar{B}B\rangle - \frac{1}{2}D\langle\bar{B}\gamma_\mu\gamma_5\{u^\mu, B\}\rangle \\ & - \frac{1}{2}F\langle\bar{B}\gamma_\mu\gamma_5[u^\mu, B]\rangle, \end{aligned} \quad (1)$$

where  $u_\mu = iu^\dagger\partial_\mu Uu^\dagger$ , with  $U(\phi) = u^2(\phi) = \exp(\sqrt{2}i\phi/f)$  containing the field  $\phi$  of the pseudoscalar octet,  $B$  stands for the  $J^P = 1/2^+$  baryon octet,  $f$  is the pseudoscalar decay constant,  $M_0$  the common baryon octet mass in the chiral limit, the constants  $D$ ,  $F$  denote the axial vector couplings of the baryons to the mesons, and the symbol  $\langle\ldots\rangle$  stands for the trace in flavor space. Finally,  $[D_\mu, B]$  stands for the covariant derivative  $[D_\mu, B] = \partial_\mu B + [\Gamma_\mu, B]$ , with  $\Gamma_\mu = [u^\dagger, \partial_\mu u]/2$ .

At next-to-leading order, the contributions of  $\mathcal{L}_{\phi B}$  to meson-baryon scattering are:

$$\begin{aligned}\mathcal{L}_{\phi B}^{(2)} = & b_D\langle\bar{B}\{\chi_+, B\}\rangle + b_F\langle\bar{B}[\chi_+, B]\rangle + b_0\langle\bar{B}B\rangle\langle\chi_+\rangle \\ & + d_1\langle\bar{B}\{u_\mu, [u^\mu, B]\}\rangle + d_2\langle\bar{B}[u_\mu, [u^\mu, B]]\rangle \\ & + d_3\langle\bar{B}u_\mu\rangle\langle u^\mu B\rangle + d_4\langle\bar{B}B\rangle\langle u^\mu u_\mu\rangle, \end{aligned} \quad (2)$$

where  $\chi_+ = 2B_0(u^\dagger\mathcal{M}u^\dagger + u\mathcal{M}u)$  breaks chiral symmetry explicitly via the quark mass matrix  $\mathcal{M} = \text{diag}(m_u, m_d, m_s)$  and  $B_0 = -\langle 0|\bar{q}q|0\rangle/f^2$  relates to the order parameter of spontaneously broken chiral symmetry.

From these lagrangians one can derive the interaction kernel up to NLO in the non-relativistic limit

$$V_{ij} = V_{ij}^{WT} + V_{ij}^{NLO} =$$

$$- \frac{C_{ij}(2\sqrt{s} - M_i - M_j)}{4f^2} N_i N_j + \frac{D_{ij} - 2(k_\mu k'^\mu) L_{ij}}{f^2} N_i N_j, \quad (3)$$

where

$$N_i = \sqrt{\frac{M_i + E_i}{2M_i}}, \quad N_j = \sqrt{\frac{M_j + E_j}{2M_j}}$$

with  $M_i, M_j$  and  $E_i, E_j$  the masses and energies, respectively, of the baryons involved in the transition. The indices  $(i, j)$  cover all the initial and final channels, which, in the case of strangeness  $S = -1$  and charge  $Q = 0$  explored here, amount to ten:  $K^-p, \bar{K}^0n, \pi^0\Lambda, \pi^0\Sigma^0, \pi^-\Sigma^+, \pi^+\Sigma^-, \eta\Lambda, \eta\Sigma^0, K^+\Xi^-,$  and  $K^0\Xi^0$ . The matrices of coefficients  $C_{ij}, D_{ij}$  and  $L_{ij}$  are shown in the appendix of [25]. They depend on the pion decay constant  $f$  and the parameters  $b_0, b_D, b_F, d_1, d_2, d_3$  and  $d_4$ , which will be determined in our fits.

The  $U_\chi$ PT method consists in solving the Bethe-Salpether equation in coupled channels

$$T_{ij} = V_{ij} + V_{il} G_l T_{lj}, \quad (4)$$

where the loop function  $G_i$  stands for the propagator of the  $i^{\text{th}}$  meson-baryon state, which is regularized employing dimensional regularization

$$\begin{aligned} G_l &= i \int \frac{d^4 q_l}{(2\pi)^4} \frac{2M_l}{(P - q_l)^2 - M_l^2 + i\epsilon} \frac{1}{q_l^2 - m_l^2 + i\epsilon} \\ &= \frac{2M_l}{(4\pi)^2} \left\{ a_l + \ln \frac{M_l^2}{\mu^2} + \frac{m_l^2 - M_l^2 + s}{2s} \ln \frac{m_l^2}{M_l^2} + \right. \\ &\quad \left. \frac{q_{\text{cm}}}{\sqrt{s}} \ln \left[ \frac{(s + 2\sqrt{s}q_{\text{cm}})^2 - (M_l^2 - m_l^2)^2}{(s - 2\sqrt{s}q_{\text{cm}})^2 - (M_l^2 - m_l^2)^2} \right] \right\}, \end{aligned} \quad (5)$$

where  $\mu = 1 \text{ GeV}$  is the regularization scale and  $a_l$  are the so called subtraction constants, which are taken as free parameters to be fitted to data. There are only 6 independent subtraction constants in  $S = -1$  meson-baryon scattering due to isospin symmetry.

This model will be supplemented by adding, to the chiral  $\bar{K}N \rightarrow K^+\Xi^-, K^0\Xi^0$  amplitudes, some of the known resonances in the  $1.89 < M < 2.35 \text{ GeV}$  energy range. From the eight resonances rated with three- and four-stars in [34], we take the  $\Sigma(2030)$  and  $\Sigma(2250)$  as good candidates, coinciding with the findings of Ref. [31], which examined various combinations of several resonances. The spin and parity  $J^\pi = 7/2^+$  of the  $\Sigma(2030)$  are well established. Those of the  $\Sigma(2250)$  are not known, but the most probable assignments are  $5/2^-$  or  $9/2^-$  [34]. We choose  $J^\pi = 5/2^-$  to simplify the calculations. An ad-hoc exponential form-factor function is also introduced to modify the energy dependence of the resonance contributions. Details on how the resonant terms are implemented can be found in Ref. [25]. The fit to the data will determine the masses, widths, form-factor cut-off values, and the product of the resonance couplings to  $\bar{K}N$  and  $K\Xi$  states.

Once the  $T$ -matrix is known, one can obtain the differential and total cross sections, the  $K^-p$  scattering length, the related energy shift and width of Kaonic hydrogen via the second order corrected Deser-type formula [35], the branching ratios at threshold, *etc.*

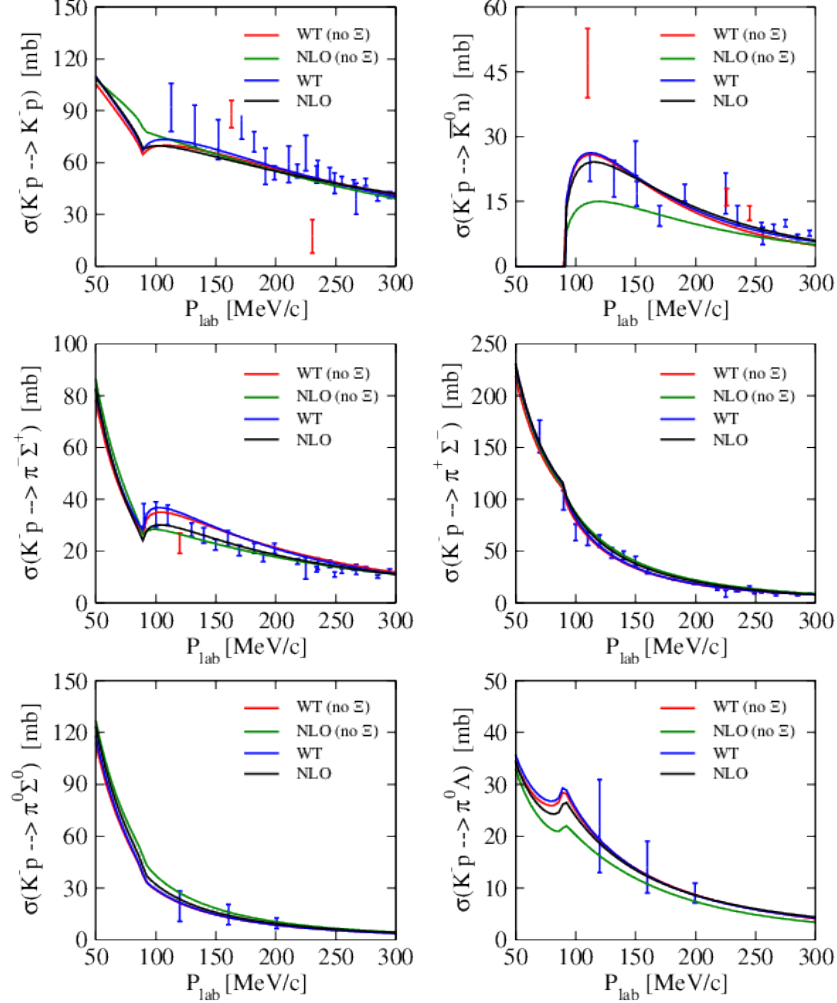


Figure 1: Total cross sections for the  $K^-p \rightarrow K^-p$ ,  $\bar{K}^0 n$ ,  $\pi^- \Sigma^+$ ,  $\pi^+ \Sigma^-$ ,  $\pi^0 \Sigma^0$ , and  $\pi^0 \Lambda$  reactions obtained from the WT (no  $K\Xi$ ) fit (red line), the NLO (no  $K\Xi$ ) fit (green line), the WT fit (blue line) and the NLO fit (black line), where the last two cases take into account the experimental data of the  $K\Xi$  channels, see text for more details. Experimental data are from [36–39]. The points in red have not been included in the fitting procedure.

### 3. Results

The elastic and inelastic cross sections are shown in Fig. 1 for several fits: ‘WT (no  $\Xi$ )’ and ‘NLO (no  $\Xi$ )’ correspond to cases employing the chiral kernel up to lowest order or NLO, respectively, without considering the  $K\Xi$  production data in the fits, as customary done by the chiral unitary models existing in the literature. The other two models, ‘WT’ and ‘NLO’, do fit in addition the  $K^-p \rightarrow K^+\Xi^-$ ,  $K^0\Xi^0$  data. It is evident from Fig. 1 that, for the observables represented there, the four fits are similarly good. The situation changes drastically for the cross sections of the  $\Xi$  production reactions represented in Fig. 2 for the same four models. The WT (no  $K\Xi$ ) fit, represented by red lines, cannot even reproduce the size of the cross section in either reaction, which is not a surprising result because there

is no direct contribution from the reactions  $K^-p \rightarrow K^0\Xi^0, K^+\Xi^-$  at lowest order. This is why these reactions are very sensitive to the NLO corrections, which is confirmed by the NLO (no  $K\Xi$ ) results represented by green lines in Fig. 2. Even if the experimental data for the  $K^-p \rightarrow K^0\Xi^0, K^+\Xi^-$  reactions have not been employed in this fit, the NLO (no  $K\Xi$ ) result gives a larger amount of strength for this channels, especially in the case of the  $K^+\Xi^-$  production reaction, where the prediction even overshoots the data considerably. When the  $K\Xi$  data is included in the fitting procedure, the NLO results, represented by the black lines, reproduce quite satisfactorily the  $K^-p \rightarrow K^0\Xi^0, K^+\Xi^-$  cross sections. For completeness, we have also attempted to reproduce these reactions employing only the lowest order Lagrangian. The corresponding WT results, represented by the blue lines, improve considerably over those of the WT (no  $K\Xi$ ) fit, but at the expense of unphysical values for the fitted subtraction constants since the strength in these channels is built mainly through unitarization.

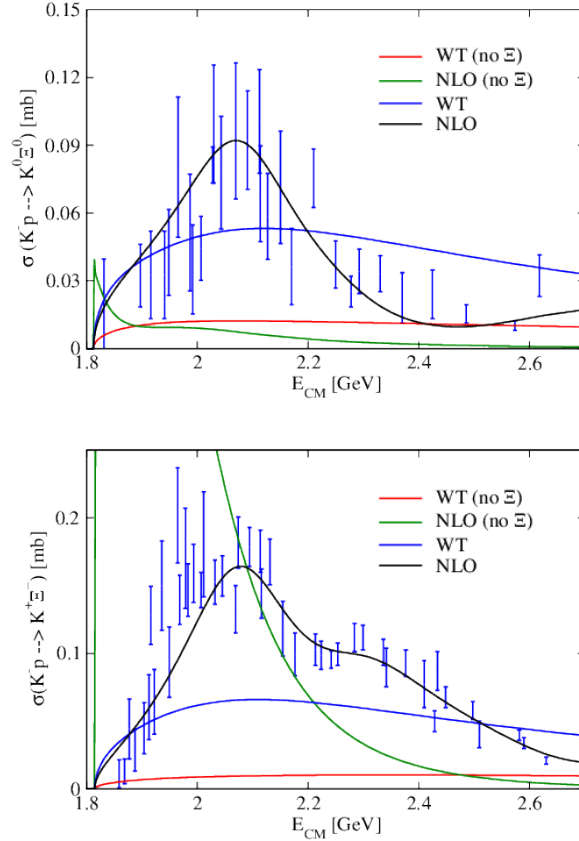


Figure 2: The total cross sections of the  $K^-p \rightarrow K^0\Xi^0, K^+\Xi^-$  reactions obtained from the WT (no  $K\Xi$ ) fit (red line), the NLO (no  $K\Xi$ ) fit (green line), the WT fit (blue line) and the NLO fit (black line). Experimental data are from [40–46].

The discrepancies between the NLO model and the data, which are larger in the vicinity of 2 GeV and around 2.2 GeV, can be improved by the explicit implementation of resonance terms coupling to the  $K\Xi$  channels. Since the resonant terms produce angular dependent

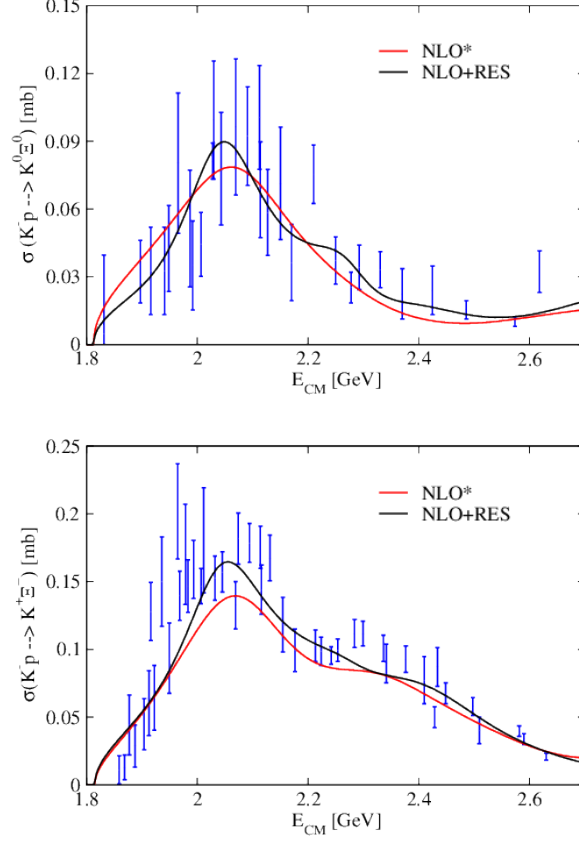


Figure 3: Total cross sections of the  $K^-p \rightarrow K^0\Xi^0, K^+\Xi^-$  reactions for the NLO\* fit (red line) and the NLO+RES fit (black line). Experimental data are from [40–46].

scattering amplitudes, we can now consider, in addition to the total cross sections and threshold observables already employed in the earlier fits, the differential cross section data of the  $K^-p \rightarrow K\Xi$  reactions. In Figs. 3, 4, and 5, we present total and differential cross section data for two different fits: ‘NLO<sup>ast</sup>’ stands for a fit that considers the chiral lagrangian up to NLO and includes all the data than the previous NLO fit plus the differential cross section data in the  $\Xi$  production channels. ‘NLO+RES’ stands for the fit employing a model that incorporates the additional effect of the two high spin resonances.

The total cross sections for  $K\Xi$  production obtained from the NLO\* fit (red lines in Fig. 3) are in reasonable agreement with the data, even if the resonant terms are not included. This NLO\* fit is in fact very similar to the NLO one but it also tries to accommodate the differential  $K\Xi$  production cross section data, which can only be adjusted on average, as shown by the red lines in Figs. 4 and 5, because of the flat distribution characteristic of  $s$ -wave models. In order to account for some structure in the differential  $K\Xi$  production cross sections we need to implement the resonant terms. On inspecting the black lines in Figs. 3, 4, and 5 one clearly sees that the NLO+RES fit reproduces satisfactorily the  $K\Xi$  total cross sections, while accounting quite reasonably for the differential ones.

In Fig. 6 we show the isopin  $I = 0$  and  $I = 1$  contributions to the  $K^-p \rightarrow K^0\Xi^0, K^+\Xi^-$



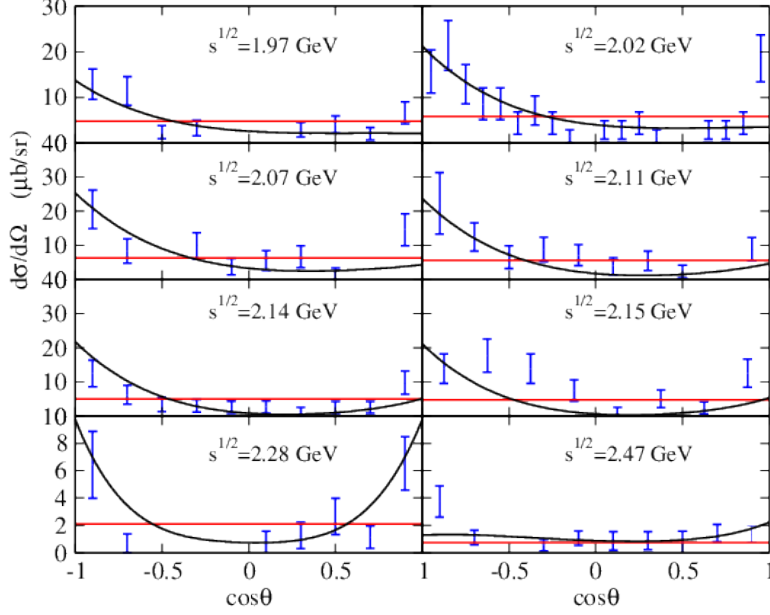


Figure 4: Differential cross section of the  $K^-p \rightarrow K^0\Xi^0$  reaction for the NLO\* fit (red line) and the NLO+RES fit (black line), see the text for more details. Experimental data are from [40–46].

cross sections, which must be summed coherently. We see that the chiral NLO\* model produces stronger  $I = 1$  amplitudes than  $I = 0$ , which is the reversed situation than one finds in the absence of unitarization. The dominance of  $I = 1$  contributions is obviously enhanced in the NLO+RES model that includes two  $I = 1$  resonances explicitly. However, other models in the literature, as that of Ref. [33] which is fitted to the same data, find a different distribution over isospin channels. For this reason, in order to pin down the details of the meson-baryon interaction in the  $S = -1$  sector, it would be very valuable to have data in this energy range with a definite value of isospin.

A recent possibility has emerged with the measurement at LHCb of the decay of the  $\Lambda_b$  into  $J/\Psi$  and a meson-baryon pair in  $S = -1$ . From the three-body final state, the reconstruction of  $J/\Psi p$  pairs permitted to find the signal of the  $P_c(4450)$  pentaquark state [47]. On the other hand, the invariant mass spectrum of the  $K^-p$  pairs gives access to study their interaction, and actually, that of any of its related coupled-channel meson-baryon ( $MB$ ) pairs, in  $I = 0$ , since it can be shown that the decay  $\Lambda_b \rightarrow J/\Psi MB$  acts as an  $I = 0$  filter [48, 49]. The invariant masses of  $I = 0$   $K\Xi$  states calculated in [49] show indeed the different predictions for the invariant mass distributions of  $K\Xi$  pairs coming from the decay of the  $\Lambda_b$ , obtained using the NLO\* and the NLO+RES models.

It would also be interesting to obtain information on the  $\bar{K}N \rightarrow K\Xi$  interaction in  $I = 1$ , of which only two points, obtained from  $K^-$  deuteron reactions in bubble chamber experiments, are known [50, 51]. The recent proposal of creating a secondary  $K_L^0$  beam at JLab offers a great opportunity for measuring the  $K_L^0 p \rightarrow K^+\Xi^0$  reaction, which would proceed through the  $\bar{K}^0$  component of the  $K_L^0$  and is of pure  $I = 1$  character. Our predictions for

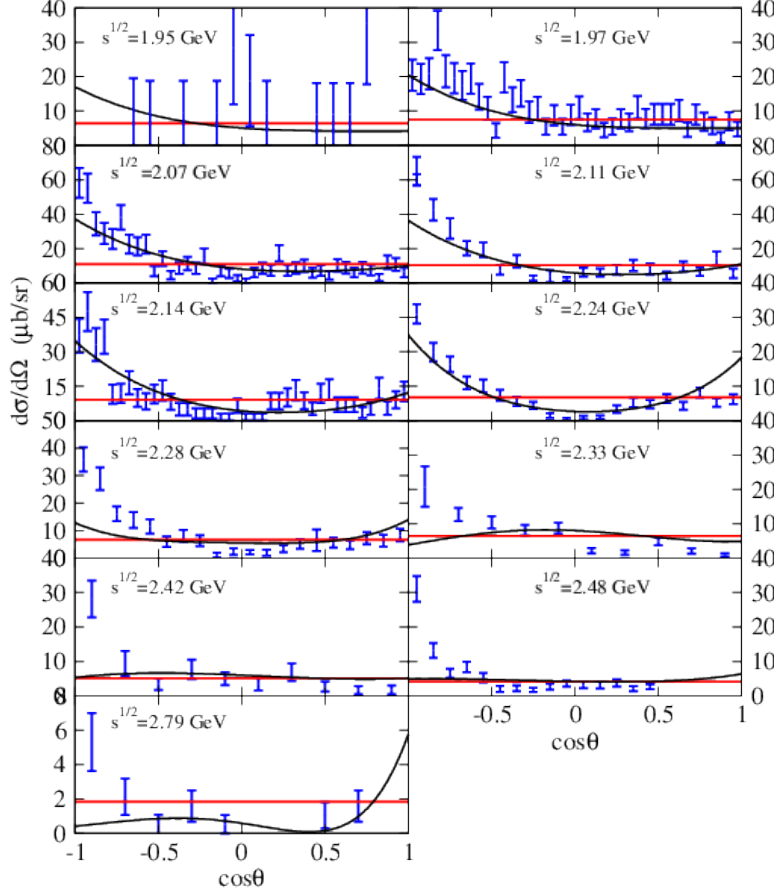


Figure 5: Differential cross section of the  $K^-p \rightarrow K^+\Xi^-$  reaction for the NLO\* fit (red line) and the NLO+RES fit (black line), see the text for more details. Experimental data are from [40–46].

this reaction are shown in Fig. 7 for the WT (green dotted line), NLO\* (red dashed line) and NLO+RES (black solid line) models, together with the experimental points of the  $I = 1$   $K^-n \rightarrow K^0\Xi^-$  reaction, which have been divided by two to properly account for the size of the strangeness  $-1$  component of the  $K_L^0$ . Since these two data points have not been used in the fit, our predictions for the most complete NLO\* or NLO+RES models are not good, especially for the data point around 2 GeV. New data from modern experiments, as the proposed measurement of the  $K_L^0 p \rightarrow K^+\Xi^0$  reaction with a secondary  $K_L^0$  beam at Jlab, would certainly be very helpful in constraining the models describing the meson-baryon interaction in the  $S = -1$  sector around 2 GeV tighter.

#### 4. Conclusions

We have presented a study of the  $S = -1$  meson-baryon interaction, employing a chiral SU(3) Lagrangian up to next-to-leading order and implementing unitarization in coupled channels. The model has been supplemented by the explicit consideration of two resonances. The parameters of the Lagrangian and of the resonances have been fitted to a large set of experimental scattering data in different two-body channels, to threshold branching ratios, and to the precise SIDDHARTA value of the energy shift and width of Kaonic hydrogen. In

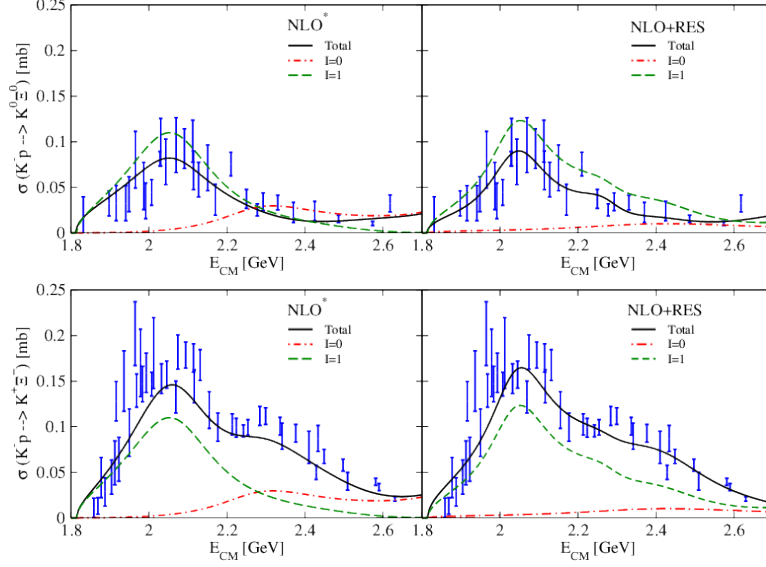


Figure 6: Total cross sections of the  $K^-p \rightarrow K^0\Xi^0, K^+\Xi^-$  reactions for the NLO\* fit (left panels) and the NLO+RES fit (right panels), splitted into their  $I = 0$  (red dot-dashed lines) and  $I = 1$  (green dashed lines) components. Experimental data are from [40–46].

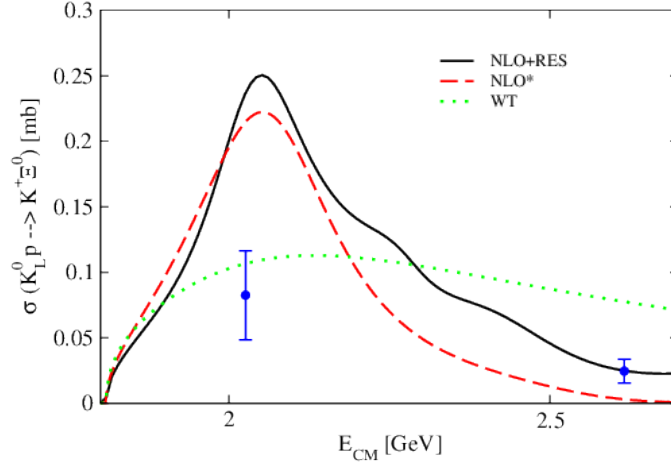


Figure 7: Total cross sections of the  $K_L^0 \rightarrow K^+\Xi^0$  reactions for the WT (green dotted line), NLO\* (red dashed line) and NLO+RES (black solid line) models, together with the experimental points of the  $I = 1$   $K^-n \rightarrow K^0\Xi^-$  reaction (divided by two). Experimental data are from [50, 51].

contrast to other works, we have also constrained our model to also reproduce the  $K^-p \rightarrow K^+\Xi^-, K^0\Xi^0$  reactions, since they become especially sensitive to the NLO terms.

While a good account of the  $K^-p \rightarrow K^+\Xi^-, K^0\Xi^0$  total and differential cross sections is achieved, the isospin decompositions of the models studied here show some differences, and they also differ from other works in the literature. We find a disagreement of our predictions with the scarce available data in the  $I = 1$  sector. Measuring the  $K_L^0p \rightarrow K^+\Xi^0$  reactions

with a secondary  $K_L^0$  beam at Jlab would be extremely valuable to further constrain the parameters of the chiral lagrangian describing the meson-baryon interaction in the  $S = -1$  sector.

## 5. Acknowledgments

This work is partly supported by the Spanish Ministerio de Economía y Competitividad (MINECO), under the project MDM–2014–0369 of ICCUB (Unidad de Excelencia ‘María de Maeztu’) and under the contract FIS2014–54762–P (with additional European FEDER funds), and by the Generalitat de Catalunya under the contract 2014SGR–401.

## References

- [1] J.A. Oller, E. Oset, and A. Ramos, Prog. Part. Nucl. Phys. **45**, 157 (2000).
- [2] R.H. Dalitz and S.F. Tuan, Annals Phys. **8** (1959) 100; R.H. Dalitz and S.F. Tuan, Phys. Rev. Lett. **2** (1959) 425; M. Jones, R.H. Dalitz and R.R. Horgan, Nucl. Phys. B **129**, 45 (1977).
- [3] N. Kaiser, P.B. Siegel, and W. Weise, Nucl. Phys. A **594**, 325 (1995).
- [4] N. Kaiser, T. Waas, and W. Weise, Nucl. Phys. A **612**, 297 (1997).
- [5] E. Oset and A. Ramos, Nucl. Phys. A **636**, 99 (1998).
- [6] J.A. Oller, U.-G. Meissner, Phys. Lett. B **500**, 263 (2001).
- [7] M.F.M. Lutz and E. Kolomeitsev, Nucl. Phys. A **700**, 193 (2002).
- [8] B. Borasoy, E. Marco, and S. Wetzel, Phys. Rev. C **66**, 055208 (2002).
- [9] D. Jido, J. A. Oller, E. Oset, A. Ramos, and U. G. Meissner, Nucl. Phys. A **725**, 181 (2003).
- [10] A. Bahaoui, C. Fayard, T. Mizutani, and B. Saghai, Phys. Rev. C **68**, 064001 (2003).
- [11] B. Borasoy, R. Nissler, W. Wiese, Eur. Phys. J. A **25**, 79 (2005).
- [12] B. Borasoy, U. G. Meissner, and R. Nissler, Phys. Rev. C **74**, 055201 (2006).
- [13] V.K. Magas, E. Oset, and A. Ramos, Phys. Rev. Lett. **95**, 052301 (2005).
- [14] M. Bazzi, G. Beer, L. Bombelli, A.M. Bragadireanu, M. Cargnelli, G. Corradi, C. Curceanu (Petrascu), and A. d’Uffizi *et al.* (SIDDARTHA Collaboration), Phys. Lett. B **704**, 113 (2011).
- [15] K. Moriya *et al.* (CLAS Collaboration), Phys. Rev. C **87**, 035206 (2013).
- [16] K. Moriya *et al.* (CLAS Collaboration), Phys. Rev. C **88**, 045201 (2013) [Addendum-ibid. C **88**, 049902 (2013)].

- [17] K. Moriya *et al.* (CLAS Collaboration), Phys. Rev. Lett. **112**, 082004 (2014).
- [18] I. Zychor, M. Buscher, M. Hartmann, A. Kacharava, I. Keshelashvili, A. Khoukaz, V. Kleber, and V. Koptev *et al.*, Phys. Lett. B **660**, 167 (2008).
- [19] G. Agakishiev *et al.* (HADES Collaboration), Phys. Rev. C **87**, 025201 (2013).
- [20] Y. Ikeda, T. Hyodo, and W. Wiese, Nucl. Phys. A **881**, 98 (2012).
- [21] T. Hyodo, D. Jido, Progress in Particle and Nuclear Physics, **67**, 55 (2012).
- [22] Zhi-Hui Guo and J.A. Oller, Phys. Rev. C **87**, 035202 (2013).
- [23] M. Mai and U.-G. Meissner, Nucl. Phys. A **900**, 51 (2013).
- [24] T. Mizutani, C. Fayard, B. Saghai, and K. Tsushima, Phys. Rev. C **87**, 035201 (2013).
- [25] A. Feijoo, V.K. Magas, and A. Ramos, Phys. Rev. C **92**, no. 1, 015206 (2015).
- [26] L. Roca and E. Oset, Phys. Rev. C **87**, 055201 (2013).
- [27] L. Roca and E. Oset, Phys. Rev. C **88**, 055206 (2013).
- [28] M. Mai and U. G. Meissner, arXiv:1411.7884 [hep-ph].
- [29] K. Nakayama, Y. Oh, and H. Haberzettl, Phys. Rev. C **74**, 035205 (2006).
- [30] J.K. S. Man, Y. Oh and K. Nakayama, Phys. Rev. C **83**, 055201 (2011).
- [31] D.A. Sharov, V.L. Korotkikh and D.E. Lanskoy, Eur. Phys. J. A **47**, 109 (2011).
- [32] R. Shyam, O. Scholten, and A.W. Thomas, Phys. Rev. C **84**, 042201 (2011).
- [33] B.C. Jackson, Y. Oh, H. Haberzettl, and K. Nakayama, Phys. Rev. C **91**, 065208 (2015).
- [34] K. A. Olive *et al.* [Particle Data Group Collaboration], Chin. Phys. C **38**, 090001 (2014).
- [35] U.G. Meissner, U. Raha, and A. Rusetsky, Eur. Phys. J. C **35**, 349 (2004).
- [36] J.K. Kim, Phys. Rev. Lett. **14**, 89 (1965).
- [37] T.S. Mast *et al.*, Phys. Rev. D **14**, 13 (1976).
- [38] R.O. Bangerter *et al.*, Phys. Rev. D **23**, 1484 (1981).
- [39] J. Ciborowski *et al.*, J. Phys. G **8**, 13 (1982).
- [40] G. Burgun *et al.*, Nucl. Phys. B **8**, 447 (1968).
- [41] J.R. Carlson *et al.*, Phys. Rev. D **7**, 2533 (1973).
- [42] P.M. Dauber *et al.*, Phys. Rev. **179**, 1262 (1969).

- [43] M. Haque *et al.*, Phys. Rev. **152**, 1148 (1966).
- [44] G.W. London *et al.*, Phys. Rev. **143**, 1034 (1966).
- [45] T.G. Trippe and P.E. Schlein, Phys. Rev. **158**, 1334 (1967).
- [46] W.P. Trower *et al.*, Phys. Rev. **170**, 1207 (1968).
- [47] R. Aaij *et al.* [LHCb Collaboration], Phys. Rev. Lett. **115**, 072001 (2015).
- [48] L. Roca, M. Mai, E. Oset and U.G. Meißner, Eur. Phys. J. C **75**, 218 (2015).
- [49] A. Feijoo, V.K. Magas, A. Ramos, and E. Oset, Phys. Rev. D **92**, 076015 (2015).
- [50] J.P. Berge *et al.*, Phys. Rev. **147**, 945 (1966).
- [51] J.C. Scheuer *et al.* (S.A.B.R.E. Collaboration), Nucl. Phys. B **33**, 61 (1971).

## 2.12 Hyperon Studies at JPAC

César Fernández-Ramírez

*Instituto de Ciencias Nucleares*

*Universidad Nacional Autónoma de México*

*A.P. 70-543, Ciudad de México 04510, Mexico*

Adam Szczepaniak

*Center for Exploration of Energy and Matter*

*Indiana University*

*Bloomington, IN 47403, U.S.A. &*

*Theory Center*

*Thomas Jefferson National Accelerator Facility*

*Newport News, VA 23606, U.S.A.*

### Abstract

We provide an overview of the recent work developed at the Joint Physics Analysis Center (JPAC) regarding  $\bar{K}N$  scattering and the hyperon spectrum. We emphasize our findings on the nature of the two  $1/2^+$  poles present in the  $\Lambda(1405)$  region.

### 1. Hadron Reactions and Resonances as Probes of Strong QCD

Recently there have been dramatic advancements in accelerator technologies, detection techniques and on the theoretical side, algorithms for first principle QCD analyses [1]. These have led to several candidates for possible “exotic ” hadrons, *i.e.*, quark-gluon hybrids or quark-hadron molecular states. It thus appears that interpretation of the entire hadron spectrum in terms of the valence constituents of the quark model is no longer possible. If confirmed, such “exotic ” hadrons could drastically alter our understanding of strong QCD and shed new light on the confinement of quarks.

Given the wide interest in hadron spectroscopy, the Joint Physics Analysis Center (JPAC) [2] has been dedicated to the development of theoretical and phenomenological analysis methods for analysis of hadron reactions. To achieve these goals researchers affiliated with JPAC are developing amplitude models based on principles of S-matrix theory to formulate scattering amplitudes for various reactions of interest to the hadron physics community and QCD practitioners. JPAC members work in close collaboration with experimentalists on implementing theoretical innovations into the existing data analysis streams, preserving knowledge for future use and disseminating the methodology across various experiments.

Resonances are characterized by their mass and spin. Near the resonance mass a two-body cross section vary as a function of the center of mass energy while angular variations of the differential cross section reflect the resonance spin. Variations in the cross section, albeit smooth, are a manifestation of a singularity in a partial wave amplitude, which is seen when the amplitude is continued beyond the real energy axis and/or beyond the integer (or half-integer) values of spin to complex domains of these variables. Resonance parameters are therefore determined by analytical continuation of reaction amplitude models.

Analytical behavior of reaction amplitudes as functions of Mandelstam variables follows from principles of the S-matrix theory [3]. For example, the absence of singularities in the complex energy plane, *a.k.a.*, the physical sheet, follows from causality and crossing symmetry. On the physical sheet the only allowed singularities are bound state poles, *e.g.*, the nucleon pole, and cuts induced by opening of particle production thresholds. The latter lie on the real axis and discontinuity of the amplitude across cuts is constrained by unitarity. Resonance poles appear as singularities on complex planes (unphysical sheets) that are connected to the physical sheet along these discontinuities. These unphysical sheets are connected in such a way that the amplitudes change smoothly when passing from the physical to an unphysical sheet. Therefore, a resonance pole located on an unphysical sheet close to the real axis has a strong influence on the amplitude in the physical region of scattering.

S-matrix analyticity does not predict whether a resonance exists or it does not. It is the underlying dynamics, *i.e.*, QCD, that determines that. Given a model that specifies the number of expected resonances, S-matrix principles, however, enable to write amplitudes that properly continue amplitudes from poles to the real axis where they can be compared with experimental data. Resonances of different spins are not independent. This follows from crossing relations and unitarity implying analyticity of partial waves in the complex angular momentum plane [4]. This is the essence of the Regge theory [5]. Therefore, partial waves should be analyzed simultaneously as function of mass and spin. This, however, is almost never done. Typically mass dependent partial wave analyses deal with each partial wave independently. Without imposing relations between resonances of different spins, the various methods for implementing resonances in a single partial wave are closely related. These methods include, for example, the K-matrix parametrization [6], N/D parametrizations [7], or solutions of Bethe-Salpeter motivated equations with contact interactions [8]. When appropriate, all these parameterizations can be supplemented with additional constraints, *e.g.*, from chiral symmetry at low-energies or Regge asymptotics. It is worth noting that the extraction of resonance properties based on a first principle QCD analysis, *i.e.*, using lattice gauge techniques, requires the same amplitude parametrizations as data analysis [9].

## 2. Hyperons: Terra Incognita in the Baryon Landscape

Even though the spectrum of baryons has been investigated for several decades, only a handful of hyperon resonances has been well established [10]. One of the key aspects of confinement is the (approximate) linearity of Regge trajectories. In the isoscalar sector [ $\Lambda$ , Fig. 1] the leading natural parity, even ( $1/2^+$ ,  $5/2^+$ , ...) and odd ( $3/2^-$ ,  $7/2^-$ , ...) trajectories have two well-established states each. If one assumes exchange degeneracy, then the four states do appear to lie on a straight line. Unfortunately, only a few more  $\Lambda$ 's are reasonably well established and the identification of other trajectories remains ambiguous. For example, it is unclear whether the first excited  $1/2^+$  state, the  $\Lambda(1600)$ , belongs to the same trajectory as the  $5/2^+$   $\Lambda(2110)$  resonance or to a different one. Similar ambiguity appears in the leading unnatural parity ( $1/2^-$ ,  $5/2^-$ , ...) trajectory where, given that there is a strong indication that what is known as the  $\Lambda(1405)$  could actually correspond to two resonances, it is unclear which  $1/2^-$  pole should be connected with the  $5/2^-$   $\Lambda(1830)$ . Similar ambiguities exist in the isovector sector [ $\Sigma$ , Fig. 1]. Except for the leading even natural parity trajectory, other trajectories have, at best, one well-established resonance, thus their shape cannot be estab-



lished. The  $3/2^- \Sigma(1940)$  should be the first resonance on the leading odd natural-parity trajectory, however there is weak evidence of such a pole in mass dependent partial-wave analysis of  $\bar{K}N$  scattering. The situation with the  $\Xi$  and  $\Omega$  baryons is even worse [10].

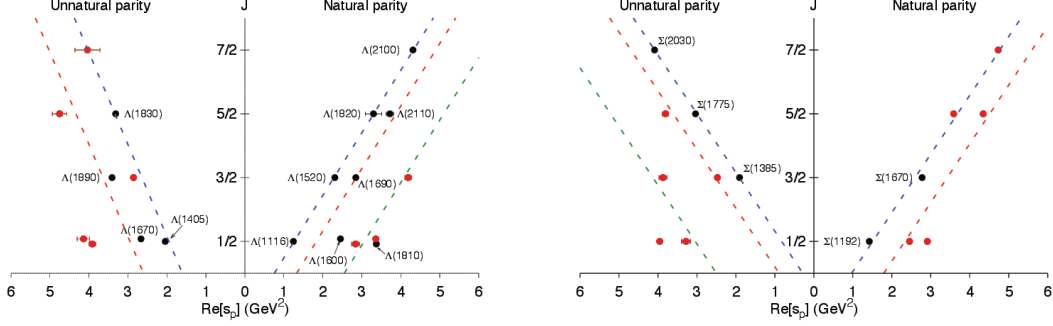


Figure 1: Chew–Frautschi plot for the  $\Lambda$  and  $\Sigma$  Regge trajectories. Black dots represent resonances with a four-star status in the *Review of Particle Properties* [10]. All resonances are taken from JPAC analysis in [11]. Dashed lines are displayed to guide the eye.

The most recent (and advanced) mass-dependent partial-wave analysis of the single-energy partial waves of the KSU data analysis of  $\bar{K}N$  scattering in the resonant region [12] was performed by JPAC in [11]. The partial-wave model is based on a coupled-channel K-matrix approach. It incorporates up to 13 channels per partial wave, analyticity, unitarity, and the appropriate threshold (angular momentum barrier) factors for the partial waves. Here we sketch the building blocks of the model. For further details, the analysis, the fitting, and the obtained spectrum we refer the reader to [11].

The partial-wave expanded scattering matrix  $S_\ell$  can be written in terms of the amplitude  $T_\ell$  as follows

$$S_\ell = \mathbb{I} + 2iR_\ell(s) = \mathbb{I} + 2i [C_\ell(s)]^{1/2} T_\ell(s) [C_\ell(s)]^{1/2}, \quad (1)$$

where  $\mathbb{I}$  is the identity matrix and the diagonal matrix

$$C_\ell(s) = \frac{q_k(s)}{q_0} \left[ \frac{r^2 q_k^2(s)}{1 + r^2 q_k^2(s)} \right]^\ell \quad (2)$$

takes into account the phase space. We define  $q_k(s) = \sqrt{(m_a m_b)(s - s_k)/(m_a + m_b)}$ , where  $m_a$  and  $m_b$  are the masses of the outgoing particles,  $s_k$  is the threshold center-of-mass energy squared of channel  $k$ , and  $q_0 = 2 \text{ GeV}$  and  $r = 1 \text{ fm}$  are normalization factors.

We employ the  $K$  matrix approach to guarantee unitarity through

$$T_\ell(s) = [K(s)^{-1} - i\rho(s, \ell)]^{-1}, \quad (3)$$

where  $\rho(s, \ell)$  is obtained from  $C_\ell(s)$  by means of a dispersive integral

$$i\rho(s, \ell) = \frac{s - s_k}{\pi} \int_{s_k}^{\infty} \frac{C_\ell(s')}{s' - s} \frac{ds'}{s' - s_k}. \quad (4)$$

In this way,  $T_\ell(s)$  can be analytically continued to both  $s$  and  $\ell$  complex planes. To build the  $K(s)$  matrix in equation (3) we add up to six  $K$  matrices

$$[K(s)]_{kj} = \sum_a x_k^a K_a(s) x_j^a. \quad (5)$$

Each  $K_a(s)$  matrix can either represent a *pole*,

$$[K_P(s)]_{kj} = x_k^P \frac{M_P}{M_P^2 - s} x_j^P, \quad (6)$$

or a *background* term,

$$[K_B(s)]_{kj} = x_k^B \frac{M_B}{M_B^2 + s} x_j^B. \quad (7)$$

The relative contribution of *pole* vs. *background* terms depends on the individual partial wave. The parameters  $M_P$ ,  $x_k^P$ ,  $M_B$  and  $x_k^B$  are fixed by fitting the single-energy partial waves from the KSU analysis [12] using MINUIT [13] and a genetic algorithm [14]. Once these parameters have been fitted to the data we can analytically continue the amplitudes to the unphysical Riemann sheets and search for poles (hyperon resonances). In Fig. 1 we show the Chew-Frautschi [15] plot of the obtained hyperon resonances.

The codes to compute the partial waves and the observables (cross sections and asymmetries) can be downloaded from or run online on the JPAC web page [2, 16].

### 3. On the Nature of the $\Lambda(1405)$

The nature of  $\Lambda(1405)$  hyperon resonance has been an open question for more than half a century [17]. The interest in this state has been renewed recently because of the new precision data from CLAS that enabled to resolve its spin and parity and confirm the  $J^P = 1/2^-$  assignment [18]. There have also been new developments in chiral unitary models [19–21], large  $N_c$  QCD calculations [22], lattice QCD [23, 24], quark-diquark models [25, 26], and Regge phenomenology [27].

Chiral unitary models applied to  $\bar{K}N$  scattering and  $\pi\Sigma K^+$  photoproduction have been able to establish that the  $\Lambda(1405)$  is not a single state but it corresponds to two resonances [19–21, 28] located at  $1429_{-7}^{+8} - i 12_{-3}^{+2}$  MeV and at  $1325_{-15}^{+15} - i 90_{-18}^{+12}$  MeV [20]. In these papers the  $\Lambda(1405)$  poles are interpreted as of molecular nature. However, the poles are generated by effective interactions and there is no reference to the fundamental, *i.e.*, QCD, composition of the resonances. Hence, the answer to the question of the nature of the poles remains open. Especially if we consider that large  $N_c$  QCD calculations of the baryon spectrum indicate that a (mostly) three-quark state should appear in the  $\Lambda(1405)$  region [22]. Furthermore, recent quark-diquark models obtain a state in the  $\Lambda(1405)$  region at 1431 MeV in [25] and at 1406 MeV in [26].

Regarding lattice QCD, the available simulations lead to inconclusive results. In [23]  $\Lambda(1405)$  appears to be a three-quark state while in [24] it seems to be more like a  $\bar{K}N$  molecule. However, it has to be taken into account that the resonant nature of the  $\Lambda(1405)$  has been ignored in these calculations [29].

In [27], we use Regge phenomenology and connect the  $\Lambda(1405)$  to the rest of the hyperon spectrum. In Fig. 2 we show the leading Regge trajectories for  $\Lambda$  and  $\Sigma$  hyperons. It is apparent how one of the  $\Lambda(1405)$  poles ( $1429^{+8}_{-7} - i12^{+2}_{-3}$  MeV) fits within the leading natural-parity  $\Lambda$  Regge trajectory while the other ( $1325^{+15}_{-15} - i90^{+12}_{-18}$  MeV) does not. The presence of a new narrow-width  $3/2^+$  state in the leading natural-parity  $\Lambda$  Regge trajectory is essential to reach this conclusion. The first evidence of such state was provided in [30] and latter confirmed by JPAC analysis [11].

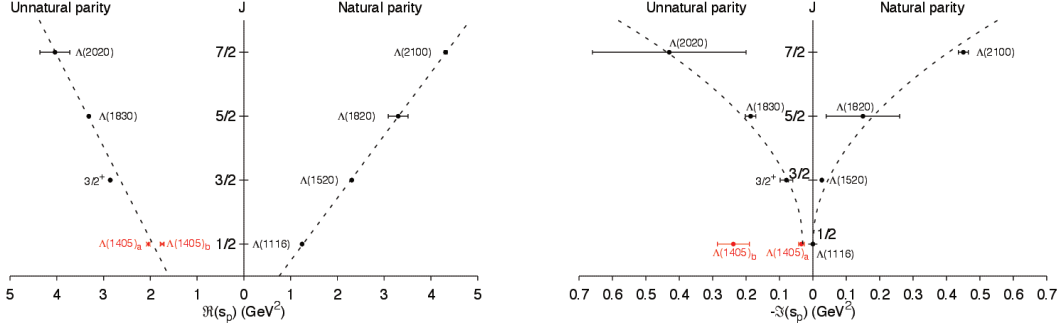


Figure 2: Leading Regge trajectories for the  $\Lambda$  resonances. Dashed lines are displayed to guide the eye.

In [27], we confirm what is apparent from inspecting Fig. 2 through extensive numerical calculations by performing fits to various physically motivated parametrizations of the Regge trajectories. We used  $\Sigma$  Regge trajectories and the natural-parity  $\Lambda$  trajectory to benchmark our approach. This analysis lead to the conclusion that the higher-mass pole belongs to the leading Regge trajectory and is compatible with a three-quark structure, while the lower-mass one does not belong either to the leading or to a nearby daughter Regge trajectory.

#### 4. Conclusions

JPAC encourages close collaboration between experimentalists and theorists on implementing theoretical innovations into the existing data analysis stream to order to obtain robust information on the hadron spectrum and hadron structure.

Recently we have developed in [11] a  $\bar{K}N$  model in the resonance region guided by S-matrix unitarity and analyticity (both in the  $s$  and the  $\ell$  complex planes). We have obtained the most comprehensive picture of the  $\Lambda$  and  $\Sigma$  spectra to the date. Both spectra show a remarkable alignment of hyperons in Regge trajectories. The codes to compute the partial waves and the observables (cross sections and asymmetries) can be run online and downloaded from [2].

Regge phenomenology seems to indicate that the higher-mass  $\Lambda(1405)$  pole belongs to the leading Regge trajectory and that it is compatible with a (mostly) three-quark structure, while the lower-mass one is either a molecule or a pentaquark. If confirmed, by for example new data with  $K_L$  beams, this finding becomes of prominent importance in identifying a two-component hybrid resonance. It also sheds a valuable light on the success/failure of approaches based on  $\bar{K}N$ , three-quark, or five-quark states embodying genuine intrinsic light

quark-antiquark pairs. The work presented in [27] gives a new direction for investigation of the origin of poles associated with the  $\Lambda(1405)$  that can also be extended to other sectors of the baryon spectrum.

## 5. Acknowledgments

This material is based upon work supported in part by the U.S. Department of Energy, Office of Science, Office of Nuclear Physics under contract DE-AC05-06OR23177. This work was also supported in part by the U.S. Department of Energy under Grant DE-FG0287ER40365, National Science Foundation under Grants PHY-1415459 and PHY-1205019, and IU Collaborative Research Grant.

## References

- [1] M. Battaglieri *et al.*, Acta Phys. Polon. B **46**, 257 (2015).
- [2] <http://www.indiana.edu/~jpac/index.html>
- [3] R.J. Eden, P.V. Landshoff, D.I. Olive, J.C. Polkinghorne, *The Analytic S-Matrix* (Cambridge University Press, Cambridge, England, 2003).
- [4] V.N. Gribov, *The Theory of Complex Angular Momenta* (Cambridge University Press, Cambridge, England, 2003).
- [5] P.D. B. Collins, *An Introduction to Regge Theory and High-Energy Physics* (Cambridge University Press, Cambridge, England, 1977).
- [6] E.P. Wigner, Phys. Rev. **70**, 15 (1946); A.M. Badalyan, L.P. Kok, and Y.A. Simonov, Phys. Rep. **82**, 31 (1982).
- [7] G.F. Chew and S. Mandelstam, Phys. Rev. **119**, 467 (1960).
- [8] E. Oset and A. Ramos, Nucl. Phys. A **635**, 99 (1998); E. Oset, *these proceedings*.
- [9] J.J. Dudek, R.G. Edwards, C.E. Thomas, and D.J. Wilson, Phys. Rev. Lett. **113**, 182001 (2014); D.J. Wilson *et al.*, Phys. Rev. D **92** 094502 (2015); J.J. Dudek, R.G. Edwards, and D.J. Wilson, arXiv:1602.05122 [hep-ph]; R.A. Briceño and M.T. Hansen, arXiv:1509.08507 [hep-lat].
- [10] K.A. Olive *et al.* (Particle Data Group), Chin. Phys. C **38**, 090001 (2014).
- [11] C. Fernández-Ramírez *et al.*, Phys. Rev. D **93**, 034029 (2016).
- [12] H. Zhang, J. Tulpan, M. Shrestha, and D.M. Manley, Phys. Rev. C **88**, 035204 (2013).
- [13] F. James and M. Roos, Comput. Phys. Commun. **10**, 343 (1975).
- [14] C. Fernández-Ramírez, E. Moya de Guerra, A. Udías, and J.M. Udías, Phys. Rev. C **77**, 065212 (2008).

- [15] G.F. Chew and S.C. Frautschi, Phys. Rev. Lett. **8**, 41 (1962).
- [16] V. Mathieu, arXiv:1601.01751 [hep-ph].
- [17] R.H. Dalitz and S.F. Tuan, Phys. Rev. Lett. **2**, 425 (1959); M.H. Alston *et al.*, Phys. Rev. Lett. **6**, 698 (1961); A. Engler *et al.*, Phys. Rev. Lett. **15**, 224 (1965).
- [18] K. Moriya *et al.*, Phys. Rev. Lett. **112**, 082004 (2014).
- [19] L. Roca and E. Oset, Phys. Rev. C **87**, 055201 (2013).
- [20] M. Mai and U.-G. Meißner, Eur. Phys. J. A **51**, 30 (2015).
- [21] D. Jido *et al.*, Nucl. Phys. A **725**, 181 (2003); T. Hyodo and W. Weise, Phys. Rev. C **77**, 035204 (2008).
- [22] C.L. Schat, J.L. Goity, and N.N. Scoccola, Phys. Rev. Lett. **88**, 102002 (2002); C.L. Schat, J.L. Goity, and N.N. Scoccola, Phys. Rev. D **66**, 114014 (2002).
- [23] G.P. Engel, C.B. Lang, and A. Schäfer, Phys. Rev. D **87**, 034502 (2013); G.P. Engel, C.B. Lang, D. Mohler, and A. Schäfer, Phys. Rev. D **87**, 074504 (2013).
- [24] J.M.M. Hall *et al.*, Phys. Rev. Lett. **114**, 132002 (2015).
- [25] E. Santopinto and J. Ferretti, Phys. Rev. C **92**, 025202 (2015).
- [26] R.N. Faustov and V.O. Galkin, Phys. Rev. D **92**, 054005 (2015).
- [27] C. Fernández-Ramírez, I.V. Danilkin, V. Mathieu, and A.P. Szczepaniak, arXiv:1512.03136 [hep-ph].
- [28] R.H. Dalitz and S.F. Tuan, Ann. Phys. (NY), **10**, 307 (1960); R.H. Dalitz, T.C. Wong, and G. Rajasekaran, Phys. Rev. **153**, 1617 (1967); N. Kaiser, T. Waas, and W. Weise, Nucl. Phys. A **612**, 297 (1997); J.A. Oller and U.-G. Meißner, Nucl. Phys. B **500**, 263 (2001); L. Roca, T. Hyodo, and D. Jido, Nucl. Phys. A **809**, 65 (2008); T. Hyodo and D. Jido, Prog. Part. Nucl. Phys. **67**, 55 (2012); L. Roca and E. Oset Phys. Rev. C **88**, 055206 (2013); Y. Kamiya *et al.*, arXiv:1602.08852.
- [29] C. Fernández-Ramírez, J. Phys.: Conf. Ser. (in press), arXiv:1603.00868 [hep-ph].
- [30] J. Shi and B.S. Zou, Phys. Rev. C **91**, 035202 (2015).

## 2.13 Spectrum and Quantum Numbers of $\Xi$ Resonances

Yongseok Oh

*Department of Physics*

*Kyungpook National University*

*Daegu 41566, Korea &*

*Institute for Nuclear Studies and Department of Physics*

*The George Washington University*

*Washington, DC 20052, U.S.A.*

### Abstract

Hyperons with strangeness  $-2$  and  $-3$  provide a useful tool to investigate the structure of baryons and the underlying dynamics. They are expected to give information which is hard to be seen in nonstrange or strangeness  $-1$  baryons. In this presentation, we analyze the spectrum of  $\Xi$  resonances in various models and make comments on the problems and puzzles. In particular, the hyperon spectrum in the bound state approach of the Skyrme model is discussed to identify the analog states of  $\Lambda(1405)$  in strangeness  $-2$  and  $-3$  sector. In addition, sum rules in hyperons masses and magnetic moments are presented, which can be used to predict unmeasured masses and magnetic moments of hyperons. The planned Kaon beam facility will have a crucial role to resolve these issues and open a new way to understand baryon structure.

### 1. Introduction

Understanding the structure of baryons is essential to investigate strong interactions. In particular, establishing baryon spectrum requires rigorous studies both in theoretical and experimental investigations and identifying quantum numbers and various physical quantities of baryons is crucial to resolve questions and puzzles in baryon structure and strong interactions. In theoretical side, there many phenomenological models have been developed to explain the observed baryon spectrum and to predict unobserved states. Since Quantum Chromodynamics, the underlying theory of strong interactions, cannot be directly used to explain baryon spectrum, those models inevitably introduce several model parameters. These parameters are fitted to observed physical properties of baryons and then the model can be used to make predictions. Since such parameters are mostly determined in the non-strange baryon sector or strangeness  $-1$  sector, there is little, if any, freedom to introduce more parameters in the multi-strangeness sector. In this respect, the importance of studying multistrangeness sector cannot be overemphasized as it can provide a very useful tool to test various models.

In spite of the early efforts for studying  $\Xi$  and  $\Omega$  spectra, our understanding on the multi-strangeness sector is still far from complete and opens many questions. As mentioned by the Particle Data Group, there are several serious difficulties in studying  $\Xi$  and  $\Omega$  resonances experimentally. First of all, the cross sections of producing multistrangeness from nonstrange initial state are very small and precise studies on the spectrum and properties of  $\Xi$  and  $\Omega$  hyperons are extremely difficult. An example can be found in the case of the  $\Omega^-$  hyperon that has strangeness  $-3$ . Although the ground state of  $\Omega^-$  baryon was discovered at BNL

in mid 60s [1], which confirmed the prediction of Gell-Mann [2], it took about 40 years to confirm that it has spin-3/2 [3]. Furthermore, the parity of the ground state of  $\Xi$  hyperon has not been measured [4]. The lack of Kaon beam facility, therefore, lead to the conclusion that any new significant information on the multi-strangeness baryons has not been accumulated during the last two decades [4]. Nevertheless, the continuous efforts to study multistrangeness system cause, albeit slow, progress in our knowledge in this system. This includes the measurement of the magnetic moment of  $\Omega^-(1672)$  [5], experimental studies on  $\Xi$  resonances [6], measuring weak decays of  $\Xi^0$  hyperon [7, 8], and the production of  $\Xi$  resonances in relativistic heavy-ion collisions [9]. In addition, BABAR Collaboration claimed that the spin-parity quantum number of the  $\Xi(1690)$  would be  $\frac{1}{2}^-$  [10].

Recently interests in multistrangeness systems are renewed by the advent of new facilities. Indeed, the cascade physics program of the CLAS Collaboration at the Thomas Jefferson National Accelerator Facility (JLab) has been launched and some preliminary results were already reported [11–14]. This activity continues to initiate a  $\Xi$  spectroscopy program using photoproduction reactions at the upgraded 12-GeV machine, which also includes a plan to measure exclusive  $\Omega$  photoproduction [15]. J-PARC has a Kaon beam facility and is going to study the  $\Xi$  baryons via the  $\bar{K}N$  scattering although the energy is not large enough to produce most  $\Xi$  resonances. It also plans to study the  $\pi N$  reaction to produce  $\Xi$  and  $\Omega$  hyperons. These reactions can also be used to identify the spin-parity quantum numbers of produced hyperons [16–18]. The plan for having a  $K_L$  beam at JLab will be complementary to J-PARC facility and unique place to produce  $\Xi$  and  $\Omega$  resonances by offering higher energy Kaon beams.

Table 1 lists the multistrangeness baryons compiled in the review of the Particle Data Group (PDG) [4], which includes eleven  $\Xi$  baryons and four  $\Omega$  baryons. Among them only the ground states,  $\Xi(1318)$ ,  $\Xi(1530)$ , and  $\Omega(1672)$ , have four-star ratings with definite spin-parity, and there are four  $\Xi$  baryons and one  $\Omega$  baryon with three-star ratings. Among the three-star-rated baryons, the  $\Xi(1820)$  is the only state whose spin-parity quantum numbers are reported.

In this presentation, we discuss the predictions of various models on hyperon spectrum. We will see that these predictions are not consistent with experimental observations and are even contradictory to each other. This shows the importance of high-quality and high-energy Kaon beam facilities to understand the underlying dynamics of hyperon structure.

## 2. Model Dependence of Hyperon Spectrum

There have been various theoretical studies on the excited states of multi-strangeness baryons based on phenomenological models. Although those models could reproduce the masses of the ground states of octet and decuplet, it is mainly due to the SU(3) group structure. Because of this, most models have the same mass sum rules for the ground state baryons. However they have very different and even contradictory predictions on the spectrum of excited states, in particular, for multistrangeness baryons. The most evident example is the third state of  $\Xi$  baryons as will be explained below. (See also Ref. [19].)

The most straightforward application of the SU(3) group structure is finding the SU(3) multiplets and their members. Early efforts in this direction were summarized, for example,

Table 1:  $\Xi$  and  $\Omega$  baryons compiled by the Particle Data Group [4].

Particle	$I(J^P)$	rating	Particle	$I(J^P)$	rating
$\Xi(1318)$	$\frac{1}{2}(\frac{1}{2}^+)$	****	$\Omega(1672)$	$0(\frac{3}{2}^+)$	****
$\Xi(1530)$	$\frac{1}{2}(\frac{3}{2}^+)$	****	$\Omega(2250)$	$0(?)^?$	***
$\Xi(1620)$	$\frac{1}{2}(\frac{1}{2}^?)$	*	$\Omega(2380)$	$?(?)^?$	**
$\Xi(1690)$	$\frac{1}{2}(\frac{1}{2}^-?)$	***	$\Omega(2470)$	$?(?)^?$	**
$\Xi(1820)$	$\frac{1}{2}(\frac{3}{2}^-)$	***			
$\Xi(1950)$	$\frac{1}{2}(\frac{1}{2}^?)$	***			
$\Xi(2030)$	$\frac{1}{2}(\geq \frac{5}{2}^?)$	***			
$\Xi(2120)$	$\frac{1}{2}(\frac{1}{2}^?)$	*			
$\Xi(2250)$	$\frac{1}{2}(\frac{1}{2}^?)$	**			
$\Xi(2370)$	$\frac{1}{2}(\frac{1}{2}^?)$	**			
$\Xi(2500)$	$\frac{1}{2}(\frac{1}{2}^?)$	*			

in Refs. [20–22]. However, such approaches ignore the dynamics of the constituents of baryons. A more detailed study on the excited states of  $\Xi$  and  $\Omega$  baryons was done by Chao, Isgur, and Karl [23] employing a non-relativistic quark model as the quark dynamics. In this model, the  $\Xi(1820)\frac{3}{2}^-$  is well explained and the third lowest state following  $\Xi(1318)$  and  $\Xi(1530)$  is predicted to be at a mass of 1695 MeV having  $J^P = \frac{1}{2}^+$ . Although this model predicts the almost correct mass for  $\Xi(1690)$ , its prediction on the spin-parity quantum numbers is not consistent with the experimental observation of Ref. [10].

The relativized quark model of Capstick and Isgur, however, gives a very different predictions on  $\Xi$  resonances [24]. In this model, the first excited state of  $\Xi(\frac{1}{2}^+)$  has a higher mass of around 1840 MeV. Furthermore, the third lowest  $\Xi$  state would have a mass of 1755 MeV with  $J^P = \frac{1}{2}^-$ . Although the spin-parity quantum numbers are consistent with  $\Xi(1690)$ , its mass is much larger than the mass of  $\Xi(1690)$ . This pattern is also confirmed by a more recent relativistic quark model of Ref. [25].

In the one-boson exchange model, Glozman and Riska predicted that the third lowest state would have odd parity at a mass of 1758 MeV with  $J = 1/2$  or  $3/2$  [26]. This mass is in the middle of the masses of  $\Xi(1820)$  and  $\Xi(1690)$ . As a result, this model overestimates the mass of  $\Xi(1690)$  and underestimates that of  $\Xi(1820)$  [27, 28].

One may construct a mass operator based on large  $N_c$  approximation of QCD, where  $N_c$  is the number of colors. Then the coefficients of the mass operator can be fitted by some known masses and then it can predict the masses of other baryons. The results can be found in Refs. [29–33], where a quite different  $\Xi$  spectrum can be found. In this approach, the third lowest state would have  $J^P = \frac{1}{2}^-$  at a mass of 1780 MeV. Therefore, this model gives a prediction on the third lowest  $\Xi$  resonance mass similar to that of relativistic quark models. (See Ref. [34] for a connection between the quark models and the large  $N_c$  expansion.)

In the algebraic model of Bijker *et al.* [35], the third lowest state has  $J^P = \frac{1}{2}^+$  at a mass around 1730 MeV. Thus it is not consistent with the BABAR result. This model predicts two



Table 2: Low-lying  $\Xi$  and  $\Omega$  baryon spectrum of spin 1/2 and 3/2 predicted by the non-relativistic quark model of Chao *et al.* [23] (CIK), relativized quark model of Capstick and Isgur [24] (CI), Glozman-Riska model [26] (GR), large  $N_c$  analysis [29–33], algebraic model [35] (BIL), and QCD sum rules [36, 37] (SR). The recent quark model prediction [25] (QM), and the Skyrme model results [19] (SK) are given as well. The mass is given in the unit of MeV.

State	CIK	CI	GR	Large- $N_c$	BIL	SR	QM	SK
$\Xi(\frac{1}{2}^+)$	1325	1305	1320		1334	1320 (1320)	1325	1318
	1695	1840	1798	1825	1727		1891	1932
	1950	2040	1947	1839	1932		2014	
$\Xi(\frac{3}{2}^+)$	1530	1505	1516		1524		1520	1539
	1930	2045	1886	1854	1878		1934	2120
	1965	2065	1947	1859	1979		2020	
$\Xi(\frac{1}{2}^-)$	1785	1755	1758	1780	1869	1550 (1630)	1725	1614
	1890	1810	1849	1922	1932		1811	1660
	1925	1835	1889	1927	2076			
$\Xi(\frac{3}{2}^-)$	1800	1785	1758	1815	1828	1840	1759	1820
	1910	1880	1849	1973	1869		1826	
	1970	1895	1889	1980	1932			
$\Omega(\frac{1}{2}^+)$	2190	2220	2068	2408	2085		2175	2140
	2210	2255	2166		2219		2191	
$\Omega(\frac{3}{2}^+)$	1675	1635	1651		1670		1656	1694
	2065	2165	2020	1922	1998		2170	2282
	2215	2280	2068	2120	2219		2182	
$\Omega(\frac{1}{2}^-)$	2020	1950	1991	2061	1989		1923	1837
$\Omega(\frac{3}{2}^-)$	2020	2000	1991	2100	1989		1953	1978

$\Xi(\frac{3}{2}^-)$  states which lie close to the observed  $\Xi(1820)$ . As a result, it predicts richer hyperon spectrum than quark models and, in particular, it makes very different predictions for the  $J^P = \frac{1}{2}^-$  states.

The QCD sum rule approaches were also used to identify the lowest states of each spin-parity quantum numbers [36, 37]. All results are summarized in Table 2 for low-lying  $\Xi$  and  $\Omega$  resonances. It shows that the predictions on  $\Xi$  and  $\Omega$  spectrum are highly model-dependent and having precise information on these resonances is crucial to distinguish the underlying dynamics and baryon structure.

### 3. The Skyrme Model

As can be seen in Table 2, the quark models have a difficulty in explaining the mass and spin-parity quantum numbers of  $\Xi(1690)$ . Furthermore, the presence of  $\Xi(1620)$ , if confirmed, raises a serious question on the prediction of quark models. This is very similar to the puzzle of  $\Lambda(1405)$ , where the low mass of the  $\Lambda(1405)$  hyperon makes it hard to be described as a

$P$ -wave three-quark state [38, 39]. Instead, interpreting the  $\Lambda(1405)$  as a  $\bar{K}N$  bound state has been successful to understand its physical properties [40–42]. It is then natural to search for other hyperons that have similar structure as the  $\Lambda(1405)$  and we claim that  $\Xi(1620)$  and  $\Xi(1690)$  are such states through investigating the hyperon spectrum in the bound state approach in the Skyrme model.

In the bound state approach to the Skyrme model [43], hyperons are described as bound states of the  $SU(2)$  soliton and the Kaon. (The  $K^*$  vector meson can also be included.) The underlying dynamics between the soliton and Kaon is described by a chiral Lagrangian of mesons. As shown in Ref. [43], the Wess-Zumino term in an  $SU(3)$  chiral Lagrangian has a very crucial role in hyperon spectrum by pushing up the  $S = +1$  state while pulling down the  $S = -1$  state. As a result, the  $S = +1$  pentaquark  $\Theta^+$  cannot be a bound state, and the bound states of  $S = -1$  correspond to the normal hyperons. Furthermore, this model renders two bound states, a positive parity state in  $P$ -wave and a negative parity state in  $S$ -wave. The  $P$ -wave state is strongly bound and, when quantized, it gives the ground states of hyperons with  $j^P = 1/2^+$  and  $3/2^+$ . On the other hand, the  $S$ -wave state is an excited state and, when quantized, it corresponds to the  $\Lambda(1405)$  with  $j^P = 1/2^-$ . Therefore, this model gives a natural way to describe both the  $\Lambda(1116, 1/2^+)$  and the  $\Lambda(1405, 1/2^-)$  on the same footing [44].

In this model, the mass of a hyperon with isospin  $i$  and spin  $j$  is written as [19]

$$M(i, j, j_m)M_{\text{sol}} + n_1\omega_1 + n_2\omega_2 + \frac{1}{2\mathcal{I}} \left\{ i(i+1) + c_1c_2j_m(j_m+1) + (\bar{c}_1 - c_1c_2)j_1(j_1+1) + (\bar{c}_2 - c_1c_2)j_2(j_2+1) + \frac{c_1+c_2}{2}[j(j+1) - j_m(j_m+1) - i(i+1)] + \frac{c_1-c_2}{2}\vec{R} \cdot (\vec{J}_1 - \vec{J}_2) \right\}, \quad (1)$$

where  $\vec{J}_1$  and  $\vec{J}_2$  are the grand spins of the  $P$ -wave and  $S$ -wave Kaon, respectively, and  $\vec{J}_m = \vec{J}_1 + \vec{J}_2$ . The total spin of the system is then given by  $\vec{J} = \vec{J}_{\text{sol}} + \vec{J}_m$ , where  $\vec{J}_{\text{sol}}$  is the soliton spin. The number and energy of the bound Kaons are  $n_i$  and  $\omega_i$ , respectively, and  $c_i$  are the hyperfine splitting constants of the bound states. We refer the details to Ref. [19], but we emphasize that this mass formula has three parts in large  $N_c$  expansion. First, the soliton mass  $M_{\text{sol}}$  is of  $O(N_c)$  and the energies of the bound Kaons are of  $O(N_c^0)$ . The hyperfine term, which contains  $1/2\mathcal{I}$  with  $\mathcal{I}$  being the moment of inertia, is of  $O(1/N_c)$ . This shows that the mass splitting between the  $\Lambda(1405)$  and the  $\Lambda(1116)$  mainly comes from the energy difference between the  $P$ -wave Kaon and the  $S$ -wave Kaon. In fact, its empirical value is about 300 MeV and this pattern repeats in the  $\Xi$  baryon spectrum and in the  $\Omega$  baryon spectrum.

In principle, the mass parameters in Eq. (1) can be calculated for a given dynamics of the meson-soliton system, for example, by extending the work of Refs. [45, 46]. However, this is a highly nontrivial and complicated calculation. Therefore, instead of calculating the mass parameters, we fit them to some known hyperon masses and predict the masses of other hyperons. The obtained results are illustrated in Table 3.

Table 3: Mass spectrum of the Skyrme model. The underlined values are used to determine the mass parameters. The values within the parenthesis are obtained by considering the mixing effect [19]. The question marks after the particle name mean that the spin-parity quantum numbers are not identified yet.

Particle Name	Mass (MeV)	Assigned State
$N$	<u>939</u>	
$\Delta$	<u>1232</u>	
$\Lambda_{1/2^+,0}$	<u>1116</u>	$\Lambda(1116)$
$\Lambda_{1/2^-,1}$	<u>1405</u>	$\Lambda(1405)$
$\Sigma_{1/2^+,0}$	1164	$\Sigma(1193)$
$\Sigma_{3/2^+,0}$	<u>1385</u>	$\Sigma(1385)$
$\Sigma_{1/2^-,1}$	1475	$\Sigma(1480)?$
$\Sigma_{3/2^-,1}$	1663	$\Sigma(1670)$
$\Xi_{1/2^+,0}$	<u>1318</u>	$\Xi(1318)$
$\Xi_{3/2^+,0}$	1539	$\Xi(1530)$
$\Xi_{1/2^-,1}$	1658(1660)*	$\Xi(1690)?$
$\Xi_{1/2^-,2}$	1616(1614)*	$\Xi(1620)?$
$\Xi_{3/2^-,1}$	<u>1820</u>	$\Xi(1820)$
$\Xi_{1/2^+,1}$	1932	$\Xi(1950)?$
$\Xi_{3/2^+,1}$	<u>2120</u>	$\Xi(2120)?$
$\Omega_{3/2^+,0}$	1694	$\Omega(1672)$
$\Omega_{1/2^-,1}$	1837	
$\Omega_{3/2^-,1}$	1978	
$\Omega_{1/2^+,1}$	2140	
$\Omega_{3/2^+,1}$	2282	$\Omega(2250)?$
$\Omega_{3/2^-,2}$	2604	

In this model, the parity of a hyperon changes if the  $P$ -wave Kaon is replaced by the  $S$ -wave state. Since the energy difference between the two Kaons is about 300 MeV, there always exist pairs of hyperons of having same spin and the opposite parity with a mass difference of about 300 MeV. Since the mass of the ground state of the  $\Xi(1/2^+)$  is 1318 MeV, a  $\Xi(1/2^-)$  state is expected at a mass of about 1620 MeV. Furthermore, this model requires two  $\Xi$  states of this mass scale. This is because the two Kaons, one in  $P$ -wave and one in  $S$ -wave, can make either  $j_m = 0$  or  $j_m = 1$  states. Considering the soliton spin  $j_{\text{sol}} = 1/2$ , these states can give two  $j = 1/2$  states and one  $j = 3/2$  state. This explains naturally the existence of two  $\Xi$  baryons with  $j^P = 1/2^-$  at similar masses, namely, the one-star rated  $\Xi(1620)$  and the three-star rated  $\Xi(1690)$ . However, since the observation of the  $\Xi(1620)$  at early 1980s [47], there is no other experimental confirmation of this state. Therefore, it is strongly required to resolve this issue urgently at current experimental facilities.

This analysis reveals that the  $\Xi(1620)$  and the  $\Xi(1690)$  are analogue states of the  $\Lambda(1405)$ . In addition, by replacing two  $P$ -wave Kaons in the  $\Xi(1382)$  and in the  $\Xi(1530)$ , we predict

that the  $\Xi(1950)$  has  $j^P = 1/2^+$  and the  $\Xi(2120)$  has  $j^P = 3/2^+$ . Their spin-parity quantum numbers are not known yet and should be identified by future experiments.

Comparing the predictions presented in Tables 2 and 3 shows that the predictions on the  $\Omega$  hyperon spectrum are drastically different from the quark model predictions. In quark models, the second lowest  $\Omega$  hyperon has a mass of around 2 GeV, while the second state has a mass of around 1840 MeV with  $j^P = 1/2^-$ . Again, this low mass of the  $\Omega$  excited state can hardly be explained by quark models. Thus, it is very interesting and crucial to see whether such low mass  $\Omega$  hyperon really exists. Furthermore, most quark models predict that the lowest  $\Omega$  baryon with  $j^P = 1/2^-$  is degenerate or almost degenerate in mass with the lowest  $\Omega$  baryon with  $j^P = 3/2^-$ , which is in contradiction to our predictions. These inconsistency with quark model predictions can be tested by future experiments.

If we extend our model to heavy quark baryons with a charm or a bottom quark [48], we can also find a similar pattern in heavy baryon spectra. In Ref. [49], the binding energies of the soliton-heavy-meson system were calculated in the rest frame of the heavy meson, which shows that the energy difference between the positive parity state and the negative parity state is again close to 300 MeV, which can explain the observed masses of  $\Lambda_c(2286)$  of  $j^P = 1/2^+$  and the  $\Lambda_c(2595)$  of  $j^P = 1/2^-$ . In quark models, the mass difference between the two states are estimated to be  $250 \sim 350$  MeV depending on the details of the quark dynamics [24, 50]. Therefore, more detailed studies are needed to clarify the structure of the  $\Lambda_c(2595)$ .

#### 4. Mass and Magnetic Moment Sum Rules

The mass formula of Eq. (1) can be used to derive mass sum rules. Since it contains the second order of strangeness, it satisfies the modified Gell-Mann–Okubo mass relation and the modified decuplet equal spacing rule [51],

$$\begin{aligned} 3\Lambda + \Sigma - 2(N + \Xi) &= \Sigma^* - \Delta - (\Omega - \Xi^*), \\ (\Omega - \Xi^*) - (\Xi^* - \Sigma^*) &= (\Xi^* - \Sigma^*) - (\Sigma^* - \Delta), \end{aligned} \quad (2)$$

where the symbols denote the masses of the corresponding octet and decuplet ground states. On the other hand, the hyperfine relation holds even with the second order of strangeness, and, therefore, the mass formula of Eq. (1) satisfies

$$\Sigma^* - \Sigma + \frac{3}{2}(\Sigma - \Lambda) = \Delta - N. \quad (3)$$

Since the mass relations (2) and (3) are obtained for the hyperons with the  $P$ -wave Kaons, the same relations should be true for the hyperons containing the  $S$ -wave Kaons only. Therefore, those relations are expected to be valid by replacing  $\Lambda$ ,  $\Sigma$ ,  $\Sigma^*$ ,  $\Xi$ ,  $\Xi^*$ , and  $\Omega$  by  $\Lambda_{1/2^-,1}$ ,  $\Sigma_{1/2^-,1}$ ,  $\Sigma_{3/2^-,1}$ ,  $\Xi_{1/2^+,1}$ ,  $\Xi_{3/2^+,1}$ , and  $\Omega_{3/2^-,2}$ , respectively. Note that those mass sum rules relate the mixed parity states of hyperons, *i.e.*, odd-parity  $\Lambda$  and  $\Sigma$ , even-parity  $\Xi$ , and odd-parity  $\Omega$ , and, therefore, should be distinguished by the quark model predictions.

We also derive a mass sum rule of

$$\Omega_{3/2^+,1} - \Omega_{3/2^-,1} = \Omega_{1/2^+,1} - \Omega_{1/2^-,1} \quad (4)$$

for  $\Omega$  resonances.

This reveals the character of the bound state model, namely, the mass differences between the baryons of the same spin but of opposite parity, which we call “parity partners”, are the same. Although the mass splitting of other parity partner hyperons are not exactly equal to the above formula, we observe that their mass differences are always close to  $\sim 290$  MeV and this pattern can be actually observed in some experimental data.

The magnetic moment operator in this approach can be written as [52]

$$\hat{\mu} = \hat{\mu}_s + \hat{\mu}_v, \quad (5)$$

where

$$\begin{aligned} \hat{\mu}_s &= \mu_{s,0}R^z + \mu_{s,1}J_1^z + \mu_{s,2}J_2^z, \\ \hat{\mu}_v &= -2(\mu_{v,0} + \mu_{v,1}n_1 + \mu_{v,2}n_2)D^{33}, \end{aligned} \quad (6)$$

with  $D^{33} = -I^z R^z / \mathbf{I}^2$ . Here,  $\mu_{s,0}$  and  $\mu_{v,0}$  are the magnetic moment parameters of the SU(2) sector while  $\mu_{s,1}$  and  $\mu_{v,1}$  ( $\mu_{s,2}$  and  $\mu_{v,2}$ ) are the parameters for the  $P$ -wave ( $S$ -wave) Kaon.

Instead of making predictions for the magnetic moment of each hyperon, we develop sum rules for magnetic moments. For the ground state baryons, we have the well-known results,

$$\begin{aligned} \mu(\Sigma^{*+}) - \mu(\Sigma^{*-}) &= \frac{3}{2} \{ \mu(\Sigma^+) - \mu(\Sigma^-) \}, \\ \mu(\Sigma^+) + \mu(\Sigma^-) &= \frac{4}{3} \{ \mu(p) + \mu(n) \} - \frac{2}{3} \mu(\Lambda), \\ \mu(\Sigma^{*+}) + \mu(\Sigma^{*-}) &= 2 \{ \mu(p) + \mu(n) \} + 2\mu(\Lambda), \\ \mu(\Xi^0) + \mu(\Xi^-) &= -\frac{1}{3} \{ \mu(p) + \mu(n) \} + \frac{8}{3} \mu(\Lambda), \\ \mu(\Xi^{*0}) + \mu(\Xi^{*-}) &= \mu(p) + \mu(n) + 4\mu(\Lambda), \\ \mu(\Xi^{*0}) - \mu(\Xi^{*-}) &= -3 \{ \mu(\Xi^0) - \mu(\Xi^-) \}, \\ \mu(\Omega) &= 3\mu(\Lambda) \end{aligned} \quad (7)$$

for the octet and decuplet ground state baryons. It should also be mentioned that these relations are valid by replacing  $\Sigma, \Sigma^*, \Xi, \Xi^*, \Omega$  by  $\Sigma_{1/2^-,1}, \Sigma_{3/2^-,1}, \Xi_{1/2^+,1}, \Xi_{3/2^+,1}, \Omega_{3/2^-,2}$ , respectively.

Other interesting sum rules include

$$\begin{aligned} &\mu(\Xi_{3/2^-,1}^0) - \mu(\Lambda_{1/2^-,1}) - \frac{1}{2} \{ \mu(\Sigma_{1/2^-,1}^+) - \mu(\Sigma_{1/2^-,1}^-) \} \\ &= \mu(\Xi_{3/2^+,0}^0) - \mu(\Lambda_{1/2^+,0}) - \frac{1}{2} \{ \mu(\Sigma_{1/2^+,0}^+) - \mu(\Sigma_{1/2^+,0}^-) \}, \end{aligned} \quad (8)$$

$$\begin{aligned} &\mu(\Xi_{3/2^-,1}^-) - \mu(\Lambda_{1/2^-,1}) + \frac{1}{2} \{ \mu(\Sigma_{1/2^-,1}^+) - \mu(\Sigma_{1/2^-,1}^-) \} \\ &= \mu(\Xi_{3/2^+,0}^-) - \mu(\Lambda_{1/2^+,0}) + \frac{1}{2} \{ \mu(\Sigma_{1/2^+,0}^+) - \mu(\Sigma_{1/2^+,0}^-) \}, \end{aligned} \quad (9)$$

$$\begin{aligned}\mu(\Xi_{1/2^-,1}^0) + 3\mu(\Xi_{1/2^-,2}^0) &= \mu(\Xi_{1/2^-,1}^-) + 3\mu(\Xi_{1/2^-,2}^-) \\ &= 2 \{ \mu(\Lambda_{1/2^+,0}) + \mu(\Lambda_{1/2^-,1}) \},\end{aligned}\tag{10}$$

and

$$\begin{aligned}\mu(\Omega_{1/2^-,1}) &= \frac{4}{3}\mu(\Lambda_{1116}) - \frac{1}{3}\mu(\Lambda_{1405}), \\ \mu(\Omega_{3/2^-,1}) &= 2\mu(\Lambda_{1116}) + \mu(\Lambda_{1405}), \\ \mu(\Omega_{1/2^+,1}) &= -\frac{1}{3}\mu(\Lambda_{1116}) + \frac{4}{3}\mu(\Lambda_{1405}), \\ \mu(\Omega_{3/2^+,1}) &= \frac{1}{3}\mu(\Lambda_{1116}) + 2\mu(\Lambda_{1405}).\end{aligned}\tag{11}$$

These sum rules relate the magnetic moments of positive and negative parity hyperons.

## 5. Summary

The predictions on multistrangeness baryon spectrum are highly model-dependent and new precise experimental data are strongly called for to distinguish the models on baryon structure. This shows that multistrangeness baryons provide a unique tool for investigating the underlying dynamics and the role of strange quarks. One issue is the low masses of the  $\Xi(1620)$  and the  $\Xi(1690)$ , which are hard to be explained by quark models but are regarded as the analogous states of the  $\Lambda(1405)$  in the Skyrme model. This model also leads to mass sum rules and magnetic moment sum rules which can distinguish the model from quark model predictions. Therefore, the suggested  $K_L$  beam facility will shed light on our understanding of strong interactions through the excited states of  $\Xi$  and  $\Omega$  baryons.

## 6. Acknowledgments

This research was supported by Basic Science Research Program through the National Research Foundation of Korea (NRF) under Grant No. NRF-2015R1D1A1A01059603.

## References

- [1] V.E. Barnes *et al.*, Phys. Rev. Lett. **12**, 204 (1964).
- [2] M. Gell-Mann, Phys. Lett. **8**, 214 (1964).
- [3] B. Aubert *et al.* (BABAR Collaboration), Phys. Rev. Lett. **97**, 112001 (2006).
- [4] K.A. Olive *et al.* (Particle Data Group), Chin. Phys. C **38**, 090001 (2014).
- [5] N.B. Wallace, P.M. Border, D.P. Ciampa, G. Guglielmo, K.J. Heller, D.M. Woods, K.A. Johns, Y.T. Gao, M.J. Longo, and R. Rameika, Phys. Rev. Lett. **74**, 3732 (1995).
- [6] M.I. Adamovich *et al.* (WA89 Collaboration), Eur. Phys. J. C **11**, 271 (1999).
- [7] E. Abouzaid *et al.* (KTeV Collaboration), Phys. Rev. Lett. **95**, 081801 (2005).

- [8] J.R. Batley *et al.* (NA48/1 Collaboration), Phys. Lett. B **645**, 36 (2007).
- [9] R. Witt *et al.* (STAR Collaboration), J. Phys. G **34**, S921 (2007).
- [10] B. Aubert *et al.* (BABAR Collaboration), Phys. Rev. D **78**, 034008 (2008).
- [11] J.W. Price, J. Ducote, J. Goetz, and B.M.K. Nefkens (for CLAS Collaboration), Nucl. Phys. A **754**, 272c (2005).
- [12] J.W. Price *et al.* (CLAS Collaboration), Phys. Rev. C **71**, 058201 (2005).
- [13] L. Guo and D. P. Weygand (for CLAS Collaboration), in *Proceedings of International Workshop on the Physics of Excited Baryons (NSTAR 05)*, edited by S. Capstick, V. Crede, and P. Eugenio, pp. 384–388, Singapore, 2006, World Scientific.
- [14] L. Guo *et al.* (CLAS Collaboration), Phys. Rev. C **76**, 025208 (2007).
- [15] *Photoproduction of the very strangest baryons on the proton target in CLAS12*, Spokespersons: M. Dugger, J. Goetz, L. Guo, E. Pasyuk, I.I. Strakovsky, D.P. Watts, and V. Ziegler (The Very Strange Collaboration with CLAS Collaboration), JLab Proposal E12–11–005a, Newport News, VA, USA, 2013.
- [16] K. Nakayama, Y. Oh, and H. Haberzettl, Phys. Rev. C **85**, 042201(R) (2012).
- [17] B. Jackson, Y. Oh, H. Haberzettl, and K. Nakayama, Phys. Rev. C **89**, 025206 (2014).
- [18] B.C. Jackson, Y. Oh, H. Haberzettl, and K. Nakayama, Phys. Rev. C **91**, 065208 (2015).
- [19] Y. Oh, Phys. Rev. D **75**, 074002 (2007).
- [20] D.E. Plane *et al.*, Nucl. Phys. B **22**, 93 (1970).
- [21] N.P. Samios, M. Goldberg, and B.T. Meadows, Rev. Mod. Phys. **46**, 49 (1974).
- [22] R. Horgan, Nucl. Phys. B **71**, 514 (1974).
- [23] K.-T. Chao, N. Isgur, and G. Karl, Phys. Rev. D **23**, 155 (1981).
- [24] S. Capstick and N. Isgur, Phys. Rev. D **34**, 2809 (1986).
- [25] M. Pervin and W. Roberts, Phys. Rev. C **77**, 025202 (2008).
- [26] L.Ya. Glozman and D.O. Riska, Phys. Rep. **268**, 263 (1996).
- [27] L. Ya. Glozman, W. Plessas, K. Varga, and R.F. Wagenbrunn, Phys. Rev. D **58**, 094030 (1998).
- [28] A. Valcarce, H. Garcilazo, and J. Vijande, Phys. Rev. C **72**, 025206 (2005).
- [29] C.E. Carlson and C.D. Carone, Phys. Lett. B **484**, 260 (2000).
- [30] C.L. Schat, J.L. Goity, and N.N. Scoccola, Phys. Rev. Lett. **88**, 102002 (2002).

- [31] J.L. Goity, C. Schat, and N.N. Scoccola, Phys. Lett. B **564**, 83 (2003).
- [32] N. Matagne and Fl. Stancu, Phys. Rev. D **71**, 014010 (2005).
- [33] N. Matagne and Fl. Stancu, Phys. Rev. D **74**, 034014 (2006).
- [34] C. Semay, F. Buisseret, N. Matagne, and Fl. Stancu, hep-ph/0702075.
- [35] R. Bijker, F. Iachello, and A. Leviatan, Ann. Phys. (N.Y.) **284**, 89 (2000).
- [36] F.X. Lee and X. Liu, Phys. Rev. D **66**, 014014 (2002).
- [37] D. Jido and M. Oka, arXiv:hep-ph/9611322.
- [38] N. Isgur and G. Karl, Phys. Rev. D **18**, 4187 (1978).
- [39] M. Arima, S. Matsui, and K. Shimizu, Phys. Rev. C **49**, 2831 (1994).
- [40] R.H. Dalitz and S.F. Tuan, Phys. Rev. Lett. **2**, 425 (1959).
- [41] R.C. Arnold and J.J. Sakurai, Phys. Rev. **128**, 2808 (1962).
- [42] E.A. Veit, B.K. Jennings, A.W. Thomas, and R.C. Barrett, Phys. Rev. D **31**, 1033 (1985).
- [43] C.G. Callan and I. Klebanov, Nucl. Phys. B **262**, 365 (1985).
- [44] C.L. Schat, N.N. Scoccola, and C. Gobbi, Nucl. Phys. A **585**, 627 (1995).
- [45] Y.-L. Ma, Y. Oh, G.-S. Yang, M. Harada, H.K. Lee, B.-Y. Park, and M. Rho, Phys. Rev. D **86**, 074025 (2012).
- [46] Y.-L. Ma, G.-S. Yang, Y. Oh, and M. Harada, Phys. Rev. D **87**, 034023 (2013).
- [47] J.K. Hassall, R.E. Ansorge, J.R. Carter, W.W. Neale, J.G. Rushbrooke, D.R. Ward, B.Y. Oh, M. Pratap, G.A. Smith, and J. Whitmore, Nucl. Phys. B **189**, 397 (1981).
- [48] M. Rho, D.O. Riska, and N.N. Scoccola, Z. Phys. A **341**, 343 (1992).
- [49] Y. Oh and B.-Y. Park, Z. Phys. A **359**, 83 (1997).
- [50] W. Roberts and M. Pervin, Int. J. Mod. Phys. A **23**, 2817 (2008).
- [51] Y. Oh and W. Weise, Eur. Phys. J. A **4**, 363 (1999).
- [52] Y. Oh, D.-P. Min, M. Rho, and N.N. Scoccola, Nucl. Phys. A **534**, 493 (1991).



## 2.14 Hyperon Resonance Studies from Charm Baryon Decays at BaBar

Veronique Ziegler

*Thomas Jefferson National Accelerator Facility*

*Newport News, VA 23606, U.S.A.*

### Abstract

We present studies of hyperon and hyperon resonance production in charm baryon decays at BaBar. The helicity formalism employed to measure the spin of  $\Omega^-$  was extended to three-body final states whereby the properties of the  $\Xi(1690)^0$  and  $\Xi(1690)^0$  produced in  $\Lambda_c^+$  decay were obtained.

### 1. Introduction

The data samples used for the analyses described in this note were collected with the BaBar detector at the PEP-II asymmetric-energy  $e^+e^-$  collider. In these studies, the charm baryons are inclusively produced in  $e^+e^-$  collisions at center-of-mass energies 10.58 and 10.54 GeV. The BaBar detector and reconstruction software are described elsewhere [1].

### 2. General Procedure for Charm Baryon Selection

The selection of charm baryon candidates requires the sequential reconstruction of initial and intermediate state candidates using four-momentum addition of tracks. Particle identification selectors based on specific energy loss ( $dE/dx$ ) and Cherenkov angle measurements have been used to identify proton, pion and kaon final tracks. Each intermediate state candidate is required to have its invariant mass within  $\pm 3\sigma$  of the fitted peak position of the relevant distribution, where  $\sigma$  is the mass resolution. In all cases, the fitted peak mass is consistent with the expected value, and the intermediate state invariant mass is then constrained to this value. Due to the fact that each weakly-decaying intermediate state (*i.e.*, the  $K_S$  and hyperons) is long-lived, the signal-to-background ratio is improved by imposing a vertex displacement criterion (in the direction of the momentum vector). In order to further enhance signal-to-background ratio, a selection criterion is imposed on the center-of-mass momentum  $p^*$  of the parent charm baryon. The use of charge conjugate states is implied throughout in this note.

### 3. Formalism

Measurements of the  $\Omega^-$  spin are obtained using a primary sample obtained from the decay sequence  $\Xi_c^0 \rightarrow \Omega^- K^+$ , with  $\Omega^- \rightarrow \Lambda K^-$  [2]. It is assumed that each charm baryon type has spin 1/2 and, as a result of its inclusive production, that it is described by a diagonal spin projection density matrix. The analysis does not require that the diagonal matrix elements be equal.

By choosing the quantization axis along the direction of the  $\Omega^-$  in the charm baryon rest-frame, the  $\Omega^-$  inherits the spin projection of the charm baryon [2]. It follows that, regardless of the spin  $J$  of the  $\Omega^-$ , the density matrix describing the  $\Omega^-$  sample is diagonal, with non-zero values only for the  $\pm 1/2$  spin projection elements, *i.e.*, the helicity  $\lambda_i$  of the  $\Omega^-$  can take

only the values  $\pm 1/2$ . Since the final state  $\Lambda$  and  $K^-$  have spin values 1/2 and 0, respectively, the net final state helicity  $\lambda_f$  also can take only the values  $\pm 1/2$ .

Defining the helicity angle  $\theta_h$  as the angle between the direction of the  $\Lambda$  in the rest-frame of the  $\Omega^-$  and the quantization axis, the probability for the  $\Lambda$  to be produced with Euler angles  $(\phi, \theta_h, 0)$  with respect to the quantization axis is given by the square of the amplitude  $\psi$ , characterizing the decay of an  $\Omega^-$  with spin  $J$  and helicity  $\lambda_i$  to a 2-body system with net helicity  $\lambda_f$ , where  $\psi = A_{\lambda_f}^J D_{\lambda_i \lambda_f}^{J*}(\phi, \theta_h, 0)$ , and the transition matrix element  $A_{\lambda_f}^J$  represents the coupling of the  $\Omega^-$  to the final state. The angular distribution of the  $\Lambda$  is then given by

$$I \propto \sum_{\lambda_i, \lambda_f} \rho_{ii} \left| A_{\lambda_f}^J D_{\lambda_i \lambda_f}^{J*}(\phi, \theta_h, 0) \right|^2, \quad (1)$$

where the  $\rho_{ii}$  ( $i = \pm 1/2$ ) are the diagonal density matrix elements inherited from the charm baryon, and the sum is over all initial and final helicity states.

The  $\Lambda$  angular distribution integrated over  $\phi$  is then obtained for spin hypotheses  $J_\Omega = 1/2, 3/2$ , and  $5/2$ , respectively as follows:

$$dN/d\cos\theta_h \propto 1 + \beta \cos\theta_h, \quad (2)$$

$$dN/d\cos\theta_h \propto 1 + 3 \cos^2\theta_h + \beta \cos\theta_h(5 - 9 \cos^2\theta_h), \quad (3)$$

$$dN/d\cos\theta_h \propto 1 - 2 \cos^2\theta_h + 5 \cos^4\theta_h + \beta \cos\theta_h(5 - 26 \cos^2\theta_h + 25 \cos^4\theta_h), \quad (4)$$

where the coefficient of the asymmetric term,  $\beta$  [2], may be non-zero as a consequence of parity violation in charm baryon and  $\Omega^-$  weak decay.

The angular distributions of the decay products of the  $\Omega^-$  baryon resulting from a spin 1/2 charm baryon decay are well-described by a function  $\propto 1 + 3 \cos^2\theta_h$ . These observations are consistent with spin assignments 3/2 for the  $\Omega^-$ . Values of 1/2 and greater than 3/2 for the spin of the  $\Omega^-$  yield C.L. values significantly less than 1% when spin 1/2 is assumed for the parent charm baryon.

#### (a) The Use of Legendre Polynomial Moments in Spin Determination

For spin  $J$ , the corrected angular distributions can be written

$$\frac{dN}{d\cos\theta_h} = N \left[ \sum_{l=0}^{l_{max}} \langle P_l \rangle P_l(\cos\theta_h) \right],$$

where  $P_l(\cos\theta_h)$  are normalized Legendre Polynomial functions such that  $l_{max} = 2J - 1$ , and if  $l$  is odd  $\langle P_l \rangle = 0$ . Each assumed  $J$  defines  $l_{max}$ , so that  $\langle P_l \rangle = 0$  for  $l > l_{max}$  and  $\langle P_l \rangle$  is calculable. The number of  $\Omega^-$  signal events in a given mass bin is obtained by giving each event,  $j$ , in that bin, a weight  $w_j = \frac{P_{l_{max}}(\cos\theta_{h_j})}{\langle P_{l_{max}} \rangle}$ .

In particular, for  $J = 3/2$ , giving each event a weight  $w_j = \sqrt{10} P_2(\cos\theta_{h_j})$  projects the complete  $\Omega^-$  signal. In order to test the  $J = 5/2$  hypothesis, each event is given a weight  $w_j = \frac{7}{\sqrt{2}} P_4(\cos\theta_{h_j})$ .

As expected, the  $\sqrt{10}P_2(\cos\theta_h)$  moment projects out the signal of a spin 3/2 hyperon, whereas the  $7/\sqrt{2}P_4(\cos\theta_h)$  moment does not. These moments are used in the analysis of the  $\Xi(1690)$  and  $\Xi(1530)$  resonances described in the next section.

#### 4. Study of Cascade Resonances Using Three-body Charm Baryon Decays

Although considerable advances have been made in baryon spectroscopy over the past decade, there has been very little improvement in our knowledge of hyperon resonances since 1988. The  $\Xi(1690)$  has been observed in the  $\Lambda\bar{K}$ ,  $\Sigma\bar{K}$  and  $\Xi\pi$  final states with various degrees of certainty.

##### (a) The $\Xi(1530)^0$ from $\Lambda_c^+ \rightarrow \Xi^-\pi^+K^+$ Decay

The properties of the  $\Xi(1530)$  resonance are investigated in the  $\Lambda_c^+ \rightarrow \Xi^-\pi^+K^+$  decay process [3]. The Dalitz plot for  $\Lambda_c^+ \rightarrow \Xi^-\pi^+K^+$  is dominated by the contribution from  $\Lambda_c^+ \rightarrow \Xi(1530)^0K^+$ , where  $\Xi(1530)^0 \rightarrow \Xi^-\pi^+$  by strong decay. The Dalitz plot (Fig. 1) shows evidence for only one resonant structure. A clear band can be seen at the nominal mass squared of the  $\Xi(1530)^0 \rightarrow \Xi^-\pi^+$ . The analysis of the Legendre polynomial moments of the  $\Xi(1530)^0 \rightarrow \Xi^-\pi^+$  system established quite clearly, on the basis of Figs. 2(b) and 2(c), that the  $\Xi(1530)^0$  hyperon resonance has spin 3/2. In conjunction with previous analyses [4] this also definitively establishes positive parity. However, comparison of the  $P_2(\cos\theta_\Xi)$  moment to the  $\Xi^-\pi^+$  mass distribution and fits to the angular decay distribution in the  $\Xi(1530)^0$  region indicate that it is necessary to include other  $\Xi^-\pi^+$  amplitudes in order to obtain a complete description of the data. In particular, the observation of a  $P_1(\cos\theta_\Xi)$  moment exhibiting oscillatory behavior in the  $\Xi(1530)^0$  region indicates the need for an  $S_{1/2}$  amplitude, while providing first evidence for the expected rapid BW phase motion of the  $P_{3/2}$   $\Xi(1530)^0$  amplitude. However, a simple model incorporating only these amplitudes and a  $D_{5/2}$  amplitude is ruled out because of the failure to describe the  $\Xi(1530)^0$  line shape. The presence of the  $S_{1/2}$  amplitude at high mass and the behavior of the mass distribution near 1.7 GeV/ $c^2$  suggest that a resonant  $\Xi(1690)^0$  amplitude may be adding coherently to this amplitude, thus leading to the inference of spin-parity  $1/2^-$  for the  $\Xi(1690)^0$ . It appears that a quantitative description of the  $\Xi(1530)^0$  line shape, and indeed of the entire Dalitz plot, must incorporate these features together with amplitude contributions associated with the  $K^+\pi^+$  and/or the  $\Xi^-K^+$  systems. However such an analysis requires a higher statistics data sample.

##### (b) The $\Xi(1690)^0$ from $\Lambda_c^+ \rightarrow (\Lambda\bar{K}^0)K^+$ Decay

The  $\Xi(1690)^0$  is observed in the  $\Lambda\bar{K}^0$  system produced in the decay  $\Lambda_c^+ \rightarrow (\Lambda\bar{K}^0)K^+$ , where the  $\bar{K}^0$  is reconstructed via  $K_S \rightarrow \pi^+\pi^-$ .

The selection of  $\Lambda_c^+$  candidates requires the intermediate reconstruction of oppositely-charged track pairs consistent with  $\Lambda \rightarrow p\pi^-$  and  $K_S \rightarrow \pi^+\pi^-$  decays. A clear peak, significant skewed toward high mass, is seen in the vicinity of the  $\Xi(1690)^0$ .

The second and fourth order Legendre polynomial moments as a function of the mass of the  $(\Lambda K_S)$  system display no peaking structure at the position of the  $\Xi(1690)^0$ , which suggests that the  $\Xi(1690)^0$  spin is probably 1/2. However, the  $\Lambda$  helicity cosine ( $\cos\theta_\Lambda$ ) distribution is not flat in contrast to the expectation for a spin 1/2 to 1/2 transition.

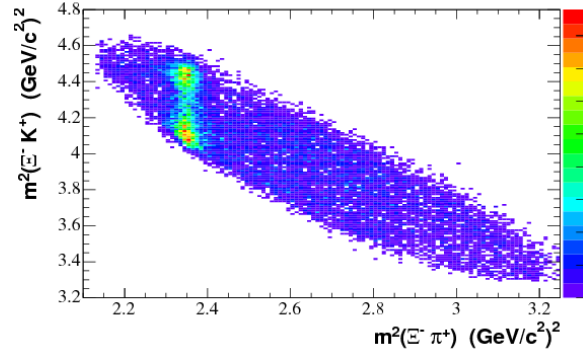


Figure 1: The Dalitz plot for  $\Lambda_c^+ \rightarrow \Xi^- \pi^+ K^+$  corresponding to the  $\Lambda_c^+$  signal region.

The Dalitz plot of  $\Lambda_c^+ \rightarrow \Lambda \bar{K}^0 K^+$  signal candidates is shown, without efficiency-correction, in Fig. 3(a). A clear band is observed in the mass-squared region of the  $\Xi(1690)^0$ , together with an accumulation of events in the  $\bar{K}^0 K^+$  threshold region; the latter is consistent with a contribution to the Dalitz plot due to the  $a_0(980)^+$  resonance. In contrast, the Dalitz plots corresponding to the  $\Lambda_c^+$  mass-sideband regions exhibit no structure.

We describe the event distribution in the Dalitz plot of Fig. 3(b) in terms of an isobar model consisting of the coherent superposition of amplitudes characterizing  $(\Lambda a_0(980)^+)$  and  $(\Xi(1690)^0 K^+)$  decay of the  $\Lambda_c^+$ . The  $a_0(980)$  is known to couple to both  $\eta\pi$  and  $\bar{K}K$  and is characterized by the Flatté parametrization [5], while a Breit-Wigner function is used to describe the amplitude for the  $\Xi(1690)^0$ .

This model is used to describe the intensity distribution at a point on the Dalitz plot by means of the squared modulus of a coherent superposition of these two amplitudes, under the assumption that the  $\Xi(1690)^0$  has spin 1/2, since the moment projections favor this choice. Fits to the Dalitz plot under the assumptions of spin 3/2 and 5/2 are ongoing. We find that no additional isobars are needed in order to accurately model the data. In order to extract the mass and width parameters of the  $\Xi(1690)^0$ , we perform a binned maximum Likelihood fit to the rectangular Dalitz plot of Fig. 3(b) (incorporating resolution smearing in mass, and a background parametrization obtained from the  $\Lambda_c^+$  mass-sidebands).

The fit reproduces accurately the skewed lineshape of the  $\Lambda K_S$  invariant mass projection (Fig. 4). The skewing results from the interference between the  $a_0(980)^+$  and the  $\Xi(1690)^0$ . The actual  $\Xi(1690)^0$  signal is symmetric and significantly smaller than the apparent signal, which is dominated by this interference effect. The fit also provides an excellent representation of the other invariant mass projections.

## 5. Conclusions

Mass and width measurements for the  $\Xi(1690)^0$  have been obtained from fits to the  $\Lambda_c^+ \rightarrow \Lambda K_S K^+$  Dalitz plot. The results indicate that the spin of the  $\Xi(1690)$  is consistent with 1/2. The properties of the  $\Xi(1530)^0$  are studied using the decay  $\Lambda_c^+ \rightarrow \Xi^- \pi^+ K^+$ . The spin of

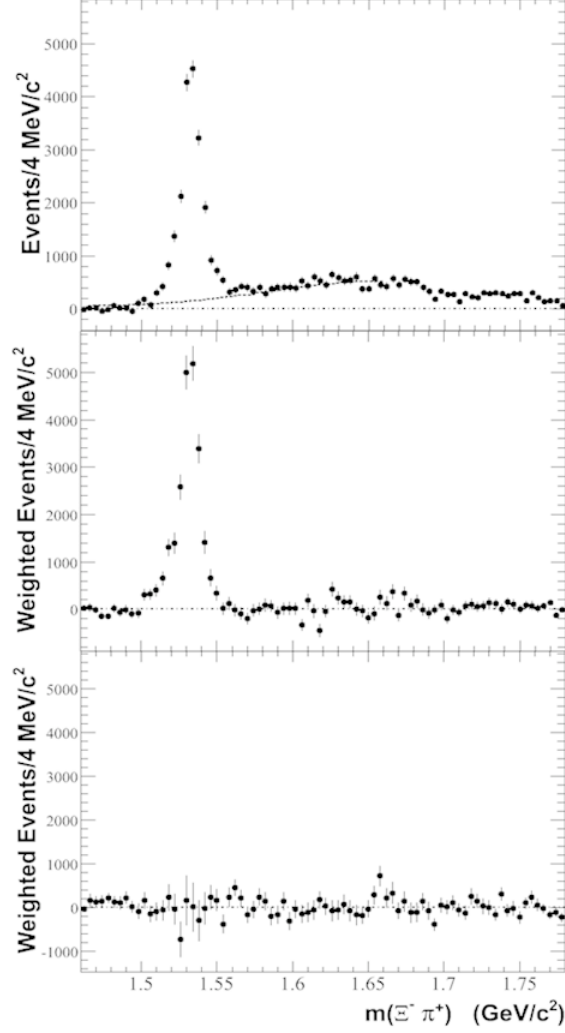


Figure 2: The efficiency-corrected  $P0, 2, 4$  moments of the  $\Xi^- \pi^+$  system invariant mass distribution for the  $\Lambda_c^+$  signal region. In (a) the dashed curve represents the estimated background contribution in the  $\Lambda_c^+$  region.

the  $\Xi(1530)$  is consistent with  $3/2$ .

Similar studies for cascade resonance production and associated spectra done at BaBar using charm baryon production can be done at GlueX with a  $K_L$  beam. Three-body systems involving two-body Cascade resonance decays require the analysis of the entire Dalitz plot when the statistical level is such that the shortcomings of a quasi-two-body approach become apparent. Therefore it is essential to have high statistics to allow for a proper fit to the entire Dalitz plot.

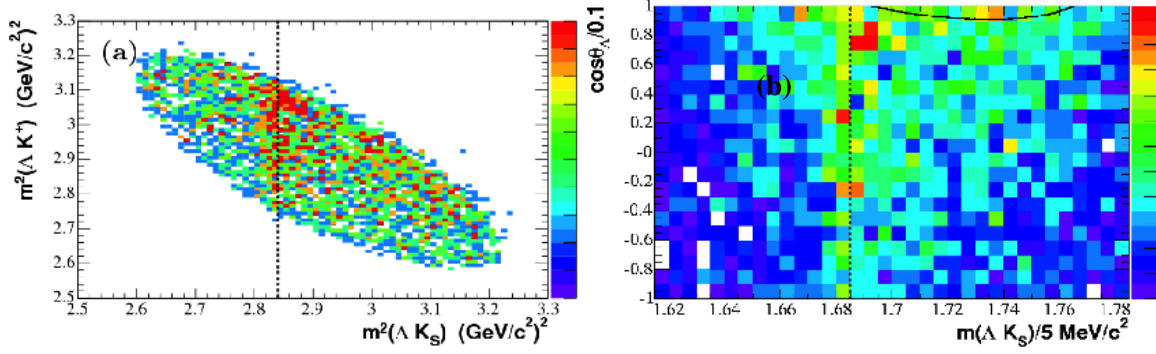


Figure 3: (a) The Dalitz plot for  $\Lambda_c^+ \rightarrow \Lambda \bar{K}^0 K^+$  corresponding to the  $\Xi(1690)^0$  signal region. The dashed line indicates the nominal mass-squared region of the  $\Xi(1690)^0$ . (b) The rectangular Dalitz plot for  $\Lambda_c^+ \rightarrow \Lambda \bar{K}^0 K^+$  corresponding to the  $\Lambda_c^+$  signal region. The black curve corresponds to the  $a_0(980)^+$  pole position.

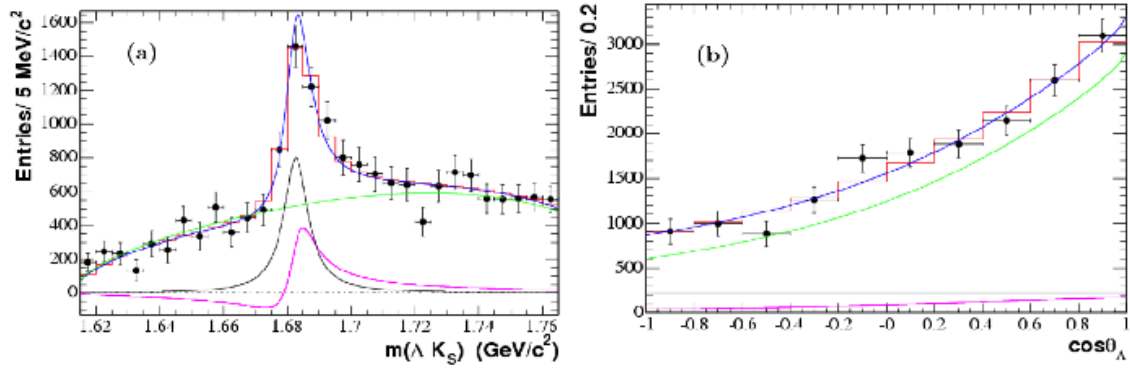


Figure 4: (a)  $\Lambda_c$ -mass-sideband-subtracted efficiency-corrected  $\Lambda K_S$  invariant mass projection. (b)  $\Lambda_c$ -mass-sideband-subtracted efficiency-corrected  $\cos\theta_\Lambda$  spectrum.

## 6. Acknowledgments

This work was supported by DOE and NSF (USA), NSERC (Canada), IHEP (China), CEA and CNRS-IN2P3 (France), BMBF and DFG (Germany), INFN (Italy), FOM (The Netherlands), NFR (Norway), MIST (Russia), and PPARC (United Kingdom).

## References

- [1] B. Aubert *et al.*, Nucl. Instr. Meth. A **479**, 1 (2002).
- [2] B. Aubert *et al.*, Phys. Rev. Lett. **97**, 112002 (2006).
- [3] B. Aubert *et al.*, Phys. Rev. D **78**, 034008 (2008).

- [4] P.E. Schlein *et al.*, Phys. Rev. Lett. **11**, 167 (1963); J. Button-Schafer *et al.*, Phys. Rev. **B142**, 883 (1966).
- [5] S.M. Flatté, Phys. Lett. B **63**, 224 (1976).

## 2.15 Evidence of Some New Hyperon Resonances – to be Checked by KL Beam

Bingsong Zou

*State Key Laboratory of Theoretical Physics*

*Institute of Theoretical Physics*

*Chinese Academy of Sciences*

*Beijing 100190, People's Republic of China*

### Abstract

Quenched and unquenched quark models predict very different patterns for the spectrum of the low excited hyperon states. Evidence is accumulating for the existence of some new hyperon resonances, such as a  $\Sigma^*$  of spin-parity  $J^P = 1/2^-$  around 1400 MeV instead of 1620 MeV as listed in PDG, a new  $\Sigma(1540)3/2^-$  resonance, a new narrow  $\Lambda(1670)3/2^-$  resonance and a new  $\Lambda(1680)3/2^+$  resonance. All these new hyperon resonances fit in the predicted pattern of the unquenched quark models very well. It is extremely important to check and establish the spectrum of these low excited hyperon states by the proposed  $K_L$  beam experiments at JLab.

### 1. Why hyperon resonances ?

Creation of quark-anti-quark pairs from gluon field plays a crucial role for understanding quark confinement and hadron spectroscopy. In the classical quenched quark model for a  $q_1\bar{q}_1$  meson, the  $q_1$  quark cannot be separated from the  $\bar{q}_1$  anti-quark due to a infinitely large confinement potential. But in reality, we know the  $q_1$  and  $\bar{q}_1$  can be easily separated from each other by creation of another quark-anti-quark pair  $q_2\bar{q}_2$  to decay to two mesons,  $q_1\bar{q}_2$  and  $q_2\bar{q}_1$ . With the creation of the  $q_2\bar{q}_2$ , instead of forming two colorless mesons, the system could also exist in the form of a tetra-quark state  $[q_1q_2][\bar{q}_1\bar{q}_2]$ . Therefore both lattice QCD and quark models should go beyond the quenched approximation which ignore the creation of quark-anti-quark pairs.

Quenched  $qqq$  quark models and unquenched  $qqq \leftrightarrow qq\bar{q}q\bar{q}$  quark models give very different predictions for the hyperon spectroscopy. For example, for the  $J^P = \frac{1}{2}^-$  SU(3) nonet partners of the  $N(1535)$  and  $\Lambda(1405)$ . While quenched quark models [1–4] predict the  $J^P = \frac{1}{2}^-$   $\Sigma$  and  $\Xi$  resonances to be around 1650 MeV and 1760 MeV, respectively, the unquenched quark models [5–7] expect them to be around 1400 MeV and 1550 MeV, respectively, a meson-soliton bound-state approach of the Skyrme model [8] and other meson-baryon dynamical models [9, 10] predict them to be around 1450 MeV and 1620 MeV, respectively. In Fig. 1, we show prediction of the lowest penta-quark states with  $J^P = 1/2^\pm, 3/2^\pm$  [5, 6] (red solid) compared with those from the classical quenched  $qqq$  model [1] (black solid). The major differences are that the lowest penta-quark hyperon states with  $J^P = 1/2^-$  and  $3/2^+$  are about 200 MeV lower those from the classical quenched  $qqq$  models [1].

Although various phenomenological models give distinguishable predictions for the lowest excited hyperon states, most of them are not experimentally established or even listed in PDG [11]. Most of our knowledge for the hyperon resonances came from analyses of old



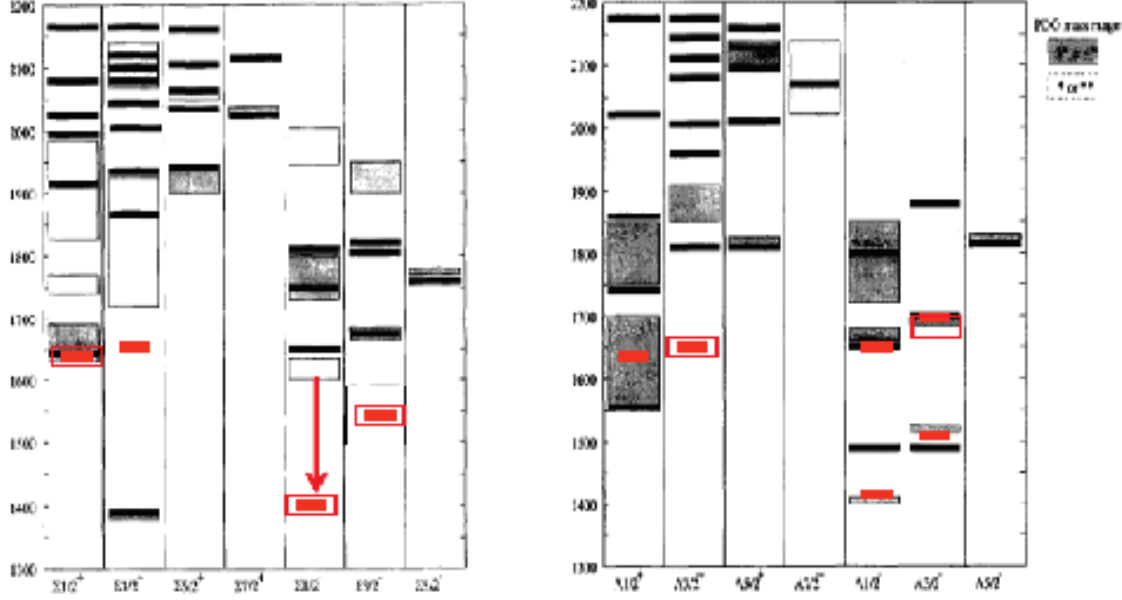


Figure 1: Prediction of the lowest penta-quark states with  $J^P = 1/2^\pm, 3/2^\pm$  [5, 6] (red solid) compared with those from the classical quenched  $qqq$  model [1] (black solid). The black boxes are experimental results from PDG while the red box are from recent new analyses.

$\bar{K}N$  experiments in the 1970s [11]. In the new century, some new measurements from Crystal Ball (CB) [12–14], LEPS [15] and CLAS [16] have started to provide us new information on  $\Sigma^*$  and  $\Lambda^*$  resonances. It is crucial to use them to clarify the spectrum of low-lying hyperon resonances to pin down the underlying dynamics for baryon spectrum and structure. Recent analyses of these new data together with old data reveal some interesting new features of the low-lying excited hyperon states. Here I will give a brief review of these new results and discuss about their further confirmation from the proposed  $K_L$  beam and other experiments.

## 2. New Results on $\Sigma^*$ and $\Lambda^*$ Resonances

### (a) On the Lowest $\Sigma^*$ Resonances with Negative Parity

The lowest  $\Sigma^*$  resonances with  $J^P = 1/2^-$  or  $3/2^-$  are still far from established. There is a  $\Sigma(1620)\frac{1}{2}^-$  listed as a 2-star resonance in the previous versions of PDG tables and downgraded to 1-star in the newest version [11]. There is also a  $\Sigma(1580)\frac{3}{2}^-$  listed as 1-star resonance [11].

The  $\Sigma(1620)\frac{1}{2}^-$  seems supporting the prediction of quenched quark models. However, for the 2-star  $\Sigma(1620)\frac{1}{2}^-$  resonance, only four references [17–20] are listed in PDG tables with weak evidence for its existence. Among them, Ref. [17] and Ref. [18] are based on multi-channel analysis of the  $\bar{K}N$  reactions. Both claim evidence for a  $\Sigma(\frac{1}{2}^-)$  resonance with mass around 1620 MeV, but give totally different branching ratios for this resonance. Ref. [17] claims that it couples only to  $\pi\Lambda$  and not to  $\pi\Sigma$

while Ref. [18] claims the opposite way. Both analyses do not have  $\Sigma(1660)\frac{1}{2}^{+}$  in their solutions. However, Ref. [21] shows no sign of  $\Sigma(\frac{1}{2}^{-})$  resonance between 1600 and 1650 MeV through analysis of the reaction  $\bar{K}N \rightarrow \Lambda\pi$  with the c.m. energy in the range of 1540-2150 MeV, instead it suggests the existence of  $\Sigma(1660)\frac{1}{2}^{+}$ . Later multi-channel analyses of the  $\bar{K}N$  reactions support the existence of the  $\Sigma(1660)\frac{1}{2}^{+}$  instead of  $\Sigma(1620)\frac{1}{2}^{-}$  [11]. In Ref. [19], the total cross sections for  $K^{-}p$  and  $K^{-}n$  with all proper final states are analyzed and indicate some  $\Sigma$  resonances near 1600 MeV without clear quantum numbers. Ref. [20] analyzes the reaction  $K^{-}n \rightarrow \pi^{-}\Lambda$  and gets two possible solutions, with one solution indicating a  $\Sigma(\frac{1}{2}^{-})$  near 1600 MeV, and the other showing no resonant structure below the  $\Sigma(1670)$ . So all these claims of evidence for the  $\Sigma(1620)\frac{1}{2}^{-}$  are very shaky. Instead, some re-analyses of the  $\pi\Lambda$  relevant data suggest that there may exist a  $\Sigma(\frac{1}{2}^{-})$  resonance around 1380 MeV [22], which supports the prediction of unquenched quark models [5, 6]. This is supported by the new CLAS data on  $\gamma p \rightarrow K\Sigma\pi$  [16], although a more delicate analysis [23] of the data suggests the resonant peak to be at a higher mass around 1430 MeV.

For the study of  $\Sigma$  resonances, the  $\bar{K}N \rightarrow \pi\Lambda$  reaction is the best available channel, where the s-channel intermediate states are purely hyperons with strangeness  $S = -1$  and isospin  $I = 1$ . Recently, high statistic new data for the reaction  $K^{-}p \rightarrow \pi^0\Lambda$  are presented by the Crystal Ball Collaboration with the c.m. energy of 1560 – 1676 MeV for both differential cross sections and  $\Lambda$  polarizations [13]. In order to clarify the status of the  $\Sigma(1620)\frac{1}{2}^{-}$  and the  $\Sigma(1660)\frac{1}{2}^{+}$ , we analyzed the differential cross sections and  $\Lambda$  polarizations for both  $K^{-}p \rightarrow \pi^0\Lambda$  and  $K^{-}n \rightarrow \pi^{-}\Lambda$  reactions with an effective Lagrangian approach, using the new Crystal Ball data on  $K^{-}p \rightarrow \pi^0\Lambda$  with the c.m. energy of 1560 – 1676 MeV [13], and the  $K^{-}n \rightarrow \pi^{-}\Lambda$  data of Ref. [20] with the c.m. energy of 1550 – 1650 MeV, where the evidence of the  $\Sigma(1620)\frac{1}{2}^{-}$  was claimed. The new Crystal Ball data clearly shows that the Crystal Ball  $\Lambda$  polarization data demand the existence of a  $\Sigma$  resonance with  $J^P = \frac{1}{2}^{+}$  and mass near 1635 MeV [24], compatible with  $\Sigma(1660)\frac{1}{2}^{+}$  listed in PDG, while the  $\Sigma(1620)\frac{1}{2}^{-}$  is not needed by the data. The differential cross sections alone cannot distinguish the two solutions with either  $\Sigma(1660)\frac{1}{2}^{+}$  or  $\Sigma(1620)\frac{1}{2}^{-}$ .

This analysis also suggests a possible  $\Sigma(\frac{3}{2}^{-})$  resonance with mass around 1542 MeV and width about 25.6 MeV. This seems consistent with the resonance structure  $\Sigma(1560)$  or  $\Sigma(1580)\frac{3}{2}^{-}$  in PDG and compatible with expectation from penta-quark model [5]. Ref. [25] also proposes a  $\Sigma(\frac{3}{2}^{-})$  resonance with mass around 1570 MeV and width about 60 MeV from  $\bar{K}N\pi$  system.

After our analysis, there were three groups [26–28] having made more sophisticated coupled channel analysis of the  $\bar{K}N$  scattering data including those from the Crystal Ball experiment. The newest analysis [28] gives roughly consistent results for the lowest  $\Sigma^{*}(1/2^{\pm})$  resonances as ours. In both analyses, there is no  $\Sigma(1620)1/2^{-}$ . While in our analysis, the  $\Sigma(1635)1/2^{+}$  is definitely needed, in Ref. [28], the  $\Sigma(1635)1/2^{+}$  is split to two  $1/2^{+}$  resonances:  $\Sigma(1567)$  and  $\Sigma(1708)$ . The other two analyses claim the need of the  $\Sigma(1620)1/2^{-}$ , but with much lower energy at 1501 MeV [26] and

1551 MeV [27], respectively.

For the lowest  $\Sigma^*(3/2^-)$ , Ref. [27] gives a similar result as ours with mass around 1550 MeV. Refs. [26, 28] give a higher mass around 1670 MeV.

So there are strong evidences for the lowest  $\Sigma^*(1/2^-)$  to be in the range of 1380  $\sim$  1500 MeV and the lowest  $\Sigma^*(3/2^-)$  to be around 1550 MeV. But this is not conclusive.

(b) **On the Lowest  $\Lambda^*(3/2^\pm)$  Resonances**

Many studies have been carried out to investigate the  $\Lambda$  resonances. Oset *et al.* [29, 30] used a chiral unitary approach for the meson-baryon interactions and got two  $J^P = \frac{1}{2}^-$  resonances with one mass near 1390 MeV and the other around 1420 MeV. They believe the well established  $\Lambda(1405)\frac{1}{2}^-$  resonance listed in PDG [11] is actually a superposition of these two  $\frac{1}{2}^-$  resonances. Manley *et al.* [26] and Kamano *et al.* [27] made multichannel partial-wave analysis of  $\bar{K}N$  reactions and got results with some significant differences. Zhong *et al.* [31] analyzed the  $K^-p \rightarrow \pi^0\Sigma^0$  reaction with the chiral-quark model and discussed characteristics of the well established  $\Lambda$  resonances. Liu *et al.* [32] analyzed the  $K^-p \rightarrow \eta\Lambda$  reaction [12] with an effective Lagrangian approach and implied a  $D_{03}$ -resonance with mass about 1670 MeV but much smaller width compared with the well established  $\Lambda(1690)\frac{3}{2}^-$ . So there are still some ambiguities of the  $\Lambda$  resonant structures needing to be clarified.

Recently, the most precise data on the differential cross sections for the  $K^-p \rightarrow \pi^0\Sigma^0$  reaction have been provided by the Crystal Ball experiment at AGS/BNL [13, 14]. The  $\Sigma^0$  polarization data were presented for the first time. However, with different data selection cuts and reconstructions, two groups in the same collaboration, *i.e.*, VA group [14] and UCLA group [13], got inconsistent results for the  $\Sigma^0$  polarizations. Previous multi-channel analysis [26, 27, 31] of the  $\bar{K}N$  reactions failed to reproduce either set of the polarization data.

In our recent work [33], we concentrate on the most precise data by the Crystal Ball Collaboration on the pure isospin scalar channel of  $\bar{K}N$  reaction to see what are the  $\Lambda$  resonances the data demand and how the two groups' distinct polarization data [13, 14] influence the spectroscopy of  $\Lambda$  resonances. Consistent differential cross sections of earlier work by Armenteros *et al.* [34] at lower energies are also used. It is found that the 4-star  $\Lambda(1670)\frac{1}{2}^-$  and 3-star  $\Lambda(1600)\frac{1}{2}^+$  resonances listed in PDG [11] are definitely needed no matter which set of CB data is used. In addition, there is strong evidence for the existence of a new  $\Lambda(\frac{3}{2}^+)$  resonance around 1680 MeV no matter which set of data is used. It gives large contribution to this reaction, replacing the contribution from the 4-star  $\Lambda(1690)\frac{3}{2}^-$  resonance included by previous fits to this reaction.

Replacing the PDG  $\Lambda(1690)\frac{3}{2}^-$  resonance by a new  $\Lambda(1680)\frac{3}{2}^+$  resonance has important implications on hyperon spectroscopy and its underlying dynamics. While the classical qqg constituent quark model [2] predicts the lowest  $\Lambda(\frac{3}{2}^+)$  resonance to be around 1900 MeV in consistent with the  $\Lambda(1890)\frac{3}{2}^+$  listed in PDG, the penta-quark dynamics [5] predicts to be below 1700 MeV in consistent with  $\Lambda(1680)\frac{3}{2}^+$  claimed in this work.

A recent analysis [32] of CB data on the  $K^-p \rightarrow \eta\Lambda$  reaction requires a  $\Lambda(\frac{3}{2}^-)$  reso-

nance with mass about 1670 MeV and width about 1.5 MeV instead of the well established  $\Lambda(1690)\frac{3}{2}^-$  resonance with width around 60 MeV. Together with  $N^*(1520)\frac{3}{2}^-$ ,  $\Sigma(1542)\frac{3}{2}^-$  suggested in Ref. [24] and either  $\Xi(1620)$  or  $\Xi(1690)$ , they fit in a nice  $3/2^-$  baryon nonet with large penta-quark configuration, *i.e.*,  $N^*(1520)$  as  $|[ud]\{uq\}\bar{q} >$  state,  $\Lambda(1520)$  as  $|[ud]\{sq\}\bar{q} >$  state,  $\Lambda(1670)$  as  $|[ud]\{ss\}\bar{s} >$  state, and  $\Xi(16xx)$  as  $|[ud]\{ss\}\bar{q} >$  state. Here  $\{q_1q_2\}$  means a diquark with configuration of flavor representation **6**, spin 1 and color  $\bar{3}$ . The  $\Lambda(1670)$  as  $|[ud]\{ss\}\bar{s} >$  state gives a natural explanation for its dominant  $\eta\Lambda$  decay mode with a very narrow width due to its very small phase space meanwhile a D-wave decay [35].

Recent analyses [27, 28] also support possible existence of the  $\Lambda(1680)\frac{3}{2}^+$ , but with a narrower width.

### 3. Summary and Prospects

Taking into account new data from Crystal Ball (CB) [12–14], LEPS [15] and CLAS [16], new analyses show strong evidences for the lowest  $\Sigma^*(1/2^-)$  to be in the range of 1380  $\sim$  1500 MeV, the lowest  $\Sigma^*(3/2^-)$  to be around 1550 MeV and the lowest  $\Lambda^*(3/2^+)$  to be around 1680 MeV. There is also evidence for a very narrow  $\Lambda^*(3/2^-)$  around 1670 MeV decaying to  $\Lambda\eta$ . All these new hyperon resonances fit in the expected pattern of unquenched quark models very well. It is very important to pin down the existence of these new resonances.

Various processes could be used to study these hyperon resonances. The neutrino induced hyperon production processes  $\bar{\nu}_{e/\mu} + p \rightarrow e^+/\mu^+ + \pi + \Lambda/\Sigma$  may provide a unique clean place for studying low energy  $\pi\Lambda/\Sigma$  interaction and hyperon resonances below  $KN$  threshold [36]. With plenty production of  $\Lambda_c$  at BESIII, J-PARC, BelleII,  $\Lambda_c^+ \rightarrow \pi^+\pi^0\Lambda$  could also be used to study  $\Sigma^*$ . The  $K^-$ ,  $K_L$  beam experiments at JPARC and Jlab could provide an elegant new source for  $\Lambda^*$ ,  $\Sigma^*$ , and  $\Xi^*$  hyperon spectroscopy.  $K_L p \rightarrow \Lambda\pi^+$ ,  $\Sigma^0\pi^+$ ,  $\Sigma^+\pi^0$ ,  $\Sigma^{*0}\pi^+$ , and  $\Sigma^{*+}\pi^0$  could pin down the  $\Sigma^*(1540)3/2^-$ ;  $K_L p \rightarrow \Sigma^0\pi^0\pi^+$ , and  $\Lambda\pi^0\pi^+$  could shed light on the  $\Sigma^*(1380 \sim 1500)1/2^-$ ,  $\Sigma^*(1540)3/2^-$ ,  $\Lambda^*(1680)3/2^+$ ;  $K_L p \rightarrow \Sigma^0\eta\pi^+$ , and  $\Lambda\eta\pi^+$  may check  $\Sigma^*(1380 \sim 1500)1/2^-$ ,  $\Sigma^*(1540)3/2^-$ , and  $\Lambda^*(1670)3/2^-$ . We believe the proposed  $K_L$  beam experiments at JLab could settle down the spectrum of the low excited hyperon states which provide complementary information to the study of penta-quark states with hidden charm [37, 38] and play a crucial role for understanding the hadron dynamics and hadron structure.

### 4. Acknowledgments

I thank S. Dulat, Puze Gao, Jun Shi, J.J. Wu, and J.J. Xie for collaboration works reviewed here. This work is supported by the National Natural Science Foundation of China under Grant 11261130311 (CRC110 by DFG and NSFC).

## References

- [1] S. Capstick and W. Roberts, Prog. Part. Nucl. Phys. **45**, S241 (2000).

- [2] S. Capstick and N. Isgur, Phys. Rev. D **34**, 2809 (1986).
- [3] L.Y. Glozman and D.O. Riska, Phys. Rept. **268**, 263 (1996).
- [4] U. Loring, B.C. Metsch, and H.R. Petry, Eur. Phys. J. A **10**, 395 (2001).
- [5] C. Helminen and D.O. Riska, Nucl. Phys. A **699**, 624 (2002).
- [6] A. Zhang *et al.*, High Energy Phys. Nucl. Phys. **29**, 250 (2005).
- [7] B.S. Zou, Nucl. Phys. A **835**, 199 (2010); Eur. Phys. J. A **35**, 325 (2008); B.C. Liu and B.S. Zou, Phys. Rev. Lett. **96**, 042002 (2006).
- [8] Y. Oh, Phys. Rev. D **75**, 074002 (2007).
- [9] K.P. Khemchandani *et al.*, Phys. Rev. D **84**, 094018 (2011).
- [10] A. Ramos, E. Oset, and C. Bennhold, Phys. Rev. Lett. **89**, 252001 (2002).
- [11] K.A. Olive *et al.* (Particle Data Group Collaboration), Chin. Phys. C **38**, 090001 (2014).
- [12] A. Starostin *et al.* (Crystal Ball Collaboration), Phys. Rev. C **64**, 055205 (2001).
- [13] S. Prakhov *et al.*, Phys. Rev. C **80**, 025204 (2009).
- [14] R. Manweiler *et al.*, Phys. Rev. C **77**, 015205 (2008).
- [15] K. Hicks *et al.* (LEPS Collaboration), Phys. Rev. Lett. **102**, 012501 (2009).
- [16] K. Moriya *et al.* (CLAS Collaboration), Phys. Rev. C **87**, 035206 (2013).
- [17] J.K. Kim, Phys. Rev. Lett. **27**, 356 (1971).
- [18] W. Langbein and F. Wagner, Nucl. Phys. B **47**, 477 (1972).
- [19] A.S. Carroll *et al.*, Phys. Rev. Lett. **37**, 806 (1976).
- [20] W.A. Morris *et al.*, Phys. Rev. D **17**, 55 (1978).
- [21] P. Baillon and P.J. Litchfield, Nucl. Phys. B **94**, 39 (1975).
- [22] J.J. Wu, S. Dulat, and B.S. Zou, Phys. Rev. D **80**, 017503 (2009); Phys. Rev. C **81**, 045210 (2010); P. Gao, J.J. Wu, and B.S. Zou, Phys. Rev. C **81**, 055203 (2010); J.J. Xie, J.J. Wu, and B.S. Zou, Phys. Rev. C **90**, 055204 (2014).
- [23] L. Roca and E. Oset, Phys. Rev. C **88**, 055206 (2013).
- [24] P. Gao, J. Shi, and B.S. Zou, Phys. Rev. C **86**, 025201 (2012); P. Gao, B.S. Zou, and A. Sibirtsev, Nucl. Phys. A **867**, 41 (2011).
- [25] A. Gal and H. Garcilazo, Nucl. Phys. A **864**, 153 (2011).
- [26] H. Zhang, J. Tulpan, M. Shrestha, and D. M. Manley, Phys. Rev. C **88**, 035205 (2013).

- [27] H. Kamano, S. X. Nakamura, T.-S. H. Lee, and T. Sato, Phys. Rev. C **92**, 025205 (2015).
- [28] C. Fernandez-Ramirez, I.V. Danilkin, D.M. Manley, V. Mathieu, and A.P. Szczepaniak, Phys. Rev. D **93**, 034029 (2016).
- [29] D. Jido *et al.*, Nucl. Phys. A **725**, 181 (2003).
- [30] V.K. Magas, E. Oset, and A. Ramos, Phys. Rev. Lett. **95**, 052301 (2005).
- [31] X.H. Zhong and Q. Zhao, Phys. Rev. C **79**, 045202 (2009); Phys. Rev. C **88**, 015208 (2013).
- [32] B.C. Liu and J.J. Xie, Phys. Rev. C **85**, 038201 (2012); Phys. Rev. C **86**, 055202 (2012).
- [33] J. Shi and B.S. Zou, Phys. Rev. C **91**, 035202 (2015).
- [34] R. Armenteros *et al.*, Nucl. Phys. B **21**, 15 (1970).
- [35] B.S. Zou, Nucl. Phys. A **914**, 454 (2013).
- [36] J.J. Wu and B.S. Zou, Few Body Syst. **56**, 165 (2015).
- [37] J.J. Wu, R. Molina, E. Oset, and B.S. Zou, Phys. Rev. Lett. **105**, 232001 (2010); Phys. Rev. C **84**, 015202 (2011).
- [38] R. Aaij *et al.* (LHCb Collaboration), Phys. Rev. Lett. **115**, 072001 (2015).

## 2.16 Can Spectroscopy with Kaon Beams at JLab Discriminate between Quark Diquark and Three Quark Models ?

Elena Santopinto

*I.N.F.N., Sezione di Genova*

*via Dodecaneso 33*

*16146 Genova, Italy*

### Abstract

Different three quark models exhibit different missing states but also quark diquark models still exhibit missing states, even if they have a reduced space states. Moreover even quark diquark models show some differences in their missing states. After many years still we are not able to answer the question if nature is completely described by three quark models or if diquark correlations in quark diquark models have to be dismissed, or even if one of the two pictures is the dominant one at different scales, as suggested in [1, 2]. A new experiment based on Kaon beam and with polarization techniques, just as can be planned at Jlab will be able to answer to that fundamental open question. The most recent LQCD effort show a three quark clustering of their states at least at lower energy, but still they are not at the pion mass physical point, thus they are still not able to encode the complexity of the chiral symmetry breaking that as shown on the other side by heroic efforts in Dyson Swinger approach to QCD, underline the emerging of the importance of diquark correlations. The quark diquark model corresponds in first approximation to the leading Regge trajectories and still all the resonances belonging to those trajectories are waiting for, to be discovered, but we expect that at least those that correspond to the leading Regge trajectories should be there, so considering that each piece of knowledge is closely interlocked and interconnected, the poor knowledge of some of the Lambda excited states, can be reflected also in an early stage in the Pentaquark analysis. Finally, a review of the underlying ideas of the Interacting Quark Diquark Model (IQDM) that assesses the baryon spectroscopy and structure in terms of quark diquark degrees of freedom is given, together with a discussion of the missing resonance problem. In respect to the early quark diquark models, we found that the IQDM is able to describe the three star.  $N^{3/2+}(1930)$ , that is missing in the old quark diquark models.

### 1. Introduction: Missing States and Kaon Beams

Different three quark models exhibit different missing states (as confirmed [3] also in the study of strong decays with different quark models) but also quark diquark models still exhibit missing states [4–6], even if they have a reduced space state. Moreover even quark diquark models show some differences in their missing states (let's compare the old [7, 8] with the new [4–6, 9]). After many years still we are not able to answer the question if nature is completely described by three quark models or if diquark correlations in quark diquark models have to be dismissed, or even if one of the two pictures is the dominant one at different scales, as suggested in Ref. [1, 2]. A new experiment based on Kaon beam and with polarization techniques, just as can be planned at Jlab will be able to answer to that fundamental open question.

In parallel, recently, theoretical approaches based on QCD have been strongly developed. Lattice QCD performs ab initio calculation for hadron spectroscopy, even if it is not easy

to approach hadron states at the physical pion mass or with heavy flavor. Nevertheless, the recent progress of the Lattice simulations are really impressive and hadron structures and interactions have been discussed extensively in Refs. [10, 11].

The most recent LQCD effort show a three quark like clustering at least at lower energy, but still LQCD results are not at the pion mass physical point, thus they are still not able to encode the complexity and richness of the chiral symmetry breaking. A bit of that, it is on the contrary kept by the efforts in Dyson Swinger approach to QCD [12], that on the contrary is able to show that any interaction that binds  $\pi$  mesons in the rainbow-ladder approximation of the DSE will produce also diquarks as can be seen in Ref. [12]. Nevertheless even if starting from the QCD Lagrangian with a DSE equation, due to the many approximations that are necessary to be able to do calculations, we still turn out dealing with a model even if rooted in QCD.

On the contrary, quark diquark models are by definition only phenomenological models, and they corresponds in first approximation to the leading Regge trajectories, but many of those resonances belonging to those trajectories are still waiting to be discovered. It is reasonable to expect that at least those resonances that correspond to the leading Regge trajectories should exist.

Considering up to only 2 GeV the Interacting Quark Diquark model has 8 missing  $\Lambda$ s in the octet and 6 in the singlet, so that many more can be expected up to 10 GeV. It seems reasonable to expect that at least the quark diquark subset of states will be found by the experiments if we believe in a string like Regge behavior at higher energies where the quark diquark picture should be the dominant one, but also those resonances are still waiting to be discovered. In this respect, the study of the higher energy part of the spectrum will shed light on the confinement mechanism [13, 14] and the generation of the strange baryon and meson masses, as due to the breaking of chiral symmetry, and this will be one of the main task for a JLab Kaon beam experiment.

Considering the same problem but as a three quark follower, we can argue in another way, but still the conclusions will be the same: the number of  $\Lambda$ 's states (but the same can be said for  $\Sigma$  or  $\Omega$ 's states) should be expected in nature at least in equal number than the  $N^*$  or  $\Delta^*$  states (around 26), if we believe in three quark  $SU(3)$  flavor symmetry (or at least only a subset of those if we on the contrary believe in a quark diquark like clustering of states). Considering that up to now only few strange states are experimentally known, and very few also with their quantum numbers *etc.*, thus for sure a 10 GeV Kaon beam experiment, as it can be planned at JLab, should be rated to have a sure important result, also considering that there will be not only expertise in the hardware, but also in the analysis techniques.

Considering that each piece of knowledge is closely interlocked and interconnected, for example the poor knowledge of some of the  $\Lambda$ 's excited states, can be reflected also in a early stage of the charmonium like Pentaquark analysis [15]. Comparing the number of  $\Lambda$ 's states predicted by the relativistic Interacting Quark Diquark models (8 for the octet and 6 for the singlet under 2 GeV) that are only a subset of those predicted by three-quark models, we can try to suggest a next generation Pentaquark analysis that evaluates the systematic error on the background due to the missing  $\Lambda$ 's states (see Ref. [4]). The future discovering of missing  $\Lambda$  resonances by a new JLab Kaon beam experiment maybe will not change the structures



seen in the Dalitz Plot by the LHCb analysis, but eventually modify some parameters. In a similar way, the poor knowledge of strange hadrons can be reflected into an early stage of strangeness physics and beyond the standard model analysis, if (as very often happen) hadron physics pieces are involved in the analysis too.

Various aspects of the hadron structures have been investigated by many experimental and theoretical approaches in the last years. The observations of the hadron states with an exotic structure have attracted a lot of interest. In particular, regarding the light flavor region, we can remind the exotic states found in the accelerator facilities such as the scalar mesons  $a_0(980)$  and  $f_0(980)$ , or the  $\Lambda(1405)$  which are expected to have an exotic structure as multiquarks, hadronic molecules, but also hybrid states and so forth [16, 17], that with Kaon beam could be better studied. On the other hand in the heavy counterpart, there are now accumulating evidences of exotic heavy hadrons, we can cite states such as the  $Z_c$  [18, 19] and  $Z_b^{(\prime)}$  [20] which can not be explained by the simple quark model picture.

The chiral effective field theory respecting the chiral symmetry provides the hadron-hadron scatterings at low energy with the Nambu-Goldstone bosons exchange. This is a powerful tool to investigate hadronic molecules as the meson-meson [21–23], meson-baryon [24, 25], and baryon-baryon [26, 27] states appearing near thresholds, but they need a fine tuning of their parameters that can only be obtained with high precision Kaon beam experiments.

Finally, in the last part of this article, we will discuss briefly some new results obtained within the formalism of the Unquenched Quark Model (UQM): when LQCD or Chiral effective models can not be applied, it can provide anyway predictions, making up with the three quark model defects, but again also the UQM like chiral effective field theory needs a good knowledge of the strange couplings that can be a sub-product of a Kaon beam experiment.

## 2. Phenomenological Motivation for Quark Diquark Model

The notion of diquark is as old as the quark model itself. Gell-Mann [28] mentioned the possibility of diquarks in his original paper on quarks, just as the possibility of tetra and pentaquark. Soon afterwards, Ida and Kobayashi [7] and Lichtenberg and Tassie [8] introduced effective degrees of freedom of diquarks in order to describe baryons as composed of a constituent diquark and quark. Since its introduction, many articles have been written on this subject [1, 29–39] up to the most recent ones [5, 6, 9], and, more recently, also in tetraquark spectroscopy. Moreover different phenomenological indications for diquark correlations have been collected during the years, such as some regularities in hadron spectroscopy, the  $\Delta I = \frac{1}{2}$  rule in weak nonleptonic decays [40], some regularities in parton distribution functions and in spin-dependent structure functions [41] and in the  $\Lambda(1116)$  and  $\Lambda(1520)$  fragmentation functions. Although the phenomenon of color superconductivity [42] in quark dense matter cannot be considered an argument in support of diquarks in the vacuum, it is nevertheless of interest since it stresses the important role of Cooper pairs of color superconductivity, which are color antitriplet, flavor antisymmetric, scalar diquarks. The concept of diquarks in hadronic physics has some similarities to that of correlated pairs in condensed matter physics (superconductivity [43]) and in nuclear physics (interacting boson model [44]), where effective bosons emerge from pairs of electrons [45] and nucleons [46],

respectively. Any interaction that binds  $\pi$  and  $\rho$  mesons in the rainbow-ladder approximation of the DSE will produce diquarks as can be seen in Ref. [12], and finally there are even some indication of diquark confinement. The quark-diquark effective degrees of freedom have shown their usefulness also in the study of transversity problems and fragmentation functions (see Ref. [47]), even in an oversimplified form, *i.e.* with the spatial part of the quark-diquark ground state wave function parametrized by means of a gaussian. The microscopic origin of the diquark as an effective degrees of freedom, it is not completely clear, nevertheless, as in nuclear physics, one may attempt to correlate the data in terms of a phenomenological model, and in many cases it has already shown its usefulness. In this short contribution, we will review the Interacting Quark Diquark model in its original formulation [1], discussing also the Point Form relativistic reformulation [1,5,6]. We shall focus on its differences and extension to the strange spectra [6]. We will point out some important consequences on the ratio of the electric and magnetic form factor of the proton, that is a presence of a zero at  $Q^2 = 8 \text{ GeV}^2$ , while impossible with three quark models. The new  $12 \text{ GeV}^2$  experiment planned at JLab will eventually shed light on the three quark versus diquark structure of the nucleon.

### 3. The Interacting Quark Diquark Model

The model is an attempt to arrive to a systematic description and correlation of data in term of q-diquark effective degrees of freedom. By formulating a quark- diquark model with explicit interactions, in particular with a direct and an exchange interaction, we will show the spectrum which emerges from this model. In respect to the prediction shown in Ref. [1] we have extended our calculation up to  $2.4 \text{ GeV}$ , and so we have predicted more states. Up to an energy of about  $2 \text{ GeV}$ , the diquark can be described as two correlated quarks with no internal spatial excitations [1, 5], thus its color-spin-flavor wave function must be antisymmetric. Moreover, as we consider only light baryons, made up of  $u, d, s$  quarks, the internal group is restricted to  $\text{SU}_{\text{sf}}(6)$ . If we denote spin by its value, flavor and color by the dimension of the representation, the quark has spin  $s_2 = \frac{1}{2}$ , flavor  $F_2 = \mathbf{3}$ , and color  $C_2 = \mathbf{3}$ . The diquark must transform as  $\bar{\mathbf{3}}$  under  $\text{SU}_c(3)$ , hadrons being color singlets. Then, one only has the symmetric  $\text{SU}_{\text{sf}}(6)$  representation  $\mathbf{21}_{\text{sf}}(\text{S})$ , containing  $s_1 = 0$ ,  $F_1 = \bar{\mathbf{3}}$ , and  $s_1 = 1$ ,  $F_1 = \mathbf{6}$ , *i.e.* the scalar and axial-vector diquarks, respectively. This is because we think of the diquark as two correlated quarks in an antisymmetric nonexcited state. We assume that the baryons are composed of a valence quark and a valence diquark.

The relative configurations of two body can be described by the relative coordinate  $\vec{r}$  and its conjugate momenta  $\vec{p}$ . The Hamiltonian contains a direct and an exchange interaction. The direct interaction is Coulomb plus linear interaction, while the exchange one is of the type spin-spin, isospin-isospin etc. A contact term has to be present to describe the splitting between the nucleon and the  $\Delta$ :

$$H = E_0 + \frac{p^2}{2m} - \frac{\tau}{r} + \beta r + (B + C\delta_0)\delta_{S_{12},1} \\ + (-1)^{l+1} 2Ae^{-\alpha r} [s_{12} \cdot \vec{s}_3 + t_{12} \cdot \vec{t}_3 + 2s_{12} \cdot \vec{s}_3 t_{12} \cdot \vec{t}_3]. \quad (1)$$

For a purely Coulomb-like interaction the problem is analytically solvable. The solution is

trivial, with eigenvalues

$$E_{n,l} = -\frac{\tau^2 m}{2n^2} \quad , \quad n = 1, 2 \dots \quad (2)$$

Here  $m$  is the reduced mass of the diquark-quark configuration and  $n$  the principal quantum number. The eigenfunctions are the usual Coulomb functions

$$R_{n,l}(r) = \sqrt{\frac{(n-l-1)!(2g)^3}{2n[(n+l)!]^3}} (2gr)^l e^{-gr} L_{n-l-1}^{2l+1}(2gr), \quad (3)$$

where for the associated Laguerre polynomials  $g = \frac{\tau m}{n}$ . We treat all the other interactions as perturbations, so the model is completely analytical. The matrix elements of  $\beta r$  can be evaluated in closed form as

$$\Delta E_{n,l} = \int_0^\infty \beta r [R_{n,l}(r)]^2 r^2 dr = \frac{\beta}{2m\tau} [3n^2 - l(l+1)]. \quad (4)$$

Next comes the exchange interaction of Eq. (5). The spin-isospin part is obviously diagonal in the basis of Eq. (7)

$$\begin{aligned} \langle \vec{s}_{12} \cdot \vec{s}_3 \rangle &= \frac{1}{2} [S(S+1) - s_{12}(s_{12}+1) - s_3(s_3+1)], \\ \langle \vec{t}_{12} \cdot \vec{t}_3 \rangle &= \frac{1}{2} [T(T+1) - t_{12}(t_{12}+1) - t_3(t_3+1)]. \end{aligned} \quad (5)$$

To complete the evaluation, we need the matrix elements of the exponential. These can be obtained in analytic form

$$I_{n,l}(\alpha) = \int_0^\infty e^{-\alpha r} [R_{n,l}(r)]^2 r^2 dr. \quad (6)$$

The results are straightforward. Here, by way of example, we quote the result for  $l = n - 1$

$$I_{n,l=n-1}(\alpha) = \left( \frac{1}{1 + \frac{n\alpha}{2\tau m}} \right)^{2n+1}. \quad (7)$$

Our results are in present in Tables 1 and 2.

#### 4. The Relativistic Interacting Quark Diquark Model

The exstention of the Interacting quark diquark model [1] in Point Form can be easily done [5, 6]. This is a potential model, constructed within the point form formalism [48], where baryon resonances are described as two-body quark-diquark bound states; thus, the relative motion between the two constituents and the Hamiltonian of the model are functions of the relative coordinate  $\vec{r}$  and its conjugate momentum  $\vec{q}$ . The Hamiltonian contains just as in the 2005 paper [1], the two basic ingredients: a Coulomb-like plus linear confining interaction and an exchange one, depending on the spin and isospin of the quark and the diquark. The mass operator is given by

$$M = E_0 + \sqrt{\vec{q}^2 + m_1^2} + \sqrt{\vec{q}^2 + m_2^2} + M_{\text{dir}}(r) + M_{\text{ex}}(r) \quad , \quad (8)$$

Table 1: Mass spectrum of  $N$ -type resonances (up to 2.1 GeV) in the interacting quark diquark model [1]. The value of the parameters are those obtained and reported in Ref. [10] based on the fit of the 3 and 4 star resonances known at the time. The table reports also the prediction for the remaining resonances, including the recent upgraded 3\*  $P_{13}(1900)$ . The experimental values are taken from Ref. [49].

Baryon $L_{2I,2J}$	Status	Mass (MeV)	$J^p$	$M_{\text{cal}}$ (MeV)
$N(939)P_{11}$	*****	939	$1/2^+$	940
$N(1440)P_{11}$	****	1410-1450	$1/2^+$	1538
$N(1520)D_{13}$	*****	1510-1520	$3/2^-$	1543
$N(1535)S_{11}$	*****	1525-1545	$1/2^-$	1538
$N(1650)S_{11}$	*****	1645-1670	$1/2^-$	1673
$N(1675)D_{15}$	*****	1670-1680	$5/2^-$	1673
$N(1680)F_{15}$	*****	1680-1690	$5/2^+$	1675
$N(1700)D_{13}$	***	1650-1750	$3/2^-$	1673
$N(1710)P_{11}$	***	1680-1740	$1/2^+$	1640
$N(1720)P_{13}$	*****	1700-1750	$3/2^+$	1675
$N(1860)F_{15}$	**	1820-1960	$5/2^+$	1975
$N(1875)D_{13}$	***	1820-1920	$3/2^-$	1838
$N(1880)P_{11}$	**	1835-1905	$1/2^+$	1838
$N(1895)S_{11}$	**	1880-1910	$1/2^-$	1838
$N(1900)P_{13}$	***	1875-1935	$3/2^+$	1967
$N(1990)F_{17}$	**	1995-2125	$7/2^+$	2015
$N(2000)F_{15}$	**	1950-2150	$5/2^+$	2015
$N(2040)P_{13}$	*	2031-2065	$3/2^+$	2015
$N(2060)D_{15}$	**	2045-2075	$5/2^-$	2078
$N(2100)P_{11}$	**	2050-2200	$1/2^+$	2015
$N(2120)D_{13}$	**	2090-2210	$3/2^-$	2069

Table 2: As Table 1, but for  $\Delta$ -type resonances.

Baryon $L_{2I,2J}$	Status	Mass (MeV)	State	$M_{\text{cal}}$ (MeV)
$\Delta(1232)P_{33}$	****	1230-1234	$3/2^+$	1235
$\Delta(1600)P_{33}$	***	1500-1700	$3/2^+$	1709
$\Delta(1620)S_{31}$	****	1600-1660	$1/2^-$	1673
$\Delta(1700)D_{33}$	****	1670-1750	$3/2^-$	1673
$\Delta(1900)S_{31}$	**	1840-1920	$1/2^-$	2003
$\Delta(1905)F_{35}$	****	1855-1910	$5/2^+$	1930
$\Delta(1910)P_{31}$	****	1860-1910	$1/2^+$	1967
$\Delta(1920)P_{33}$	***	1900-1970	$3/2^+$	1930
$\Delta(1930)D_{35}$	***	1900-2000	$5/2^-$	2003
$\Delta(1940)D_{33}$	**	1940-2060	$3/2^-$	2003
$\Delta(1950)F_{37}$	****	1915-1950	$7/2^+$	1930
$\Delta(2000)F_{35}$	**	$\approx 2000$	$5/2^+$	2015

where  $E_0$  is a constant,  $M_{\text{dir}}(r)$  and  $M_{\text{ex}}(r)$  the direct and the exchange diquark-quark interaction, respectively,  $m_1$  and  $m_2$  stand for diquark and quark masses. The direct term, we consider,

$$M_{\text{dir}}(r) = -\frac{\tau}{r} (1 - e^{-\mu r}) + \beta r \quad (9)$$

is the sum of a Coulomb-like interaction with a cut off plus a linear confinement term. We also have an exchange interaction, since this is the crucial ingredient of a quark-diquark description of baryons that has to be extended to contain flavor  $\lambda$  matrices in such a way to be able to describe in a simultaneous way both the non strange and the strange sector [1, 6]. We have also generalized the exchange interaction in such a way to be able to describe strange baryons, simply considering

$$M_{\text{ex}}(r) = (-1)^{L+1} e^{-\sigma r} \left[ A_S \vec{s}_1 \cdot \vec{s}_2 + A_F \vec{\lambda}_1^f \cdot \vec{\lambda}_2^f + A_I \vec{t}_1 \cdot \vec{t}_2 \right], \quad (10)$$

where  $\vec{\lambda}^f$  are the  $\text{SU}_f(3)$  Gell-Mann matrices. In a certain sense, we can consider it as a Gürsey-Radicati inspired interaction [9, 50]. In the nonstrange sector, we also have to keep a contact interaction [5] in the mass operator

$$M_{\text{cont}} = \left( \frac{m_1 m_2}{E_1 E_2} \right)^{1/2+\epsilon} \frac{\eta^3 D}{\pi^{3/2}} e^{-\eta^2 r^2} \delta_{L,0} \delta_{s_1,1} \left( \frac{m_1 m_2}{E_1 E_2} \right)^{1/2+\epsilon} \quad (11)$$

as necessary to reproduce the  $\Delta - N$  mass splitting.

The results for the strange and non-strange baryon spectra from Ref. [1, 6] (See Tables 1, 2, and 3) were obtained by diagonalizing the mass operator of Eq.(8) by means of a numerical variational procedure, based on harmonic oscillator trial wave functions. With a basis of 150 harmonic oscillator shells, the results converge very well.

It is interesting to compare our results [6] to those of three-quark quark models (see Refs. [2, 5, 54–60]). It is clear that a larger number of experiments and analysis, looking for missing

Table 3: Mass predictions [6] for  $\Lambda$ -type resonances compared with PDG data; APS copyright.

Resonance	Status	$M^{\text{exp.}}$ (MeV)	$J^P$	$L^P$	$S$	$s_1$	$Q^2 q$	<b>F</b>	<b>F<sub>1</sub></b>	$I$	$t_1$	$n_r$	$M^{\text{calc.}}$ (MeV)
$\Lambda(1116) P_{01}$	****	1116	$\frac{1}{2}^+$	$0^+$	$\frac{1}{2}$	0	$[n, n]_s$	<b>8</b>	$\bar{\mathbf{3}}$	0	0	0	1116
$\Lambda(1600) P_{01}$	***	1560 - 1700	$\frac{1}{2}^+$	$0^+$	$\frac{1}{2}$	0	$[n, s]_n$	<b>8</b>	$\bar{\mathbf{3}}$	0	$\frac{1}{2}$	0	1518
$\Lambda(1670) S_{01}$	****	1660 - 1680	$\frac{1}{2}^-$	$1^-$	$\frac{1}{2}$	0	$[n, n]_s$	<b>8</b>	$\bar{\mathbf{3}}$	0	0	0	1650
$\Lambda(1690) D_{03}$	****	1685 - 1695	$\frac{3}{2}^-$	$1^-$	$\frac{1}{2}$	0	$[n, n]_s$	<b>8</b>	$\bar{\mathbf{3}}$	0	0	0	1650
$\Lambda(1800) S_{01}$	***	1720 - 1850	$\frac{1}{2}^-$	$1^-$	$\frac{1}{2}$	0	$[n, s]_n$	<b>8</b>	$\bar{\mathbf{3}}$	0	$\frac{1}{2}$	0	1732
$\Lambda(1810) P_{01}$	***	1750 - 1850	$\frac{1}{2}^+$	$0^+$	$\frac{1}{2}$	0	$[n, n]_s$	<b>8</b>	$\bar{\mathbf{3}}$	0	0	1	1666
$\Lambda(1820) F_{05}$	****	1815 - 1825	$\frac{5}{2}^+$	$2^+$	$\frac{1}{2}$	0	$[n, n]_s$	<b>8</b>	$\bar{\mathbf{3}}$	0	0	0	1896
$\Lambda(1830) D_{05}$	****	1810 - 1830	$\frac{5}{2}^-$	$1^-$	$\frac{3}{2}$	1	$\{n, s\}_n$	<b>8</b>	<b>6</b>	0	$\frac{1}{2}$	0	1785
$\Lambda(1890) P_{03}$	****	1850 - 1910	$\frac{3}{2}^+$	$0^+$	$\frac{3}{2}$	1	$\{n, s\}_n$	<b>8</b>	<b>6</b>	0	$\frac{1}{2}$	0	1896
missing	—	—	$\frac{3}{2}^-$	$1^-$	$\frac{1}{2}$	0	$[n, s]_n$	<b>8</b>	$\bar{\mathbf{3}}$	0	$\frac{1}{2}$	0	1732
missing	—	—	$\frac{1}{2}^-$	$1^-$	$\frac{3}{2}$	1	$\{n, s\}_n$	<b>8</b>	<b>6</b>	0	$\frac{1}{2}$	0	1785
missing	—	—	$\frac{3}{2}^-$	$1^-$	$\frac{1}{2}$	0	$[n, n]_s$	<b>8</b>	$\bar{\mathbf{3}}$	0	0	1	1785
missing	—	—	$\frac{1}{2}^+$	$0^+$	$\frac{1}{2}$	1	$\{n, s\}_n$	<b>8</b>	<b>6</b>	0	$\frac{1}{2}$	0	1955
missing	—	—	$\frac{1}{2}^+$	$0^+$	$\frac{1}{2}$	0	$[n, s]_n$	<b>8</b>	$\bar{\mathbf{3}}$	0	$\frac{1}{2}$	1	1960
missing	—	—	$\frac{1}{2}^-$	$1^-$	$\frac{1}{2}$	1	$\{n, s\}_n$	<b>8</b>	<b>6</b>	0	$\frac{1}{2}$	0	1969
missing	—	—	$\frac{3}{2}^-$	$1^-$	$\frac{1}{2}$	1	$\{n, s\}_n$	<b>8</b>	<b>6</b>	0	$\frac{1}{2}$	0	1969
$\Lambda^*(1405) S_{01}$	****	1402 - 1410	$\frac{1}{2}^-$	$1^-$	$\frac{1}{2}$	0	$[n, n]_s$	<b>1</b>	$\bar{\mathbf{3}}$	0	0	0	1431
$\Lambda^*(1520) D_{03}$	****	1519 - 1521	$\frac{3}{2}^-$	$1^-$	$\frac{1}{2}$	0	$[n, n]_s$	<b>1</b>	$\bar{\mathbf{3}}$	0	0	0	1431
missing	—	—	$\frac{1}{2}^-$	$1^-$	$\frac{1}{2}$	0	$[n, s]_n$	<b>1</b>	$\bar{\mathbf{3}}$	0	$\frac{1}{2}$	0	1443
missing	—	—	$\frac{3}{2}^-$	$1^-$	$\frac{1}{2}$	0	$[n, s]_n$	<b>1</b>	$\bar{\mathbf{3}}$	0	$\frac{1}{2}$	0	1443
missing	—	—	$\frac{1}{2}^-$	$1^-$	$\frac{1}{2}$	0	$[n, n]_s$	<b>1</b>	$\bar{\mathbf{3}}$	0	0	1	1854
missing	—	—	$\frac{3}{2}^-$	$1^-$	$\frac{1}{2}$	0	$[n, n]_s$	<b>1</b>	$\bar{\mathbf{3}}$	0	0	1	1854
missing	—	—	$\frac{1}{2}^-$	$1^-$	$\frac{1}{2}$	0	$[n, s]_n$	<b>1</b>	$\bar{\mathbf{3}}$	0	$\frac{1}{2}$	1	1928
missing	—	—	$\frac{3}{2}^-$	$1^-$	$\frac{1}{2}$	0	$[n, s]_n$	<b>1</b>	$\bar{\mathbf{3}}$	0	$\frac{1}{2}$	1	1928

resonances, are necessary because many aspects of hadron spectroscopy are still unclear. In particular the number of  $\Lambda$  states reported by the PDG are still very few in respect to the predictions both of the Lattice QCD and by the models. In particular the relativistic version of the interacting quark diquark model predict seven  $\Lambda$  missing states belonging to the octet and other six missing states belonging to the singlet (considering only states under 2.0 GeV), otherwise much more states should be considered, and looked for, by a 10 GeV secondary Kaon beam experiment at Jlab. Typical three quark models will predict much more  $\Lambda$  missing states, and in short they should be in the same number then the already known  $N$  or  $\Delta$  states, so at least so 24 for the octet and the same for the singlet. New experiments should be dedicated to the hunting of those elusive missing  $\Lambda$  states.

Without relying on models only considering the  $^{***}$  and  $^{***}$  Nstar and using  $SU(3)$  symmetry, for each Nstar belonging to an octet, one can expect to complete with the corresponding  $\Lambda$  state belonging to the same octet. That will give us an expectation for its mass by means of an evaluation via a Guersey and Radicati mass formula (see table ). The  $\Lambda$ 's states that are partners of the same octet multiplet for which at least an  $N$  star state has been already seen or viceversa will be denoted with the same colors.

It is also worthwhile noting that in our model [6]  $\Lambda(1116)$  and  $\Lambda^*(1520)$  are described as bound states of a scalar diquark  $[n, n]$  and a quark  $s$ , where the quark-diquark system is in  $S$  or  $P$ -wave, respectively [6]. This is in accordance with the observations of Refs. [35, 36] on  $\Lambda$ 's fragmentation functions, that the two resonances can be described as  $[n, n] - s$  systems.

The present work can be expanded to include charmed and/or bottomed baryons, which can be quite interesting in light of the recent experimental effort to study the properties of heavy hadrons.

We should also underline that the interacting quark-diquark model gives origin to wave functions that can describe in a reasonable way the elastic electromagnetic form factors of the nucleon. In particular they give origin to a reproduction of the existing data for the ratio of the electric and magnetic form factor of the proton that predict a zero at  $Q^2 = 8 \text{ GeV}^2$  (see Fig. 1) like in vector meson parametrizations. On the contrary, we have found impossible to get this zero with a three quark model [52] (see Fig. 2). The new experiment planned at JLab will be able to distinguish between the two scenarios ruling out one of the two models.

## 5. The Unquenched Quark Model

The behavior of observables such as the spectrum and the magnetic moments of hadrons are well reproduced by the constituent quark model (CQM) [2, 5, 53–60], but it neglects quark-antiquark pair-creation (or continuum-coupling) effects. The unquenching of the quark model for hadrons is a way to take these components into account.

The unquenching of CQM were initially done by Törnqvist and collaborators, who used an unitarized quark model [61, 62], while Van Beveren and Rupp used an t-matrix approach [63, 64]. These techniques were applied to study of scalar meson nonet ( $a_0$ ,  $f_0$ , etc.) of Ref. [64, 65] in which the loop contributions are given by the hadronic intermediate states that each meson can access. It is via these hadronic loops that the bare states become “dressed” and the hadronic loop contributions totally dominate the dynamics of the

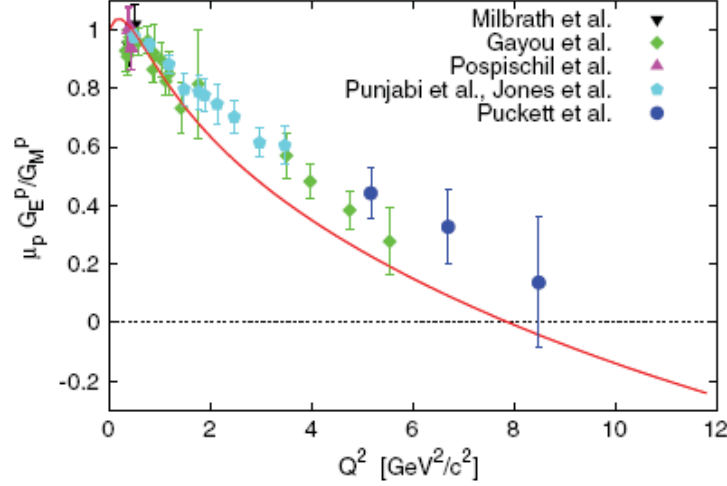


Figure 1: Ratio  $\mu_p G_E^p(Q^2)/G_M^p(Q^2)$ , the solid line correspond to the relativistic quark-diquark calculation, figure taken from Ref. [51]; APS copyright.

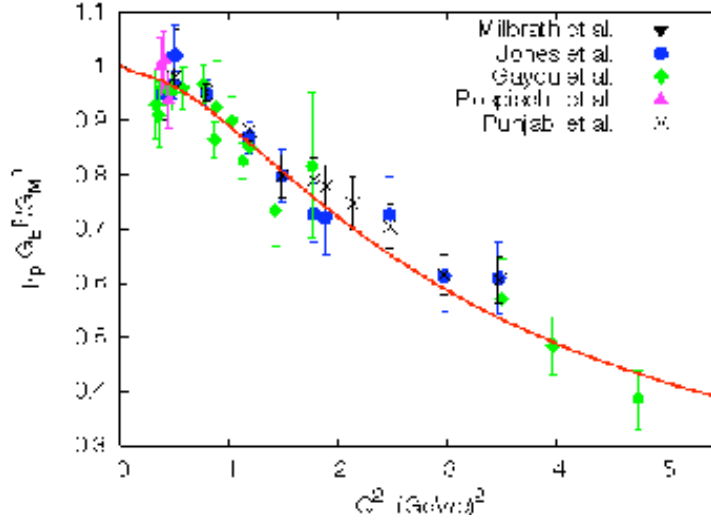


Figure 2: Ratio  $\mu_p G_E^p(Q^2)/G_M^p(Q^2)$ , the solid line correspond to the relativistic Hypercentral quark model, Figure taken from Ref. [52]; APS copyright.

process. A similar approach was developed by Pennington in Ref. [66], where they have investigated the dynamical generation of the scalar mesons by initially inserting only one “bare seed”. Also, the strangeness content of the nucleon and electromagnetic form factors were investigated in [67], whereas Capstick and Morel in Ref. [68] analyzed baryon meson loop effects on the spectrum of nonstrange baryons. In the meson sector, Eichten *et al.* explored the influence of the open-charm channels on the charmonium properties using the Cornell coupled-channel model [53] to assess departures from the single-channel potential-model expectations.



In this work we present the latest applications of the UQM to study the orbital angular momenta contribution to the spin of the proton in which the effects of the sea quarks were introduced into the CQM in a systematic way and the wave functions given explicitly. In another contribution of the same workshop are on the contrary discussed the flavor asymmetry and strangeness of the proton. Finally, the UQM is applied to describe meson observables and the spectroscopy of the charmonium and bottomonium, developing the formalism to take into account in a systematic way, the continuum components.

## 6. The UQM Formalism

In the UQM for baryons [67, 69–71] and mesons [72–75], the hadron wave function is made up of a zeroth order  $qqq$  ( $q\bar{q}$ ) configuration plus a sum over the possible higher Fock components, due to the creation of  ${}^3P_0$   $q\bar{q}$  pairs. Thus, we have

$$|\psi_A\rangle = \mathcal{N} \left[ |A\rangle + \sum_{BC\ell J} \int d\vec{K} k^2 dk |BC\ell J; \vec{K}k\rangle \frac{\langle BC\ell J; \vec{K}k | T^\dagger | A\rangle}{E_a - E_b - E_c} \right], \quad (12)$$

where  $T^\dagger$  stands for the  ${}^3P_0$  quark-antiquark pair-creation operator [72–75],  $A$  is the baryon/meson,  $B$  and  $C$  represent the intermediate state hadrons.  $E_a$ ,  $E_b$  and  $E_c$  are the corresponding energies,  $k$  and  $\ell$  the relative radial momentum and orbital angular momentum between  $B$  and  $C$  and  $\vec{J} = \vec{J}_b + \vec{J}_c + \vec{\ell}$  is the total angular momentum. It is worthwhile noting that in Refs. [72–75], the constant pair-creation strength in the operator (12) was substituted with an effective one, to suppress unphysical heavy quark pair-creation.

The introduction of continuum effects in the CQM can thus be essential to study observables that only depend on  $q\bar{q}$  sea pairs, like the strangeness content of the nucleon electromagnetic form factors [67] or the flavor asymmetry of the nucleon sea [69] it has been discussed in another contribution of the same conference (see García-Tecocoatzi *et al.*) The continuum effects can give important corrections to baryon/meson observables, like the self-energy corrections to meson masses [72–75] or the importance of the orbital angular momentum in the spin of the proton [70].

## 7. Orbital Angular Momenta Contribution to Proton Spin in the UQM Formalism

The inclusion of the continuum higher Fock components has a dramatic effect on the spin content of the proton [71]. Whereas in the CQM the proton spin is carried entirely by the (valence) quarks, while in the unquenched calculation 67.6% is carried by the quark and antiquark spins and the remaining 32.4% by orbital angular momentum. The orbital angular momentum due to the relative motion of the baryon with respect to the meson accounts for 31.7% of the proton spin, whereas the orbitally excited baryons and mesons in the intermediate state only contribute 0.7%. Finally we note, that the orbital angular momentum arises almost entirely from the relative motion of the nucleon and  $\Delta$  resonance with respect to the  $\pi$ -meson in the intermediate states.

## 8. Self-Energy Corrections in the UQM

The formalism was used to compute the charmonium ( $c\bar{c}$ ) and bottomonium ( $b\bar{b}$ ) spectra with self-energy corrections, due to continuum coupling effects [72–75]. In the UQM, the

physical mass of a meson

$$M_a = E_a + \Sigma(E_a) \quad (13)$$

is given by the sum of two terms: a bare energy,  $E_a$ , calculated within a potential model [55], and a self energy correction

$$\Sigma(E_a) = \sum_{BC\ell J} \int_0^\infty k^2 dk \frac{|M_{A \rightarrow BC}(k)|^2}{E_a - E_b - E_c}, \quad (14)$$

computed within the UQM formalism.

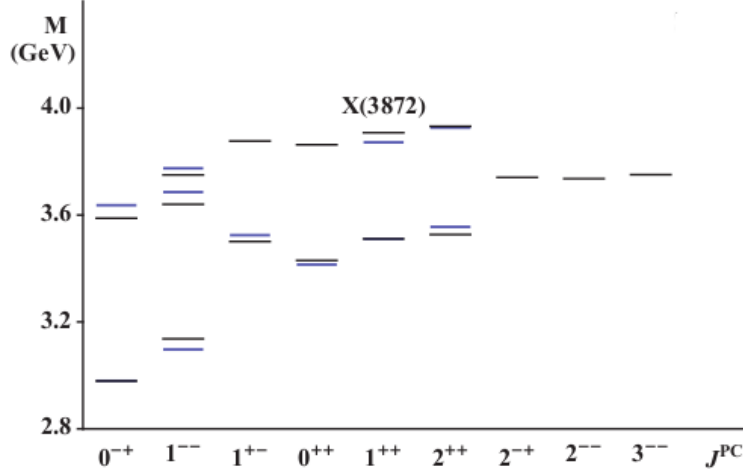


Figure 3: Charmonium spectrum with self energies corrections. Black lines are theoretical predictions and blue lines are experimental data available. Figure taken from Ref. [73]; APS copyright.

Our results for the self energies corrections of charmonia [73,75] and bottomonia [72,74,75] spectrums, are shown in Figures 3 and 4.

In our framework the  $X(3872)$  can be interpreted as a  $c\bar{c}$  core [the  $\chi_{c1}(2^3P_1)$ ], plus higher Fock components due to the coupling to the meson-meson continuum. In Ref. [75], we were the first to predict analogous states (as  $X(3872)$ ) with strong continuum components in the bottomonium sector but in the  $\chi_{b1}(3^3P_1)$  sector, due to opening of threshold of  $B\bar{B}$ ,  $B\bar{B}^*$  and  $B^*\bar{B}^*$ . We expect similar interesting effects near threshold also in the  $N^*$  sector.

It is interesting to compare the present results to those of the main three-quark quark models [2, 5, 54–60]. It is clear that a larger number of experiments and analyses, looking for missing resonances, are necessary because many aspects of hadron spectroscopy are still unclear.

## References

- [1] E. Santopinto, Phys. Rev. C **72**, 022201 (2005).

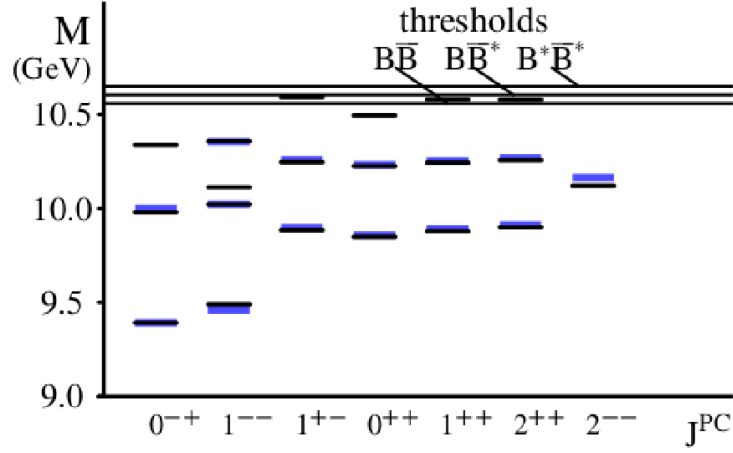


Figure 4: Bottomonium spectrum with self energies corrections. Black lines are theoretical predictions and blue lines are experimental data available. Figure taken from Ref. [74]; APS copyright.

- [2] G. Galata and E. Santopinto, Phys. Rev. C **86**, 045202 (2012).
- [3] Strong decays of baryons and missing resonances, R. Bijker, G. Galat, H. Garca-Tecocoatzi, E. Santopinto, arXiv:1506.07469 [hep-ph].
- [4] E. Santopinto, Diquark correlations in baryons: the Interacting Quark Diquark Model, accepted for publication on JPS conference Proceedings NSTAR 2015, arXiv:1512.04896.
- [5] J. Ferretti, A. Vassallo, and E. Santopinto, Phys. Rev. C **83**, 065204 (2011).
- [6] E. Santopinto and J. Ferretti, Phys. Rev. C **92**, 025202 (2015).
- [7] M. Ida and R. Kobayashi, Progr. Theor. Phys. **36**, 846 (1966).
- [8] D.B. Lichtenberg and L.J. Tassie, Phys. Rev. **155**, 1601 (1967).
- [9] M. De Sanctis, J. Ferretti, E. Santopinto, A. Vassallo, arXiv:1410.0590, accepted for publication on EPJA.
- [10] J.J. Dudek, R.G. Edwards, M.J. Peardon, D.G. Richards and C.E. Thomas, Phys. Rev. Lett. **103**, 262001 (2009).
- [11] S. Aoki *et al.* [PACS-CS Collaboration], PTEP **2012**, 01A102 (2012).
- [12] R.T. Cahill, C.D. Roberts, and J. Praschifka, Phys. Rev. D **36**, 2804 (1987).
- [13] A. Ostrander, E. Santopinto, A.P. Szczepaniak, and A. Vassallo, Phys. Rev. D **86**, 114015 (2012).
- [14] C.D. Roberts and J. Segovia, arXiv:1603.02722 [nucl-th].

- [15] R. Aaij *et al.* (LHCb Collaboration), Phys. Rev. Lett. **115**, 072001 (2015).
- [16] E. Klempt and A. Zaitsev, Phys. Rept. **454**, 1 (2007).
- [17] N. Brambilla, S. Eidelman, B.K. Heltsley, R. Vogt, G.T. Bodwin, E. Eichten, A.D. Frawley, and A.B. Meyer *et al.*, Eur. Phys. J. C **71**, 1534 (2011).
- [18] M. Ablikim *et al.* (BESIII Collaboration), Phys. Rev. Lett. **110**, 252001 (2013).
- [19] Z.Q. Liu *et al.* (Belle Collaboration), Phys. Rev. Lett. **110**, 252002 (2013).
- [20] A. Bondar *et al.* (Belle Collaboration), Phys. Rev. Lett. **108**, 122001 (2012).
- [21] J.A. Oller and E. Oset, Nucl. Phys. A **620**, 438 (1997). [Nucl. Phys. A **652**, 407 (1999)].
- [22] P. Wang and X.G. Wang, Phys. Rev. Lett. **111**, 042002 (2013).
- [23] V. Baru, E. Epelbaum, A.A. Filin, F.-K. Guo, H.-W. Hammer, C. Hanhart, U.-G. Meissner and A.V. Nefediev, Phys. Rev. D **91**, 034002 (2015).
- [24] T. Hyodo and D. Jido, Prog. Part. Nucl. Phys. **67**, 55 (2012).
- [25] Y. Yamaguchi, S. Ohkoda, S. Yasui, and A. Hosaka, Phys. Rev. D **84**, 014032 (2011).
- [26] R. Machleidt and D.R. Entem, Phys. Rept. **503**, 1 (2011).
- [27] J. Haidenbauer and U. G. Meissner, Nucl. Phys. A **881**, 44 (2012).
- [28] M. Gell-Mann, Phys. Lett. **8**, 214 (1964).
- [29] For a review, see M. Anselmino, E. Predazzi, S. Ekelin, S. Frederksson, and D.B. Lichtenberg, Rev. Mod. Phys. **65**, 1199 (1993).
- [30] R. Jakob, P.J. Mulders, and J. Rodrigues, Nucl. Phys. A **626**, 937 (1997).
- [31] S.J. Brodsky, D.S. Hwang, and I. Schmidt, Phys. Lett. B **530**, 99 (2002).
- [32] L.P. Gamberg, G.R. Goldstein, and K.A. Oganessyan, Phys. Rev. D **67**, 071504 (2003).
- [33] R.L. Jaffe and F. Wilczek, Phys. Rev. Lett. **91**, 232003 (2003).
- [34] F. Wilczek, arXiv:hep-ph/0409168; R.L. Jaffe, arXiv:hep-ph/0409065; R.L. Jaffe and F. Wilczek, Phys. Rev. Lett. **91**, 232003 (2003).
- [35] R.L. Jaffe, Phys. Rept. **409**, 1 (2005) [Nucl. Phys. Proc. Suppl. **142**, 343 (2005)].
- [36] A. Selem and F. Wilczek, hep-ph/0602128.
- [37] T. DeGrand, Z. Liu, and S. Schaefer, Phys. Rev. D **77**, 034505 (2008).
- [38] H. Forkel and E. Klempt, Phys. Lett. B **679**, 77 (2009).

- [39] A.V. Anisovich *et al.*, Int. J. Mod. Phys. A **25**, 2965 (2010); [Int. J. Mod. Phys. A **25**, 3155 (2010)].
- [40] M. Neubert and B. Stech, Phys. Lett. B **231**, 477 (1989); Phys. Rev. D **44** (1991).
- [41] F.E. Close and A.W. Thomas, Phys. Lett. B **212**, 227 (1988).
- [42] D. Bailing and A. Love, Phys. Rept. **107**, 325 (1984); M.G. Alford, K. Rajagopal, and F. Wilczek, Nucl. Phys. B **537**, 443 (1999).
- [43] J. Bardeen, L.N. Cooper and J.R. Schrieffer, Phys. Rev. **108**, 1175 (1957).
- [44] F. Iachello and A. Arima, *The Interacting Boson Model*, (Cambridge University Press, 1987).
- [45] L.N. Cooper, Phys. Rev. **104**, 1189 (1956).
- [46] T. Otsuka, A. Arima, F. Iachello, and I. Talmi, Phys. Lett. **76B**, 135 (1978).
- [47] A. Bacchetta, F. Conti, and M. Radici, Phys. Rev. D **78**, 074010 (1991).
- [48] W.H. Klink, Phys. Rev. C **58**, 3617 (1998); **58**, 3587 (1998); W.N. Polyzou *et al.*, Few Body Syst. **49**, 129 (2011); E.P. Biernat, W.H. Klink, and W. Schweiger, Few Body Syst. **49**, 149 (2011).
- [49] K.A. Olive *et al.* (Particle Data Group), Chin. Phys. C **38**, 090001 (2014).
- [50] F. Gursey and L.A. Radicati, Phys. Rev. Lett. **13**, 173 (1964).
- [51] M. De Sanctis, J. Ferretti, E. Santopinto, and A. Vassallo, Phys. Rev. C **84**, 055201 (2011).
- [52] E. Santopinto, A. Vassallo, M.M. Giannini, and M. De Sanctis, Phys. Rev. C **82**, 065204 (2010).
- [53] E. Eichten, K. Gottfried, T. Kinoshita, J.B. Kogut, K.D. Lane, and T.-M. Yan, Phys. Rev. Lett. **34** (1975) 369; E. Eichten, K. Gottfried, T. Kinoshita, K.D. Lane, and T.-M. Yan, Phys. Rev. D **17**, 3090 (1978); Phys. Rev. D **21**, 203 (1980).
- [54] N. Isgur and G. Karl, Phys. Rev. D **18**, 4187 (1978); Phys. Rev. D **19**, 2653 (1979); [Erratum-*ibid.* **23**, 817 (1981)]; Phys. Rev. D **20**, 1191 (1979).
- [55] S. Godfrey and N. Isgur, Phys. Rev. D **32**, 189 (1985).
- [56] S. Capstick and N. Isgur, Phys. Rev. D **34**, 2809 (1986).
- [57] M. Ferraris, M.M. Giannini, M. Pizzo, E. Santopinto, and L. Tiator, Phys. Lett. B **364**, 231 (1995); E. Santopinto, F. Iachello, and M.M. Giannini, Eur. Phys. J. A **1**, 307 (1998); E. ginto and G. Giannini, Phys. Rev. C **86**, 065202 (2012); M.M. Giannini, E. Santopinto, Chin. J. Phys. **53**, 020301 (2015); M. Aiello *et al.*, Phys. Lett. B **387**, 215 (1996); Aiello *et al.*, J. of Phys. G **24**, 753 (1988); R. Bijker, F. Iachello, E. Santopinto, J. of Phys. A **31**, 9041 (1988); M. De Sanctis *et al.*, Phys. Rev., C **6** 062201 (2007).

- [58] L.Y. Glozman, D.O. Riska, Phys. Rept. **268** 263 (1996); L.Y. Glozman, W. Plessas, K. Varga, R.F. Wagenbrunn, Phys. Rev. D **58**, 094030 (1998).
- [59] U. Loring, B.C. Metsch, and H.R. Petry, Eur. Phys. J. A **10**, 395 (2001).
- [60] R. Bijker, F. Iachello, and A. Leviatan, Ann. Phys. (N.Y.) **236**, 69 (1994); Phys. Rev. C **54**, 1935 (1996); Phys. Rev. D **55**, 2862 (1997); Ann. Phys. (N.Y.) **284**, 89 (2000).
- [61] S. Ono and N.A. Törnqvist, Z. Phys. C **23**, 59 (1984); K. Heikkila, S. Ono, and N.A. Törnqvist, Phys. Rev. D **29** (1984) 110. [Erratum-ibid. **29** (1984) 2136]; S. Ono, A.I. Sanda, and N.A. Törnqvist, Phys. Rev. D **34**, 186 (1986).
- [62] N.A. Törnqvist and P. Zenczykowski, Phys. Rev. D **29**, 2139 (1984); Z. Phys. C **30**, 83 (1986) P. Zenczykowski, Annals Phys. **169**, 453 (1986).
- [63] E. van Beveren, C. Dullemond, and G. Rupp, Phys. Rev. D **21**, 771 (1980) [Erratum-ibid. D **22**, 787 (1980)].
- [64] E. van Beveren, T.A. Rijken, K. Metzger, C. Dullemond, G. Rupp, and J.E. Ribeiro, Z. Phys. C **30**, 615 (1986).
- [65] N.A. Törnqvist, Z. Phys. C **68**, 647 (1995).
- [66] M. Boglione and M.R. Pennington, Phys. Rev. D **65**, 114010 (2002).
- [67] R. Bijker, J. Ferretti, and E. Santopinto, Phys. Rev. C **85**, 035204 (2012).
- [68] S. Capstick and D. Morel, arXiv:nucl-th/0204014.
- [69] E. Santopinto and R. Bijker, Phys. Rev. C **82**, 062202 (2010).
- [70] E. Santopinto and R. Bijker, Few Body Syst. **44**, 95 (2008).
- [71] R. Bijker and E. Santopinto, Phys. Rev. C **80**, 065210 (2009).
- [72] J. Ferretti, G. Galatà, E. Santopinto, and A. Vassallo, Phys. Rev. C **86**, 015204 (2012).
- [73] J. Ferretti, G. Galatà, and E. Santopinto, Phys. Rev. C **88**, 015207 (2013).
- [74] J. Ferretti and E. Santopinto, Phys. Rev. D **90**, 094022 (2014).
- [75] J. Ferretti, G. Galatà, and E. Santopinto, Phys. Rev. D **90**, 054010 (2014).

## 2.17 Reducing the Ambiguity of the AntiKaon-Nucleon Amplitude Using Modern Experimental Data

Maxim Mai

*Helmholtz–Institut für Strahlen- und Kernphysik (Theorie)*

*and Bethe Center for Theoretical Physics*

*Universität Bonn*

*D-53115 Bonn, Germany*

### Abstract

AntiKaon-nucleon scattering is studied utilizing an analytic solution of the Bethe-Salpeter equation with the interaction kernel derived from the leading and next-to leading order chiral Lagrangian. In the on-shell factorization of this solution multiple sets of parameters are found, which all allow for a good description of the existing hadronic data. We confirm the two-pole structure of the  $\Lambda(1405)$ . The narrow  $\Lambda(1405)$  pole appears at comparable positions in the complex energy plane, whereas the location of the broad pole suffers from a large uncertainty. It is demonstrated how experimental data on the photoproduction of  $K^+\pi\Sigma$  off the proton measured by the CLAS Collaboration can be used to reduce this ambiguity. Finally, an estimation is made on the desired quality of the new scattering data to constrain the parameter space of the presented model.

### 1. Introduction

The strangeness  $S = -1$  resonance  $\Lambda(1405)$  is believed to be dynamically generated through coupled-channel effects in the antiKaon-nucleon interaction. A further intricate feature is its two-pole structure. Within chiral unitary approaches, which are considered to be the best tool to address the chiral SU(3) dynamics in such type of system, the investigation of the two-pole structure was initiated in Ref. [1] and thoroughly analyzed in many publications, for a (PDG) review see Ref. [2]. However, the available scattering data alone do not allow to pin down the poles with good precision, as it is known since long, see, *e.g.*, Ref. [3].

Recently, very sophisticated measurements of the reaction  $\gamma p \rightarrow K^+\pi\Sigma$  were performed by the CLAS Collaboration at JLab, see Ref. [4]. There, the invariant mass distribution of all three  $\pi\Sigma$  channels was determined in a broad energy range and with high resolution. First theoretical analyses of this data have already been performed on the basis of a chiral unitary approach in Refs. [5, 6]. In this work, we take up the challenge to combine our next-to-leading order approach of antiKaon-nucleon scattering [7] in an on-shell approximation with the CLAS data.

First, we construct a family of solutions that lead to a good description of the scattering and the SIDDHARTA data. This reconfirms the two-pole structure of the  $\Lambda(1405)$ . As before, we find that the location of the second pole in the complex energy plane is not well determined from these data alone. Then, we address the issue how this ambiguity can be constrained from the CLAS data. Similar to Ref. [5], we use a simple semi-phenomenological model for the photoproduction process that combines the description of the hadronic scattering with a simple polynomial and energy-dependent ansatz for the photoproduction of  $K^+$  and a meson-baryon pair of strangeness  $S = -1$  off the proton. The corresponding energy- and

channel-dependent constants are fitted to the CLAS data. However, it appears that not all solutions, consistent with the scattering data, lead to a decent fit to the photoproduction data. Moreover, we find that the solutions, consistent with photoproduction and scattering data lead to similar positions of both poles of  $\Lambda(1405)$ .

## 2. AntiKaon-nucleon Scattering

The starting point of the present analysis is the meson-baryon scattering amplitude - a simplified version of the amplitude constructed and described in detail in the original publication [8] as well as in Refs. [9, 10], to which we refer the reader for conceptual details. We start from the chiral Lagrangian of leading (LO) and next-to-leading (NLO) order. For the reasons given in Refs. [8–10], the  $s$ - and  $u$ -channel one-baryon exchange diagrams are neglected, leaving us with the following chiral potential

$$V(\not{q}_2, \not{q}_1; p) = A_{WT}(\not{q}_1 + \not{q}_2) + A_{14}(q_1 \cdot q_2) + A_{57}[\not{q}_1, \not{q}_2] + A_M + A_{811} \left( \not{q}_2(q_1 \cdot p) + \not{q}_1(q_2 \cdot p) \right), \quad (1)$$

where the incoming- and outgoing-meson four-momenta are denoted by  $q_1$  and  $q_2$ , respectively, whereas the overall four-momentum of the meson-baryon system is denoted by  $p$ . The  $A_{WT}$ ,  $A_{14}$ ,  $A_{57}$ ,  $A_M$  and  $A_{811}$  are 10-dimensional matrices which encode the coupling strengths between all 10 channels of the meson-baryon system for strangeness  $S = -1$ , *i.e.*,  $\{K^-p, \bar{K}^0n, \pi^0\Lambda, \pi^0\Sigma^0, \pi^+\Sigma^-, \pi^-\Sigma^+, \eta\Lambda, \eta\Sigma^0, K^+\Xi^-, K^0\Xi^0\}$ . These matrices depend on the meson decay constants, the baryon and meson masses as well as 14 low-energy constants (LECs) as specified in the original publication [8].

Due to the appearance of the  $\Lambda(1405)$  resonance just below the  $\bar{K}N$  threshold and large momentum transfer, the strict chiral expansion is not applicable for the present system. Instead, the above potential is used as a driving term of the coupled-channel Bethe-Salpeter equation (BSE), for NLO approaches see, *e.g.*, Ref. [3, 7, 11, 12]. For the meson-baryon scattering amplitude  $T(\not{q}_2, \not{q}_1; p)$  the integral equation to be solved reads

$$T(\not{q}_2, \not{q}_1; p) = V(\not{q}_2, \not{q}_1; p) + i \int \frac{d^d l}{(2\pi)^d} V(\not{q}_2, \not{l}; p) S(\not{p} - \not{l}) \Delta(\not{l}) T(\not{l}, \not{q}_1; p), \quad (2)$$

where  $S$  and  $\Delta$  represent the baryon (of mass  $m$ ) and the meson (of mass  $M$ ) propagator, respectively, and are given by  $iS(\not{p}) = i/(\not{p} - m + i\epsilon)$  and  $i\Delta(\not{k}) = i/(k^2 - M^2 + i\epsilon)$ . Moreover,  $T$ ,  $V$ ,  $S$  and  $\Delta$  in the last expression are matrices in the channel space. The loop diagrams appearing above are treated using dimensional regularization and applying the usual  $\overline{\text{MS}}$  subtraction scheme in the spirit of our previous work [10]. Note that the modified loop integrals are still scale-dependent. This scale  $\mu$  reflects the influence of the higher-order terms not included in our potential and is used as a fit parameter. To be precise, we have 6 such parameters in the isospin basis.

The above equation can be solved analytically if the kernel contains contact terms only, see Ref. [9] for the corresponding solution. Using this solution for the strangeness  $S = -1$  system, we have shown in Ref. [7] that once the full off-shell amplitude is constructed, one can easily reduce it to the on-shell solution, *i.e.*, setting all tadpole integrals to zero. It appears that the double pole structure of the  $\Lambda(1405)$  is preserved by this reduction and that



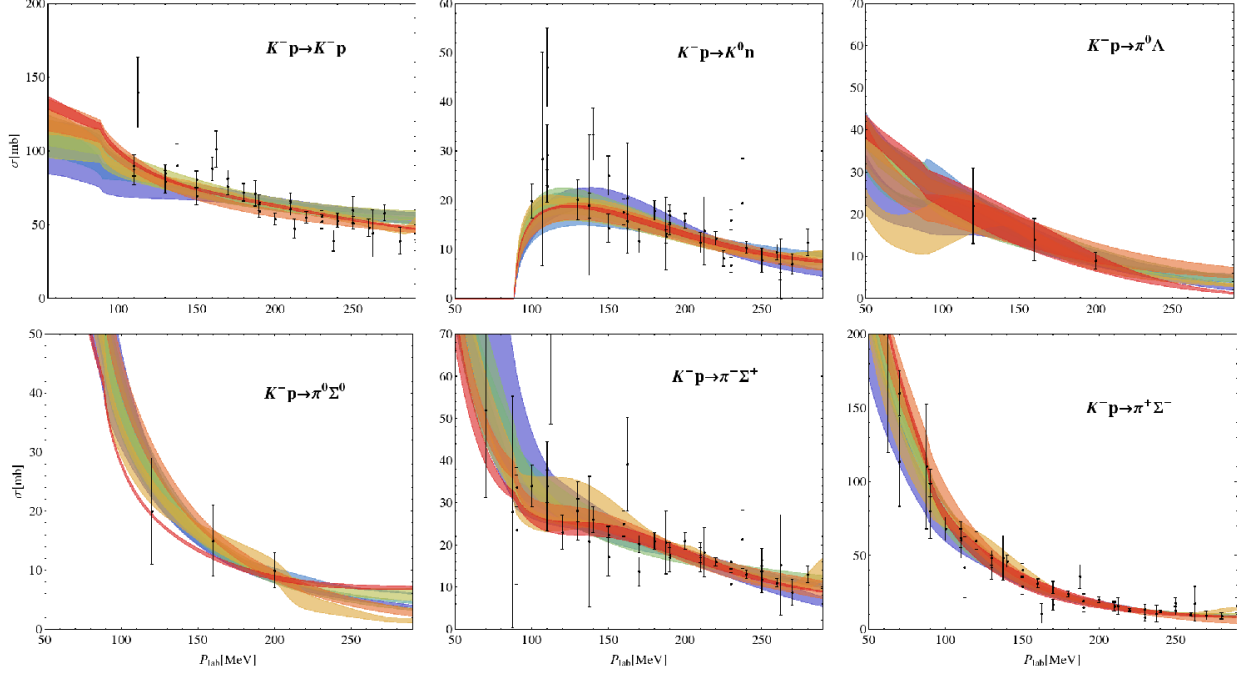


Figure 1: Fit results compared to the experimental data from Refs. [13–16]. Different colors correspond to the eight best solutions, while the bands represent the  $1\sigma$  uncertainty due to errors of the fit parameters. The color coding is specified in Fig. 2.

the positions of the two poles are changing only by about 20 MeV in imaginary part. On the other hand, the use of the on-shell approximation of the Eq. (2) reduces the computational time roughly by a factor of 30. Therefore, in order to explore the parameter space in more detail, it seems to be safe and also quite meaningful to start from the solution of the BSE (2) with the chiral potential (1) on the mass-shell. Once the parameter space is explored well enough we can slowly turn on the tadpole integrals obtaining the full off-shell solution. Such a solution will become a part of a more sophisticated two-meson photoproduction amplitude in a future work.

The free parameters of the present model, the low-energy constants as well as the regularization scales  $\mu$  are adjusted to reproduce all known experimental data in the meson-baryon sector of strangeness  $S = -1$ . The main bulk of this data consists of the cross sections

Table 1: Quality of the various fits in the description of the hadronic and the photoproduction data from CLAS. For the definition of  $\chi^2_{\text{p.p.}}$ , see the text.

Fit #	1	2	3	4	5	6	7	8
$\chi^2_{\text{d.o.f.}}$ (hadronic data)	1.35	1.14	0.99	0.96	1.06	1.02	1.15	0.90
$\chi^2_{\text{p.p.}}$ (CLAS data)	3.18	1.94	2.56	1.77	1.90	6.11	2.93	3.14

for the processes  $K^-p \rightarrow MB$ , where  $MB \in \{K^-p, \bar{K}^0n, \pi^0\Lambda, \pi^+\Sigma^-, \pi^0\Sigma^0, \pi^-\Sigma^+\}$ , and laboratory momentum  $P_{\text{lab}} < 300$  MeV, from Refs. [13–16]. Electromagnetic effects are not included in the analysis and assumed to be negligible at the measured values of  $P_{\text{lab}}$ . Additionally, at the antiKaon-nucleon threshold, we consider the decay ratios from Refs. [17, 18] as well as the energy shift and width of Kaonic hydrogen in the 1s state from the SIDDHARTA experiment at DAΦNE [19] related to the  $K^-p$  scattering length via the modified Deser-type formula [20]. Due to the precision of the experiment, the latter two values have already become the most important input in this sector. In principle, both  $\bar{K}N$  scattering lengths can be determined directly, performing a complementary measurement on the Kaonic deuterium, see Refs. [21, 22] for the proposed experiments. The strong energy shift and width of the latter can again be related to the antiKaon-deuteron scattering length, using the the modified Deser-type formula [20] and finally to the antiKaon-nucleon scattering lengths as described in Ref. [23].

The fit to the above data was performed minimizing  $\chi_{\text{d.o.f.}}^2$  using several thousands randomly distributed sets of starting values of the free parameters. The latter were assumed to be of natural size, while the unphysical solutions, *e.g.*, poles on the first Riemann sheet for  $\text{Im}(W) < 200$  MeV ( $W := \sqrt{p^2}$ ), were sorted out. For more details on the fitting procedure and results, we refer the reader to the original publication [8]. Eight best solutions were obtained by this, see second row of Tab. 1, whereas the next best  $\chi_{\text{d.o.f.}}^2$  are at least one order of magnitude larger. The results of the fits compared to experimental data are presented in Fig. 1, where every solution is represented by a distinct color.

The data are described equally well by all eight solutions, showing, however, different functional behaviour of the cross sections as a function of  $P_{\text{lab}}$ . When continued analytically to the complex  $W$  plane, all eight solutions confirm the double pole structure of the  $\Lambda(1405)$ , see Fig. 2. There, the narrow pole lies on the Riemann sheet, connected to the real axis between the  $\pi\Sigma - \bar{K}N$  thresholds for every solution. The second poles lie on the Riemann sheets, connected to the real axis between the following thresholds:  $\pi\Sigma - \bar{K}N$  for solution 1, 2, 4, 5 and 8;  $\pi\Lambda - \pi\Sigma$  for solution 3;  $\bar{K}N - \eta\Lambda$  for solutions 6 and 7. Please note that the second pole of the solution 5 has a shadow pole ( $5'$  in Fig. 2) on the Riemann sheet, connected to the real axis between  $\bar{K}N - \eta\Lambda$  thresholds. The scattering amplitude is restricted around the  $\bar{K}N$  threshold by the SIDDHARTA measurement quite strongly. Therefore, in the complex  $W$  plane we observe a very stable behaviour of the amplitude at this energy, *i.e.*, the position of the narrow pole agrees among all solutions within the  $1\sigma$  parameter errors, see Fig. 2. This is in line with the findings of other groups [3, 11, 12], *i.e.*, one observes stability of the position of the narrow pole. Quantitatively, the first pole found in these models is located at somewhat lower energies and is slightly broader than those of our model. In view of the stability of the pole position, we trace this shift to the different treatment of the Born term contributions to the chiral potential utilized in Refs. [3, 11, 12].

The position of the second pole is, on the other hand, less restricted. To be more precise, for the real part we find three clusters of these poles: around the  $\pi\Sigma$  threshold, around the  $\bar{K}N$  threshold as well as around 1470 MeV. For several solutions, there is some agreement in the positions of the second pole between the present analysis and the one of Ref. [12] and of our previous work [7]. However, as the experimental data is described similarly well by all fit solutions, one can not reject any of them. Thus, the distribution of poles represents

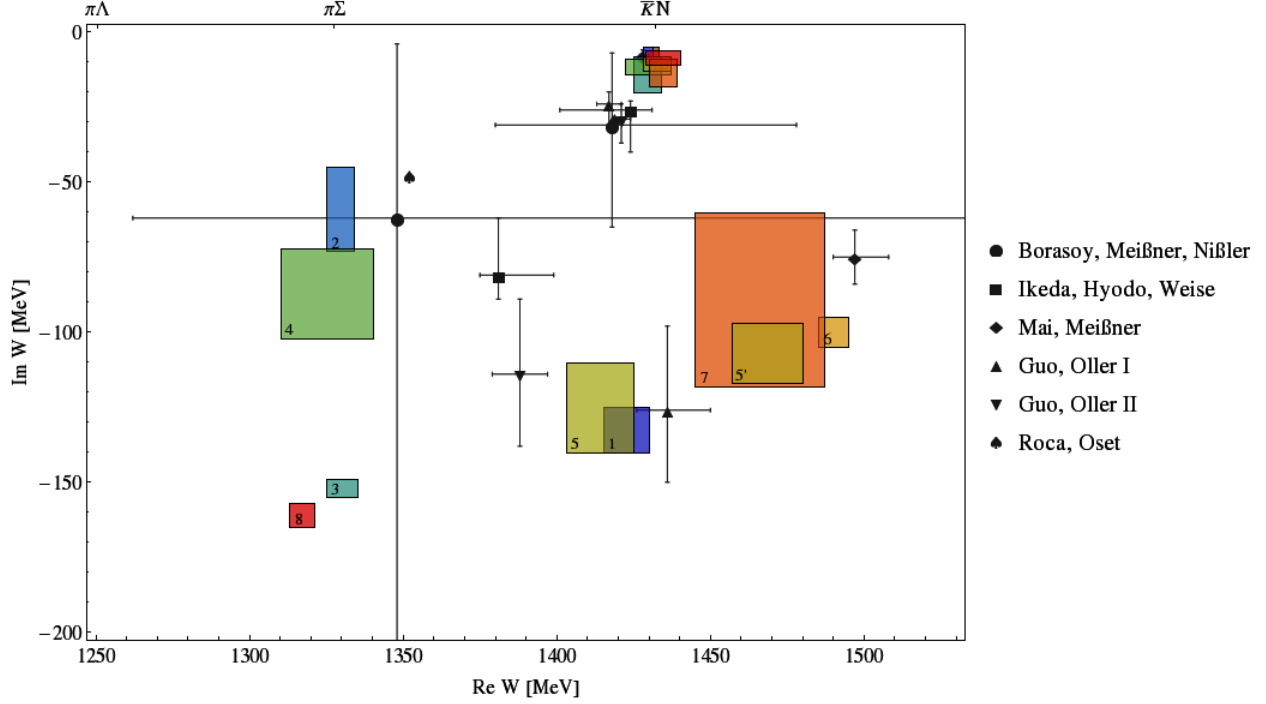


Figure 2: Double pole structure of the  $\Lambda(1405)$  in the complex energy plane for the eight solutions that describe the scattering and the SIDDHARTA data. For easier reading, we have labeled the second pole of these solutions by the corresponding fit #, where 5 and 5' denote the second pole on the second Riemann sheet, connected to the real axis between the  $\pi\Sigma - \bar{K}N$  and  $\bar{K}N - \eta\Lambda$  thresholds, respectively. For comparison, various results from the literature are also shown, see Refs. [3, 5, 7, 11, 12].

the systematic uncertainty of the present approach. It appears to be quite large, but is still significantly smaller than the older analysis of Ref. [3]. Recall that no restrictions were put on the parameters of the model, except for naturalness.

### 3. Photoproduction Amplitude

We have demonstrated above that the present model for the meson-baryon interaction possesses at least eight different solutions, which all describe the hadronic data similarly well. In this Section, we wish to see whether these solutions are compatible with the photoproduction data, if they are considered as a final-state interaction of the reaction  $\gamma p \rightarrow K^+\Sigma\pi$ . For this purpose it is sufficient to consider the simple ansatz

$$\mathcal{M}^j(\tilde{W}, M_{\text{inv}}) = \sum_{i=1}^{10} C^i(\tilde{W}) G^i(M_{\text{inv}}) f_{0+}^{i,j}(M_{\text{inv}}), \quad (3)$$

where  $\tilde{W}$  and  $M_{\text{inv}}$  denote the total energy of the system and the invariant mass of the  $\pi\Sigma$  subsystem, respectively. For a specific meson-baryon channel  $i$ , the energy-dependent

(and in general complex valued) constants  $C^i(\tilde{W})$  describe the reaction mechanism of  $\gamma p \rightarrow K^+ M_i B_i$ , whereas the final-state interaction is captured by the standard Höhler partial waves  $f_{0+}$ . For a specific meson-baryon channel  $i$ , the Greens function is denoted by  $G^i(M_{\text{inv}})$  and is given by the one-loop meson baryon function in dimensional regularization.

The regularization scales appearing in the Eq. (3) via the  $G^i(M_{\text{inv}})$  have already been fixed in the fit to the hadronic cross sections and the SIDDHARTA data. Thus, the only new parameters of the photoproduction amplitude are the constants  $C^i(\tilde{W})$  which, however, are quite numerous (10 for each  $\tilde{W}$ ). These parameters are adjusted to reproduce the invariant mass distribution  $d\sigma/dM_{\text{inv}}(M_{\text{inv}})$  for the final  $\pi^+\Sigma^-$ ,  $\pi^0\Sigma^0$  and  $\pi^-\Sigma^+$  states and for all 9 measured total energy values  $\tilde{W} = 2.0, 2.1, \dots, 2.8$  GeV. The achieved quality of the photoproduction fits is listed in the third row of Tab. 1, whereas the  $\chi^2_{\text{d.o.f.}}$  of the hadronic part are stated in the second row. Note that for the comparison of the photoproduction fits the quantity  $\chi^2_{\text{d.o.f.}}$  is not meaningful due to the large number of generic parameters  $C_i(\tilde{W})$ . Therefore, we compare the total  $\chi^2$  divided by the total number of data points for all three  $\pi\Sigma$  final states, denoted by  $\chi^2_{\text{p.p.}}$ . For the same reason it is not meaningful to perform a global fit, minimizing the total  $\chi^2_{\text{d.o.f.}}$ .

It turns out that even within such a simple and flexible photoproduction amplitude, only the solutions #2, #4 and #5 of the eight hadronic solutions allow for a decent description of the CLAS data. While the total  $\chi^2$  per data point of these solutions is very close to each other, the next best solution has a 40% larger total  $\chi^2_{\text{p.p.}}$  than the best one.

We have checked this statement for a large number of hadronic solutions randomly distributed within  $1\sigma$  band around the central ones. For every such solution a fit to the CLAS data was performed independently and no significantly better fit was found to those of the central solution. Therefore, we consider the above exclusion principle of the hadronic solutions as statistically stable. For further discussion on this aspect see Ref. [8].

The best solution is indeed #4, which, incidentally, has also the lowest  $\chi^2_{\text{d.o.f.}}$  for the hadronic part. This solution also gives an excellent description of the  $\Sigma\pi\pi$  mass distribution from Ref. [24], calculated using the method developed in Ref. [1]. With respect to these data, solution #2 is also satisfactory but #5 is not. Therefore, the photoproduction data combined with the scattering and the SIDDHARTA data lead to a sizable reduction in the ambiguity of the second pole of the  $\Lambda(1405)$ . The locations of the two poles in these surviving solutions are  $(1434^{+2}_{-2} - i 10^{+2}_{-1})$  MeV  $((1330^{+4}_{-5} - i 56^{+17}_{-11})$  MeV) and  $(1429^{+8}_{-7} - i 12^{+2}_{-3})$  MeV  $((1325^{+15}_{-15} - i 90^{+12}_{-18})$  MeV) for the first (second) pole of the solution #2 and #4, respectively. In fact, the second pole of the surviving solutions is close to the value found in Ref. [5], see Fig. 2, and also close to the central value of the analysis based on scattering data only [3].

We conclude that the inclusion of the CLAS data as experimental input can serve as a new important constraint on the antiKaon-nucleon scattering amplitude. However, for future studies a theoretically more robust model for the two-meson photoproduction amplitude is required. We propose that a generalization of the one-meson photoproduction model, presented in Ref. [9, 25], may be the next logical step for this endeavor.

#### 4. New Scattering (Pseudo-) Data

In the last Section, we have demonstrated that modern data indeed allows to put additional

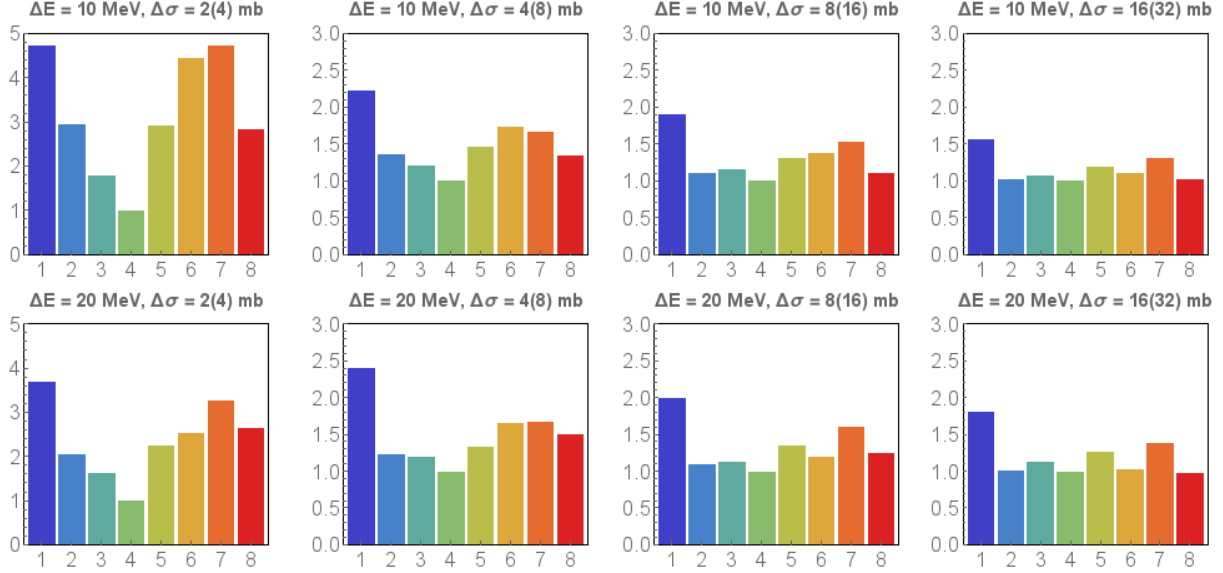


Figure 3: Comparison of  $\chi^2_{\text{d.o.f.}}$  for all 8 solutions and all available as well as pseudo scattering data. The values are normalized by the  $\chi^2_{\text{d.o.f.}}$  of solution #4, which is used to generate the pseudo-data. Each plot label denotes the assumed energy binning  $\Delta E$  and measurement uncertainty  $\Delta\sigma$  for the charged (neutral) final states.

constraints on the antiKaon-nucleon scattering amplitude. To use these data we have used a very simple ansatz for the two-meson photoproduction amplitude. Another and actually more direct way to put new constraints on the scattering amplitude is to improve the (currently very old) cross section data on  $K^-p \rightarrow \dots$  as proposed in, *e.g.*, Ref. [26] using Kaon beams at JLab. In the following we study the impact of such, in the future available data if used complementary to the already available data. In particular, we will estimate the minimal resolution required for such new data to be capable to rule out some of our 8 solutions.

We start from generating realistic pseudo-data, without discussing further the details of such measurements. For this we assume our best solution (#4) to be a realistic one and calculate total cross sections in all six channels  $K^-p \rightarrow MB$ , where  $MB \in \{K^-p, \bar{K}^0n, \pi^0\Lambda, \pi^+\Sigma^-, \pi^0\Sigma^0, \pi^-\Sigma^+\}$  in the energy range  $P_{\text{lab}} = 100 \dots 300$  MeV for various values of the energy resolution  $\Delta E$ . To account for the uncertainty of the new measurement, we assume several values  $\Delta\sigma$ . Since neutral channels are usually more complicated to measure the uncertainty  $\Delta\sigma$  is assumed to be twice as large as in the charged channels. Finally, realistic pseudo-data is obtained as a random value around the central one (predicted by the solution #4) normally distributed with the standard deviation of  $\Delta\sigma$ .

For the fixed parameter sets of the model we calculate the new  $\chi^2_{\text{d.o.f.}}$  using all available data together with the new pseudo-data. The results of such a test for different values of  $\Delta E$  and  $\Delta\sigma$  are depicted in Fig. 3. There, the individual values  $\chi^2_{\text{d.o.f.}}$  are normalized to the one of the solution #4, which is used to generate pseudo-data. It is seen that even at

quite low energy resolution of  $\Delta E = 20$  MeV already 3 solutions have twice as large  $\chi^2_{\text{d.o.f.}}$  as the one of solution #4. Thus such solutions could presumably be ruled out by the new data. On the other hand, it looks like given a too large measurement uncertainty  $\Delta\sigma$  none of the above solutions can be ruled out that easily. Therefore, we conclude from this very preliminary and qualitative study that for the new data to be restrictive enough the desired measurement precision should be  $\Delta\sigma \lesssim 4(8)$  mb for the charged (neutral) final states. The energy resolutions seems to play a minor role.

## 5. Acknowledgments

The speaker thanks the organizers and in particular Igor Strakovsky for the invitation to this very inspiring workshop. The work of the speaker was performed with Ulf-G. Meißner and supported in part by the DFG and the NSFC through funds provided to the Sino-German CRC 110 “Symmetries and the Emergence of Structure in QCD” (NSFC Grant No. 11261130311).

## References

- [1] J. A. Oller and U.-G. Meißner, Phys. Lett. B **500**, 263 (2001).
- [2] U.-G. Meißner and T. Hyodo, *Pole structure of the  $\Lambda(1405)$  region* in *Review of Particle Physics*, <http://pdg.lbl.gov/2015/reviews/rpp2015-rev-lam-1405-pole-struct.pdf>.
- [3] B. Borasoy, U.-G. Meißner, and R. Nisßler, Phys. Rev. C **74** 055201, (2006).
- [4] K. Moriya *et al.* (CLAS Collaboration), Phys. Rev. C **87**, 035206 (2013).
- [5] L. Roca and E. Oset, Phys. Rev. C **87**, 055201 (2013).
- [6] S.X. Nakamura and D. Jido, PTEP **2014**, 023D01 (2014).
- [7] M. Mai and U.-G. Meißner, Nucl. Phys. A **900**, 51 (2013).
- [8] M. Mai and U.-G. Meißner, Eur. Phys. J. A **51**, 30 (2015).
- [9] M. Mai, P.C. Bruns, and U.-G. Meißner, Phys. Rev. D **86**, 094033 (2012).
- [10] P.C. Bruns, M. Mai, and U.-G. Meißner, Phys. Lett. B **697**, 254 (2011).
- [11] Y. Ikeda, T. Hyodo, and W. Weise, Nucl. Phys. A **881**, 98 (2012).
- [12] Z.H. Guo and J.A. Oller, Phys. Rev. C **87**, 035202 (2013).
- [13] J. Ciborowski *et al.*, J. Phys. G **8** (1982) 13.
- [14] W.E. Humphrey and R.R. Ross, Phys. Rev. **127**, 1305 (1962).
- [15] M. Sakitt, T.B. Day, R.G. Glasser, N. Seeman, J.H. Friedman, W.E. Humphrey, and R. R. Ross, Phys. Rev. **139**, B719 (1965).

- [16] M.B. Watson, M. Ferro-Luzzi, and R. D. Tripp, Phys. Rev. **131**, 2248 (1963).
- [17] D.N. Tovee *et al.*, Nucl. Phys. B **33**, 493 (1971).
- [18] R.J. Nowak *et al.*, Nucl. Phys. B **139**, 61 (1978).
- [19] M. Bazzi *et al.* (SIDDARTHA Collaboration), Phys. Lett. B **704**, 113 (2011).
- [20] U.-G. Meißner, U. Raha, and A. Rusetsky, Eur. Phys. J. C **35**, 349 (2004).
- [21] SIDDHARTA-2 Collaboration, Proposal at Laboratori Nazionali di Frascati of INFN, *The upgrade of the SIDDHARTA apparatus for an enriched scientific case*, 2010.
- [22] C. Berucci *et al.*, Letter of Intent for J-PARC, *Measurement of the strong interaction induced shift and width of the  $1s$  state of Kaonic deuterium*, 2013.
- [23] M. Mai, V. Baru, E. Epelbaum, and A. Rusetsky, Phys. Rev. D **91**, 054016 (2015).
- [24] R.J. Hemingway, Nucl. Phys. B **253**, 742 (1985).
- [25] B. Borasoy, P.C. Bruns, U.-G. Meißner, and R. Nissler, Eur. Phys. J. A **34**, 161 (2007).
- [26] W.J. Briscoe, M. Döring, H. Haberzettl, D.M. Manley, M. Naruki, I.I. Strakovsky, and E.S. Swanson, Eur. Phys. J. A **51**, 129 (2015).

## 2.18 Opportunities in the Hyperon Spectrum with Neutral Kaon Beam

Vincent Mathieu

*Center for Exploration of Energy and Matter*

*Indiana University*

*Bloomington, IN 47403, U.S.A.*

### Abstract

In this talk, I presented the features of the webpage of our model for  $\bar{K}N$  scattering. The future directions concerning these reactions were also discussed.

1. As explained in these Proceedings,<sup>1</sup> the hyperon spectrum is of importance for the understanding of the strong interaction. In Ref. [1], we presented a unitary multichannel model for  $\bar{K}N$  scattering in the resonance region that fulfills unitarity. This project has led to deliverables (such as the partial waves or codes for the various observables). We decided to create an interactive webpage [2], where the practitioners can download and simulate online our models.<sup>2</sup>

Several coupled channels, indicated in the publication, were considered in the fitting procedure. In the JPAC webpage, the observables and partial waves for the following channels can be computed

$$K^-p \rightarrow K^-p, \bar{K}^0n, \pi^-\Sigma^+, \pi^+\Sigma^-, \pi^0\Sigma^0, \pi^0\Lambda.$$

All observables, differential cross section  $d\sigma/dz_s$ , polarization observable  $P$  and total cross section  $\sigma$ , are expressed in terms of the spin-non-flip  $f(s, z_s)$  and the spin-flip  $g(s, z_s)$  amplitudes with the relations

$$\begin{aligned} \frac{d\sigma}{dz_s}(s, z_s) &= \frac{1}{q^2} [|f(s, z_s)|^2 + |g(s, z_s)|^2], \\ P \frac{d\sigma}{dz_s}(s, z_s) &= \frac{2}{q^2} \text{Im} [f(s, z_s)g^*(s, z_s)], \quad \sigma(s) = \int_{-1}^1 \frac{d\sigma}{dz_s}(s, z_s) dz_s. \end{aligned} \quad (1)$$

For a given channel (the channel index is omitted), the amplitudes admit a partial wave expansion

$$f(s, z_s) = \sum_{\ell=0}^{\infty} [(\ell+1)R_{\ell+}(s) + \ell R_{\ell-}(s)] P_{\ell}(z_s), \quad (2)$$

$$g(s, z_s) = \sum_{\ell=1}^{\infty} [R_{\ell+}(s) - R_{\ell-}(s)] \sqrt{1 - z_s^2} P'_{\ell}(z_s). \quad (3)$$

In a given meson-baryon channel  $\ell$  labels the relative orbital angular momentum and the total angular momentum is given by  $J = \ell \pm 1/2$ . For a detailed relation, in all channels, between the orbital momentum and the partial waves we refer the reader to Ref. [1].

<sup>1</sup>See the contribution, in these Proceedings, by César Fernández-Ramírez and Adam Szczepaniak.

<sup>2</sup>Other projects performed by the Joint Physics Analysis Center are also available online. A short description of these projects are presented in Ref. [3].



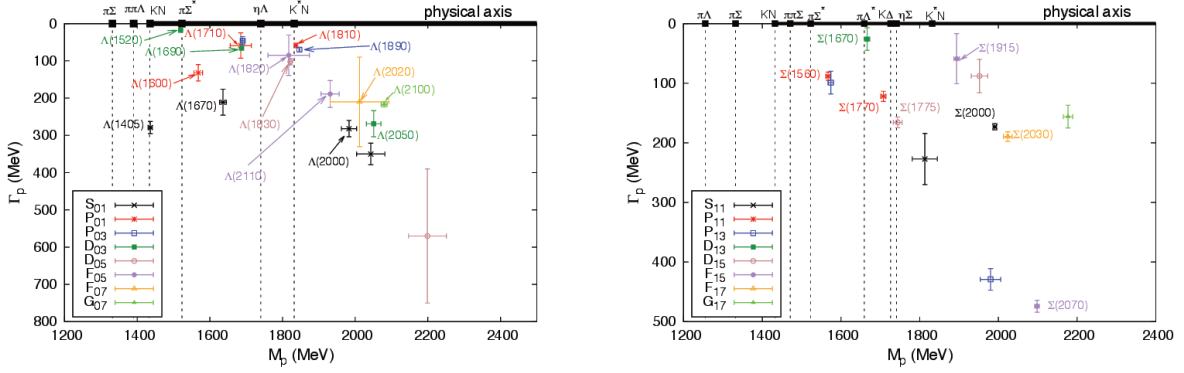


Figure 1: Spectrum of the  $\Lambda$  ( $I=0$ ) and  $\Sigma$  ( $I=1$ ) baryons from Ref. [1].

After removing the barrier factor, the partial waves are parametrized with a  $K$ -matrix to ensure proper 2-body unitarity in the resonance region. The  $K$ -matrix is the sum of the resonance contributions and an empirical background term. Each wave is parametrized and fitted independently. The detailed procedure is described in Ref. [1]. Finally the partial waves are analytically continue on the unphysical sheet and the pole positions are extracted. The resulting spectrum for  $\Lambda$  and  $\Sigma$  baryons is displayed on Figure 1.

The partial waves, binned in energy supplied by the user, can be downloaded online . The Fortran code yielding the partial is also available. The differential cross section (together with the polarization) and the total cross section have also their dedicated pages. The codes for producing the observables can be both simulated online and downloaded.

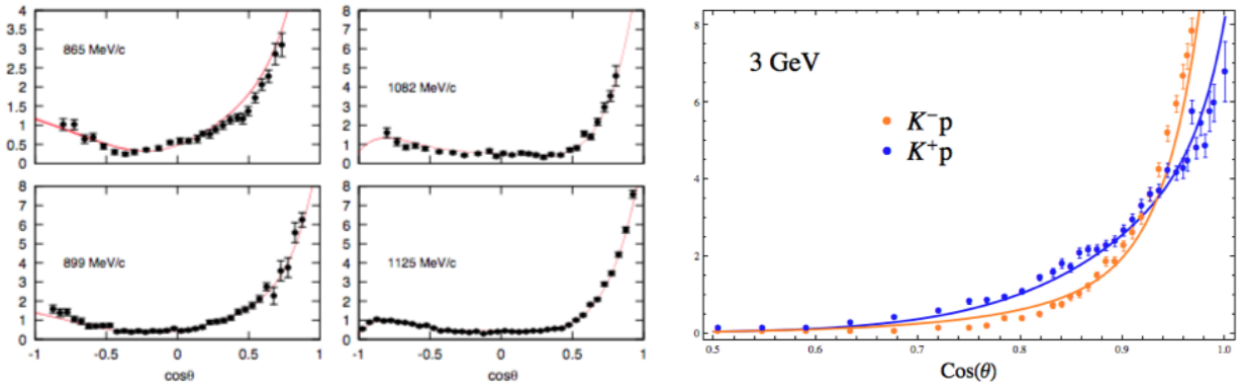


Figure 2:  $K^-p \rightarrow K^-p$  differential cross section from Ref. [1] (left) and from Ref. [4] (right).

The differential cross section peaks in the forward direction as the energy increases as can be seen on Fig. 2. This is characteristic of the Regge poles. Indeed at high energy, the reaction is driven by singularities in the complex angular momentum plane. Those Regge poles display an exponential suppression in the momentum transferred squared  $t = -2q^2(1 - \cos\theta)$ . The smooth continuation from the resonance region to the Regge region is suggested on Fig. 2.

We can formalize this phenomenon by a mathematical relation between the resonances and the Regge poles, the so-called finite energy sum rules. An example of these sum rules read (for the notation, their derivation and their applications to pion-nucleon scattering, see Ref. [5]):

$$\frac{1}{\Lambda} \int_0^\Lambda \text{Im } A(\nu, t) d\nu = \frac{\beta(t) \Lambda^{\alpha(t)}}{\alpha(t) + 1}. \quad (4)$$

The left-hand side consists in an integration over the resonance region. The right-hand side is determined by the residue  $\beta(t)$  and the trajectory  $\alpha(t)$  of the Regge pole(s) contributing to the scalar amplitudes  $A(\nu, t)$  ( $\nu = (s - u)/2$  being the crossing variable). In practice, that means that the high energy data can be used to constrain the parameters of the fit in the resonances region. Since the energy range for the kaon long beam in this proposal extend above the resonance region, one could fully exploit the data and the finite energy sum rules to better constrain the hyperon spectrum.

## 2. Acknowledgments

This material is based upon work supported in part by the U.S. Department of Energy, Office of Science, Office of Nuclear Physics under contract DE-AC05-06OR23177. This work was also supported in part by the U.S. Department of Energy under Grant No. DE-FG0287ER40365 and National Science Foundation under Grants PHY-1415459 and NSF-PHY-1205019.

## References

- [1] C. Fernández-Ramirez, I.V. Danilkin, D.M. Manley, V. Mathieu, and A.P. Szczepaniak, Phys. Rev. D **93**, 034029 (2016).
- [2] <http://www.indiana.edu/jpac/index.html>.
- [3] V. Mathieu, arXiv:1601.01751 [hep-ph].
- [4] V. Mathieu, unpublished.
- [5] V. Mathieu, I.V. Danilkin, C. Fernández-Ramirez, M.R. Pennington, D. Schott, A.P. Szczepaniak, and G. Fox, Phys. Rev. D **92**, 074004 (2015).

## 2.19 Establishing $S = -1$ Hyperon Resonances Using Kaon-Induced Meson Productions within Dynamical Coupled-Channels Approach

Hiroyuki Kamano

*Research Center for Nuclear Physics*

*Osaka University*

*Ibaraki, Osaka 567-0047, Japan*

### Abstract

We give an overview of our recent effort for the spectroscopy of strangeness  $S = -1$  hyperon resonances ( $Y^*$ ), which has been made through a comprehensive partial-wave analysis of the  $K^-p \rightarrow \bar{K}N, \pi\Sigma, \pi\Lambda, \eta\Lambda, K\Xi$  reactions within a dynamical coupled-channels (DCC) approach. It is found that the existing  $K^-p$  reaction data are not sufficient to unambiguously determine partial-wave amplitudes and properties (pole masses and residues, etc.) of  $Y^*$  resonances. We then discuss what new data are actually needed for further establishing  $Y^*$  resonances.

### 1. Introduction

So far, a number of  $\Lambda^*$  and  $\Sigma^*$  resonances with strangeness  $S = -1$  (collectively referred to as  $Y^*$ ) have been reported as listed by Particle Data Group (PDG) [1]. However, those are much less understood than the nonstrange  $N^*$  and  $\Delta^*$  resonances. For example, most of the  $\Sigma^*$  resonances are poorly established. In fact, just 6 out of 26 reported  $\Sigma^*$  resonances are rated as “four-star” by PDG, and unlike the  $N^*$  and  $\Delta^*$  resonances, even the existence of low-lying resonances is still uncertain. Furthermore, the spin and parity quantum numbers have not been determined for quite a few  $Y^*$  resonances [1].

Another issue that should be noted for  $Y^*$  resonances is that until very recently, only the so-called Breit-Wigner mass and width were listed by PDG with a few exception (see, *e.g.*, 2012 edition of PDG [2]). This is also in contrast to the  $N^*$  and  $\Delta^*$  cases, where resonances defined by poles of scattering amplitudes have also been extensively studied, and both of the pole and Breit-Wigner results have been listed by PDG for a long time. It is known (see, *e.g.*, Ref. [3]) that a resonance mass defined by the pole of scattering amplitudes is equivalent to an exact (complex-)energy eigenvalue of the *full* Hamiltonian of the underlying theory, namely the Quantum Chromodynamics (QCD) in this case, under the purely outgoing boundary condition. Thus extracting resonances defined by poles from reaction data is essential to testing QCD in the confinement domain, and such a test is now becoming reality with the help of the Lattice QCD simulations (see, *e.g.*, Refs. [4–7]).

In this situation, a first attempt of a comprehensive and systematic partial-wave analysis of  $K^-p$  reactions to extract  $Y^*$  resonances defined by poles was accomplished by the Kent State University (KSU) group in 2013 [8, 9], and then by our group using the dynamical coupled-channels (DCC) approach [10, 11]. (Recently, a reanalysis of the KSU single-energy solution [8] using an on-shell  $K$ -matrix approach has been done in Ref. [12].) Here it is emphasized again that it is only in recent years that this kind of comprehensive study to extract pole information from reaction data began for the  $Y^*$  resonances.

The basic formula of our DCC approach [10,13,14] is the coupled-channels integral equation for the partial-wave amplitudes:

$$T_{b,a}^{(J^P I)}(p_b, p_a; W) = V_{b,a}^{(J^P I)}(p_b, p_a; W) + \sum_c \int dp_c p_c^2 V_{b,c}^{(J^P I)}(p_b, p_c; W) G_c(p_c; W) T_{c,a}^{(J^P I)}(p_c, p_a; W). \quad (1)$$

Here, the subscripts  $(a, b, c)$  represent the meson-baryon channels we have considered, *i.e.*,  $\bar{K}N$ ,  $\pi\Sigma$ ,  $\pi\Lambda$ ,  $\eta\Lambda$ ,  $K\Xi$ ,  $\pi\Sigma^*$ , and  $\bar{K}^*N$ , where the last two are the quasi-two-body channels that subsequently decay into the three-body  $\pi\pi\Lambda$  and  $\pi\bar{K}N$  channels, respectively;  $V_{b,a}^{(J^P I)}(p_b, p_a; W)$  denotes the potential driving the transition from the channel  $a$  to the channel  $b$ ; and  $G_c(p_c; W)$  denotes the Green's function for the channel  $c$ . In our approach, the transition potential consists of hadron-exchange diagrams derived from effective Lagrangians. By solving Eq. (1), one can sum up all the possible transition processes between reaction channels considered, and this ensures the multichannel two-body as well as three-body unitarity for the resulting amplitudes. Furthermore, off-shell rescattering effects, which are usually neglected in on-shell approaches, are also taken into account properly through the momentum integral appearing in the right hand side of Eq. (1). Actually, these features make our model quite unique among existing models of meson production reactions.

In this contribution, we first give an overview of our recent efforts for the  $Y^*$  spectroscopy through the comprehensive partial-wave analysis of the  $K^-p$  reactions within our DCC approach in Sec. 2. Then, in Sec. 3, we discuss and give prospects for what new data for anti-Kaon induced reactions are needed for further establishing  $Y^*$  resonances.

## 2. Results of DCC Analysis for $K^-p$ Reactions

In Ref. [10], we have constructed models for the  $S = -1$  sector within the DCC approach by analyzing the data of  $K^-p \rightarrow \bar{K}N, \pi\Sigma, \pi\Lambda, \eta\Lambda$ , and  $K\Xi$  reactions up to  $W = 2.1$  GeV. The analysis takes into account all available data for both unpolarized and polarized observables as far as we found in the considered energy region, and it results in fitting to more than 17,000 data points. From this analysis, we have determined the partial-wave amplitudes for the  $K^-p \rightarrow \bar{K}N, \pi\Sigma, \pi\Lambda, \eta\Lambda$ , and  $K\Xi$  reactions not only for  $S$  wave but also higher partial waves including  $P$ ,  $D$ , and  $F$  waves. Furthermore, the threshold parameters such as scattering lengths and effective ranges have also been determined for the  $\bar{K}N$ ,  $\eta\Lambda$ , and  $K\Xi$  scatterings. We then extracted in Ref. [11] the parameters associated with  $Y^*$  resonances such as mass, width, and coupling constants defined by poles of scattering amplitudes within our constructed models.

In Fig. 1, we present several results of our fits to the data for  $K^-p \rightarrow K^-p$  (see Refs. [10,11] for the full details of our analysis). Here it is found that two curves (red solid and blue dashed curves) are plotted in each panel. As will be discussed later, this is because the available  $K^-p$  reaction data are not sufficient to constrain our reaction model unambiguously, but it allows us to have two distinct sets of our model parameters, yet both give almost the same  $\chi^2$  value. Thus these two curves may be viewed as a measure of ambiguity in our analysis originating from the insufficient amount and accuracy of the current existing data. Hereafter we call them Model A and Model B, respectively. Our two models reproduce not only the total cross sections but also the “angle-dependent quantities” such as the differential cross section

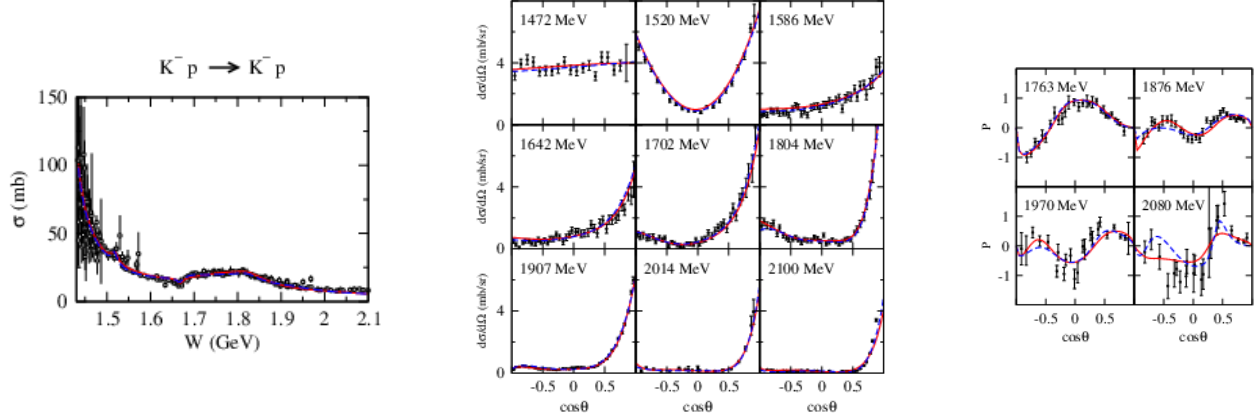


Figure 1: Several results of our fits to the data for  $K^- p \rightarrow K^- p$  scattering from Ref. [10]. Total cross section  $\sigma$  (the leftest panel), differential cross section  $d\sigma/d\Omega$  (middle panels), and recoil polarization  $P$  (right panels) are presented. Red solid and blue dashed curves represent the results of our two analyses, Model A and Model B, respectively. The references for the data can be found in Ref. [10].

$(d\sigma/d\Omega)$  and recoil polarization ( $P$ ) very well over the entire kinematical region where the data are available. We have confirmed that the other reaction data are also well reproduced.

Figure 2 shows a comparison of extracted  $Y^*$  mass spectra between our two models [10, 11] and the KSU analysis [8, 9]. The extracted masses show an excellent agreement for several resonances, but in overall, they are still fluctuating between our two models and the KSU analysis. Again, this is because the existing  $K^- p$  reaction data are not sufficient to determine the  $Y^*$  mass spectrum, and without new data this level of analysis dependence will not be avoidable. Although the extracted spectrum is still analysis dependent, we found a couple of new  $Y^*$  resonances that are quite interesting. One is a new  $J^P = 3/2^-$   $\Lambda$  resonance located near the  $\eta\Lambda$  threshold found in Model B. The width of this new resonance is  $\sim 10$  MeV, which is much narrower than usually expected for light-quark baryon resonances. As shown in Ref. [10], the contribution of this new resonance is hardly seen in most of the reaction observables considered in our analysis, but it is turned out that the new resonance is responsible for reproducing the concave-up behavior of differential cross section for  $K^- p \rightarrow \eta\Lambda$  near the threshold. Thus the angular dependence of the  $K^- p \rightarrow \eta\Lambda$  differential cross section data seems to favor the existence of this narrow resonance. Another interesting finding is that Model B further presents a new  $J^P = 1/2^-$   $\Lambda$  resonance with the mass close to  $\Lambda(1520)3/2^-$ . It is often discussed in quark models that the  $\Lambda(1405)1/2^-$  is the spin partner of  $\Lambda(1520)3/2^-$ . However, from this result, this new  $S$ -wave resonance might be the true spin partner. It would also be worthwhile to mention that a number of low-lying  $\Sigma^*$  resonances located just above the  $\bar{K}N$  threshold are found, and those may correspond to the one-star and two-star resonances assigned by PDG. For further confirmation of these interesting  $Y^*$  resonances, however, more extensive and accurate data of anti-Kaon induced reactions are definitely needed.

Figure 3 shows the branching ratios for the  $Y^*$  resonances extracted from our two models,

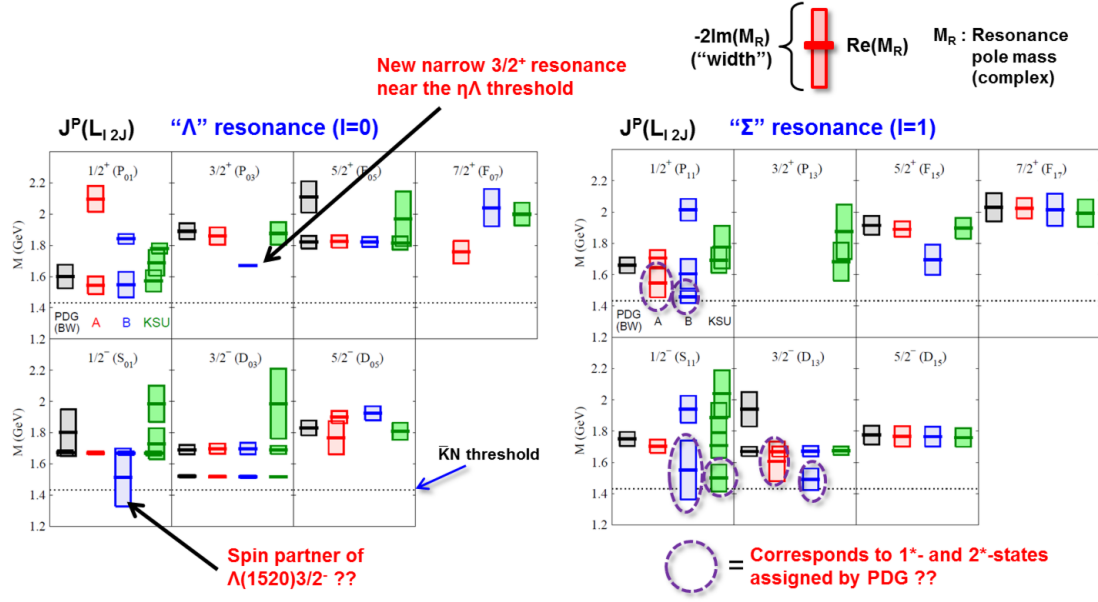


Figure 2: Comparison of mass spectra for  $Y^*$  resonances defined by poles of scattering amplitudes [11]. Spectra in red and blue are the results from Model A and Model B [11], respectively, while the spectrum in green is obtained by the KSU analysis [9]. As a reference, the Breit-Wigner masses and widths for the four- and three-star resonances assigned by PDG [1] are also presented in black.

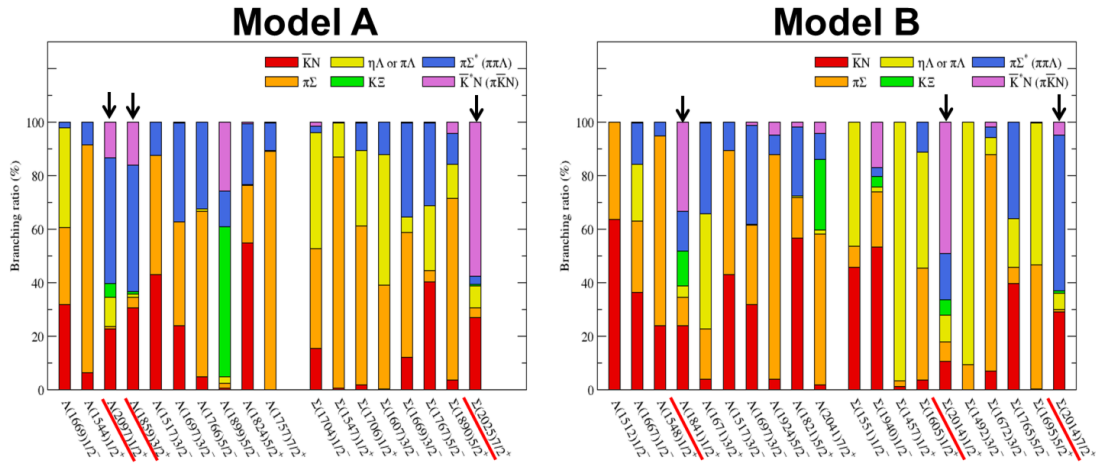


Figure 3: Branching ratios for  $Y^*$  resonances extracted from Model A and Model B [11].

Models A and B. It is found that most resonances have large branching ratios for the  $\bar{K}N$  and  $\pi\Sigma$  channels, and also for the  $\pi\Lambda$  channel for the  $\Sigma^*$  resonances. However, as indicated by

black arrows in Fig. 3, high-mass resonances also have large branching ratios for the quasi-two-body  $\pi\Sigma^*$  and  $\bar{K}^*N$  channels, which subsequently decay into the three-body  $\pi\pi\Lambda$  and  $\pi\bar{K}N$  channels. This suggests that the three-body production reactions would also play an important role for establishing high-mass  $Y^*$  resonances. This situation is quite similar to the  $N^*$  and  $\Delta^*$  resonances, where the high-mass resonances decay dominantly to the three-body  $\pi\pi N$  channel (see, *e.g.*, Fig. 6 of Ref. [15]), and the  $\pi\pi N$  production data are expected to be the key to establishing high-mass  $N^*$  and  $\Delta^*$  resonances (see, *e.g.*, Refs. [16, 17]). In fact, this is the motivation for the planned measurement of  $\pi N \rightarrow \pi\pi N$  reactions at the J-PARC E45 experiment [15]. It is also worthwhile to mention the  $J^P = 7/2^+$   $\Sigma$  resonance. This resonance is assigned as a four-star resonance by PDG [1] [ $\Sigma(2030)7/2^+$  in the PDG notation], and our two models actually give almost the same mass value, *i.e.*,  $\text{Re}(M_R) = 2025$  MeV for Model A and  $\text{Re}(M_R) = 2014$  MeV for Model B. However, one can see that the component of the branching ratios for the quasi-two-body channels is rather different between the two models: In Model A, it is dominated by  $\bar{K}^*N$  ( $\pi\bar{K}N$ ) channel, while in Model B it is dominated by  $\pi\Sigma^*$  ( $\pi\pi\Lambda$ ) channel. This indicates that our knowledge on the three-body channels is still poor even for the four-star resonance.

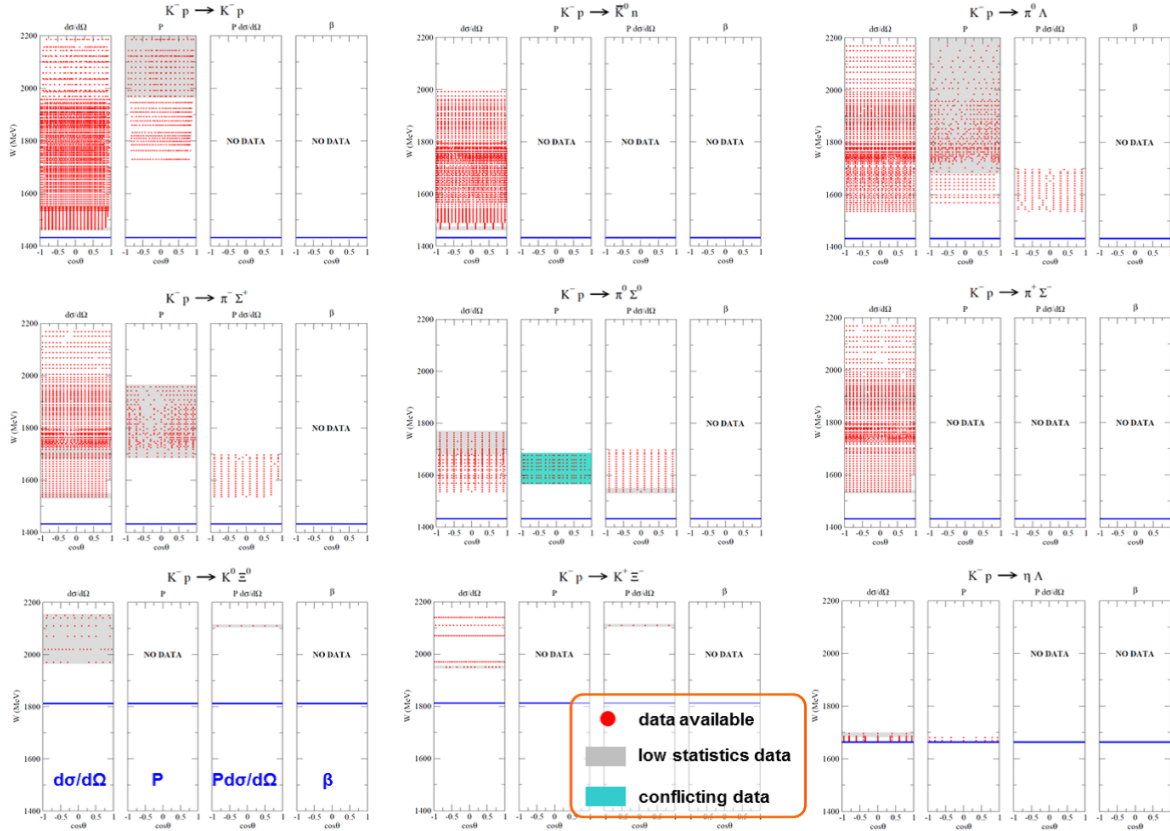


Figure 4: Kinematical coverage of  $K^- p$  reaction data included in our analysis. The horizontal axis is cosine of the scattering angle in the center-of-mass frame and the vertical axis is the total scattering energy. The blue line in each panel represents the threshold of the corresponding reaction.

Now we make some comments on the kinematical coverage of the data for  $K^-p \rightarrow \bar{K}N, \pi\Sigma, \pi\Lambda, \eta\Lambda$ , and  $K\Xi$  included in our analysis. It is summarized in Fig. 4. It is well known that for  $(0^-) + (1/2^+) \rightarrow (0^-) + (1/2^+)$  reactions the differential cross section ( $d\sigma/d\Omega$ ), recoil polarization ( $P$ ), and spin-rotation angle ( $\beta$ ) form a “complete set” of observables [18, 19]. Therefore, one needs to have high statistics data for all the three observables in order to determine the scattering amplitudes accurately and accomplish a reliable extraction of resonance parameters. However, from Fig. 4 one can see that the existing data are *far from complete*. The kinematical coverage of  $d\sigma/d\Omega$ ,  $P$ , and their products  $P \times d\sigma/d\Omega$  are still small for most reactions, and no data of  $\beta$  are available for all reactions. Furthermore, even though the data exist, some data sets have large statistical errors and are even conflicting with each other (see Ref. [10] for the details). Because of this, there still exist ambiguities in our constructed models, even though they reproduce the existing data very well. Actually, this can be seen, *e.g.*, from the spin-rotation angles predicted from our two models and the KSU analysis, which can be found in Fig. 28 of Ref. [10]. Although the three analyses reproduce the existing data equally well, significant difference appears in the predicted value of the spin-rotation angles, particularly at higher  $W$ . It is therefore highly desirable that the complete experiments of  $\bar{K}N$  reactions will be performed at J-PARC using charged Kaon beam as well as at JLab using neutral Kaon beam.

### 3. Discussions and Prospects for $Y^*$ Spectroscopy using anti-Kaon Induced Reactions

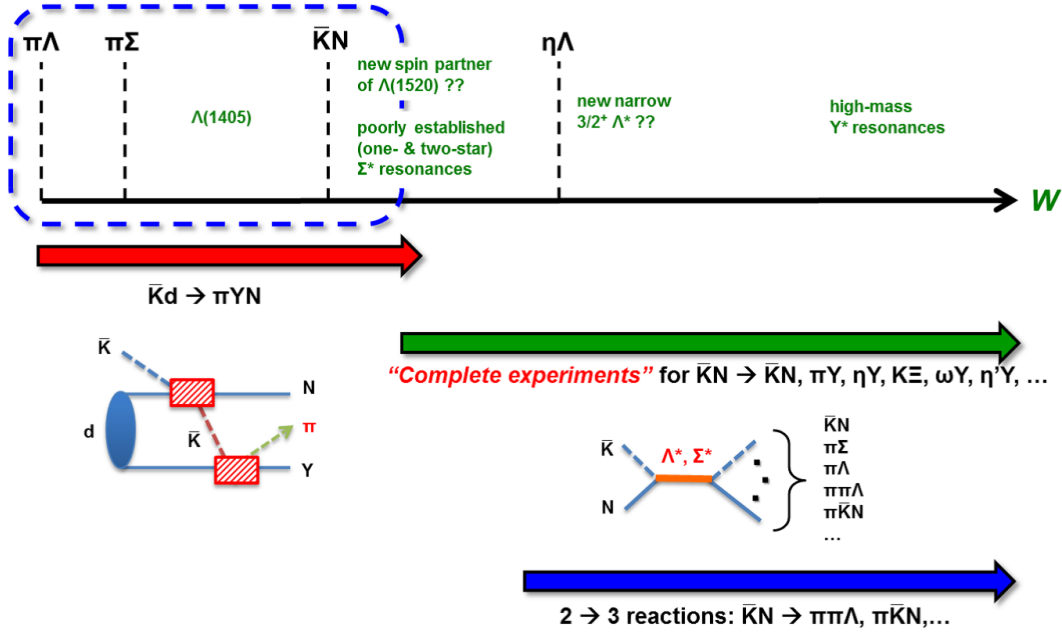


Figure 5: Strategy and necessary data for establishing  $Y^*$  resonances using anti-Kaon induced reactions.

As we have seen in the previous Section, the existing  $\bar{K}N$  reaction data are not sufficient to eliminate analysis dependence in the extracted  $Y^*$  resonance parameters, and, as depicted in Fig. 5, more extensive and accurate data for both two-body and three-body productions are necessary for further establishing  $Y^*$  resonances. In particular, the complete experiments



measuring all polarization observables will be the key to resolving this issue. In this regard, some discussions are ongoing with experimentalists to examine possible new experiments measuring  $\bar{K}N$  reactions at J-PARC [20]. Experiments using neutral Kaon beam at JLab is also highly desirable. Actually,  $K_L^0 p$  reaction has a great advantage since it exclusively produces  $\Sigma^*$  resonances in the direct  $s$ -channel processes due to the isospin selection, and thus the combined analysis of both charged- and neutral-Kaon induced reactions off the nucleon would be the best way for completing the  $Y^*$  spectroscopy.

On the other hand, the  $\bar{K}N$  reactions are not so suitable for studying the low energy region, indicated by the blue dashed circle in Fig. 5. There are two reasons for this: (i) the  $\bar{K}N$  reactions cannot directly access the region below the  $\bar{K}N$  threshold, and (ii) experimentally it is not easy to measure the  $\bar{K}N$  reactions in the region just above the  $\bar{K}N$  threshold because of difficulty in producing low momentum Kaon beam. However, studying this energy region is very important because a number of interesting  $Y^*$  resonances exist or are suggested to exist, such as  $\Lambda(1405)$ , poorly established low-lying  $\Sigma^*$  resonances, and a possible new  $S$ -wave  $\Lambda$  resonance that might be a “true” spin partner of  $\Lambda(1520)3/2^+$  as mentioned in Sec. 2. Therefore, we have recently started an application of our DCC approach to the deuteron-target reaction,  $\bar{K}d \rightarrow \pi Y N$ , which is being measured at the J-PARC  $E31$  experiment [21]. This is because for this reaction the  $\pi Y$  system in the final state can access the low energy region indicated by the blue dashed circle in Fig. 5, even if the momentum of the incoming Kaon is rather high. With this application, we aim at a combined analysis of both  $\bar{K}N$  and  $\bar{K}d$  reactions so that we can cover the whole energy region relevant to the  $Y^*$  spectroscopy. The construction of the model for the deuteron-target reactions is underway, and it will be presented elsewhere.

#### 4. Acknowledgments

The author thanks T.-S. H. Lee, S.X. Nakamura, and T. Sato for their collaboration. This work was supported by the Japan Society for the Promotion of Science (JSPS) KAKENHI Grant No. 25800149 and by the HPCI Strategic Program (Field 5 *The Origin of Matter and the Universe*) of Ministry of Education, Culture, Sports, Science and Technology (MEXT) of Japan.

## References

- [1] K. Olive *et al.* (Particle Data Group), Chin. Phys. C **38**, 090001 (2014).
- [2] J. Beringer *et al.* (Particle Data Group), Phys. Rev. D **86**, 010001 (2012).
- [3] *Proceedings of the workshop on Resonances - Models and Phenomena*, edited by S. Albeverio, L.S. Ferreira, and L. Streit, published in Lecture Notes in Physics, **211** (1984).
- [4] J.J. Dudek, *et al.* (Hadron Spectrum Collaboration), Phys. Rev. Lett. **113**, 182001 (2014).
- [5] J.-J. Wu, T.-S.H. Lee, A.W. Thomas, and R.D. Young, Phys. Rev. C **90**, 055206 (2014).
- [6] R. Molina and M. Döring, arXiv:1512.05831 .

- [7] T.-S.H. Lee, J.-J. Wu, and H. Kamano, arXiv:1602.01169 .
- [8] H. Zhang, J. Tulpan, M. Shrestha, and D. M. Manley, Phys. Rev. C **88**, 035204 (2013).
- [9] H. Zhang, J. Tulpan, M. Shrestha, and D.M. Manley, Phys. Rev. C **88**, 035205 (2013).
- [10] H. Kamano, S.X. Nakamura, T.-S.H. Lee, and T. Sato, Phys. Rev. C **90**, 065204 (2014).
- [11] H. Kamano, S.X. Nakamura, T.-S.H. Lee, and T. Sato, Phys. Rev. C **92**, 025205 (2015).
- [12] C. Fernández-Ramírez, I.V. Danilkin, D.M. Manley, V. Mathieu, and A.P. Szczepaniak, arXiv:1510.07065 .
- [13] A. Matsuyama, T. Sato, and T.-S.H. Lee, Phys. Rep. **439**, 193 (2007).
- [14] H. Kamano, S.X. Nakamura, T.-S.H. Lee, and T. Sato, Phys. Rev. C **88**, 035209 (2013).
- [15] K. Hicks and H. Sako *et al.* (J-PARC E45 Experiment), *3-Body Hadronic Reactions for New Aspects of Baryon Spectroscopy*, [http://j-parc.jp/researcher/Hadron/en/pac\\_1207/pdf/P45\\_2012-3.pdf](http://j-parc.jp/researcher/Hadron/en/pac_1207/pdf/P45_2012-3.pdf) .
- [16] H. Kamano, Phys. Rev. C **88**, 045203 (2013).
- [17] H. Kamano, B. Juliá-Díaz, T.-S.H. Lee, A. Matsuyama, and T. Sato, Phys. Rev. C **79**, 025206 (2009).
- [18] R.L. Kelly, J.C. Sandusky, and R.E. Cutkosky, Phys. Rev. C **10**, 2309 (1974).
- [19] D.H. Saxon and J.B. Whittaker, Z. Phys. C **9**, 35 (1981).
- [20] H. Sako (private communication).
- [21] H. Noumi *et al.* (J-PARC E31 Experiment), *Spectroscopic study of hyperon resonances below  $\bar{K}N$  threshold via the  $(K^-, n)$  reaction on deuteron*, [http://j-parc.jp/researcher/Hadron/en/pac\\_1207/pdf/E31\\_2012-9.pdf](http://j-parc.jp/researcher/Hadron/en/pac_1207/pdf/E31_2012-9.pdf) .

## 2.20 Strangeness Physics at CLAS in the 6 GeV Era

Reinhard Schumacher

*Department of Physics*

*Carnegie Mellon University*

*Pittsburgh, PA 15213, U.S.A.*

### Abstract

A very brief overview is presented of varied strangeness-physics studies that have been conducted with the CLAS system in the era of 6 GeV beam at Jefferson Lab. A full bibliography of articles related to open strangeness production is given, together with some physics context for each work. One natural place where these studies could be continued, using a  $K_L$  beam and the GlueX detector, is in the further investigation of the  $\Lambda(1405)$  baryon. The line shapes and cross sections of this state were found, using photoproduction at CLAS, to differ markedly in the three possible  $\Sigma\pi$  final states. The analogous strong-interaction reactions using a  $K_L$  beam could further bring this phenomenon into focus.

1. The CLAS program ran from 1998 to 2012, during the time when the maximum Jefferson Lab beam energy was 6 GeV. An important thrust of this program was to investigate the spectrum of  $N^*$  and  $\Delta^*$  (non-strange) baryon resonances using photo- and electro-production reactions. To this end, final states containing strange particles ( $K$  mesons and low-mass hyperons) played a significant role. The reason for this is partly due to favorable kinematics. When the total invariant energy  $W(= \sqrt{s})$  of a baryonic system exceeds 1.6 GeV it becomes possible to create the lightest strangeness-containing final state,  $K^+\Lambda$ . This is a two-body final state that is straightforward to reconstruct in the CLAS detector system [1], and theoretically it is easier to deal with two-body reaction amplitudes than with three- and higher-body reaction amplitudes. In the mass range  $W > 1.6$  GeV the decay modes of excited nucleons tend to not to favor two-body  $\pi$ -nucleon final states but rather multi-pion states. As input to partial-wave decompositions and resonance-extraction models, therefore, the strangeness-containing final states of high-mass nucleon excitations have had importance. Excited baryons decay through all possible channels simultaneously, constrained by unitarity of course, and channel-coupling is crucial to determining the spectrum of excitations. Within this mix of amplitudes, however, the  $KY$  decay modes have proven useful. The end result has been, as summarized in the recent edition of the Review of Particle Properties [2], clearer definition of the spectrum of baryonic excitations, with definite contributions from the strangeness sector channels.

To this end, strangeness photoproduction cross sections measurements at CLAS for the  $K^+\Lambda$ ,  $K^+\Sigma^0$  and  $K^0\Sigma^+$  channels on a proton target were published [3–6]. Cross sections are not enough, in general, to define the reaction mechanism, including the underlying  $N^*$  excitation spectrum. Photoproduction of pseudo-scalar mesons is described by four complex amplitudes, leading to fifteen spin observables in addition to the cross section. Full knowledge of these spin observables would exhaust the information that can be gleaned experimentally about any given reaction channel. Here the hyperonic channels offer another advantage when compared with the non-strange reaction channels: the polarization of most hyperons can be measured directly through their parity-violating weak decay asymmetries. Unlike

the polarization of nucleons, that require recoil polarimeter instrumentation and secondary scattering to measure, the hyperons reveal their polarization states directly in the angular distribution of their decay products. CLAS published photoproduction measurements for a number of the observables that involve the recoiling hyperons and/or circularly polarized photons, specifically  $P$ ,  $C_x$  and  $C_z$  [3, 5, 7–9]. Additional work was done on observables involving linearly polarized photons [10] and/or a polarized hydrogen target in the FROST program, both in combination with hyperon polarization. This included the observables  $\Sigma$ ,  $T$ ,  $E$ ,  $O_x$  and  $O_z$ . Other spin observables are still under analysis. In principle, a complete set of observables can be measured for the  $KY$  photoproduction reactions, meaning that at any given energy and production angle all 16 observables can be separated using a finite number of measurements. The CLAS program has, in principle, enough data in hand to make this a reality for the  $K^+\Lambda$  and  $K^+\Sigma^0$  reactions on the proton, but it has not been achieved so far, mainly on account of limits in statistical precision. Exploratory cross section measurements on a neutron (deuteron) target have also been published [11]. On the model-building side, all these observables have been analyzed, for example, in the framework of K-matrix coupled channels PWA calculations by the Bonn-Gatchina group and collaborators [12–18], and also the Argonne-Osaka Collaboration [19].

Photoproduction measurements probe nucleon excitations with zero net 4-momentum transfer to the target ( $Q^2 = 0$ ). Electroproduction measurements add the degree of freedom of  $Q^2 > 0$ , which brings in the “longitudinal” virtual photon degree of freedom and the associated interference amplitudes between the photon polarization components. CLAS results on electroproduction of  $K^+\Lambda$  and  $K^+\Sigma^0$  final states off the proton have been published for values of  $0.3 < Q^2 < 2.6 \text{ GeV}^2$  [20–26]. The results include separation of the cross sections into 5 structure functions, as well as measurement of the hyperon recoil polarization and the beam-hyperon polarization transfer observables. Model-building approaches have generally followed in the path of photoproduction work, with the addition of hadronic form factors to address the  $Q^2$  dependence of resonance contributions.

One can inquire into hadronization properties of quarks propagating in the nuclear medium as a function of variable such as the hadronic fraction  $z$  of the detected final-state meson and the hadron transverse momentum. CLAS investigated this nuclear dependence for neutral Kaons, comparing multiplicities of Kaons in heavy nuclei to those in deuterium [27]. This was the only study done at CLAS in the area of nuclear effects with strange particles.

Cross sections for pseudo-scalar meson photoproduction are predicted to scale as  $s^7$  at high energies and large  $t$  in perturbative QCD [28] and also some other reaction models. This phenomenon was confirmed decades ago for pion photoproduction. Analysis of CLAS data confirmed this behavior for the first time in  $K^+\Lambda$  photoproduction as well [29]. The same study also illustrated the transition in  $W$  from the resonance region, where high-mass resonances near 1920 and 2100 MeV contribute to the mechanism, to the scaling behavior that dominates at higher  $W$ .

At the partonic level, in many high-energy reactions, phenomenology shows that the creation of  $s\bar{s}$  quark pairs is suppressed by a factor of roughly 5 compared to creation of  $u\bar{u}$  and  $d\bar{d}$  pairs. The mass difference between the quarks is presumably at the root of this effect. It was shown with CLAS that this suppression extends to electroproduction reactions

at the comparatively low energies leading to exclusive  $KY$  final states when compared to exclusive  $\pi N$  final states [30]. Also, new limits on baryon non-conservation in the decay of the  $\Lambda$  hyperon [31] have been published. Furthermore, the structure of excited baryons can be related to their radiative decay branching fractions. CLAS published radiative decay fractions for the  $\Sigma^0(1385)$ , the  $\Sigma^+(1385)$ , and the  $\Lambda(1520)$  [32–34].

The possibility of an exotic pentaquark state known as the  $\Theta^+(1520)$  caused world-wide excitement in the hadronic physics community over a decade ago. Initially, a hint of such a state was seen and reported by CLAS based on some already-existing data [35, 36], but subsequent dedicated searches with higher statistics and better background control found no support for this or similar states [37–41].

Differential photoproduction cross sections for the excited hyperons were measured simultaneously for the  $\Sigma(1385)$ , the  $\Lambda(1405)$  and the  $\Lambda(1520)$  [42], and for the  $\Lambda(1520)$  in electroproduction [43]. All three hyperons showed  $t$ -channel-like behavior at high  $W$ , with some evidence for high-mass  $N^*$  contributions near their respective thresholds. However, the  $\Lambda(1405)$  showed an unexpected and unexplained charge dependence among the three available decay modes,  $\Sigma^+\pi^-$ ,  $\Sigma^-\pi^+$  and  $\Sigma^0\pi^0$ , near the reaction threshold. The effect was not seen in the case of the  $\Lambda(1520)$ , indicated that something is special about the  $\Lambda(1405)$ .

The structure of the  $\Lambda(1405)$  was investigated in the reaction  $\gamma + p \rightarrow K^+ + \Sigma + \pi$  to determine the invariant mass distributions or “line shapes” of the  $\Sigma^+\pi^-$ ,  $\Sigma^-\pi^+$  and  $\Sigma^0\pi^0$  final states, from threshold at 1328 MeV/ $c^2$  through the mass range of the  $\Lambda(1405)$  and the  $\Lambda(1520)$ , for center-of-mass energies  $1.95 < W < 2.85$  GeV [44, 45]. The three mass distributions differ strongly in the vicinity of the  $I = 0$   $\Lambda(1405)$ , indicating the presence of substantial  $I = 1$  strength in the reaction. Background contributions to the data from the  $\Sigma^0(1385)$  and from  $K^*\Sigma$  production were studied and shown to have negligible influence. The nature of this  $I = 1$  component has not been understood fully, but initial model calculations based on the chiral unitary ansatz have been made [46–49]. The  $I = 0$  nature of the  $\Lambda(1405)$  is consistent with chiral unitary model approaches that indicate a composite structure of two pole. One couples strongest to the  $\bar{K}N$  channel (subthreshold) and the other couples strongest to the  $\Sigma\pi$  channel (the open decay channels) [50–54]. It was furthermore experimentally determined at CLAS for the first time that the spin and parity of the  $\Lambda(1405)$  is  $J^P = (1/2)^-$  [55], as had long been assumed. A first-time measurement of electroproduction of the  $\Lambda(1405)$  was published [56] that suggested again that the line shape of this hyperon is indicative of structure more complex than a single Breit-Wigner-type resonance.

The next category of hyperons investigated at CLAS were the  $S = -2$  cascade resonances. Photoproduction of the  $\Xi^-(1321)$  and its first excitation, the  $\Xi^-(1530)$ , were measured [57, 58]. However, none of the expected higher-mass cascades that are expected in the quark model were revealed in the available energy range, despite considerable effort.

All the reaction channels itemized above involved hyperon production in association with the ground-state pseudo-scalar Kaons. But there has also been some investigation of vector strange meson photoproduction leading to the final states  $K^{*+}\Lambda$  and  $K^{*+}\Sigma^0$  [59] and also  $K^0\Sigma^*$  [60].

Looking ahead, the CLAS12 program [61] is scheduled to begin data taking in about 2017, and there are hyperon spectroscopy measurements planned for that new era of research. A

continued search for excited cascade hyperons is one example, and there are even plans to detect photoproduction of the triply-strange  $\Omega^-$  baryon.

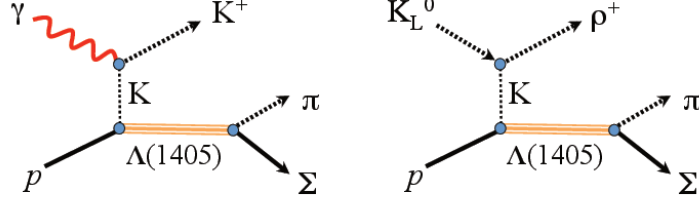


Figure 1: Creation and decay of the  $\Lambda(1405)$  baryon via photoproduction (left) and via hadronic production using a  $K_L$  beam (right). In either case the exchange of an off-shell Kaon allows production of the  $\Lambda(1405)$ , which lies below the  $\bar{K}N$  threshold.

Turning to the prospects of using a  $K_L$  beam in conjunction with the GlueX detector, one can ask whether the CLAS program, as it has been very briefly outlined here, serves as an impetus for new research. One idea to consider is to extend the cited studies of the still-mysterious  $\Lambda(1405)$  hyperon. Does its line shape depend on the manner in which it is produced, as currently thought, in light of the chiral unitary model approaches? Can its line shape be precisely measured using a  $K_L$  beam and the excellent resolution and particle identification capabilities of GlueX [62]? Figure 1 shows a comparison of sample diagrams for production of this hyperon via photon and Kaon beams. What they have in common is that the exchanged Kaon is off shell, allowing entry into the sub-threshold  $\bar{K}N$  regime where this hyperon exists. The method proved fruitful in the photoproduction case, and so by analogy one may expect to create the state in the  $K_L$  beam case as well. A very preliminary check of existing data, which is exceedingly sparse, suggests that the cross section is in the range of 250 micro-barns, which in turn could lead to a reaction rate of, very roughly, one event per few seconds. One favorable aspect of such a measurement program would be that no Kaons need to be detected in the final state with GlueX, while photon detection capability would be very important indeed. No acceptance calculations for an actual experiment have been carried out yet for this discussion.

In conclusion, the CLAS program of hyperon physics has produced a sizable harvest of hyperon and strangeness-related results. These have helped define the spectrum of non-strange excited states, reveal the reaction mechanisms for the photo- and electro- production of several ground state and excited state hyperons, test some quark model and QCD-related phenomenology, and shed further light onto the nature of the  $\Lambda(1405)$  state. The further study of the latter state may be one place where future work using a  $K_L$  beam in conjunction with GlueX would be of interest.

## 2. Acknowledgments

This work was supported by DOE grant DE-FG02-87ER40315.

## References

- [1] B.A. Mecking *et al.* (CLAS Collaboration), Nucl. Instrum. Meth. A **503**, 513 (2003).
- [2] K.A. Olive *et al.* (Particle Data Group), Chin. Phys. C **38**, 090001 (2014).
- [3] J.W.C. McNabb *et al.* (CLAS Collaboration), Phys. Rev. C **69**, 042201 (2004).
- [4] R. Bradford *et al.* (CLAS Collaboration), Phys. Rev. C **73**, 035202 (2006).
- [5] M.E. McCracken *et al.* (CLAS Collaboration), Phys. Rev. C **81**, 025201 (2010).
- [6] F.J. Klein (for CLAS Collaboration), *Proceedings on 8th International Conference on Hypernuclear and strange particle physics* (HYP 2003), Nucl. Phys. A **754**, 321 (2005).
- [7] R.K. Bradford *et al.* (CLAS Collaboration), Phys. Rev. C **75**, 035205 (2007).
- [8] B. Dey *et al.* (CLAS Collaboration), Phys. Rev. C **82**, 025202 (2010).
- [9] C.S. Nepali *et al.* (CLAS Collaboration), Phys. Rev. C **87**, 045206 (2013).
- [10] C. Paterson *et al.* (CLAS Collaboration), to be submitted, 2016.
- [11] S. Anefalos Pereira *et al.* (CLAS Collaboration), Phys. Lett. B **688**, 289 (2010).
- [12] A.V. Sarantsev, V.A. Nikonov, A.V. Anisovich, E. Klempt, and U. Thoma, Eur. Phys. J. A **25**, 441 (2005).
- [13] A.V. Anisovich, V. Kleber, E. Klempt, V.A. Nikonov, A.V. Sarantsev, and U. Thoma, Eur. Phys. J. A **34**, 243 (2007).
- [14] V.A. Nikonov, A.V. Anisovich, E. Klempt, A.V. Sarantsev, and U. Thoma, Phys. Lett. B **662**, 245 (2008).
- [15] A.V. Anisovich, E. Klempt, V.A. Nikonov, A.V. Sarantsev, and U. Thoma, Eur. Phys. J. A **47**, 153 (2011).
- [16] A.V. Anisovich, R. Beck, E. Klempt, V.A. Nikonov, A.V. Sarantsev, and U. Thoma, Eur. Phys. J. A **48**, 15 (2012).
- [17] A.V. Anisovich, R. Beck, E. Klempt, V.A. Nikonov, A.V. Sarantsev, and U. Thoma, Eur. Phys. J. A **48**, 88 (2012).
- [18] A.V. Anisovich, R. Beck, V. Burkert, E. Klempt, M.E. McCracken, V.A. Nikonov, A.V. Sarantsev, R.A. Schumacher, and U. Thoma, Eur. Phys. J. A **50**, 129 (2014).
- [19] H. Kamano, S.X. Nakamura, T.S.H. Lee, and T. Sato, Phys. Rev. C **88**, 035209 (2013).
- [20] D.S. Carman *et al.* (CLAS Collaboration), Phys. Rev. Lett. **90**, 131804 (2003).
- [21] B.A. Raue and D.S. Carman, Phys. Rev. C **71**, 065209 (2005).

- [22] P. Ambrozewicz *et al.* (CLAS Collaboration), Phys. Rev. C **75**, 045203 (2007).
- [23] D.S. Carman, K. Park, B.A. Raue, and V. Crede *et al.* (CLAS Collaboration), Phys. Rev. C **87**, 025204 (2013).
- [24] R. Nasseripour *et al.* (CLAS Collaboration), Phys. Rev. C **77**, 065208 (2008).
- [25] D.S. Carman *et al.* (CLAS Collaboration), Phys. Rev. C **79**, 065205 (2009).
- [26] M. Gabrielyan *et al.* (CLAS Collaboration), Phys. Rev. C **90**, 035202 (2014).
- [27] A. Daniel *et al.* (CLAS Collaboration), Phys. Lett. B **706**, 26 (2011).
- [28] S.J. Brodsky and G.R. Farrar, Phys. Rev. Lett. **31**, 1153 (1973).
- [29] R.A. Schumacher and M.M. Sargsian, Phys. Rev. C **83**, 025207 (2011).
- [30] M. Mestayer *et al.* (CLAS Collaboration), Phys. Rev. Lett. **113**, 152004 (2014).
- [31] M.E. McCracken *et al.* (CLAS Collaboration), Phys. Rev. D **92**, 072002 (2015).
- [32] S. Taylor *et al.* (CLAS Collaboration), Phys. Rev. C **71**, 054609 (2005), [Erratum: Phys. Rev. C **72**, 039902 (2005)].
- [33] D. Keller *et al.* (CLAS Collaboration), Phys. Rev. D **83**, 072004 (2011).
- [34] D. Keller *et al.* (CLAS Collaboration), Phys. Rev. D **85**, 052004 (2012).
- [35] S. Stepanyan *et al.* (CLAS Collaboration), Phys. Rev. Lett. **91**, 252001 (2003).
- [36] V. Kubarovsky *et al.* (CLAS Collaboration), Phys. Rev. Lett. **92**, 032001 (2004).
- [37] B. McKinnon *et al.* (CLAS Collaboration), Phys. Rev. Lett. **96**, 212001 (2006).
- [38] M. Battaglieri *et al.* (CLAS Collaboration), Phys. Rev. Lett. **96**, 042001 (2006).
- [39] R. De Vita *et al.* (CLAS Collaboration), Phys. Rev. D **74**, 032001 (2006).
- [40] V. Kubarovsky *et al.* (CLAS Collaboration), Phys. Rev. Lett. **97**, 102001 (2006).
- [41] S. Niccolai *et al.* (CLAS Collaboration), Phys. Rev. Lett. **97**, 032001 (2006).
- [42] K. Moriya *et al.* (CLAS Collaboration), Phys. Rev. C **88**, 045201 (2013), [Addendum: Phys. Rev. C **88**, 049902 (2013)].
- [43] S.P. Barrow *et al.* (CLAS Collaboration), Phys. Rev. C **64**, 044601 (2001).
- [44] K. Moriya *et al.* (CLAS Collaboration), Phys. Rev. C **87**, 035206 (2013).
- [45] R.A. Schumacher and Kei Moriya, *Proceedings, 11th International Conference on Hypernuclear and Strange Particle Physics* (HYP 2012), Nucl. Phys. A **914**, 51 (2013).
- [46] J.C. Nacher, E. Oset, H. Toki, and A. Ramos, Phys. Lett. B **455**, 55 (1999).



- [47] L. Roca and E. Oset, Phys. Rev. C **87**, 055201 (2013).
- [48] L. Roca and E. Oset, Phys. Rev. C **88**, 055206 (2013).
- [49] Bing-Song Zou, Nucl. Phys. A **835**, 199 (2010).
- [50] J.A. Oller and U.G. Meissner, Phys. Lett. B **500**, 263 (2001).
- [51] D. Jido, J.A. Oller, E. Oset, A. Ramos, and U.G. Meissner, Nucl. Phys. A **725**, 181 (2003).
- [52] V.K. Magas, E. Oset, and A. Ramos, Phys. Rev. Lett. **95**, 052301 (2005).
- [53] B. Borasoy, R. Nissler, and W. Weise, Eur. Phys. J. A **25**, 79 (2005).
- [54] T. Hyodo and D. Jido, Prog. Part. Nucl. Phys. **67**, 55 (2012).
- [55] K. Moriya *et al.* (CLAS Collaboration), Phys. Rev. Lett. **112**, 082004 (2014).
- [56] H.Y. Lu and R.A. Schumacher *et al.* (CLAS Collaboration), Phys. Rev. C **88**, 045202 (2013).
- [57] J.W. Price *et al.* (CLAS Collaboration), Phys. Rev. C **71**, 058201 (2005).
- [58] L. Guo *et al.* (CLAS Collaboration), Phys. Rev. C **76**, 025208 (2007).
- [59] W. Tang *et al.* (CLAS Collaboration), Phys. Rev. C **87**, 065204 (2013).
- [60] I. Hleiqawi *et al.* (CLAS Collaboration), Phys. Rev. C **75**, 042201 (2007), [Erratum: Phys. Rev. C **76**, 039905(2007)].
- [61] S. Stepanyan, *Proceedings, 13th International Conference on Hadron spectroscopy* (Hadron 2009), AIP Conf. Proc. **1257**, 121 (2010).
- [62] H. Al Ghouli *et al.* (GlueX Collaboration), *16th International Conference on Hadron Spectroscopy* (Hadron 2015), Newport News, Virginia, USA, September, 2015 (2015); arXiv:1512.03699 [nucl-ex].

## 2.21 Lattice Studies of Hyperon Spectroscopy

David Richards

Thomas Jefferson National Accelerator Facility  
Newport News, VA 23606, U.S.A.

### Abstract

I describe recent progress at studying the spectrum of hadrons containing the strange quark through lattice QCD calculations. I emphasise in particular the richness of the spectrum revealed by lattice studies, with a spectrum of states at least as rich as that of the quark model. I conclude by prospects for future calculations, including in particular the determination of the decay amplitudes for the excited states.

### 1. Introduction

The calculation of the spectrum of QCD using lattice simulations has long been a key quest of the lattice community. For the case of the lowest-lying hadrons, they form a vital benchmark of our ability to describe the strong interactions through lattice calculations: the spectrum is well established from experiment. A noticeably high-profile example of such a calculation is that of the BMW Collaboration [1], whereby the spectrum of the lowest-lying states containing the  $u$ ,  $d$  and  $s$  quarks exhibited remarkable agreement with experiment. Such calculations require a high degree of control over the systematic uncertainties inherent to lattice calculations, namely those arising from the finite volume in which they are performed, finite lattice spacing, and, finally, the need until recently to extrapolate from unphysical  $u$  and  $d$  quark masses to the physical light quark masses. It worth noting here that the quark masses are not themselves physical observables, but are tunable parameters in the calculations that are tuned to ensure that certain mass ratios attain their physical values.

The calculation of the excitations of the theory, the excited-state spectrum, provides an important *predictive* opportunity for lattice QCD, yet imposes still further challenges. Nowhere are the opportunities for predictions more apparent than in the spectrum of hyperons, where so few of the states anticipated have been seen in experiment, and where the quantum numbers of the states that have been observed are often poorly established. The aim of this talk is to review our current knowledge of hyperon spectroscopy, to outline the challenges that are being overcome to advance that knowledge, and to emphasise the role that lattice calculations will play in the future hyperon physics program.

### 2. The flavor structure of excited baryons

Lattice QCD is formulated in Euclidean space, thereby admitting the use of importance sampling that is essential to numerical calculations of QCD. The spectrum of the theory is determined through observing the temporal decay of time-sliced correlation functions, *i.e.*,

$$C(t) = \sum_{\vec{x}} \langle 0 | \mathcal{O}^{J^P}(\vec{x}, t) \bar{\mathcal{O}}^{J^P}(\vec{0}, 0) | 0 \rangle \longrightarrow A^n e^{-M_n t}, \quad (1)$$

where  $\mathcal{O}^{J^P}$  is an interpolating operator of specified spin and parity  $J^P$ , and  $M_n$  are the masses of the states of those quantum numbers. That these are real, rather than imaginary,

exponentials is reflective of working in Euclidean space. Extracting subleading terms in a sum of exponentials from a single correlation function is a challenging task, though various techniques, such as the sequential-Bayes method [2], have been attempted. A robust way of extracting the subleading contributions is by means of the variational method, whereby we compute a matrix of correlation functions

$$C_{ij}(t) = \sum_{\vec{x}} \langle 0 | \mathcal{O}_i^{JP}(\vec{x}, t) \bar{\mathcal{O}}_j^{JP}(\vec{0}, 0) | 0 \rangle \longrightarrow A_{ij}^n e^{-M_n t}, \quad (2)$$

where  $\{\mathcal{O}_i^{JP} : i = 1, \dots, N\}$  is a basis of operators, each having common quantum numbers. We now solve the generalized eigenvalue equation

$$C(t)u(t, t_0) = \lambda(t, t_0)C(t_0)u(t, t_0) \quad (3)$$

yielding a set of real eigenvalues  $\{\lambda_n(t, t_0) : n = 1, \dots, N\}$  with corresponding eigenvectors  $\{u^n(t, t_0) : n = 1, \dots, N\}$ , where, for sufficiently large  $t$ , we have  $\lambda_0 \geq \lambda_1 \geq \dots$ . These eigenvalues have the property that, for sufficiently large  $t$  and  $t_0$

$$\lambda_n(t, t_0) \rightarrow (1 - A)e^{-M_n(t-t_0)} + Ae^{-(M_n + \Delta M)(t-t_0)}. \quad (4)$$

We have thus delineated between the different subleading exponentials. Furthermore, the eigenvector corresponding to a particular state in the spectrum provides important information as to the structure of the state. In particular, we can express the spectral decomposition of the correlation functions as

$$C_{ij}(t) = \sum_n \frac{Z_i^{n*} Z_j^n}{2M_n} e^{-M_n t},$$

where

$$Z_i^n \equiv \langle n | \mathcal{O}_i^\dagger | 0 \rangle = \sqrt{2M_n} e^{M_n t_0/2} u_j^{n*} C_{ji}(t_0) \quad (5)$$

for an eigenvectors  $u^n$  obtained at some reference time  $t = t_{\text{ref}}$ . We will exploit this feature below to determine the dominant operators corresponding to the various states in the spectrum.

The efficacy of the variational method relies on three features. Firstly, on a basis of operators that faithfully spans the structure of the different states. Secondly, on an efficient means of computing the correlation functions of Eqn.(2). Thirdly, on having a sufficiently large signal-to-noise ratio to render the solution of the generalized eigenvalue equation feasible. In the calculations of the *Hadron Spectrum Collaboration* that I will emphasise in this talk, the second requirement is satisfied through the use of “distillation” [3] and its stochastic variants [4], whilst the third through the use of a so-called anisotropic lattice [5, 6] with a fine temporal lattice spacing to allow the exponential fall-off of correlation functions to be resolved at small temporal separations, and through exploiting the translational symmetry of the lattice to make many calculations of the correlation function on a single gauge configuration. For this workshop, I will focus on this first of these issues, namely the construction of a suitable operator basis.

Table 1: The table shows the different baryons that can be constructed from the light  $u$ ,  $d$  and  $s$  quarks, together with their isospin, strangeness and  $SU(3)_F$  flavor content.

Baryon	$I$	$S$	$SU(3)_F$
$N$	$\frac{1}{2}$	0	$\mathbf{8}_F$
$\Delta$	$\frac{3}{2}$	0	$\mathbf{10}_F$
$\Lambda$	0	0	$\mathbf{1}_F$
			$\mathbf{8}_F$
$\Sigma$	1	-1	$\mathbf{8}_F$
			$\mathbf{10}_F$
$\Xi$	$\frac{1}{2}$	-2	$\mathbf{8}_F$
			$\mathbf{10}_F$
$\Omega$	0	-3	$\mathbf{10}_F$

We begin by expressing baryon interpolating operators of definite  $J^P$  as [7, 8]

$$\mathcal{O}^{J^P} \sim \left( F_{\Sigma_F} \otimes (S^{P_s})_{\Sigma_S}^n \otimes D_{L, \Sigma_D}^{[d]} \right)^{J^P}, \quad (6)$$

where  $F$ ,  $S$  and  $D$  are the flavor, Dirac spin and orbital angular momentum parts of the wave function, and the  $\Sigma$ 's express the corresponding permutation symmetry: - Symmetric (S), mixed-symmetric (MS), mixed anti-symmetric (MA), and antisymmetric (A). The construction of the flavor and spin components of the interpolating operators is straightforward.

Non-zero orbital angular momentum is introduced through the use of gauge-covariant derivatives, written in a circular basis and acting on the quark fields. In the notation above,  $D_{L, \Sigma_D}^{[d]}$  corresponds to an orbital wave function constructed from  $d$  derivatives, and projected onto orbital angular momentum  $L$ . In the calculations described here, up to two covariant derivatives are employed, enabling orbital angular momentum up to  $l = 2$  to be accessed. Of particular note is the mixed-symmetric combination  $D_{L=1, M}^{[2]}$ , the commutator of two covariant derivatives projected to  $L = 1$ , that corresponds to a chromo-magnetic field that would vanish for trivial gauge field configuration; operators with this construction we identify as *hybrid* operators, associated with a manifest gluon content [9]. Whilst the lack of rotational symmetry introduced through the discretization onto a finite space-time lattice has the consequence that angular momentum is no longer a good quantum number at any finite spacing, we find in practice that the spectrum shows a remarkable realization of rotational symmetry, enabling the “single-particle” spectrum to be classified according to the total angular momentum of the states, illustrated in Figure 1 below.

Our published work on the flavor structure of the excited baryon spectrum was obtained for three difference quark masses, corresponding to  $m_\pi = 702, 524$  and  $391$  MeV, with the strange quark maintained at its physical value; the largest pion mass corresponds to three degenerate quark masses, *i.e.*, the  $SU(3)$  flavor-symmetric point. We classify the flavor structure of the three-quark interpolating operators that can be constructed from the  $ud$ ,  $d$  and

$s$  quarks according to their  $SU(3)_F$  flavor composition, corresponding to octet ( $8_F$ ), decuplet ( $10_F$ ) and singlet ( $1_F$ ), detailed in Table 1. We find that, even at the lightest pion mass used in our calculations, where  $SU(3)_F$  is most severely broken, the states are dominated by a particular  $SU(3)_F$  representation, illustrated in Figure 1.

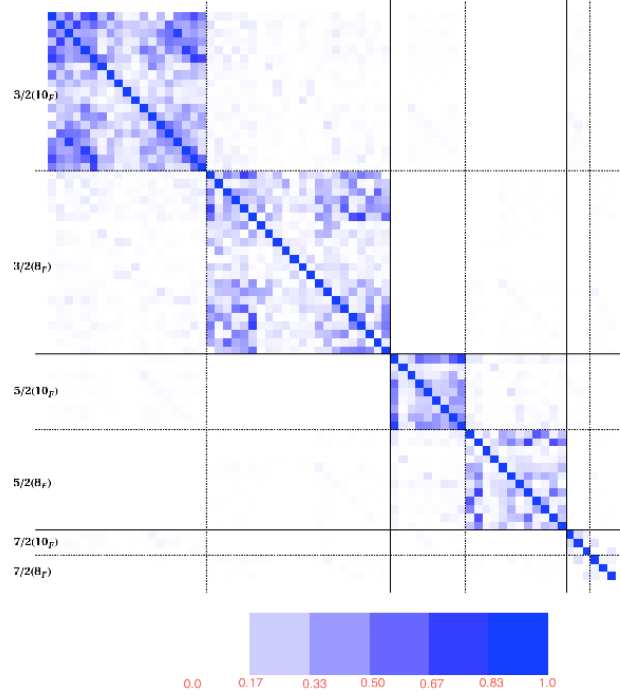


Figure 1: The magnitudes  $C_{ij} / \sqrt{C_{ii}C_{jj}}$  of the elements of the correlator matrix of Eqn.(2), normalized to the diagonal elements, at a separation of 5 time slices and at a pion mass of 391 MeV. The plot shows the correlation matrix not only to be block-diagonal in spin, but also block diagonal in flavor.

The spectrum is encapsulated in Figure 2, for the calculation at  $m_\pi = 391$  MeV, showing the dominant flavor structure for each state represented as blue ( $8_F$ ), yellow ( $10_F$ ) and beige ( $1_F$ ). The spectrum that emerges has several remarkable features:

- (a) The spectrum is remarkably rich, displaying a counting of states satisfying  $SU(6) \otimes O(3)$  symmetry, and beyond that expected in a simple quark-diquark picture of a baryon.
- (b) There are additional positive-parity states which we label “hybrid” baryons, denoted in the figure by the bold borders, with a mass around 1.2 GeV above their non-hybrid cousins, that we identify through their dominant coupling to the hybrid operators introduced above, illustrated in Figure 3 [9].
- (c) The mixed-flavor states, the  $\Lambda$ ,  $\Sigma$  and  $\Xi$ , exhibit multiplicities expected from exact  $SU(3)$  flavor symmetries. Thus the  $\Xi$ , for example, has a spectrum corresponding to the superposition of multiplicities of the  $8_F$  and  $10_F$  exact  $SU(3)_F$  expectations, seen

clearly by comparing the low-lying band for the  $\Xi$  with that of the octet Nucleon and decuplet  $\Delta$ .

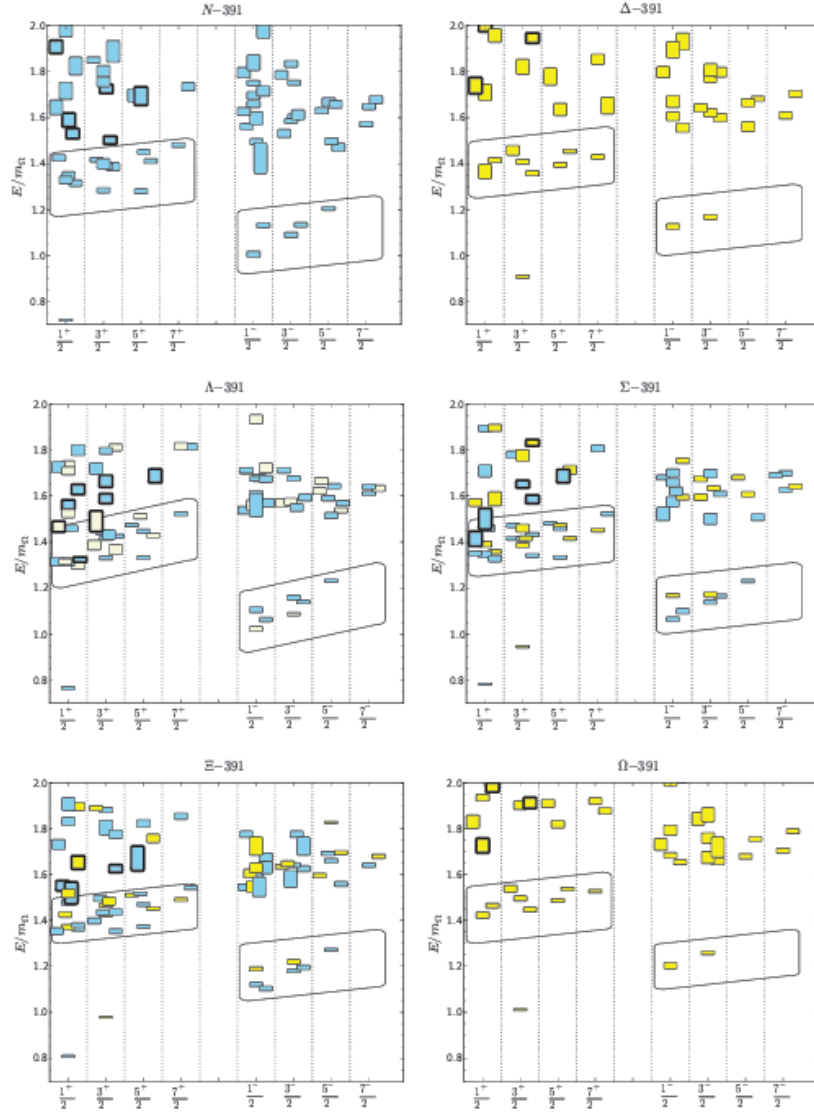


Figure 2: The figures show the spectrum of baryon states composed of  $u$ ,  $d$  and  $s$  quarks, obtained on a  $16^3 \times 48$  anisotropic lattice [8]. The bands denote the lowest-lying states identified with  $SU(6) \otimes O(3)$  symmetry, whilst the states with bold borders denote those identified as *hybrid* states, as discussed in the text.

There are features of the calculated spectrum that are qualitatively different to experiment,

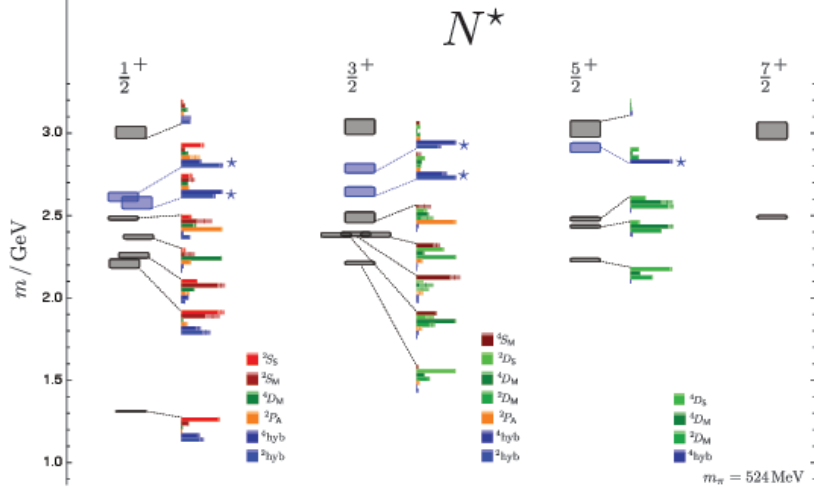


Figure 3: The figure, taken from Ref. [9], shows the relative overlaps, defined through Eqn.(5), of the lowest-lying states in the positive parity nucleon spectrum. Those operators labelled  $^2\text{hyb}$  and  $^4\text{hyb}$  correspond to the commutator of two gauge-covariant derivatives; the states in blue are those dominated by such operators which we identify as “hybrid” baryons.

notably the anomalously low masses of the Roper and of the  $\Lambda(1405)^-$ . In the case of the latter, a recent calculation using different source and sink smearing radii found a level ordering consistent with that observed [10], and there are arguments that the  $\Lambda(1405)^-$  is a  $\bar{K}N$  molecule, based on the calculated vanishing of its strange magnetic form factor [11]; it should be noted, however, that the interpretation of the electromagnetic properties of a two-particle state from a calculation on a finite lattice requires considerable theoretical analysis [12]. However, a comprehensive understanding of the spectrum of hyperon must reflect the fact that in general these states are resonances, unstable under the strong interactions.

### 3. Resonances and Lattice QCD

Lattice QCD is formulated in Euclidean space, and the energies entering into the spectral decomposition of Eqn.(2) are real. In the finite spatial volume in which are calculations are performed, those energies are quantised and should include the two- and higher-body scattering states that must be present in the spectrum. For non-interacting particles, the energies of those multi-hadron states are given by the symmetries of the box in which we are performing our calculations, and the allowed three momenta of the states. The finite spatial volume forces those scattering states to interact thereby shifting the energies from their non-interacting values. For the case of elastic scattering, the so-called Lüscher method enables the shift in energies at a finite volume to be related to the infinite volume phase shift [13, 14]; this was shortly thereafter extended to states with non-zero total momentum [15], enabling a far finer resolution of the momentum-dependent phase shifts.

In the meson sector, and using the distillation method introduced above, the precise calculation of the momentum-dependent phase shifts for states such as the  $\rho$  meson in  $I = 1 \pi\pi$  scattering has now been accomplished [16]. More recently, the formalism has been extended

to the extraction of the momentum-dependent amplitudes for inelastic scattering [17–20], and applied to the  $\pi K - \eta K$  [21, 22] and the coupled  $\pi\pi - \bar{K}K$  system [23].

Analogous calculations in the baryon sector are less advanced. Firstly, we note that the multi-hadron states that we would expect to observe in the baryon spectrum appear absent in the spectrum presented in Figure 2. The reason is simply that the three-quark interpolating operators that forms the basis for the application of the variational method have a coupling to multi-hadron states in Eqn.(5) that is suppressed by the spatial volume compared to that for “single-hadron” states. Key to the meson results cited above has been the introduction into the variational basis of multi-meson operators, at both zero and non-zero total momentum, for which the coupling to two-hadron states is not suppressed. The first steps have been taken to include multi-hadron  $N\pi$  operators into the excited nucleon basis [24, 25], with the expected spectrum  $N\pi$  energy emerging, and meson-baryon phase shifts for several channels have been computed using the same anisotropic lattice formulation employed here [26]. The application of the variational method with as faithful a basis as that used in the meson sector is more limited by computational requirements, which are considerably more demanding, than by theoretical background.

#### 4. Summary

There has been enormous progress, both theoretical and computational, aimed at extracting the excited-state spectrum of QCD. Precise calculations of momentum-dependent phase shifts have been obtained for the meson spectrum, and the formalism developed that can be applied to baryons. The most important conclusion of this talk is the richness of the hyperon spectrum, encompassing not only those states expected in the quark model, but additional hybrid states in which the gluons are manifest. In the coming years, the tools that have been developed for understanding the amplitudes and decays of resonances from lattice QCD calculations, and applied to the excited meson spectrum, will be applied to the excited baryon sector, both guiding and interpreting an exciting experimental program in hyperon spectroscopy.

#### 5. Acknowledgments

The author would like to thank his colleagues in the *Hadron Spectrum Collaboration* for their collaboration on the work presented here. This material is based upon work supported by the U.S. Department of Energy, Office of Science, Office of Nuclear Physics under contract DE-AC05-06OR23177.

## References

- [1] S. Durr *et al.*, Science **322**, 1224 (2008),
- [2] Y. Chen, S.-J. Dong, T. Draper, I. Horvath, K.-F. Liu, N. Mathur, S. Tamhankar, C. Srinivasan, F.X. Lee, and J.-B. Zhang, arXiv:hep-lat/0405001 [hep-lat].
- [3] M. Peardon, J. Bulava, J. Foley, C. Morningstar, J. Dudek, R.G. Edwards, B. Joo, H.-W. Lin, D.G. Richards, and K.J. Juge (Hadron Spectrum), Phys. Rev. D **80**, 054506 (2009).



- [4] C. Morningstar, J. Bulava, J. Foley, K.J. Juge, D. Lenkner, M. Peardon, and C.H. Wong, Phys. Rev. D **83**, 114505 (2011).
- [5] C.J. Morningstar and M.J. Peardon, Phys. Rev. D **56**, 4043 (1997).
- [6] H.-W. Lin *et al.* (Hadron Spectrum), Phys. Rev. D **79**, 034502 (2009).
- [7] R.G. Edwards, J.J. Dudek, D.G. Richards, and S.J. Wallace, Phys. Rev. D **84**, 074508 (2011).
- [8] R.G. Edwards, N. Mathur, D.G. Richards, and S.J. Wallace (Hadron Spectrum), Phys. Rev. D **87**, 054506 (2013).
- [9] J.J. Dudek and R.G. Edwards, Phys. Rev. D **85**, 054016 (2012).
- [10] B.J. Menadue, W. Kamleh, D.B. Leinweber, and M.S. Mahbub, Phys. Rev. Lett. **108**, 112001 (2012).
- [11] J.M.M. Hall, W. Kamleh, D.B. Leinweber, B.J. Menadue, B.J. Owen, A.W. Thomas, and R.D. Young, Phys. Rev. Lett. **114**, 132002 (2015),
- [12] R.A. Briceo and M.T. Hansen, arXiv:1509.08507 [hep-lat].
- [13] M. Luscher, Commun. Math. Phys. **105**, 153 (1986).
- [14] M. Luscher, Nucl. Phys. B **354**, 531 (1991).
- [15] K. Rummukainen and S.A. Gottlieb, Nucl. Phys. B **450**, 397 (1995),
- [16] J.J. Dudek, R.G. Edwards, and C.E. Thomas (Hadron Spectrum), Phys. Rev. D **87**, 034505 (2013), [Erratum: Phys. Rev. D **90**, 099902(2014)].
- [17] S. He, X. Feng, and C. Liu, JHEP **07**, 011 (2005).
- [18] P. Guo, J. Dudek, R. Edwards, and A.P. Szczepaniak, Phys. Rev. D **88**, 014501 (2013).
- [19] M.T. Hansen and S.R. Sharpe, Phys. Rev. D **86**, 016007 (2012).
- [20] R.A. Briceo and Z. Davoudi, Phys. Rev. D **88**, 094507 (2013).
- [21] J.J. Dudek, R.G. Edwards, C.E. Thomas, and D.J. Wilson (Hadron Spectrum), Phys. Rev. Lett. **113**, 182001 (2014).
- [22] D.J. Wilson, J.J. Dudek, R.G. Edwards, and C.E. Thomas, Phys. Rev. D **91**, 054008 (2015).
- [23] D.J. Wilson, R.A. Briceo, J.J. Dudek, R.G. Edwards, and C.E. Thomas, Phys. Rev. D **92**, 094502 (2015),
- [24] V. Verduci and C.B. Lang, *Proceedings, 32nd International Symposium on Lattice Field Theory* (Lattice 2014), PoS **LATTICE2014**, 121 (2014).
- [25] A.L. Kiratidis, W. Kamleh, D.B. Leinweber, and B.J. Owen, Phys. Rev. D **91**, 094509 (2015).
- [26] W. Detmold and A. Nicholson, arXiv:1511.02275 [hep-lat].

## 2.22 Formation of the $f_0(980)$ and $a_0(980)$ resonances by $\bar{K}$ Induced Reactions on Protons

Eulogio Oset

*Departamento de Física Teórica and IFIC*

*Centro Mixto Universidad de Valencia-CSIC Institutos de Investigación de Paterna*

*Aptdo. 22085, 46071 Valencia, Spain &*

*Institute of Modern Physics*

*Chinese Academy of Sciences*

*Lanzhou 730000, China*

Ju-Jun Xie

*Institute of Modern Physics*

*Chinese Academy of Sciences*

*Lanzhou 730000, China &*

*State Key Laboratory of Theoretical Physics*

*Institute of Theoretical Physics*

*Chinese Academy of Sciences*

*Beijing 100190, China*

Wei-Hong Liang

*Department of Physics*

*Guangxi Normal University*

*Guilin 541004, China*

### Abstract

Results are shown for the cross section of several reactions induced by  $\bar{K}$  scattering on protons. The reactions studied are  $K^-p \rightarrow \Lambda\pi^+\pi^-$ ,  $K^-p \rightarrow \Sigma^0\pi^+\pi^-$ ,  $K^-p \rightarrow \Lambda\pi^0\eta$ ,  $K^-p \rightarrow \Sigma^0\pi^0\eta$ ,  $K^-p \rightarrow \Sigma^+\pi^-\eta$ ,  $\bar{K}^0p \rightarrow \Lambda\pi^+\eta$ ,  $\bar{K}^0p \rightarrow \Sigma^0\pi^+\eta$ ,  $\bar{K}^0p \rightarrow \Sigma^+\pi^+\pi^-$ ,  $\bar{K}^0p \rightarrow \Sigma^+\pi^0\eta$ . In the reactions with a final  $\pi^+\pi^-$  a clear peak is seen for the  $f_0(980)$  formation, with no trace of the  $f_0(500)$ . In the cases of  $\pi\eta$  production the  $a_0(980)$  resonance shows up, with a characteristic strong cusp shape.

### 1. Introduction

Kaon beams are increasingly becoming a good source for new information in hadron physics. At intermediate energies J-PARC offers good intensity secondary Kaon beams up to about 2 GeV/c [1, 2]. DAPHNE at Frascati provides low energy Kaon beams [3, 4]. Plans are been made for a secondary meson beam Facility at Jefferson Lab, which would include Kaons, both charged and neutral [5]. One of the purposes is to produce hyperons ( $\equiv Y$ ) [6], and cascade states, which are poorly known [7, 8]. Here we address a different problem using Kaon beams: the Kaon induced production of the  $f_0(980)$  and  $a_0(980)$  resonances. We show some results for the reactions  $\bar{K}p \rightarrow \pi\pi Y$  and  $\bar{K}p \rightarrow \pi\eta Y$ , which produce the  $f_0(980)$  and  $a_0(980)$  resonances, respectively. These two scalar resonances have generated an intense debate as to their nature, as  $q\bar{q}$ , tetraquarks, meson molecules, glueballs, dynamically generated states, *etc.* [9]. By now it is commonly accepted that these mesons are not standard  $q\bar{q}$

states but “extraordinary” states [10]. The advent of chiral dynamics in its unitarized form in coupled channels, the chiral unitary approach, has shown how these resonances appear from the interaction of pseudoscalar mesons, with a kernel, or potential, extracted from the chiral Lagrangians [11], and using the coupled channels Bethe Salpeter equation [12–15], or similar methods, like the inverse amplitude method [16, 17]. A recent review on this issue is given in [18].

New information on these states has come from the study of  $B$  and  $D$  decays [19, 20], which has stimulated much theoretical work [21–28]. However, not much has been done in reactions involving baryons, with the exception of  $f_0(980)$  photoproduction, measured in Refs. [29, 30], which had been addressed theoretically earlier in Ref. [31]. Other theoretical studies have been done after the experiment in [32, 33]. With this perspective, the use of Kaon induced reactions on proton targets to produce these states promises to be a new good source of information which should help us understand better the nature of these resonances.

In chiral unitary theories the  $f_0(980)$  couples strongly to  $K\bar{K}$ , and much less to  $\pi\pi$  which becomes the decay channel. Similarly, the  $a_0(980)$  couples both to  $K\bar{K}$  and to  $\pi\eta$ , the latter being the decay channel. This is why the use of Kaon beams to produce these resonances provides a new method to test these ideas.

## 2. The Chiral Unitary Approach for the $f_0(980)$ and $a_0(980)$ Resonances

Following Refs. [12, 34], The first step is the use of the transition potentials from the lowest order chiral Lagrangians of Ref. [11] with the coupled channels,  $\pi^+\pi^-$ ,  $\pi^0\pi^0$ ,  $\pi^0\eta$ ,  $\eta\eta$ ,  $K^+K^-$ ,  $K^0\bar{K}^0$ , for which explicit expressions in  $s$  wave can be seen in Refs. [21, 22]. By using the on shell factorization of the Bethe-Salpeter equation in coupled channels [35, 36], one finds in matrix form

$$T = V + VGT; \quad T = [1 - VG]^{-1}V, \quad (1)$$

where  $V$  is the transition potential and  $G$  the loop function for two intermediate meson propagators. This function is regularized in dimensional regularization or taking a cut off in three momenta. For the reactions studied on needs the  $t_{K^+K^- \rightarrow \pi^+\pi^-}$ ,  $t_{K^0\bar{K}^0 \rightarrow \pi^+\pi^-}$ ,  $t_{K^+K^- \rightarrow \pi^0\eta}$ ,  $t_{K^0\bar{K}^0 \rightarrow \pi^0\eta}$  matrix elements, which contain a pole associated to the  $f_0(980)$  (the first two), or to the  $a_0(980)$  (the last two). The  $a_0(980)$  appears usually as a big cusp around the  $K\bar{K}$  threshold, both in the theory as in experiments [37, 38].

## 3. Formalism

In our formalism the picture for  $f_0(980)$  and  $a_0(980)$  anti-Kaon induced production proceeds via the creation of one  $K$  by the  $\bar{K}p$  initial state in a first step followed by the interaction of the  $K$  and  $\bar{K}$  which generates the resonances. This is shown by the Feynman diagram depicted in Fig. 1.

We first take the  $K^-p \rightarrow \Lambda(\Sigma^0)\pi^+\pi^-(\pi^0\eta)$  as a reference and from this reaction we construct the other five reactions with minimal changes. In this case, the  $K^-$  must couple with another  $K^+$  to form the resonances. In this case one of the Kaons (the  $K^+$ ) is necessarily off shell, which would require the use of the  $K^+K^- \rightarrow \pi^+\pi^-(\pi^0\eta)$  amplitude with the  $K^+$  leg off shell, which readily comes from the chiral Lagrangians. Yet, the structure of these

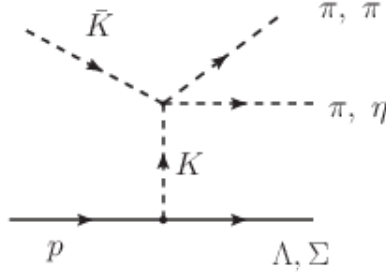


Figure 1: Feynman diagram for the  $\bar{K}p \rightarrow \pi\pi(\pi^0\eta)Y$  reaction.

Lagrangians is such that the potential can be written as [12]

$$V_{K^+K^- \rightarrow \pi^+\pi^-}(p_{K^-}, q) = V_{K^+K^- \rightarrow \pi^+\pi^-}^{\text{on}}(M_{\text{inv}}) + b(q^2 - m_{K^+}^2), \quad (2)$$

where  $p_{K^-}$  and  $q$  are the four momenta of  $K^-$  and  $K^+$  mesons, respectively, with  $M_{\text{inv}} = \sqrt{(p_{K^-} + q)^2}$  the invariant mass of the  $K^+K^-$  system. The off shell term with  $b$  is unphysical while  $V^{\text{on}}$  is a physical quantity. Then, the term  $b(q^2 - m_{K^+}^2)$  multiplied by the  $K^+$  propagator of Fig. 1 leads to a contact term as depicted in Fig. 2.

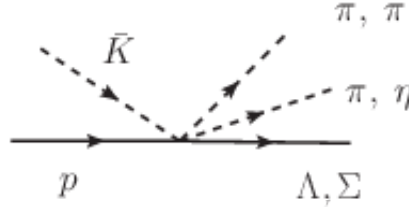


Figure 2: Contact term stemming from the Feynman diagram of Fig. 1 from the off shell part of the  $K^+K^- \rightarrow \pi^+\pi^-(\pi^0\eta)$  transition potential.

The interesting thing is that the same chiral Lagrangian for meson baryon [39,40], expanding on the number of pion fields, contains a contact term with the same topology as the one obtained from the off shell part of the amplitude [41] and it cancels this off shell term. Hence, only the physical on shell  $K\bar{K} \rightarrow \pi\pi(\pi\eta)$  amplitude is needed in Fig. 1 for the evaluation of the diagrams. These cancellations were already observed in Ref. [42] in the study of the  $\pi N \rightarrow \pi\pi N$  reaction and in Ref. [43] for the study of the pion cloud contribution to the Kaon nucleus optical potential.

One also needs the Lagrangians for the Yukawa meson-baryon-baryon vertex of Fig. 1 which is given by

$$\begin{aligned} \mathcal{L} &= \frac{D}{2} \langle \bar{B} \gamma^\mu \gamma_5 \{u_\mu, B\} \rangle + \frac{F}{2} \langle \bar{B} \gamma^\mu \gamma_5 [u_\mu, B] \rangle \\ &= \frac{D+F}{2} \langle \bar{B} \gamma^\mu \gamma_5 u_\mu B \rangle + \frac{D-F}{2} \langle \bar{B} \gamma^\mu \gamma_5 B u_\mu \rangle, \end{aligned} \quad (3)$$

where the symbol  $\langle \rangle$  stands for the trace of SU(3). The term linear in meson field gives

$$u_\mu \simeq -\sqrt{2} \frac{\partial_\mu \Phi}{f} \quad (4)$$

with  $f$  the pion decay constant,  $f = f_\pi = 93$  MeV, and  $\Phi$ ,  $B$  the meson and baryon SU(3) field matrices given by

$$\Phi = \begin{pmatrix} \frac{1}{\sqrt{2}}\pi^0 + \frac{1}{\sqrt{6}}\eta & \pi^+ & K^+ \\ \pi^- & -\frac{1}{\sqrt{2}}\pi^0 + \frac{1}{\sqrt{6}}\eta & K^0 \\ K^- & \bar{K}^0 & -\frac{2}{\sqrt{6}}\eta \end{pmatrix}, \quad (5)$$

$$B = \begin{pmatrix} \frac{1}{\sqrt{2}}\Sigma^0 + \frac{1}{\sqrt{6}}\Lambda & \Sigma^+ & p \\ \Sigma^- & -\frac{1}{\sqrt{2}}\Sigma^0 + \frac{1}{\sqrt{6}}\Lambda & n \\ \Xi^- & \Xi^0 & -\frac{2}{\sqrt{6}}\Lambda \end{pmatrix}. \quad (6)$$

We take  $D = 0.795$ ,  $F = 0.465$  [44]. The explicit evaluation of the SU(3) matrix elements of Eq. (3) leads to the following expression

$$\mathcal{L} \rightarrow i \left( \alpha \frac{D+F}{2f} + \beta \frac{D-F}{2f} \right) \bar{u}(p', s'_B) \not{q} \gamma_5 u(p, s_B), \quad (7)$$

where  $u(p, s_B)$  and  $\bar{u}(p', s'_B)$  are the ordinary Dirac spinors of the initial and final baryons, respectively, and  $p, s_B$  and  $p', s'_B$  are the four-momenta and spins of the baryons, while  $q = p - p'$  is the four momentum of the meson. The values of  $\alpha$  and  $\beta$  are tabulated in Table 1.

Table 1: Coefficients for the  $\bar{K}NY$  couplings of Eq. (7).

	$K^-p \rightarrow \Lambda$	$K^-p \rightarrow \Sigma^0$	$K^-n \rightarrow \Sigma^-$
$\alpha$	$-\frac{2}{\sqrt{3}}$	0	0
$\beta$	$\frac{1}{\sqrt{3}}$	1	$\sqrt{2}$
	$\bar{K}^0n \rightarrow \Lambda$	$\bar{K}^0n \rightarrow \Sigma^0$	$\bar{K}^0p \rightarrow \Sigma^+$
$\alpha$	$-\frac{2}{\sqrt{3}}$	0	0
$\beta$	$\frac{1}{\sqrt{3}}$	-1	$\sqrt{2}$

Finally the amplitude for the diagram of Fig. 1 can be written as

$$T = -it_{K\bar{K} \rightarrow MM} \frac{1}{q^2 - m_K^2} \left( \alpha \frac{D+F}{2f} + \beta \frac{D-F}{2f} \right) \times \bar{u}(p', s'_{\Lambda/\Sigma}) \not{q} \gamma_5 u(p, s_p) F(q^2), \quad (8)$$

where we have added the usual Yukawa form factor that we take of the form

$$F(q^2) = \frac{\Lambda^2}{\Lambda^2 - q^2} \quad (9)$$

with typical values of  $\Lambda$  of the order of 1 GeV.

The sum and average of  $|T|^2$  over final and initial polarization of the baryons is easily done and the full expression can be seen in [45].

We can write  $q^2$  in terms of the variables of the external particles and have

$$q^2 = M_p^2 + M'^2 - 2EE' + 2|\vec{p}||\vec{p}'| \cos \theta, \quad (10)$$

where  $\vec{p}, \vec{p}'$  and  $E, E'$  are the momenta and energies of the proton and the final baryon, and  $\theta$  is the angle between the direction of the initial and final baryon, all of them evaluated in the global center of mass frame (CM).

We can write the differential cross section as

$$\frac{d^2\sigma}{dM_{\text{inv}}d\cos\theta} = \frac{M_p M'}{32\pi^3} \frac{|\vec{p}'|}{|\vec{p}|} \frac{|\vec{p}|}{s} \overline{\sum_{s_p} \sum_{s'_{\Lambda/\Sigma}} |T|^2}, \quad (11)$$

with  $|\vec{p}|$  the momentum of one of the mesons in the frame where the two final mesons are at rest,

We study nine reactions:

$$\begin{aligned} K^- p &\rightarrow \Lambda \pi^+ \pi^-, \quad K^- p \rightarrow \Sigma^0 \pi^+ \pi^-, \quad K^- p \rightarrow \Lambda \pi^0 \eta, \\ K^- p &\rightarrow \Sigma^0 \pi^0 \eta, \quad K^- p \rightarrow \Sigma^+ \pi^- \eta, \quad \bar{K}^0 p \rightarrow \Lambda \pi^+ \eta, \\ \bar{K}^0 p &\rightarrow \Sigma^0 \pi^+ \eta, \quad \bar{K}^0 p \rightarrow \Sigma^+ \pi^+ \pi^-, \quad \bar{K}^0 p \rightarrow \Sigma^+ \pi^0 \eta. \end{aligned} \quad (12)$$

The Yukawa vertices for  $KBB$  are summarized in Table 1. For the  $K\bar{K} \rightarrow MM$  amplitudes only the  $I_3 = 0$  components, corresponding to zero charge, are needed here. We have three cases with  $\pi\eta$  where the charge is non zero,  $K^- p \rightarrow \Sigma^+ \pi^- \eta$ ,  $\bar{K}^0 p \rightarrow \Lambda \pi^+ \eta$  and  $\bar{K}^0 p \rightarrow \Sigma^0 \pi^+ \eta$ , which can be easily related to the  $K^+ K^- \rightarrow \pi^0 \eta$  using isospin symmetry [45].

With these ingredients, we use Eq. (11) to evaluate the cross section in each case, changing the  $t_{K\bar{K},MM}$  in each case and the values of  $\alpha$  and  $\beta$ . These magnitudes are summarized in Table 2.

#### 4. Results

The cross section depend on the energy,  $M_{\text{inv}}$ , and the scattering angle  $\theta$  given by Eq. (10). We first evaluate the cross section for  $\theta = 0$ , in the forward direction. In Fig. 3, we show the numerical results of  $d\sigma/dM_{\text{inv}}d\cos\theta$  for  $\cos(\theta) = 1$  as a function of  $M_{\text{inv}}$  of the  $\pi^+ \pi^-$  for  $K^- p \rightarrow \Lambda(\Sigma^0) \pi^+ \pi^-$  reactions. We take  $\sqrt{s} = 2.4$  GeV, which corresponds to the  $K^-$  momentum  $p_{K^-} = 2.42$  GeV in the laboratory frame. One can see a clear peak around  $M_{\text{inv}} = 980$  MeV which is the signal of the  $f_0(980)$  resonance produced by the initial  $K^+ K^-$  coupled channel interactions and decaying into  $\pi^+ \pi^-$  channel. We also see that the magnitude of the cross section for  $\Lambda$  production is about ten times larger than for  $\Sigma^0$  production, because the coupling of  $KN\Lambda$  is bigger than the  $KN\Sigma$  one.

Table 2: Matrices  $t_{K\bar{K} \rightarrow MM}$ ,  $\alpha$ ,  $\beta$  used in each reaction and resonance obtained.

Reaction	$t_{K\bar{K} \rightarrow MM}$	$\alpha$	$\beta$	Resonance
$K^- p \rightarrow \Lambda \pi^+ \pi^-$	$t_{K^+ K^- \rightarrow \pi^+ \pi^-}$	$-\frac{2}{\sqrt{3}}$	$\frac{1}{\sqrt{3}}$	$f_0(980)$
$K^- p \rightarrow \Sigma^0 \pi^+ \pi^-$	$t_{K^+ K^- \rightarrow \pi^+ \pi^-}$	0	1	$f_0(980)$
$K^- p \rightarrow \Lambda \pi^0 \eta$	$t_{K^+ K^- \rightarrow \pi^0 \eta}$	$-\frac{2}{\sqrt{3}}$	$\frac{1}{\sqrt{3}}$	$a_0(980)$
$K^- p \rightarrow \Sigma^0 \pi^0 \eta$	$t_{K^+ K^- \rightarrow \pi^0 \eta}$	0	1	$a_0(980)$
$K^- p \rightarrow \Sigma^+ \pi^- \eta$	$\sqrt{2} t_{K^+ K^- \rightarrow \pi^0 \eta}$	0	$\sqrt{2}$	$a_0(980)$
$\bar{K}^0 p \rightarrow \Lambda \pi^+ \eta$	$\sqrt{2} t_{K^+ K^- \rightarrow \pi^0 \eta}$	$-\frac{2}{\sqrt{3}}$	$\frac{1}{\sqrt{3}}$	$a_0(980)$
$\bar{K}^0 p \rightarrow \Sigma^0 \pi^+ \eta$	$\sqrt{2} t_{K^+ K^- \rightarrow \pi^0 \eta}$	0	1	$a_0(980)$
$\bar{K}^0 p \rightarrow \Sigma^+ \pi^+ \pi^-$	$t_{K^0 \bar{K}^0 \rightarrow \pi^+ \pi^-}$	0	$\sqrt{2}$	$f_0(980)$
$\bar{K}^0 p \rightarrow \Sigma^+ \pi^0 \eta$	$t_{K^0 \bar{K}^0 \rightarrow \pi^0 \eta}$	0	$\sqrt{2}$	$a_0(980)$

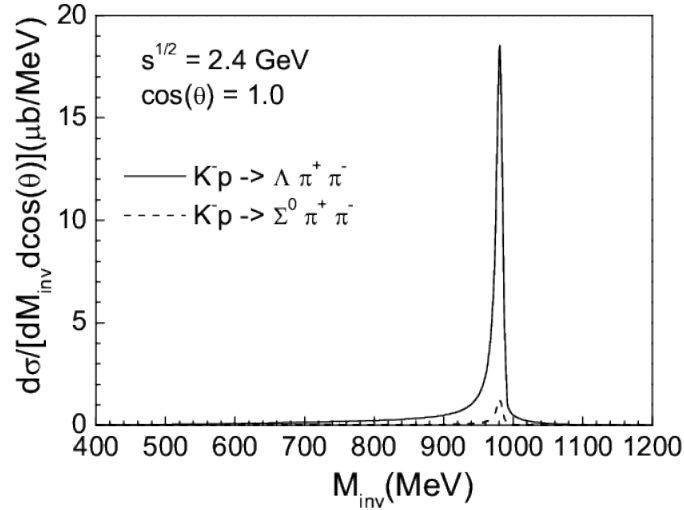


Figure 3: Theoretical predictions for  $S$  wave  $\pi^+ \pi^-$  mass distributions for  $K^- p \rightarrow \Lambda(\Sigma^0) \pi^+ \pi^-$  reactions at  $\sqrt{s} = 2.4$  GeV and  $\cos(\theta) = 1$ .

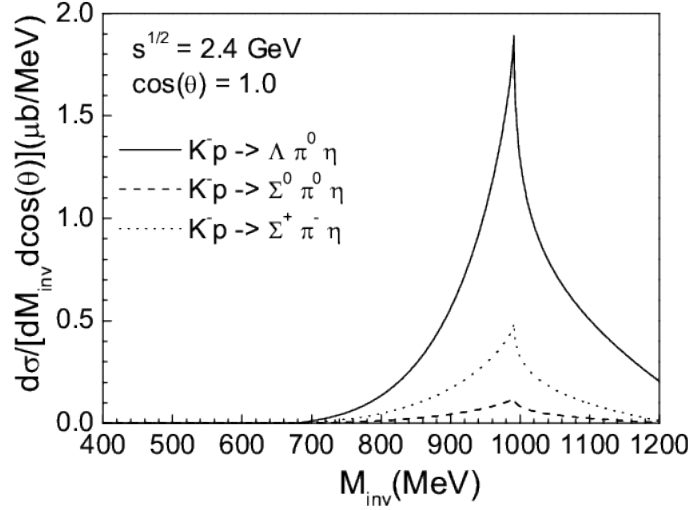


Figure 4: Theoretical predictions for  $S$  wave  $\pi\eta$  mass distributions for  $K^-p \rightarrow \Lambda(\Sigma^0)\pi^0\eta$  and  $K^-p \rightarrow \Sigma^+\pi^-\eta$  reactions at  $\sqrt{s} = 2.4$  GeV and  $\cos(\theta) = 1$ .

In Fig. 4, we can see the numerical results of  $d\sigma/dM_{\text{inv}}d\cos\theta$  for  $\cos(\theta) = 1$  as a function of  $M_{\text{inv}}$  of the  $\pi\eta$  for  $K^-p \rightarrow \Lambda(\Sigma^0)\pi^0\eta$  and  $K^-p \rightarrow \Sigma^+\pi^-\eta$  reactions. In this case one also observes a clear peak/cusp around  $M_{\text{inv}} = 980$  MeV, corresponding to the  $a_0(980)$  state.

The results for  $\bar{K}^0p$  reactions are shown in Fig. 5. One observes again the clear peaks for  $a_0(980)$  and  $f_0(980)$  resonances around  $M_{\text{inv}} = 980$  MeV.

In all the reactions mentioned above, one observes clear peaks for the  $f_0(980)$  with the  $\pi^+\pi^-$  production or for the  $a_0(980)$  with  $\pi\eta$  production. One should note that in the case of the  $f_0(980)$  production there is no signal for  $f_0(500)$  ( $\sigma$ ) production. This is similar to what was found in  $B_s^0 \rightarrow J/\psi\pi^+\pi^-$ , where a clear peak was seen for the  $f_0(980)$  but no trace was observed of the  $f_0(500)$  [19]. An explanation for this fact was given in Ref. [21] using the chiral unitary approach.

The reactions with  $\pi\eta$  in the final state produce the  $a_0(980)$  resonance, with a cusp around the  $K\bar{K}$  threshold, but with a large strength.

In Figs. 6 to 8, we show the results for  $d\sigma/dM_{\text{inv}}d\cos\theta$  for the  $\bar{K}p$  reactions at the peak of the invariant mass of,  $f_0(980)$ ,  $a_0(980)$  respectively, as a function of  $\cos\theta$ . The reactions peak forward because we considered only the contributions from the  $t$  channel  $K$  exchange. One can see that the cross section falls down from forward to backward angles by about a factor ten.

Finally, by fixing  $M_{\text{inv}} = 980$  MeV at the peak of the resonance and  $\cos\theta = 1$  we show the results by looking at the dependence of the cross section with the energy of the  $\bar{K}$  beam. We only show the results for the  $\Lambda$  production in Fig. 9 because the  $\Lambda$  production is larger than the  $\Sigma$  production. One can observe that the cross section grows fast from the reaction threshold and reaches a peak around  $p_{\bar{K}} = 2.5$  GeV.



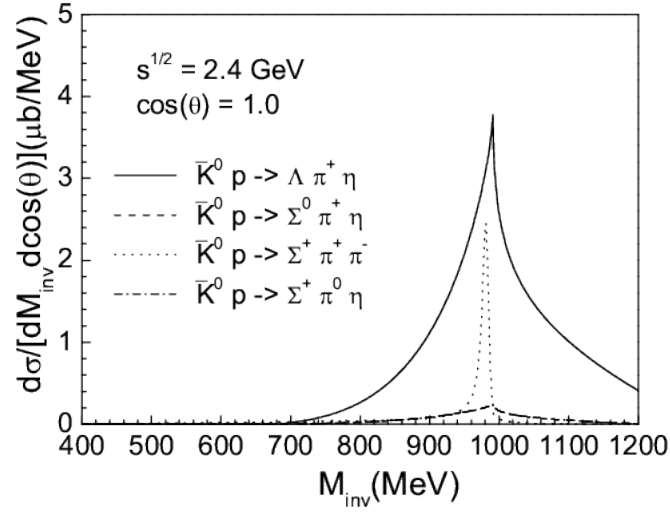


Figure 5: Theoretical predictions for  $S$  wave  $\pi\eta$  and  $\pi^+\pi^-$  mass distributions for  $\bar{K}^0 p \rightarrow \Lambda(\Sigma^0)\pi^+\eta$  and  $K^- p \rightarrow \Sigma^+\pi^0\eta(\pi^+\pi^-)$  reactions at  $\sqrt{s} = 2.4$  GeV and  $\cos(\theta) = 1$ .

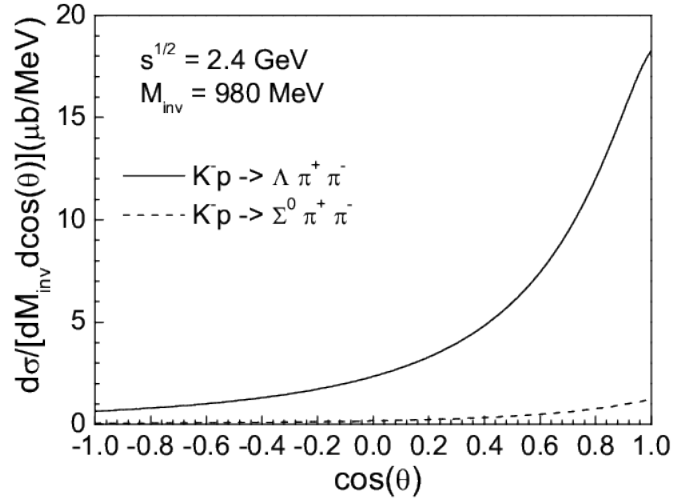


Figure 6: Theoretical predictions for  $d\sigma/dM_{\text{inv}}d\cos\theta$  as a function of  $\cos(\theta)$  for  $K^- p \rightarrow \Lambda(\Sigma^0)\pi^+\pi^-$  reactions at  $\sqrt{s} = 2.4$  GeV and  $M_{\text{inv}} = 980$  MeV.

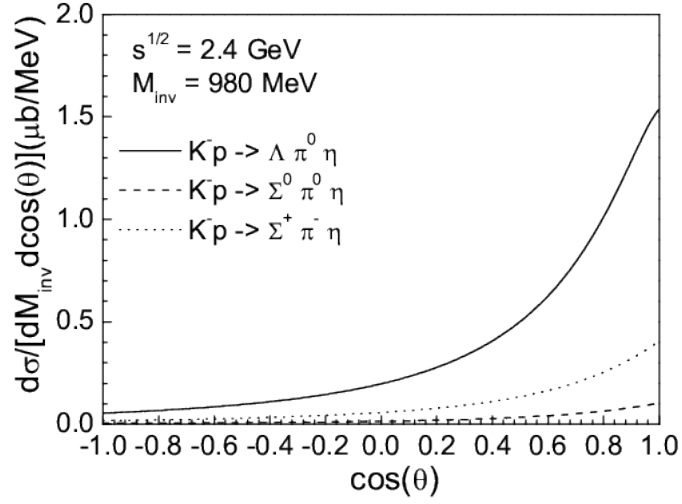


Figure 7: Theoretical predictions for  $d\sigma/dM_{\text{inv}}d\cos\theta$  as a function of  $\cos(\theta)$  for  $K^-p \rightarrow \Lambda(\Sigma^0)\pi^0\eta$  and  $K^-p \rightarrow \Sigma^+\pi^-\eta$  reactions at  $\sqrt{s} = 2.4$  GeV and  $M_{\text{inv}} = 980$  MeV.

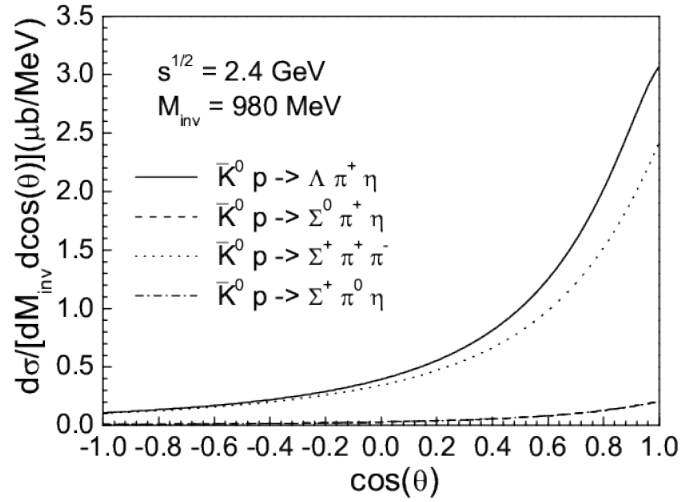


Figure 8: Theoretical predictions for  $d\sigma/dM_{\text{inv}}d\cos\theta$  as a function of  $\cos(\theta)$  for  $\bar{K}^0p \rightarrow \Lambda(\Sigma^0)\pi^+\eta$  and  $\bar{K}^0p \rightarrow \Sigma^+\pi^0\eta(\pi^+\pi^-)$  reactions at  $\sqrt{s} = 2.4$  GeV and  $M_{\text{inv}} = 980$  MeV.

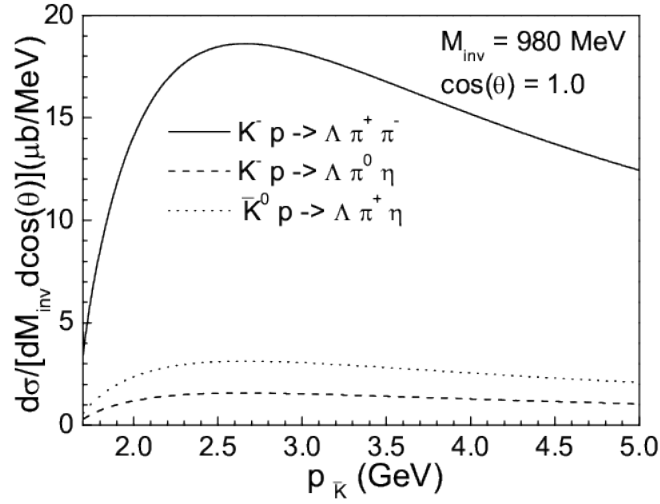


Figure 9: Theoretical predictions for  $d\sigma/dM_{\text{inv}}d\cos\theta$  as a function of  $p_{\bar{K}}$  for  $K^-p \rightarrow \Lambda\pi^+\pi^-$  ( $\pi^0\eta$ ) and  $\bar{K}^0p \rightarrow \Lambda\pi^+\eta$  reactions at  $\cos\theta = 1$  and  $M_{\text{inv}} = 980$  MeV.

## 5. Conclusions

We have shown results of the cross sections for the production of  $f_0(980)$  and  $a_0(980)$  resonances in  $\bar{K}p$  reactions from the perspective that these two resonances are dynamically generated from the coupled pseudoscalar-pseudoscalar channels interaction in  $I = 0$  and 1, respectively. These results provide the first evaluation of the cross section for these reactions. In the cases of  $\pi^+\pi^-$  final states, we find a neat peak for the  $f_0(980)$  production and no trace of the  $f_0(500)$ . This feature is related to the fact that the resonance is produced from  $K\bar{K}$  and the  $f_0(980)$  has a strong coupling  $K\bar{K}$  while the  $f_0(500)$  has a smaller coupling to this component. This feature was also observed in the  $B_s \rightarrow J/\psi\pi^+\pi^-$  reaction and one finds a natural explanation of both reactions within the chiral unitary approach. It would be most interesting to have the reactions proposed measured in actual experiments to bring further light on possible interpretations of the nature of these resonances.

The reactions with the  $\pi\eta$  production give also rise to a clear peak corresponding to the  $a_0(980)$ . This resonance appears as a limit of a resonance in the chiral unitary approach, corresponding to a state slightly unbound, or barely bound. Consequently, it shows up in form of a strong cusp around the  $K\bar{K}$  threshold, a feature which is observed in recent experiments with large statistics. We should also note that our theoretical results provide the absolute strength for both the  $f_0(980)$  and  $a_0(980)$  production as a consequence of the theoretical framework that generates dynamically these two resonances. Comparison of the strength of these reactions, when measured, could serve to assert the accuracy of the production model that we have considered, and help us narrow the scope on pictures for the nature of the  $f_0(980)$  and  $a_0(980)$  resonances.

## 6. Acknowledgments

One of us, E.O., wishes to acknowledge support from the Chinese Academy of Sciences in the Program of Visiting Professorship for Senior International Scientists (Grant No. 2013T2J0012). This work is partly supported by the Spanish Ministerio de Economía y Competitividad and European FEDER funds under the contract number FIS2011–28853–C02–01 and FIS2011–28853–C02–02, and the Generalitat Valenciana in the program Prometeo II-2014/068. This work is also partly supported by the National Natural Science Foundation of China under Grant Nos. 11165005, 11565007 and 11475227. This work is also supported by the Open Project Program of State Key Laboratory of Theoretical Physics, Institute of Theoretical Physics, Chinese Academy of Sciences, China (No. Y5KF151CJ1).

## References

- [1] T. Sato, T. Takahashi, and K. Yoshimura, *Lect. Notes Phys.* **781**, 193 (2009).
- [2] S. Kumano, arXiv:1504.05264 [hep-ph].
- [3] S. Okada *et al.*, *EPJ Web Conf.* **3**, 03023 (2010).
- [4] M. Bazzi *et al.* [SIDDHARTA Collaboration], *Nucl. Phys. A* **907**, 69 (2013).
- [5] W.J. Briscoe, M. Döring, H. Haberzettl, D.M. Manley, M. Naruki, I.I. Strakovsky and E.S. Swanson, *Eur. Phys. J. A* **51**, 129 (2015).
- [6] H. Zhang, J. Tulpan, M. Shrestha, and D.M. Manley, *Phys. Rev. C* **88**, 035204 (2013).
- [7] B. Jackson, Y. Oh, H. Haberzettl, and K. Nakayama, *Phys. Rev. C* **89**, 025206 (2014).
- [8] B. C. Jackson, Y. Oh, H. Haberzettl, and K. Nakayama, *Phys. Rev. C* **91**, 065208 (2015).
- [9] E. Klempt and A. Zaitsev, *Phys. Rept.* **454**, 1 (2007).
- [10] R.L. Jaffe, talk at the *Hadron Conference 2015*, Jefferson Lab, <https://www.jlab.org/conferences/hadron2015/talks/monday/>
- [11] J. Gasser and H. Leutwyler, *Nucl. Phys. B* **250**, 465 (1985).
- [12] J.A. Oller and E. Oset, *Nucl. Phys. A* **620**, 438 (1997); [Erratum-ibid. A **652**, 407 (1999)].
- [13] N. Kaiser, *Eur. Phys. J. A* **3**, 307 (1998).
- [14] M.P. Locher, V.E. Markushin, and H.Q. Zheng, *Eur. Phys. J. C* **4**, 317 (1998).
- [15] J. Nieves and E. Ruiz Arriola, *Nucl. Phys. A* **679**, 57 (2000); *Phys. Lett. B* **455**, 30 (1999).
- [16] J. A. Oller, E. Oset, and J.R. Pelaez, *Phys. Rev. D* **59**, 074001 (1999); [*Phys. Rev. D* **60**, 099906 (1999)]; [*Phys. Rev. D* **75**, 099903 (2007)].

- [17] J.R. Pelaez and G. Rios, Phys. Rev. Lett. **97**, 242002 (2006).
- [18] J.R. Pelaez, arXiv:1510.00653 [hep-ph].
- [19] R. Aaij *et al.* (LHCb Collaboration), Phys. Lett. B **698**, 115 (2011).
- [20] H. Muramatsu *et al.* (CLEO Collaboration), Phys. Rev. Lett. **89**, 251802 (2002); [Phys. Rev. Lett. **90**, 059901 (2003)].
- [21] W. H. Liang and E. Oset, Phys. Lett. B **737**, 70 (2014).
- [22] J.J. Xie, L. R. Dai, and E. Oset, Phys. Lett. B **742**, 363 (2015).
- [23] J.-P. Dedonder, R. Kaminski, L. Lesniak, and B. Loiseau, Phys. Rev. D **89**, 094018 (2014).
- [24] J.T. Daub, C. Hanhart, and B. Kubis, arXiv:1508.06841 [hep-ph].
- [25] M. Döring, U. G. Meißner, and W. Wang, JHEP **1310**, 011 (2013).
- [26] W.F. Wang, H.n. Li, W. Wang, and C.D. Lü, Phys. Rev. D **91**, 094024 (2015).
- [27] T. Sekihara and E. Oset, Phys. Rev. D **92**, 054038 (2015).
- [28] W.H. Liang, J.J. Xie, and E. Oset, Phys. Rev. D **92**, 034008 (2015).
- [29] M. Battaglieri *et al.* [CLAS Collaboration], Phys. Rev. Lett. **102**, 102001 (2009).
- [30] M. Battaglieri *et al.* [CLAS Collaboration], Phys. Rev. D **80**, 072005 (2009).
- [31] E. Marco, E. Oset, and H. Toki, Phys. Rev. C **60**, 015202 (1999).
- [32] M.L.L. da Silva and M.V.T. Machado, Phys. Rev. C **87**, 065201 (2013).
- [33] A. Donnachie and Y.S. Kalashnikova, arXiv:1507.07408 [hep-ph].
- [34] D. Gamermann, E. Oset, D. Strottman, and M.J. Vicente Vacas, Phys. Rev. D **76**, 074016 (2007).
- [35] J.A. Oller and E. Oset, Phys. Rev. D **60**, 074023 (1999).
- [36] J.A. Oller and U.G. Meissner, Phys. Lett. B **500**, 263 (2001).
- [37] P. Rubin *et al.* [CLEO Collaboration], Phys. Rev. Lett. **93**, 111801 (2004).
- [38] G.S. Adams *et al.* [CLEO Collaboration], Phys. Rev. D **84**, 112009 (2011).
- [39] G. Ecker, Prog. Part. Nucl. Phys. **35**, 1 (1995).
- [40] V. Bernard, N. Kaiser, and U. G. Meissner, Int. J. Mod. Phys. E **4**, 193 (1995).
- [41] K.P. Khemchandani, A. Martinez Torres, and E. Oset, Eur. Phys. J. A **37**, 233 (2008).
- [42] E. Oset and M.J. Vicente-Vacas, Nucl. Phys. A **446**, 584 (1985).

- [43] C. Garcia-Recio, J. Nieves, and E. Oset, Phys. Rev. C **51**, 237 (1995).
- [44] B. Borasoy, Phys. Rev. D **59**, 054021 (1999).
- [45] J.J. Xie, W.H. Liang, and E. Oset, arXiv:1512.01888 [nucl-th]. Phys. Rev. C, in print.

## 2.23 TREK @ J-PARC: Beyond the Standard Model with Stopped $K^+$

Michael Kohl

*Hampton University*

*Hampton, VA 23668, U.S.A. &*

*Thomas Jefferson National Accelerator Facility*

*Newport News, VA 23606, U.S.A.*

*(TREK/E36 Collaboration)*

### Abstract

The TREK/E36 experiment has been carried out at J-PARC to provide a precision test of lepton universality in the  $K_{e2}/K_{\mu2}$  ratio to search for new physics beyond the Standard Model. Simultaneously it will be sensitive to light U(1) gauge bosons and sterile neutrinos below 300 MeV/ $c^2$ , which could be associated with dark matter or explain established muon-related anomalies such as the muon  $g - 2$  and the proton radius puzzle. The experiment has been set up at the J-PARC K1.1BR kaon beamline since fall 2014, it has been fully commissioned in spring 2015, and completed the accumulation of production data in fall 2015. The experiment has used a scintillating fiber target to stop a beam of up to 1.2 Million  $K^+$  per spill. The kaon decay products were detected with a large-acceptance toroidal spectrometer capable of tracking charged particles with high resolution, combined with a photon calorimeter with large solid angle and particle identification systems. The status and recent progress of the experiment will be presented.

### 1. Introduction

High precision electroweak tests represent a powerful tool to test the Standard Model (SM) and to obtain indirect hints of new physics. Lepton universality is a central characteristic of the SM, describing the flavor independence of the electroweak couplings of the charged leptons. Experimentally, lepton universality has been tested and established rather well in many processes – for an overview see, *e.g.*, Ref. [1]. However, there have also been a few exceptions. Small deviations from lepton universality at the 2-3  $\sigma$  level have been observed in the  $\tau$  sector [2–4]. More recently, universality violation has also been reported in the  $\mu$  sector with a 2.6  $\sigma$  deviation from lepton universality in the LHCb result of  $B^+$  mesons decaying to  $K^+l^+l^-$  [5].

Although not strictly referring to the electroweak couplings, the unresolved proton radius puzzle [6] can also be interpreted as a violation of lepton universality. The proton radius puzzle is the seven standard deviation difference in Lamb shift measurements of the proton radius with muonic hydrogen [7, 8] and radius measurements with electrons [9–11].

The observation of any non-universal behavior could imply new physics beyond the SM. Lepton universality can be tested with high precision experiments that aim at measuring certain observables very precisely which can be calculated in the SM very accurately and where new physics effects would be enhanced. Such an observable is the ratio of leptonic decay widths of the charged kaon,  $R_K$ , defined as

$$R_K = \frac{\Gamma(K^+ \rightarrow e^+ \nu_e)}{\Gamma(K^+ \rightarrow \mu^+ \nu_\mu)} . \quad (1)$$

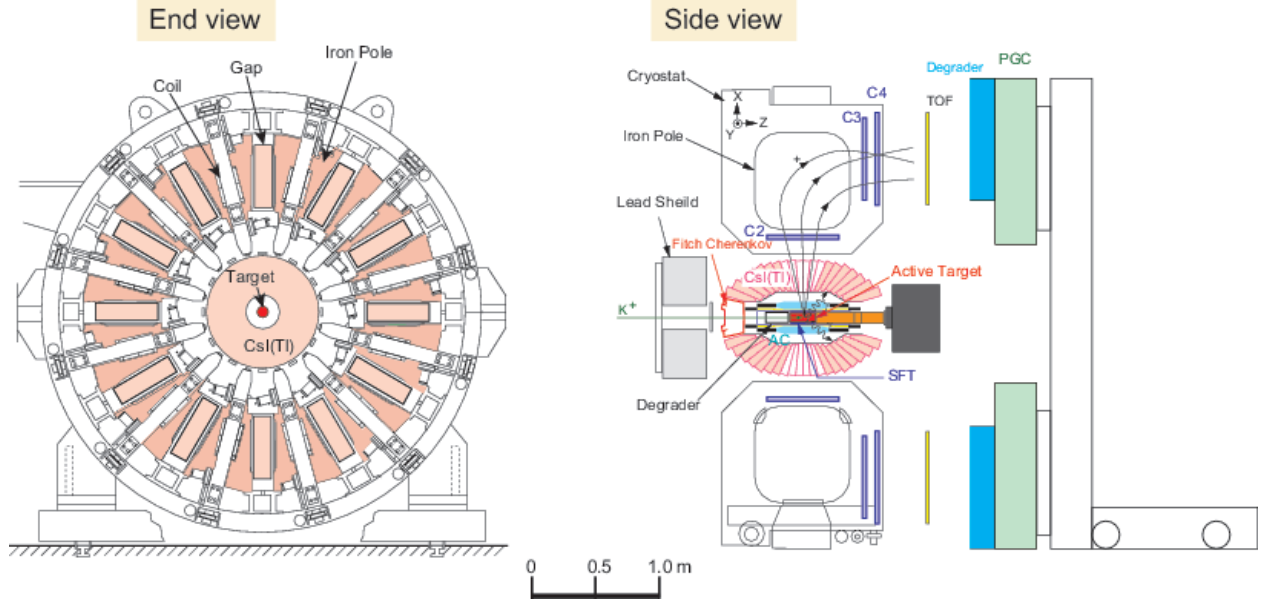


Figure 1: Schematic end and side views of the E36 setup. See text for description.

Since the hadronic uncertainties associated with the form factor of the decay drops out in leading order from the ratio of decay widths, the SM prediction is very precise, as small as 0.04%, giving a value of

$$R_K^{SM} = \frac{m_e^2}{m_\mu^2} \left( \frac{m_K^2 - m_e^2}{m_K^2 - m_\mu^2} \right)^2 (1 + \delta_r) = (2.477 \pm 0.001) \times 10^{-5}, \quad (2)$$

with a radiative correction of  $\delta_r = -0.036$  [12]. Moreover, the value of  $R_K$  is helicity-suppressed, which enhances the relative size of any effect due to new physics. New physics effects in the ratio  $R_K$  have been predicted in the minimal SUSY extension of the SM (MSSM) [13–15]. In addition,  $R_K$  is also sensitive to the neutrino mixing parameters within SM extensions involving a fourth generation of quarks and leptons [16] or sterile neutrinos [17].

The ratio  $R_K$  has been measured previously with KLOE [18] and NA62 [19], averaging to  $R_K = (2.488 \pm 0.009) \times 10^{-5}$ , consistent with the SM value.

Experiment E36 at J-PARC has been designed to measure the ratio  $R_K$  to test lepton universality with a total uncertainty of 0.25% using stopped kaons [20]. As such it provides a complementary method to the in-flight decay measurements of NA62 and KLOE, governed by different systematics.

In addition, E36 is sensitive to byproduct searches for light neutral particles in the exotic decay modes  $K^+ \rightarrow \mu^+ \nu V$  or  $K^+ \rightarrow \pi^+ V$ , with  $V \rightarrow e^+ e^-$ . Such a particle, also known as the dark or hidden photon  $A'$  or also dark  $Z'$ , could represent the hidden force carrier of a dark sector associated with dark matter [21, 22]. If it is sufficiently light and weakly coupled to the SM, it could lead to observable decays into electron-positron pairs, which can



be used to reconstruct the invariant mass of the hypothetical dark particle. Further, a possible resolution of the proton radius could be due to the existence of light neutral particles [23–27]. Such hypothetical particles can be conceived without violating existing constraints if they are fine-tuned and non-universally coupled [25–27]. In this case there would be a prediction of a strong observable signals in kaon decays, in particular in the calculable leptonic radiative mode  $K^+ \rightarrow \mu^+ \nu e^+ e^-$  [26].

## 2. Experimental Setup

Experiment E36 [20] has been part of the TREK program at J-PARC, where TREK stands for Time Reversal Experiment with Kaons. E36 has been mounted from fall 2014 – spring 2015 and completed data taking in fall 2015 at the K1.1BR beamline at J-PARC, using the existing E-246 apparatus [28] from a previous T-violation search via transverse polarization of muons in  $K^+ \rightarrow \mu^+ \pi^0 \nu_\mu$  ( $K_{\mu 3}$ ) decays at KEK [29–31]. A next-generation T-violation search in  $K_{\mu 3}$  decays (E06) has been proposed at J-PARC to take place when sufficient primary proton beam power of 100-300 kW becomes available [32]. The E-246 apparatus has been upgraded for E36 and features

- a smaller-diameter scintillating fiber target to stop the kaon beam to minimize multiple scattering and energy loss of the outgoing decay particles,
- redundant particle ID systems to distinguish  $e$  and  $\mu$  with high efficiency and low misidentification probability,
- improved near-target tracking with a Spiraling Fiber Tracker (SFT), and
- a faster readout of the CsI(Tl) calorimeter with a pile-up capable data acquisition system using FPGA based wave form digitization.

The E36 setup is shown schematically in Fig. 1. The incoming  $K^+$  is tagged with the Fitch Cherenkov and moderated down to range out inside the active volume of the stopping target, a matrix of 256 scintillating fibers oriented longitudinally along the beam, which determines the location of the kaon stop in the transverse plane. The target is surrounded by a Spiraling Fiber Tracker (SFT), consisting of two pairs of fiber layers spiraling in either helicity around the target, providing a longitudinal coordinate of the outgoing decay particle [33]. The target+SFT assembly is further surrounded by 12 time-of-flight scintillators (TOF1) and 12 aerogel (AC) counters [34] aligned with the 12 sectors of the toroidal spectrometer. Photons and positron-electron pairs from  $\pi^0$  or directly from  $K^+$  decays are registered in the highly segmented large-acceptance CsI(Tl) calorimeter barrel covering a solid angle of about  $3\pi$ . The calorimeter features 12 gaps aligned with the sectors of the toroid, allowing energetic charged  $\pi^+$ ,  $\mu^+$ , and  $e^+$  to be momentum-analyzed through the magnetic field and tracked with Multi-Wire Proportional Chambers C2-C4 in each of 12 gaps of the magnetic toroid. At the exit of each magnet gap, another set of fast scintillators (TTC and TOF2), and leadglass (PGC) counters [35] are providing trigger signals and particle identification to discriminate between  $\mu$  and  $e$ .

Three particle identification systems allow to redundantly distinguish between positrons, and muons or pions: The threshold Aerogel Cerenkov (AC) counters sensitive to positrons surround the target bundle, the time of flight (TOF) is measured between scintillators near the

target (TOF1) and in each gap (TTC and TOF2), and leadglass counters (PGC) are located at the end of each gap to identify positrons by their shower.

The data acquisition was set up for three different trigger types. All trigger types required a good kaon stop defined by the Fitch counter and minimal signals in the target. The “Positron” trigger required a good kaon stop in combination with a good gap trigger and an additional sector aerogel hit for positron candidates. The “Muon” trigger did not have any gap positron requirement and was prescaled by an order of magnitude. The third trigger type was dedicated to the light neutral boson search, by requiring at least three TOF1 counters for three charged particle to be observed, in coincidence with a good gap trigger, but no PID constraints otherwise, resulting in a tolerable count rate.

### 3. Status of E36

The E36 experiment has been performed with the TREK apparatus at J-PARC employing a  $K^+$  beam stopped in an active target consisting of scintillating fibers. The technique is different from the NA62 and KLOE experiments which used the in-flight-kaon decay method. The  $K_{e2}$  ( $p_{e^+} = 247$  MeV/c) and  $K_{\mu2}$  ( $p_{\mu^+} = 236$  MeV/c) events were detected using the TREK toroidal spectrometer. In order to compare the experimental  $R_K$  value with the SM prediction, the internal bremsstrahlung process in radiative  $K^+ \rightarrow e^+ \nu \gamma$  ( $K_{e2\gamma}^{IB}$ ) and  $K^+ \rightarrow \mu^+ \nu \gamma$  ( $K_{\mu2\gamma}^{IB}$ ) decays is included into the  $K_{e2}$  and  $K_{\mu2}$  samples, respectively. The  $R_K$  value is derived from the accepted  $K_{e2}$  and  $K_{\mu2}$  events after correcting for the detector acceptance. Charged particles from the kaon stopping target are tracked and momentum-analyzed using four-point tracking with the target+SFT and three multi-wire proportional chambers in each toroidal sector. The tracking redundancy allows to determine the efficiency of each tracking element. The  $K_{e2}$ ,  $K_{\mu2}$ , and their radiative decays were collected for a central magnetic field of the spectrometer,  $B = 1.4$  T. In order to remove  $K^+ \rightarrow \pi^0 e^+ \nu$  ( $K_{e3}$ ) and  $K^+ \rightarrow \pi^0 \mu^+ \nu$  ( $K_{\mu3}$ ) backgrounds, the  $K_{e2}$  and  $K_{\mu2}$  events are identified by requiring the  $e^+$  and  $\mu^+$  momentum to be higher than the  $K_{e3}$  and  $K_{\mu3}$  endpoints ( $p_{max} = 228$  and 215 MeV/c). Particle discrimination between  $e^+$  and  $\mu^+$  is carried out using aerogel Cherenkov (AC) counters surrounding the target, by measuring the time-of-flight (TOF) between the TOF1 and TOF2 scintillation counters, and by a lead glass shower calorimeter (PGC). The TOF1 and AC counters surround the fiber target, and the TOF2 and PGC counters are located at the exit of the spectrometer. Simulations have shown that a muon misidentification probability  $< 10^{-6}$  is adequate and achievable by using the particle ID systems in combination with the momentum selection. ... The  $R_K = \Gamma(K_{e2})/\Gamma(K_{\mu2})$  ratio can be obtained from the number of accepted events (N),  $\tilde{K}_{e2} = K_{e2} + K_{e2\gamma}^{IB}$  and  $\tilde{K}_{\mu2} = K_{\mu2} + K_{\mu2\gamma}^{IB}$ , corrected for the detector acceptance. The acceptance ratio can be calculated by a Monte Carlo simulation, and dedicated calibration datasets have been taken to validate the simulations. It should be noted that the analysis procedure is identical for both  $K_{e2}$  and  $K_{\mu2}$  except for the particle identification in order to reduce the systematic error due to the analysis. The statistical error of the  $R_K$  value will be dominated by that of the accepted  $K_{e2}$  events because the  $BR(K_{e2})/BR(K_{\mu2}) \approx 10^{-5}$ . The number of  $K_{e2}$  events has been estimated to be  $\approx 2.5 \times 10^5$  assuming 1,500 kWdays of data collection, corresponding to a statistical error of  $\Delta R_K = 0.0054$  ( $\Delta R_K/R_K = 0.2\%$ ). At the end of data taking, the actually delivered integrated beam amounted to about 1,000 kWdays.

Systematic errors have been considered due to (1) uncertainty of the detector acceptance ratio, (2) imperfect reproducibility of the experimental conditions by a Monte Carlo simulation, (3) performance of particle identification, and (4) background contamination. The total systematic error has been estimated with detailed simulation to be  $\Delta R_K/R_K = 0.15\%$  by adding all items in quadrature.

For the byproduct search of light neutral bosons  $A'$  in the processes  $K^+ \rightarrow \mu^+ \nu_\mu A'$  or  $K^+ \rightarrow \pi^+ A'$  as possible signals from the dark sector, the  $A'$  particle would be identified as a narrow peak in the  $e^+e^-$  invariant-mass distribution through its decay,  $A' \rightarrow e^+e^-$ . In the E36 experiment the  $e^+e^-$  pair has been detected in the CsI(Tl) calorimeter in coincidence with the charged muon or pion tracked in the toroidal spectrometer. A multiplicity of at least three TOF1 elements has been required for the dedicated trigger type, while the less biased muon trigger type was prescaled during data taking.

Data taking of E36 has recently been completed at J-PARC by the end of 2015. Two independent analyses have been started in two teams, one based in Japan and another in North America.

#### 4. Acknowledgments

This work has been supported by DOE Early Career Award DE-SC0003884 and DE-SC0013941 in the US, NSERC in Canada and Kaken-hi in Japan.

## References

- [1] A. Pich, arXiv:1201.0537.
- [2] K. Nakamura *et al.* (Particle Data Group), J. Phys. G **37**, 075021 (2010).
- [3] J.P. Lee *et al.* (BABAR Collaboration), Phys. Rev. D **88**, 072012 (2013).
- [4] A. Bozek *et al.* (Belle Collaboration), Phys. Rev. D **82**, 072005 (2010).
- [5] R. Aaij *et al.* (LHCb Collaboration), Phys. Rev. Lett. **113**, 151601 (2014).
- [6] R. Pohl, R. Gilman, G.A. Miller, and K. Pachucki, Annu. Rev. Nucl. Part. Sci. **63** (2013).
- [7] R. Pohl *et al.* (CREMA Collaboration), Nature, **466**, 213 (2010).
- [8] A. Antognini *et al.* (CREMA Collaboration), Science, **339**, 417 (2013).
- [9] J.C. Bernauer *et al.*, Phys. Rev. Lett. **105**, 242001 (2010).
- [10] J.C. Bernauer *et al.*, Phys. Rev. C **90**, 015206 (2014).
- [11] P.J. Mohr, B.N. Taylor, and D.B. Newell (CODATA2010), Rev. Mod. Phys. **84**, 1527 (2012).
- [12] V. Cirigliano and I. Rosell, Phys. Rev. Lett. **99**, 231801 (2007).

- [13] A. Masiero, P. Paradisi, and R. Petronzio, Phys. Rev. D **74**, 011701 (2006).
- [14] A. Masiero, P. Paradisi, and R. Petronzio, JHEP **0811**, 042 (2008).
- [15] J. Gierbach and U. Nierste, arXiv:1202.4906.
- [16] H. Lacker and A. Menzel, JHEP **1007**, 006 (2010).
- [17] A. Abada *et al.*, JHEP **1302**, 048 (2013).
- [18] F. Ambrosino *et al.* (KLOE Collaboration), Eur. Phys. J. C **64**, 627 (2009).
- [19] C. Lazzeroni *et al.* (NA62 Collaboration), Phys. Lett. B **719**, 326 (2013).
- [20] TREK/E36 proposal for J-PARC, submitted to the 10th PAC, July 2010, *Measurement of  $\Gamma(K^+ \rightarrow e^+\nu)/\Gamma(K^+ \rightarrow \mu^+\nu)$  and Search for heavy sterile neutrinos using the TREK detector system*, M. Kohl and S. Shimizu, spokespersons, [http://j-parc.jp/NuclPart/pac\\_1007/pdf/KEK\\_J-PARC-PAC2010-04.pdf](http://j-parc.jp/NuclPart/pac_1007/pdf/KEK_J-PARC-PAC2010-04.pdf); Addendum to E36, submitted to the 11th PAC, January 2011, <http://trek.kek.jp/e36/reports/addendum1.pdf>; Addendum II to E36, submitted to the 13th PAC, January 2012, [http://trek.kek.jp/e36/reports/kl2add2\\_submitted.pdf](http://trek.kek.jp/e36/reports/kl2add2_submitted.pdf).
- [21] J.D. Bjorken, R. Essig, P. Schuster, and N. Toro, Phys. Rev. D **80**, 075018 (2009).
- [22] M. Pospelov, Phys. Rev. D **80**, 095002 (2009).
- [23] V.Barger, C.W. Chiang, W.Y. Keung, D. Marfatia, Phys. Rev. Lett. **106**, 153001 (2011).
- [24] D. Tucker-Smith and I. Yavin, Phys. Rev. D **83**, 101702 (2011).
- [25] C.E. Carlson and B.C. Rislow, Phys. Rev. D **86**, 035013 (2012).
- [26] C.E. Carlson and B.C. Rislow, Phys. Rev. D **89**, 035003 (2014).
- [27] B. Batell, D. McKeen, and M. Pospelov, Phys. Rev. Lett. **107**, 011803 (2011).
- [28] J.A. Macdonald *et al.*, Nucl. Instrum. and Meth. A **506**, 60 (2003).
- [29] M. Abe *et al.* (E-246 Collaboration), Phys. Rev. D **73**, 072005 (2006).
- [30] M. Abe *et al.* (E-246 Collaboration), Phys. Rev. Lett. **93**, 131601 (2004).
- [31] M. Abe *et al.* (E-246 Collaboration), Phys. Rev. Lett. **83**, 4253 (1999).
- [32] TREK/E06 proposal for J-PARC, submitted to the 1st PAC, June 2006, *Measurement of  $T$ -violating Transverse Muon Polarization in  $K^+ \rightarrow \pi^0 \mu^+ \nu$  Decays*, J. Imazato and M. Kohl, spokespersons, [http://j-parc.jp/researcher/Hadron/en/pac\\_0606/pdf/p06-Imazato\\_2.pdf](http://j-parc.jp/researcher/Hadron/en/pac_0606/pdf/p06-Imazato_2.pdf).
- [33] O. Mineev *et al.* (TREK Collaboration), *The design and performance of a Spiral Fiber Tracker for the J-PARC E36 experiment*, to be published.

- [34] M. Tabata *et al.* (TREK Collaboration), Nucl. Instr. and Meth. in Physics Research A **795**, 206 (2015).
- [35] Y. Miyazaki *et al.* (TREK Collaboration), Nuclear Instruments and Methods in Physics Research A **779**, 13 (2015).

## 2.24 Simulation Study of $K_L$ Beam: $K_L$ Rates and Background

Ilya Larin

*Department of Physics*

*Old Dominion University*

*Norfolk, VA 23529, U.S.A.*

### Abstract

We report our simulation results for  $K_L$ -beam and neutron background production, estimated rates for certain run conditions and resolution for  $K_L$ -beam momentum.

#### 1. $K_L$ Beam Line

Our calculations have been performed for Jefferson Lab Hall D setup geometry. Primary  $K_L$ -production target has been placed in Hall D collimator cave. For the target material, we selected beryllium as for thick targets  $K_L$ -yield roughly proportional to the radiation length and density, which gives beryllium as the best candidate. Beam plug and sweeping magnet are placed right after the target. For our calculations we took a simple beam plug: 15 cm thick piece of lead. Sweeping magnet is cleaning up charged component and has a field integral 2 Tesla . meter, which is enough to remove all charged background coming out of the beam plug. Vacuum beam pipe has 7 cm diameter and preventing neutron rescattering in air. Where are two collimators: one placed before the wall between collimator cave and experimental hall, another - in front of the Hall D detector. Distance between primary Be target and liquid hydrogen (LH<sub>2</sub>) target (located inside Hall D detector) has been taken 16 m in our calculations, it can be increased upto 20 m.

#### 2. $K_L$ Production

We simulated  $K_L$ -production in photon bremsstrahlung beam produced by 12 GeV electron beam in Hall D tagger amorphous radiator. We analyzed  $K_L$ -production via  $\phi$ -meson photoproduction in detail. This is one of the main mechanisms of  $K_L$ -production at our energy range. It gives the same number of  $K^0$  and  $\bar{K}^0$ . Another mechanism is hyperon photoproduction (which gives only  $K^0$ ) was not studied in our simulations separately. Instead, we have taken as an alternative model Pythia generator [1], which includes hyperon production.  $\phi$ -meson photoproduction total and differential cross sections on proton and complex nuclei (coherent and incoherent) were taken from Refs. [2,3]. Angular distributions for  $\phi \rightarrow K_L K_S$  decay, we used are from Ref. [2, 4, 5]. These calculations show that  $\phi$  decay in its rest frame is going mostly perpendicular to the axis of  $\phi$  momentum. Since  $K_L$ s need to stay on original photon beam direction to get LH<sub>2</sub> target, this condition requires that  $\phi$  production and decay angles in laboratory frame should be about the same. That means we will have in the LH<sub>2</sub> only  $K_L$ s from  $\phi$ -mesons produced at relatively high  $t$ . It suppresses the number of "useful"  $K_L$ s by factor of  $\sim 3$  or more (in comparison with the case if  $K_L$  and  $K_S$  momenta are parallel to  $\phi$  momentum).  $K_L$  absorption used in our calculations was studied in Ref. [6] very well. About 80% of produced  $K_L$ s will be absorbed in Be target itself and beam plug. This value of absorbed  $K_L$ s can be reduced by optimizing beam plug setup.

### 3. $K_L$ Beam Parameters

One of the main  $K_L$ -beam parameters is momentum distribution. Momentum spectrum is a function of the distance and angle. We are giving here resulting spectra for  $K_L$  reaching  $\text{LH}_2$  target. Results of our simulations for  $K_L$  momentum spectrum is shown on Fig. 1. The spectrum first has increasing shape since  $\phi$  decay cone angle decreasing at higher  $\gamma$ -beam and  $K_L$  momentum. This selecting lower  $\phi$  production  $t$  values, which are more favorable according to  $\phi$  differential cross section. At certain point highest possible  $\gamma$ -beam momentum is reached and  $K_L$  momentum spectrum is dying out pretty fast. For comparison, we selected part of  $K_L$  spectrum from Pythia generator originated only from  $\phi$  decays and showed it on the same plot (red histogram).

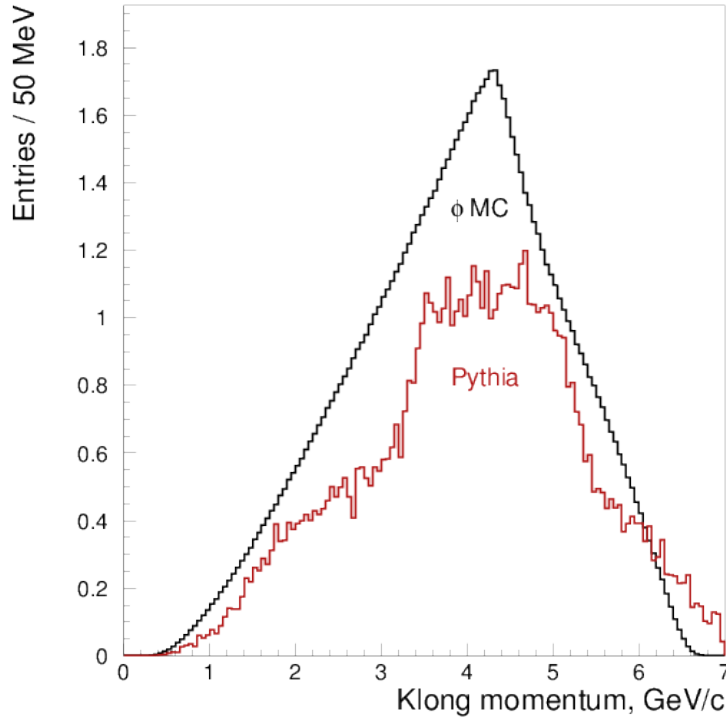


Figure 1:  $K_L$  momentum spectra originated from  $\phi$  decays: black histogram - our simulation using GEANT [7], red - Pythia generator result [1].

Pythia shows, that  $\phi$  decays give about 30% of  $K_L$ s. Number of  $K^0$  exceeds number of  $\bar{K}^0$  by 30% according to this generator for our conditions. Their momentum spectra are shown on Fig. 2 separately.

To estimate expected rate of  $K_L$  at  $\text{LH}_2$  target we used the following conditions: electron beam current is  $3.2 \mu\text{A}$ , tagger radiator thickness is 1% of radiation length, Be target thickness is 40 cm, distance Be to  $\text{LH}_2$  target is 16 m, radius of  $\text{LH}_2$  target is 2 cm. Our calculations are related to the  $K_L$  flux at that distance and solid angle. For  $K_L$ -beam intensity under the above condition, we got 100  $K_L$ s per second for our  $\phi$  photoproduction simulation and

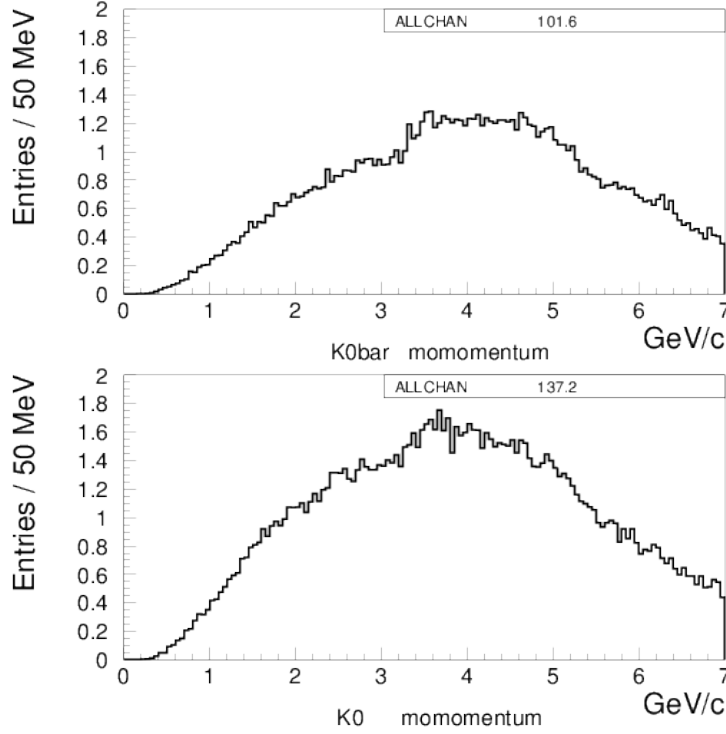


Figure 2:  $\bar{K}^0$  (top plot) and  $K^0$  (bottom plot) momentum spectra from Pythia generator.

240  $K_L$ s per second from all sources from Pythia. There are ways to increase the  $K_L$ -beam intensity by increasing tagger radiator thickness, electron beam current and other parameters. Increasing  $LH_2$  target radius will increase number of  $K_L$ s reaching it proportionally to the solid angle. For example for  $LH_2$  target radius 4 cm, electron beam current 5  $\mu A$ , 5% rad. length radiator and increased Be target sizes we shall be able to obtain beam rate about 7,000  $K_L$ s per second from all production mechanisms at  $LH_2$  target face. For comparison this value corresponds to  $\sim 10$  million of produced  $K_L$ s in Be target per second.

#### 4. $K_L$ Beam Resolution

$K_L$ -beam momentum can be measured using TOF - time between accelerator bunch and reaction in  $LH_2$  target detected by start counter. Hall D tagger timing can not be used at such high intensity conditions. Thus TOF resolution is a quadratic sum of accelerator time and start counter time resolutions. Since accelerator signal has very good time resolution ( $\sim 0.1$  ns or better), TOF resolution will be defined by start counter. Hall D start counter has resolution  $\sim 0.35$  ns. This value can be hopefully improved with upgrading counter design and parameters. In our calculations we used an optimistic value of 0.25 ns start counter time resolution. Of course to get TOF information electron beam needs to have narrow bunch time structure with the distance between bunches at least 30 ns. At low ( $< 1$  GeV/c)  $K_L$  momenta uncertainty in  $K_L$  production point position within Be target will also affect TOF



calculation precision. Fig. 3 shows TOF and beam momentum resolution as a function of  $K_L$  beam momentum.

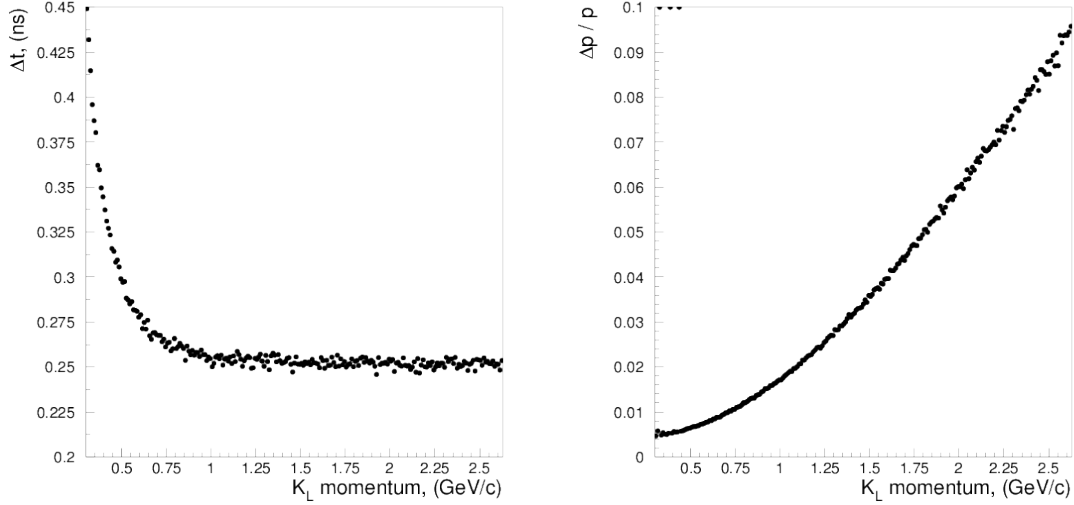


Figure 3:  $K_L$ -beam TOF (left plot) and momentum (right plot) resolution as a function of momentum.

TOF resolution is flat for momenta higher than 1 GeV/c. Momentum resolution is growing with momentum value, for 1 GeV/c it is  $\sim 1.7\%$ , for 2 GeV/c  $\sim 6\%$ .

## 5. $K_L$ Beam Background

Background conditions is one of the most important parameter of the beam. After passing through 30 radiation length beam plug and swiping out charged background component, we will have some residual  $\gamma$  background and neutrons produced by electromagnetic showers. Momentum spectrum of residual  $\gamma$ s shown on Fig. 4.

It decreases exponentially with increasing  $\gamma$  energy. For the rates we obtained  $\sim 100,000$  per second for  $\gamma$ s with energy above 50 MeV and  $\sim 1,000$  per second for  $\gamma$ s above 500 MeV.

The most important and unpleasant background for  $K_L$ -beam is neutron background. Special care needs to be taken to estimate and if possible to eliminate this kind of background. In our calculations to estimate neutron background we used two independent program packages: Pythia [1] and DINREG [8]. Both packages give the same order of magnitude neutron background level. At our condition it is  $\sim 140$  neutrons per second at LH<sub>2</sub> target for neutrons with momenta higher than 500 MeV/c. These spectra along with  $K_L$  momentum spectrum are shown on Fig. 5.

Additionally we calculated muon production level. Muon will be swiped out of the beam line thus they are not our background. But since their high penetration ability it might be important the for purposes of the shielding. We taken into account only Bethe-Heitler muon production process. Muons from pion decays and other production mechanisms will increase total muon yield only slightly. They were not included in our model. Number of produced

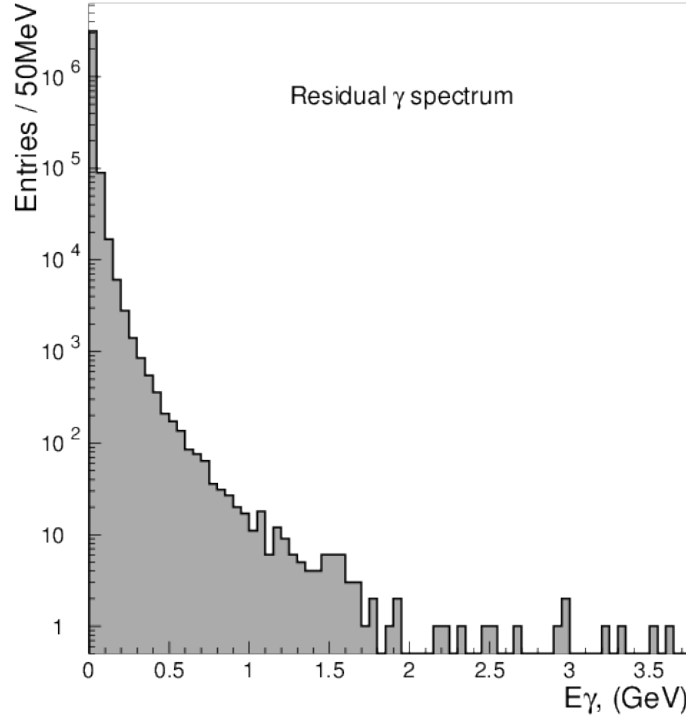


Figure 4: Momentum spectrum of residual  $\gamma$ s.

muon in Be target and lead beam plug is about the same, lead originating muons have much softer momentum spectrum. Estimated number of produced muons  $\sim 6$  million per second. Their momentum spectrum is shown on Fig. 6.

Half of muons have momentum higher than  $2 \text{ GeV}/c$ ,  $\sim 10\%$  of muons have momentum higher than  $6 \text{ GeV}/c$  and  $\sim 1\%$  of muons - momentum above  $10 \text{ GeV}/c$ .

## 6. Summary

In the summary part, we want to emphasize that  $K_L$ -beam facility opens horizons for new rich physics. Jefferson Lab GlueX spectrometer has very good acceptance and resolution parameters [9], which perfectly fit  $K_L$ -beam facility requirements. Expected rates for  $K_L$ -beam with increased  $\gamma$ -beam luminosity will allow to collect statistics order of magnitude higher than other facilities can provide. One of the main advantage of such facility is that  $K_L$ -beam is produced by  $\gamma$ -beam which provides low neutron background level comparing with hadron produced  $K_L$ -beam. To get more precise  $K_L$ -beam rates and neutron background estimations as well as radiation levels induced, it is important to conduct a few days measurements on low intensity test beam.

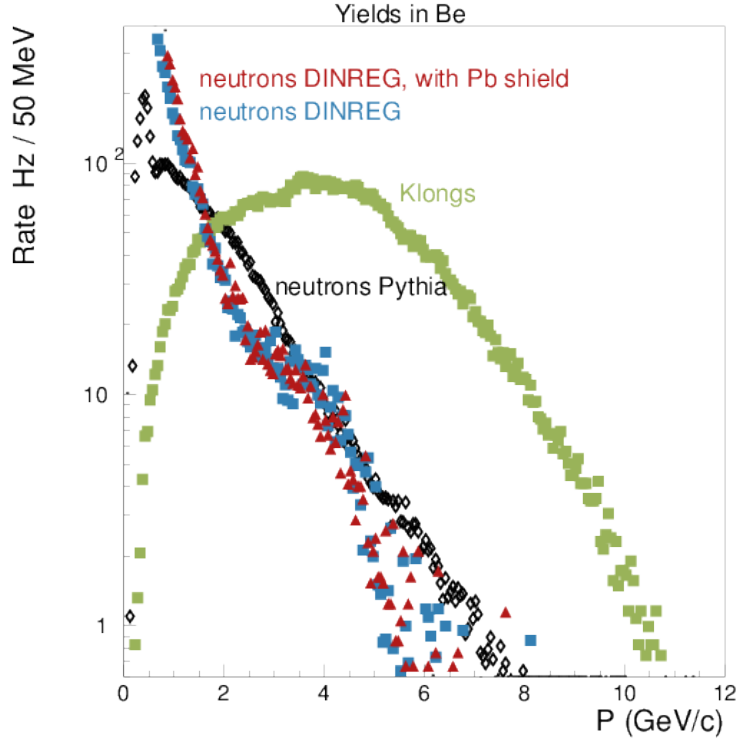


Figure 5:  $K_L$  and neutron momentum spectra obtained with different packages.

## 7. Acknowledgments

I thank the organizing committee for the possibility to participate in this Workshop. I also want to express my special thanks to Igor Strakovsky and Moskov Amaryan for fruitful discussions which help me a lot in  $K_L$ -beam analysis. This work is supported, in part, by the U.S. Department of Energy, Office of Science, Office of Nuclear Physics, under Award Number DE-FG02-96ER40960.

## References

- [1] We used the Pythia version modified for the GlueX Collaboration, Hall D at Jefferson Lab. <http://home.thep.lu.se/torbjorn/Pythia.html>.
- [2] A. Titov and T.-S. Lee, Phys. Rev. C **67**, 065205 (2003).
- [3] G. McClellan *et al.*, Phys. Rev. Lett. **26**, 149 (1971).
- [4] A. Titov and B. Kampfer, Phys. Rev. C **76**, 035202 (2007).
- [5] T. Mibe *et al.* (CLAS Collaboration), Phys. Rev. C **76**, 052202 (2007).

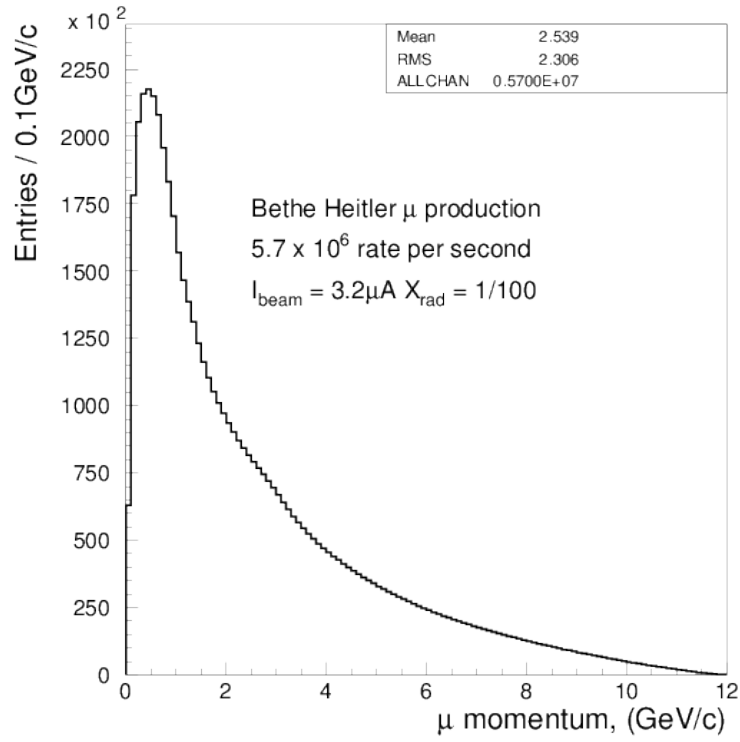


Figure 6: Muon momentum spectrum for Bethe-Heitler production.

- [6] G.W. Brandenburg *et al.*, Phys. Rev. D **7**, 708 (1973).
- [7] Application Software Group, *GEANT - Detector Description and Simulation Tool*, CERN Program Library Long Writeup W5013, CERN, Geneva, Switzerland (1994).
- [8] P. Degtiarenko, Private communications, 2015.
- [9] S. Taylor,  *$K_L$  Simulation Studies with the GlueX Detector*, these Proceedings.

## 2.25 $K_L$ Simulation Studies with the GlueX Detector

Simon Taylor

Thomas Jefferson National Accelerator Facility

Newport News, VA 23606, U.S.A.

### Abstract

Results of simulations of three reactions of interest for a potential  $K_L$  program in Hall D at Jefferson Lab, namely  $K_L p \rightarrow pK_S$ ,  $\pi^+\Lambda$ , and  $K^+\Xi^0$ , are presented.

### 1. Introduction

The GlueX detector is a large acceptance detector based on a solenoid design with good coverage for both neutral and charged particles. This article describes some simulations of events generated by  $K_L$  beam particles interacting with a liquid hydrogen target at the center of the solenoid. The GlueX detector is used to detect one or all of the final state particles. I will be focusing on a few of the simplest two-body reactions, namely  $K_L p \rightarrow pK_S$ ,  $K_L p \rightarrow \Lambda\pi^+$ , and  $K_L p \rightarrow K^+\Xi^0$ .

### 2. Event Generation, Simulation and Reconstruction

The  $K_L$  beam is generated by sampling the momentum distribution of  $K_L$  particles coming from the decays of  $\phi$  mesons produced by interactions of a photon beam with a beryllium target 16 meters upstream of the liquid hydrogen target. The  $K_L$  beam profile was assumed to be uniform within a 2 cm radius at the hydrogen target.

The cross section model for the  $pK_S$  channel was determined by parameterizing fits to the existing data for  $W \leq 2.17$  GeV and connecting the cross section at  $W = 2.17$  GeV to a power-law approximation to the cross section for higher  $W$ . The parametrization for low  $W$  took the form

$$\frac{d\sigma}{d\Omega} = f_0(W)P_0(\cos\theta) + f_1(W)P_1(\cos\theta) + f_2(W)P_2(\cos\theta), \quad (1)$$

where  $P_0$ ,  $P_1$ , and  $P_2$  are the first three Legendre polynomials and  $f_0$ ,  $f_1$ , and  $f_2$  were determined empirically. The high- $W$  behavior was modeled according to the results reported in Brandenburg *et al.*, [1]: the total cross section falls off as function of the  $K_L$  momentum  $p_K$  according to  $\sigma \propto p_K^{-2.1}$  and the angular dependence for high  $W$  depended on  $u' = u - u_{max}$ ,  $s$  and  $t$  according to

$$\frac{d\sigma}{dt} \propto p_K^{-1.33} e^{(3.1+2.8 \log s)t}, \quad (2)$$

$$\frac{d\sigma}{du'} \propto p_K^{-5.24} e^{5.4u'}. \quad (3)$$

The cross section model for the  $\Lambda\pi^+$  channel was based on distributions from Yamartino [2].

The cross section model for the  $K^+\Xi^0$  channel was based on parametrizations of functions from Jackson *et al.* [3].

The generated events were passed through a full GEANT3-based Monte Carlo of the GlueX detector. The detector consists of a solenoid magnet enclosing devices for tracking charged particles and detecting neutral particles and a forward region consisting of two layers of scintillators (TOF) and a lead-glass electromagnetic calorimeter (FCAL). A schematic view of the detector is shown in Fig. 1. The magnetic field at the center of the bore of the magnet for standard running conditions is about 2 T. The trajectories of charged particles produced by interactions of the beam with the 30-cm liquid hydrogen target at the center of the bore of the magnet are measured using the Central Drift Chamber for angles greater than  $\sim 20^\circ$  with respect to the beam line. Forward-going tracks are reconstructed using the Forward Drift Chambers. The timing of the interaction of the Kaon beam with the hydrogen target is determined using signals from the Start Counter, an array of 30 thin (3 mm thick) scintillators enclosing the target region. Photons are registered in the central region by the Barrel Calorimeter (BCAL).

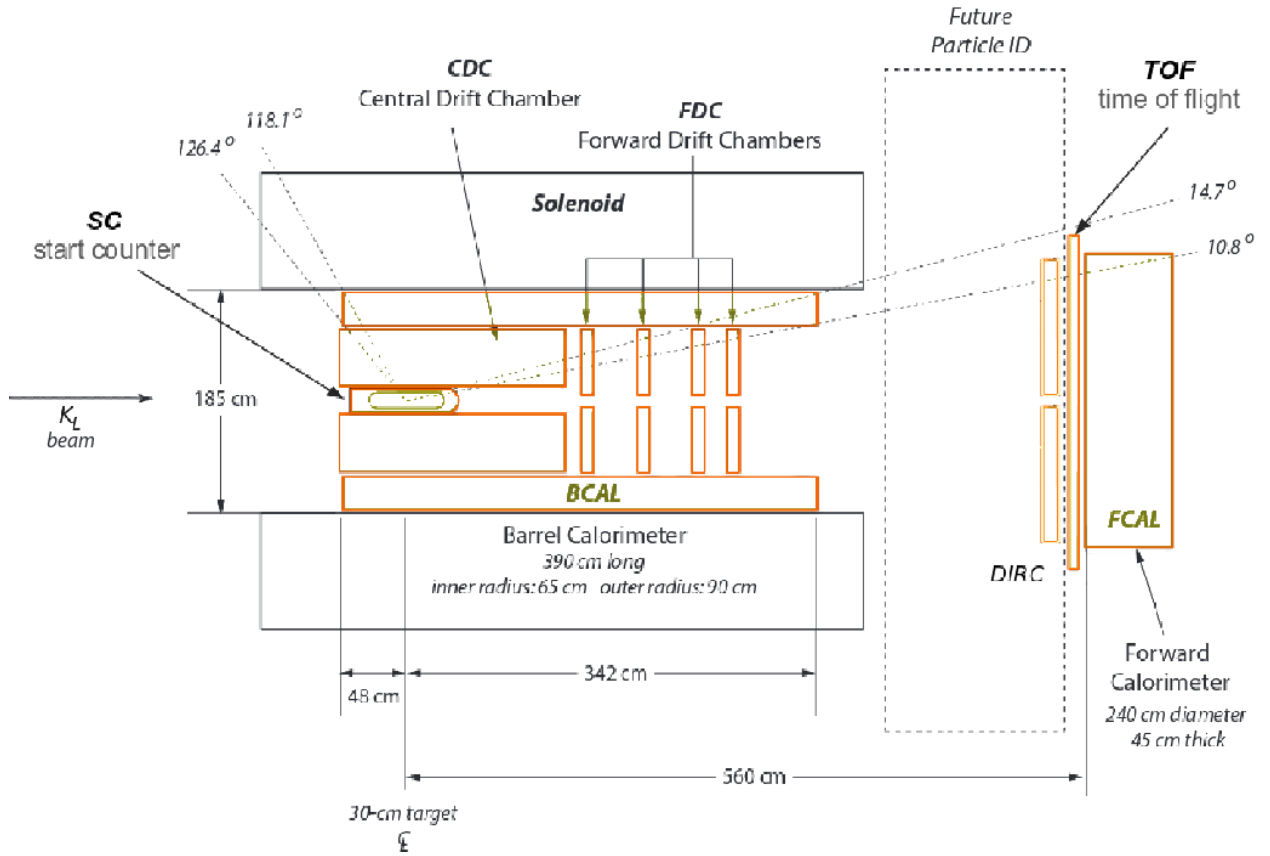


Figure 1: Schematic view of the GlueX detector.

For each topology, one particle (the proton for the  $pK_S$  channel, the  $\pi^+$  for the  $\Lambda\pi^+$  channel and the  $K^+$  for the  $K^+\Xi^0$  channel) provides a rough determination for the position of the primary vertex along the beam line that is used in conjunction with the start counter to determine the flight time of the  $K_L$  from the beryllium target to the hydrogen target. Protons, pions, and Kaons are distinguished using a combination of  $dE/dx$  in the chambers and time-of-flight to the outer detectors (BCAL and TOF). The energy loss and timing distributions

for the  $pK_S$  channel are shown in Fig. 2; the distributions are similar for the  $\Lambda\pi^+$  channel, where a proton band arises from the  $\Lambda \rightarrow p\pi^-$  decay channel. Also shown is the  $dE/dx$  distribution for the  $K^+\Xi^0$  channel, where a prominent Kaon band can be seen, along with pion and proton bands arising from  $\Lambda$  decays.

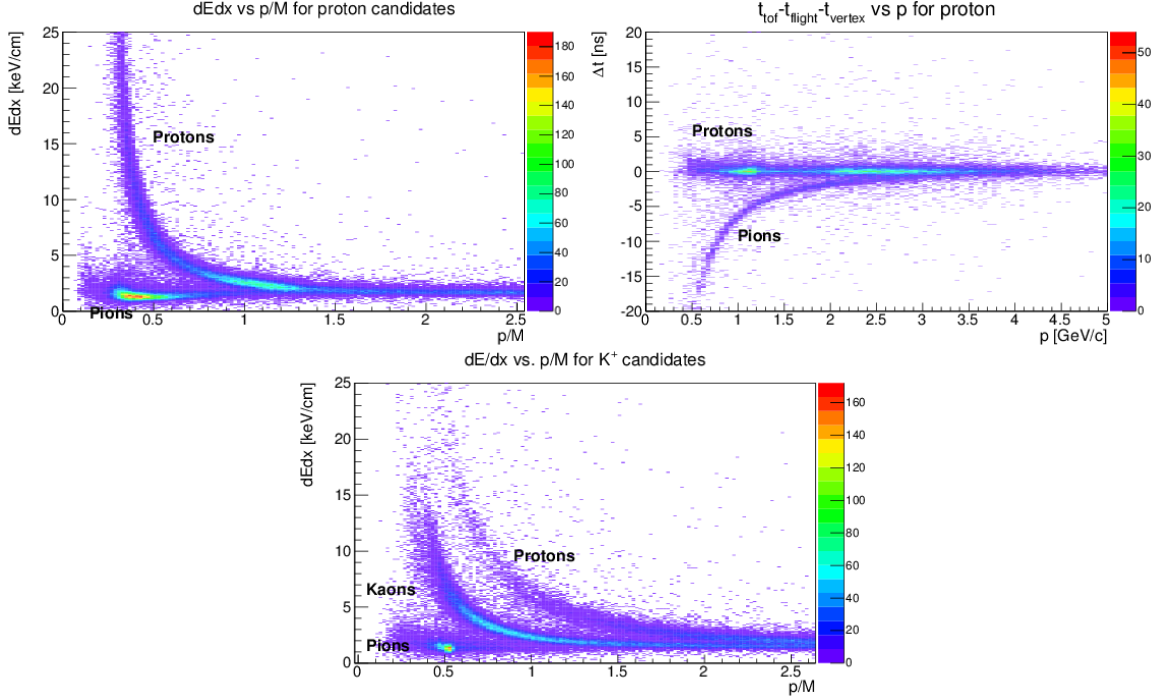


Figure 2: Particle identification: (top left)  $dE/dx$  for the  $pK_S$  channel; (top right) time difference at the primary “vertex” for the proton hypothesis for the  $pK_S$  channel using the TOF; (bottom)  $dE/dx$  for the  $K^+\Xi^0$  channel. The proton and pion bands arise from the decay of the  $\Lambda$ .

### 3. Results for each Topology

#### (a) $K_L p \rightarrow pK_S$

The  $K_L$  momentum distribution for the  $pK_S$  channel and the mass distribution for the  $K_S$  recoiling against the proton are shown in Fig. 3. The missing mass distribution suffers from long non-Gaussian tails.

Since the GlueX detector has full acceptance in  $\phi$  for charged particles and large acceptance in  $\theta$  (roughly  $1^\circ \sim 140^\circ$ ), reconstruction of full events is feasible. For the  $pK_S$  channel, I take advantage of the branching ratio of 69.2% for  $K_S \rightarrow \pi^+\pi^-$  [4]: the invariant mass of the  $\pi^+\pi^-$  pair and  $W$  as computed from the four-momenta of the proton and the two pions is shown in Fig. 4. After combining the four-momenta of the final state particles with the four-momenta of the beam and the target, the missing mass squared for the full reaction should be zero, which is also shown in Fig. 4. A comparison between two methods for computing  $W$ , one using the  $K_L$  momentum and

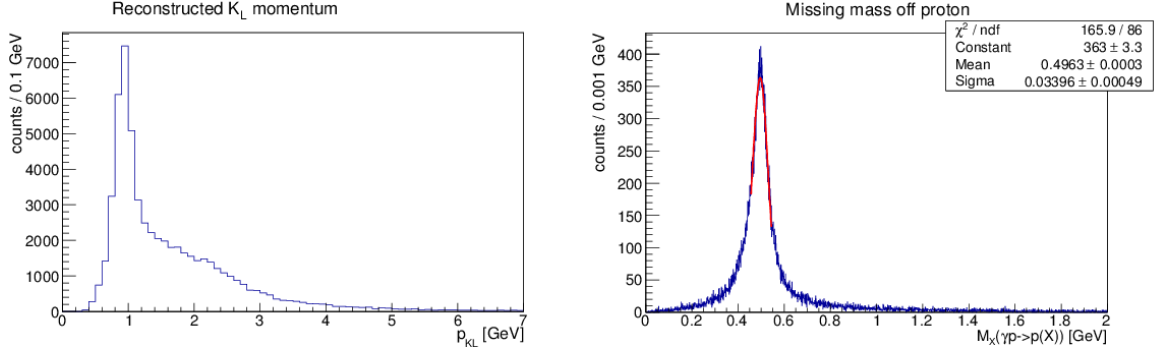


Figure 3:  $K_L$  momentum distribution (left) and missing mass off the proton (right) for the  $pK_S$  channel.

the other using the final state particles, is shown in Fig. 5. Finally, I require conservation of energy and momentum in the reaction by applying a kinematic fit to the data. After applying a 0.1 cut on the confidence level of the fit, I computed an estimate for the reconstruction efficiency as a function of  $W$  as shown in Fig. 6. The efficiency is  $\varepsilon = N(W, reconstructed)/N(W, thrown)$ . Here the efficiency includes the branching ratio for  $K_S \rightarrow \pi^+\pi^-$ . The average reconstruction efficiency is about 7%.

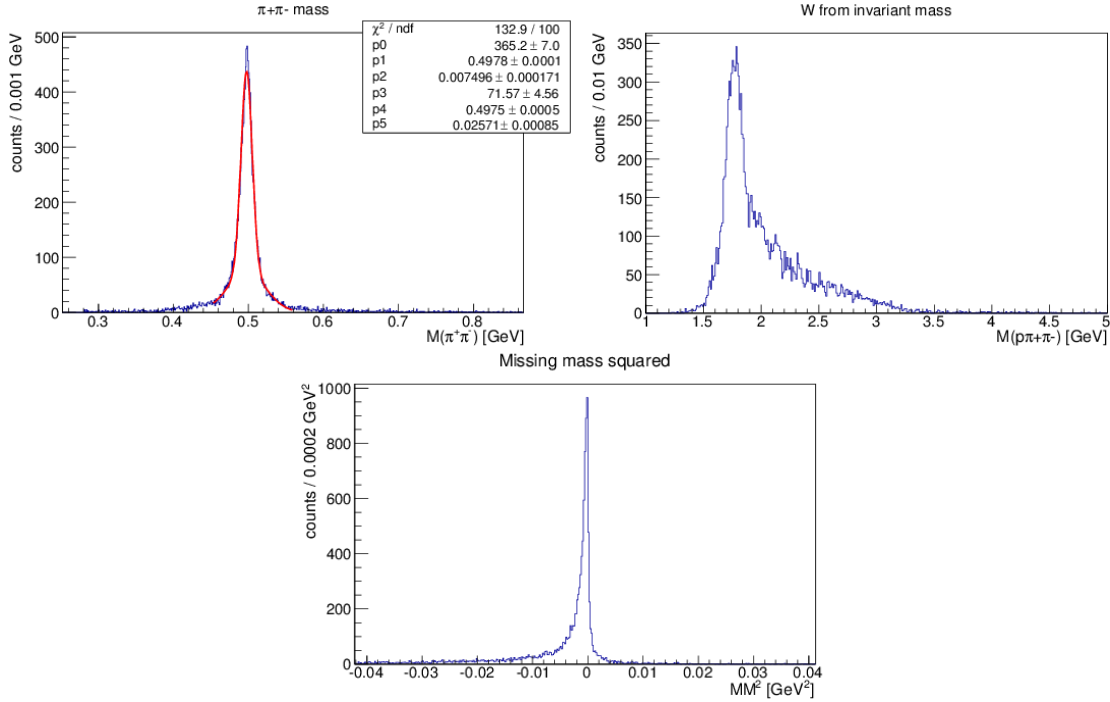


Figure 4: Full reconstruction for  $K_L p \rightarrow p K_S$ ,  $K_S \rightarrow \pi^+\pi^-$ : (top left)  $\pi^+\pi^-$  invariant mass; (top right)  $W$  computed from  $p\pi^+\pi^-$  invariant mass; (bottom) missing mass squared for the full reaction.

(b)  $K_L p \rightarrow \Lambda \pi^+$



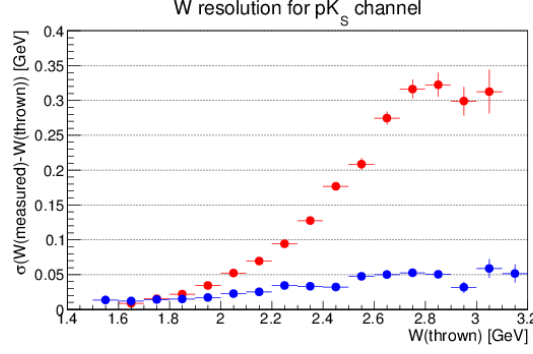


Figure 5: W resolution for the  $pK_S$  channel.

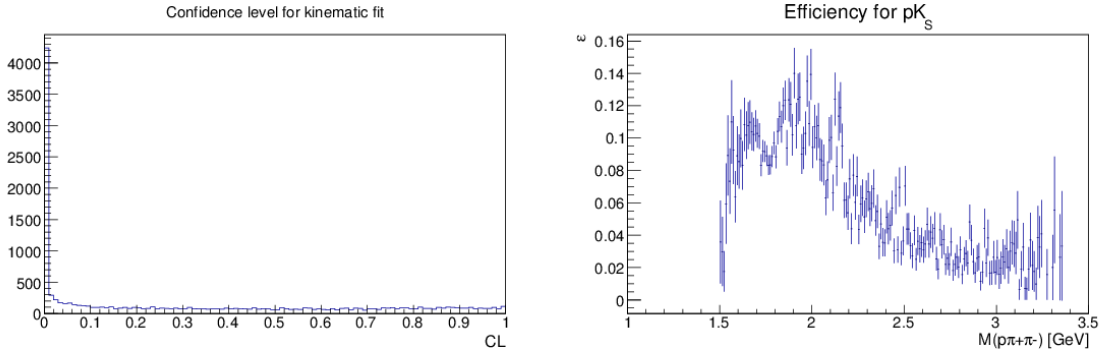


Figure 6: (left) Confidence level distribution for kinematic fit for the  $pK_S$  channel. (right) Estimate for efficiency for full reconstruction of the  $K_L p \rightarrow p K_S$ ,  $K_S \rightarrow \pi^+ \pi^-$  reaction chain as a function of  $W$ .

The reconstructed  $K_L$  momentum distribution and the missing mass off the  $\pi^+$  for the  $\gamma p \rightarrow \Lambda \pi^+$  simulation are shown in Fig. 7. As with the previous topology, the missing mass distribution has very long non-Gaussian tails.

Taking advantage of the large (63.9%) branching ratio for  $\Lambda \rightarrow p \pi^-$  [4], the full final state can be reconstructed. The mass distributions for this reaction chain are shown in Fig. 8. A comparison of the  $W$  resolution using two methods (one using the  $K_L$  momentum and the other using the four-momenta of the final state particles) is shown in Fig. 9. After applying a kinematic fit to the data and cutting at a confidence level of 0.1, I determined the efficiency as a function of  $W$ , as shown in Fig. 10. Here the efficiency includes the branching ratio for  $\Lambda \rightarrow p \pi^-$ . The average efficiency is about 2%.

(c)  $K_L p \rightarrow K^+ \Xi^0$

The reconstructed  $K_L$  momentum distribution and the missing mass off the  $K^+$  for the  $\gamma p \rightarrow K^+ \Xi^0$  simulation are shown in Fig. 11. The  $\Xi^0$  mass distribution reconstructed using the missing mass technique is broad (full-width-at-half-maximum  $\approx 300$  MeV). The  $\Xi^0$  decays almost 100% of the time to  $\Lambda \pi^0$  [4]. Here we take advantage of the large branches for  $\Lambda \rightarrow p \pi^-$  and  $\pi^0 \rightarrow \gamma \gamma$  to reconstruct  $\Xi^0$ 's using the four-momenta for all of the final state particles. The reconstructed mass distributions are shown in Fig. 12. A

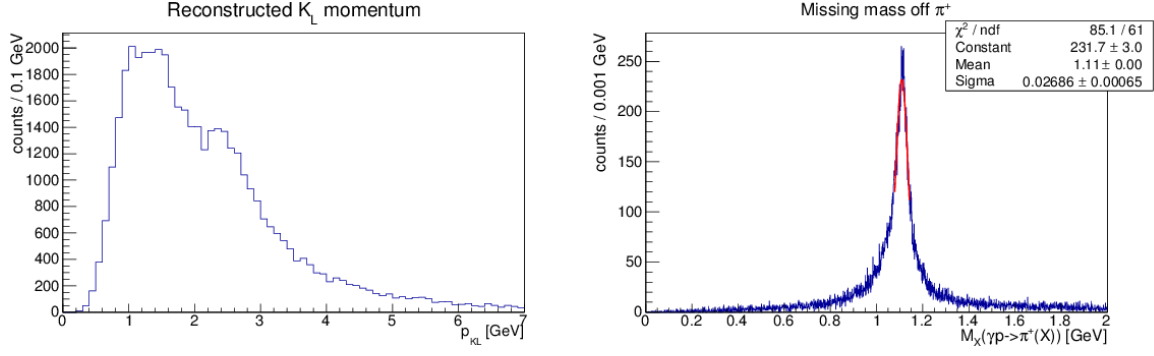


Figure 7:  $K_L$  momentum distribution (left) and missing mass off the proton (right) for the  $\Lambda\pi^+$  channel.

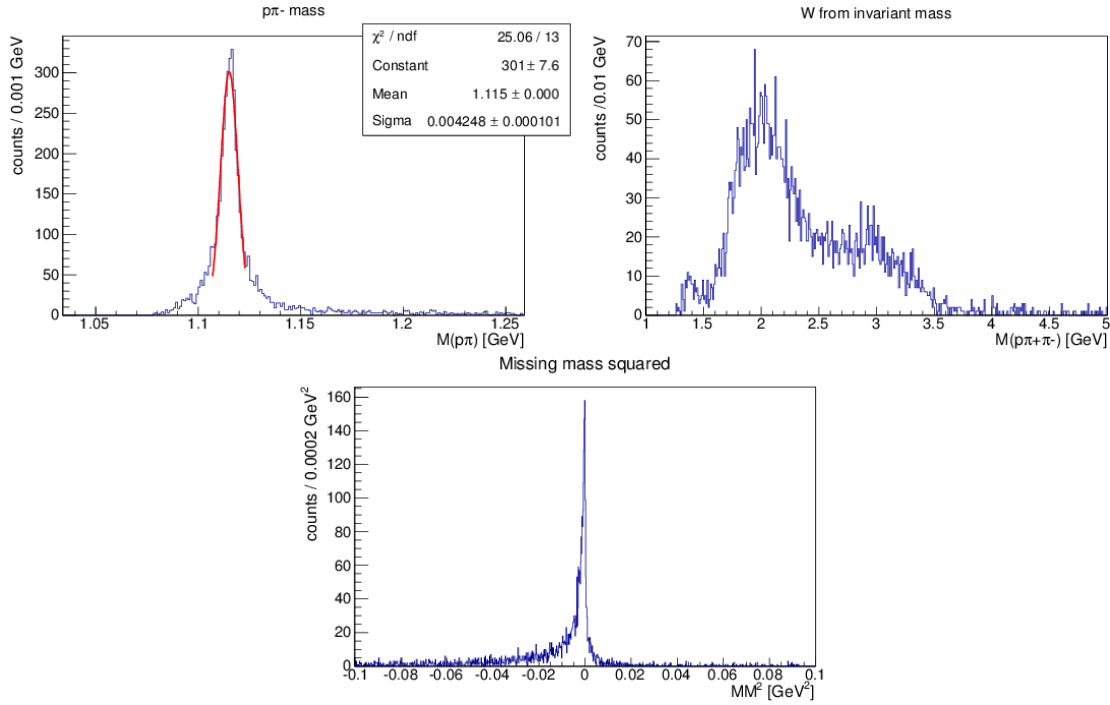


Figure 8: Full reconstruction for  $K_L p \rightarrow \Lambda\pi^+$ ,  $\Lambda \rightarrow p\pi^-$ : (top left)  $p\pi^-$  invariant mass; (top right)  $W$  computed from  $p\pi^+\pi^-$  invariant mass; (bottom) missing mass squared for the full reaction.

comparison of the two methods for computing  $W$  is shown in Fig. 13. An estimate for the efficiency as a function of  $W$  after applying a kinematic fit to the data and cutting at a confidence level of 0.1 is shown in Fig. 14. The average efficiency is about 0.4%. This efficiency includes the branching ratios for the  $\Lambda$  and  $\pi^0$  decays. Also shown is the invariant mass of the  $\Xi^0$  constructed in  $p\pi^-2\gamma$ . The peak is much narrower than the  $\Xi^0$  peak seen in missing mass.

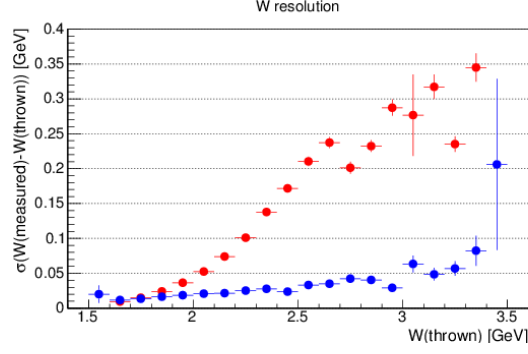


Figure 9:  $W$  resolution for the  $\Lambda\pi^+$  channel.

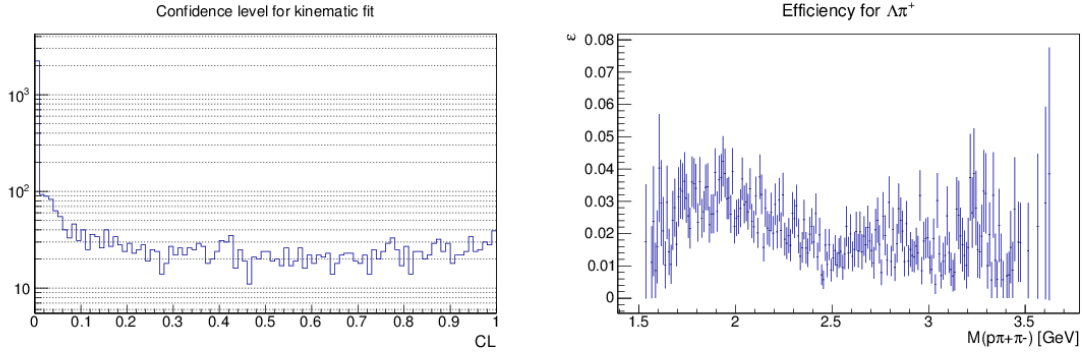


Figure 10: (left) Confidence level distribution for kinematic fit for the  $\Lambda\pi^+$  channel. (right) Estimate for efficiency for full reconstruction of the  $K_L p \rightarrow \Lambda\pi^+$ ,  $\Lambda \rightarrow p\pi^-$  reaction chain as a function of  $W$ .

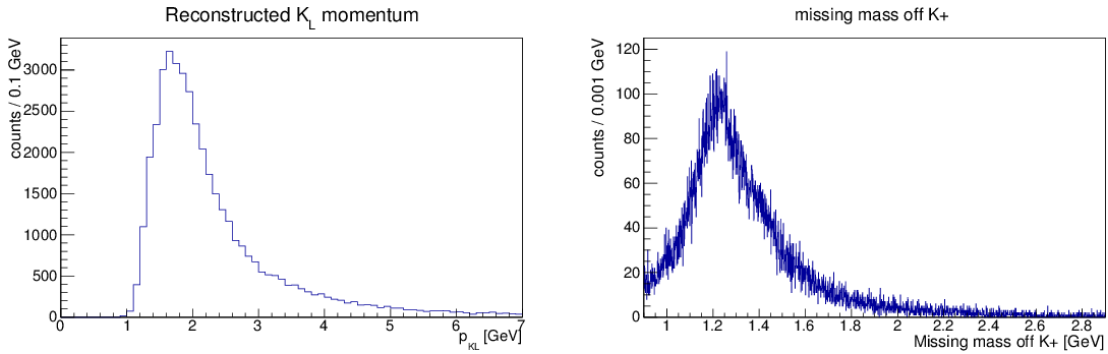


Figure 11:  $K_L$  momentum distribution (left) and missing mass off the proton (right) for the  $K^+\Xi^0$  channel.

#### 4. Remarks

For all topologies under consideration here, the  $W$  resolution using the measured  $K_L$  momentum worsens considerably as  $W$  increases, whereas the  $W$  resolution using the final state particles is flatter as a function of  $W$ . Resolution at the level of 50 MeV or less can be achieved with the latter technique, at the expense of efficiency. One source for the ineffi-

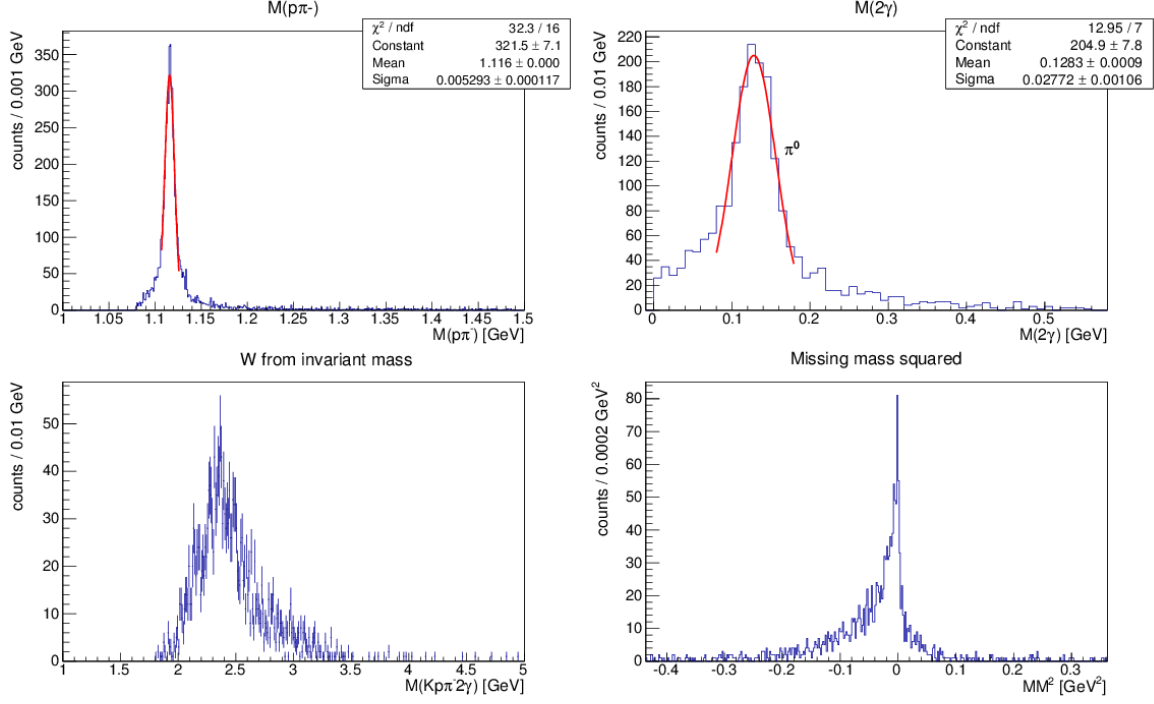


Figure 12: Full reconstruction for  $K_L p \rightarrow K^+ \Xi^0$ ,  $\Xi^0 \rightarrow \Lambda \pi^0$ ,  $\Lambda \rightarrow p \pi^-$ ,  $\pi^0 \rightarrow \gamma \gamma$ : (top left)  $p\pi^-$  invariant mass; (top right) two photon invariant mass; (bottom left)  $W$  computed from  $K^+ p \pi^- 2\gamma$  invariant mass; (bottom right) missing mass squared for the full reaction.

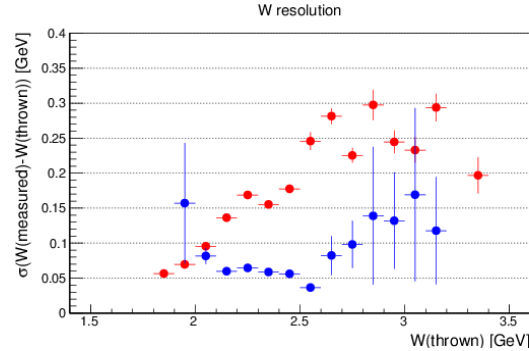


Figure 13:  $W$  resolution for the  $K^+ \Xi^0$  channel.

ciency is the spiraling of low-momentum pions in the magnetic field of the GlueX solenoid, which makes track finding and fitting difficult. This can be mitigated by running the solenoid at a lower current than the standard current for regular GlueX runs. The preliminary kinematic fitting results are encouraging and further improvement in the  $W$  resolution can be expected for the case where events are fully reconstructed.

## 5. Acknowledgments

The author would like to thank Ilya Larin for providing event generation code and Mark

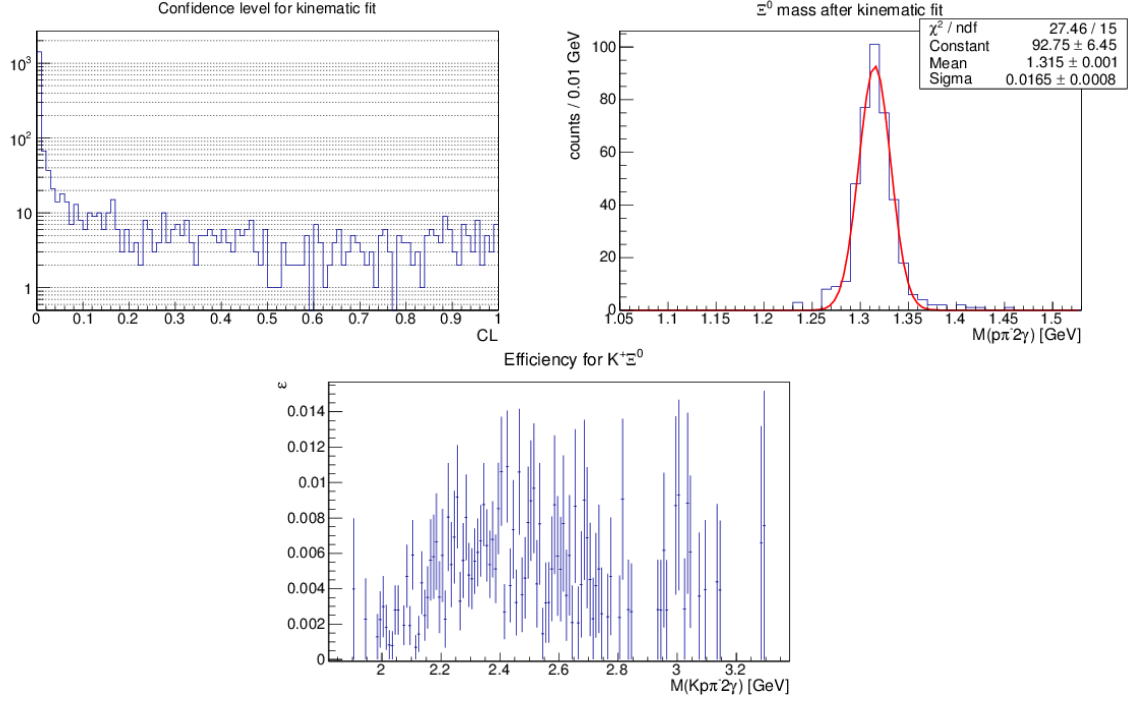


Figure 14: (top left) Confidence level distribution for kinematic fit for the  $K^+\Xi^0$  channel. (top right)  $\Xi^0$  mass distribution after kinematic fit with a 0.1 confidence level cut. (bottom) Estimate for efficiency for full reconstruction of the  $K_L p \rightarrow K^+\Xi^0$ ,  $\Xi^0 \rightarrow \Lambda\pi^0$ ,  $\Lambda \rightarrow p\pi^-$ ,  $\pi^0 \rightarrow \gamma\gamma$  reaction chain as a function of  $W$ .

Manley for providing plots of cross section data for the  $K_L p \rightarrow pK_S$  reaction. This material is based upon work supported by the U.S. Department of Energy, Office of Science, Office of Nuclear Physics under contract DE-AC05-06OR23177.

## References

- [1] G.W. Brandenburg *et al.*, Phys. Rev. D **9**, 1939 (1974).
- [2] R. Yamartino, Ph.D. Thesis, SLAC (1974); SLAC-R-0177.
- [3] B.C. Jackson, Y. Oh, H. Haberzettl, and K. Nakayama, Phys. Rev. C **91**, 065208 (2015).
- [4] K.A. Olive *et al.* (Particle Data Group), Chin. Phys. C **38**, 090001 (2014).

## 2.26 Compact Photon Source Conceptual Design

Pavel Degtyarenko and Bogdan Wojtsekhowski

*Thomas Jefferson National Accelerator Facility*

*Newport News, VA 23606, U.S.A.*

### Abstract

We describe options for the production of an intense photon beam at the CEBAF Hall D Tagger facility, needed for creating a high-quality secondary  $K_L^0$  delivered to the Hall D detector. The conceptual design for the Compact Photon Source apparatus is presented.

### 1. Introduction

An intense high energy gamma source is a pre-requisite for the production of the  $K_L^0$  beams needed for the new proposed experiments at Hall D. Here we describe a new approach to designing such photon sources. We will discuss possible practical implementation of the new approach in the design, adjusted to the parameters and limitations of the available infrastructure. The plan view of the present Tagger vault area is shown in Fig. 1.

### 2. Available facilities and Options at the Tagger Area

An electron beam at the nominal energy of 12 GeV enters the Tagger vault through the Hall D beamline tunnel and is directed into a typically thin radiator in front of the Tagger magnet. The bulk of the incident beam goes through the gap in the magnet without interaction and is then directed into the exit beam pipe, leading to the beam dump at the end of the beam dump alcove, behind the labyrinth shielding walls. Electron interactions in the radiator produce bremsstrahlung photons going straight through the opening in the magnet, and then through the long pipe leading to the Hall D beam entry port. Electrons that have lost a portion of their original energy to the photon production are deflected in the magnet and exit through the row of position-sensitive detectors at the magnet side. The energy of each corresponding photon is thus determined. The need to count and the need to determine the energy of each produced photon imposes major limitations on the maximum beam current (5  $\mu\text{A}$  at 12 GeV) and on the maximum radiator thickness (about 0.0005 radiation lengths (R.L.) for the maximum beam current). The whole area layout and design parameters, including the radiation shielding requirements, were chosen with these limitations taken into account.

### 3. Consequences of Intensity Increase by "Brute Force"

The proposal for the production of the  $K_L^0$  beams at the Hall D complex would require photon beams which are orders of magnitude more intensive than those available currently, corresponding approximately to the effective radiator thickness of 0.05 – 0.1 R.L. Simply replacing the present radiator with a much thicker one (a "brute force" solution) is possible in principle. However, such a solution would lead to several consequences which would make it practically unacceptable. The radiation levels at the vault, both prompt and post-operational due to the beam line elements' radioactivation, are evaluated to be too high. Mitigation would require removal of sensitive electronic components around the vault, building of new temporary shielding walls and disposal of radioactive beam line components after the operations. Dose rates and activation evaluation would require complex simulations and quality

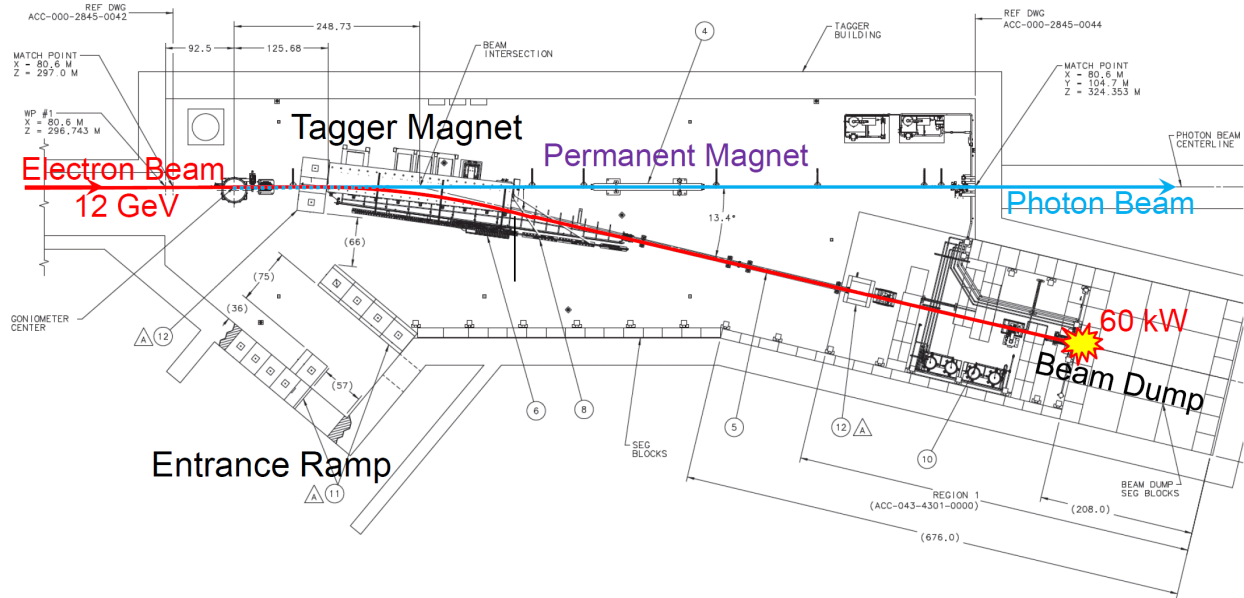


Figure 1: Tagger vault area in the Hall D complex at CEBAF.

and reliability control. That is all deemed to be expensive and risky, and it is not clear if the necessary photon beam intensity can be reached.

#### 4. Simulation of the Radiation Environment

GEANT3 [1] detector simulation package was used originally for modeling and optimizing the Tagger vault setup and finding acceptable radiation shielding solutions. An example of the GEANT3 geometry may be seen in Fig. 2. One 12 GeV beam electron trace is shown in Fig. 2 by the red curve, starting in the beam tunnel and going through the radiator, the tagger magnet, the exit vacuum volumes and beam pipes. Upon arriving at the beam dump, it cascades inside the copper core of the dump, with some blue gamma and black neutron tracks shown exiting the core and stopping in the iron shielding blocks.

Fig. 3 illustrates the major causes of the prompt radiation inside the vault during normal operations. Most of the beam electrons do not interact in the radiator and end up depositing their energy in the dump, producing a cascade of electrons and photons which are mainly absorbed in the core of the dump. The secondary neutrons escape the core but mostly stop in the surrounding iron shielding and the labyrinth walls. A couple of the beam electrons shown in the plot have produced bremsstrahlung gammas energetic enough to kick the electrons visibly away from the beam line. They end up cascading and depositing their energy in the first labyrinth wall and spraying some of the cascading electrons and gammas back into the vault. More beam electrons produce lower energy gammas in the radiator and get deflected at smaller angles, hitting exit flanges and narrower portions of the exit beam line and producing essentially full 12 GeV electromagnetic cascades in the vault. The bremsstrahlung gammas produced at the radiator go straight along the exit beam line through the magnet yoke and forward to Hall D proper.

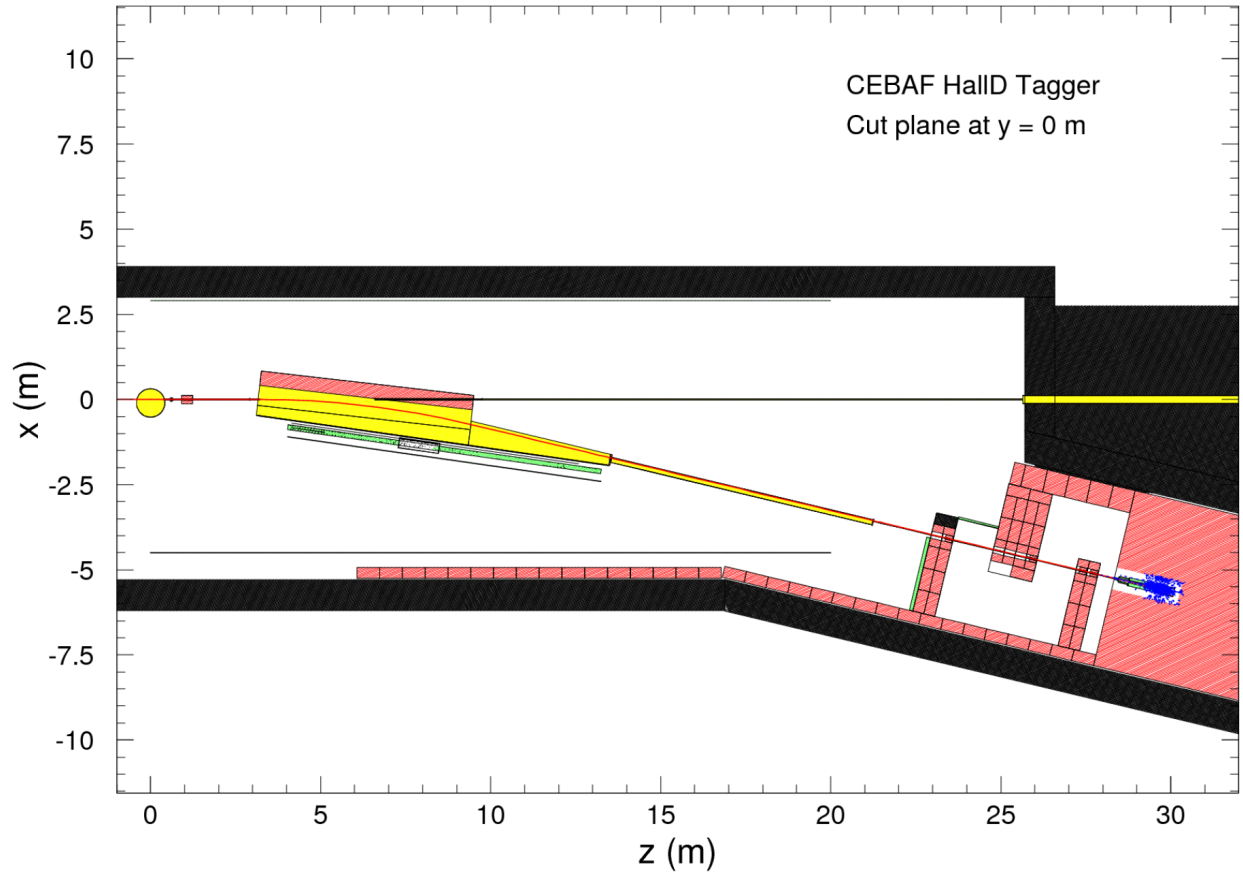


Figure 2: Plane cut of the Tagger vault model built using the GEANT3 detector simulation package. Black areas correspond to the concrete walls. Red hatch style is used for iron shielding blocks. Yellow areas correspond to the beam vacuum.

The model allowed us to simulate the operational radiation environment and optimize the shielding design at the vault, corresponding to the nominal operating conditions in the Hall D complex. The first commissioning runs in 2015 indicated that the observed radiation fields in the Tagger vault are in agreement with the calculations within a factor 2 or 3, which is acceptable given all uncertainties in the model and in the measurements. The estimates for the “brute force” solution of simply increasing the radiator thickness to produce more intensive photon beams at the vault indicate that that an increase of the prompt radiation would be way beyond the present design limitations and is indeed problematic.

## 5. New “Compact Photon Source” Solution

As a solution to this apparent problem, we suggest designing and implementing the “Compact Photon Source” (CPS) device. The new conceptual design combines in a single properly shielded assembly all elements necessary for the production of the intense photon beam, such that the overall dimensions of the setup are limited and the operational radiation dose rates around it are acceptable. The experiment does not require tagging of the produced photons,



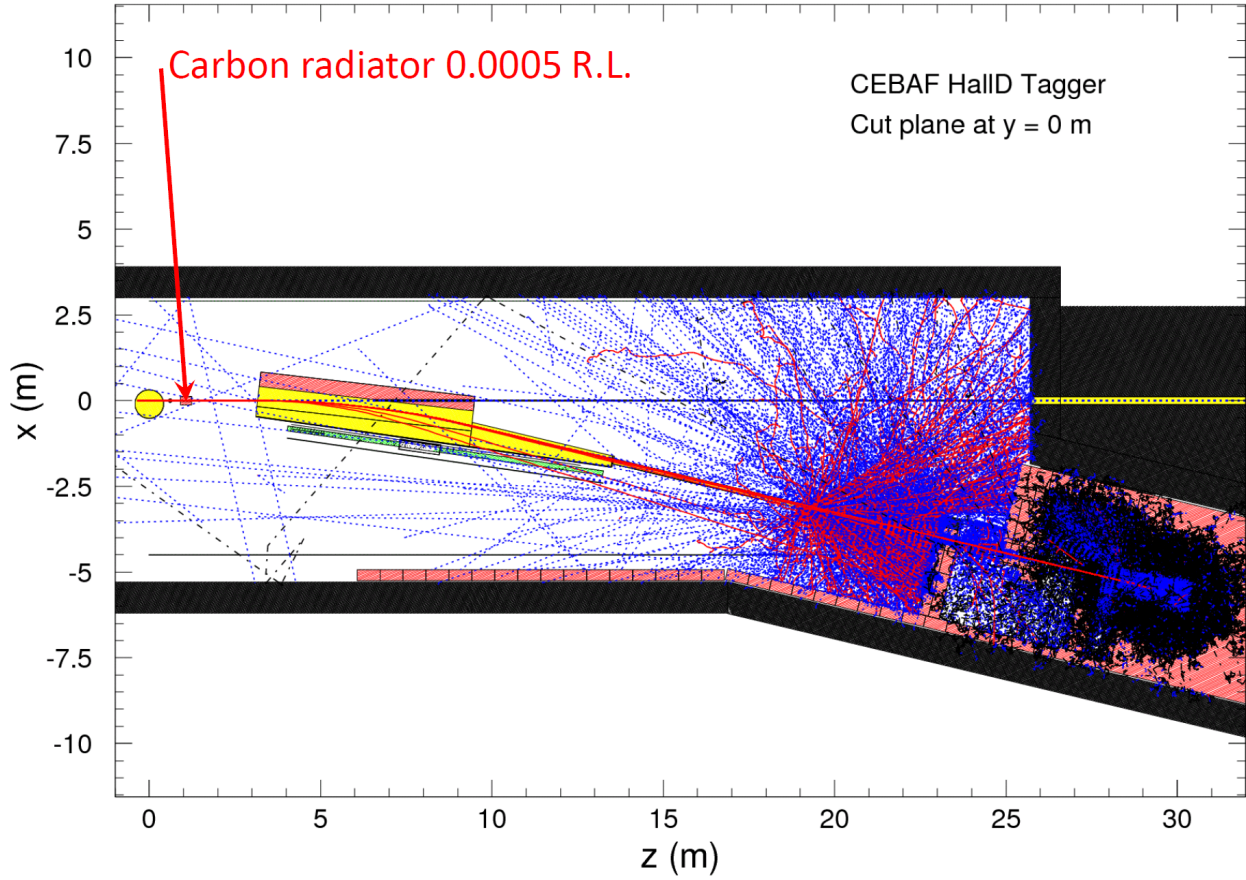


Figure 3: Same plot as in Fig. 2, but showing the simulation of 2000 beam electrons at 12 GeV. Red tracks show charged particles, mostly electrons, blue tracks are gammas, and neutrons are tracked in black.

so the new design could be compact and hermetically closed by the shielding, as opposed to the present Tagger Magnet concept. One of the earlier CPS concepts was published recently [2] and proposed for use in the WACS experiment at JLab [3].

Fig. 4 illustrates the GEANT3 model of such a device. The assembly is small enough to fit in the Tagger vault immediately after the Tagger magnet. We propose to extend the path of the incoming 12 GeV electron beam beyond the Tagger magnet by removing the standard radiator from the beam and by switching the magnetic field off. After exiting the Tagger magnet through the currently available photon beam exit pipe, the electron beam enters the well shielded CPS device. First, the beam electrons see the new radiator, as thick as necessary to produce photon beam optimized for  $K_L^0$  production downstream. After the radiator the “spent” electrons are deflected by the region of a strong magnetic field sufficient to deflect the main 12 GeV beam through the vacuum volume with the beam diagnostics equipment and into the high power beam dump, away from the straight photon beam axis. A long-bore straight collimator lets the photon beam through the assembly. An illustration of the beam propagation and absorption in the CPS device is given in Fig. 5.

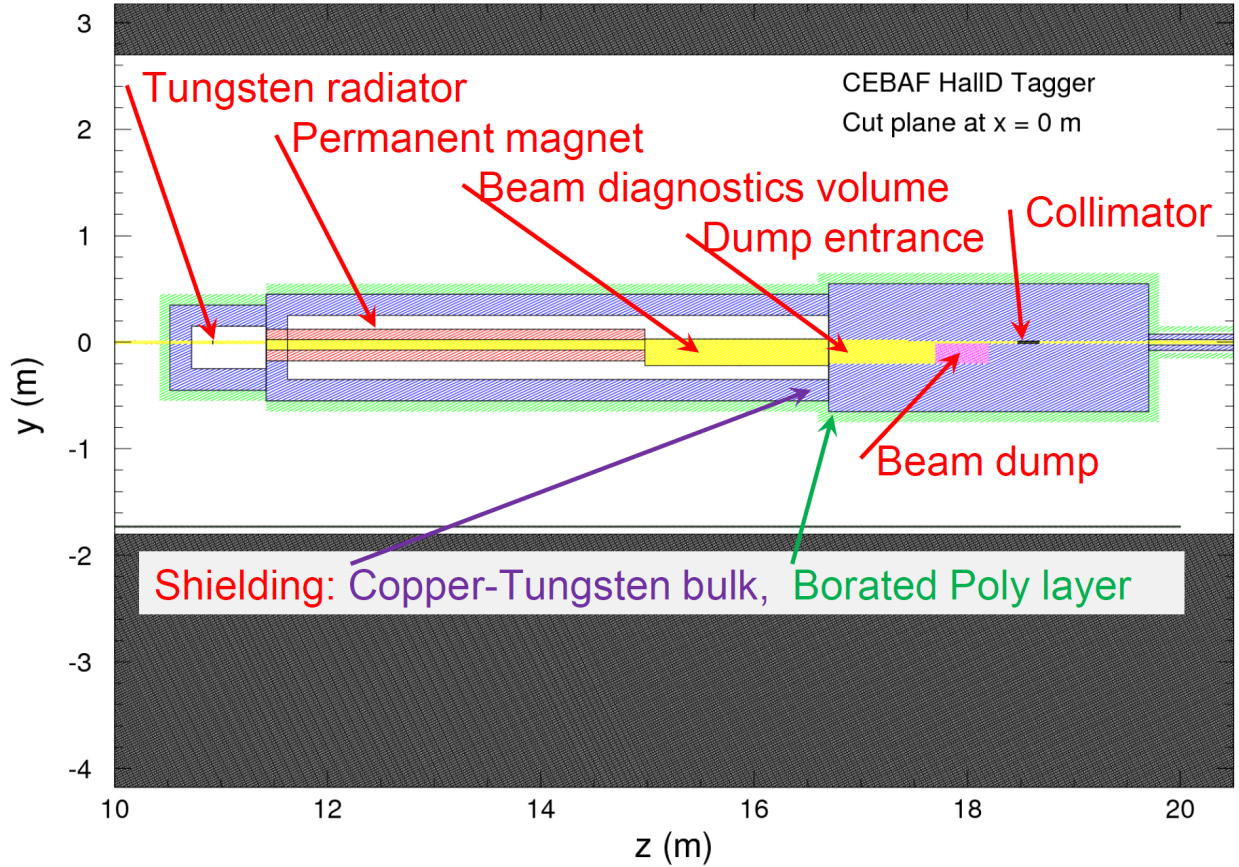


Figure 4: Vertical cut plane of the GEANT3 model of the CPS device. Elements of the design are indicated in the plot. See discussion in the text.

The dump including the shielding is by necessity the most massive element of the design, consisting of a water-cooled thermoconductive copper or silver core, surrounded by thick, high-Z, and high density material, such as Tungsten alloy or Lead. The dump design includes the entrance slit for the main electron beam and for the tail electrons that lost their energy in the radiator and are deflected farther down. The slit provides the condition for the main electron-produced cascade to originate roughly in the middle of the bulk dump volume, such that there was sufficient shielding in all directions and the products of the cascade were contained in the dump as much as possible.

The dump will also provide a long-bore channel for the main bremsstrahlung gamma beam to go through, with the critical collimation aperture placed in the middle of the bulk volume to contain most of the secondary products generated in the collimator. A Borated Poly outer layer is useful for slowing, thermalizing, and absorbing fast neutrons still exiting the bulk shielding. We suggest that the exit photon channel and beam line in the vault also be shielded properly.

The GEANT3 model calculations show that the overall dimensions of the CPS assembly could stay reasonably small (see Fig. 6), while achieving the overall dose rates at the Tagger

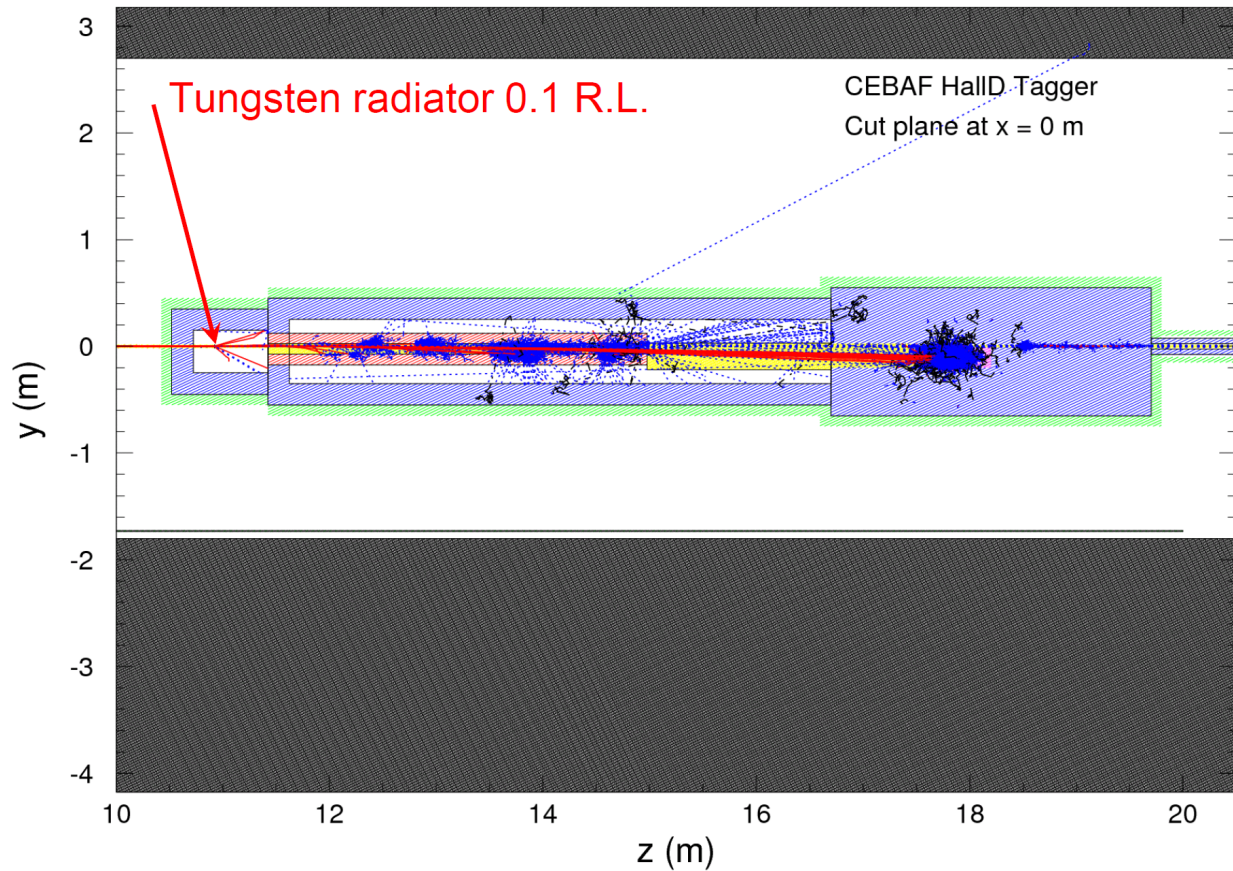


Figure 5: The same plot as in Fig. 4, but showing the simulation of 50 beam electrons at 12 GeV, with a 0.1 R.L. Tungsten radiator installed. Beam electrons interact in the radiator frequently, lose energy, and get deflected in the 0.8 Tesla magnetic field. Most of them go down to the core of the dump and deposit their energy there. The photon beam goes straight to (and through) the aperture collimator.

vault comparable to nominal Hall D operations. The dense high-Z material covering the core of the dump from all sides, together with a 2-inch layer of Borated Poly material all around, work rather effectively. The estimate shows that, for the ultimate new setup with 10% R.L. radiator, the dose rates in the vault during full 60 kW beam operations are comparable to the nominal running conditions in the vault, as shown in Fig. 7. The radiation spectral composition is different; most of the dose rate contribution in the CPS setup is from higher energy neutrons. The comparison indicates that at equal beam currents, gamma radiation dose rates are much smaller for the CPS run (an order of magnitude), and neutron dose rates in the area are comparable.

The dramatic difference between the overall dimensions of the present dump package and the new proposed compact solution is explained by using high density and high-Z material in the new design, and also by making it hermetic, that is, covering the beam dump entrance volume almost as solidly as in all other directions. The present Hall D Tagger Dump de-



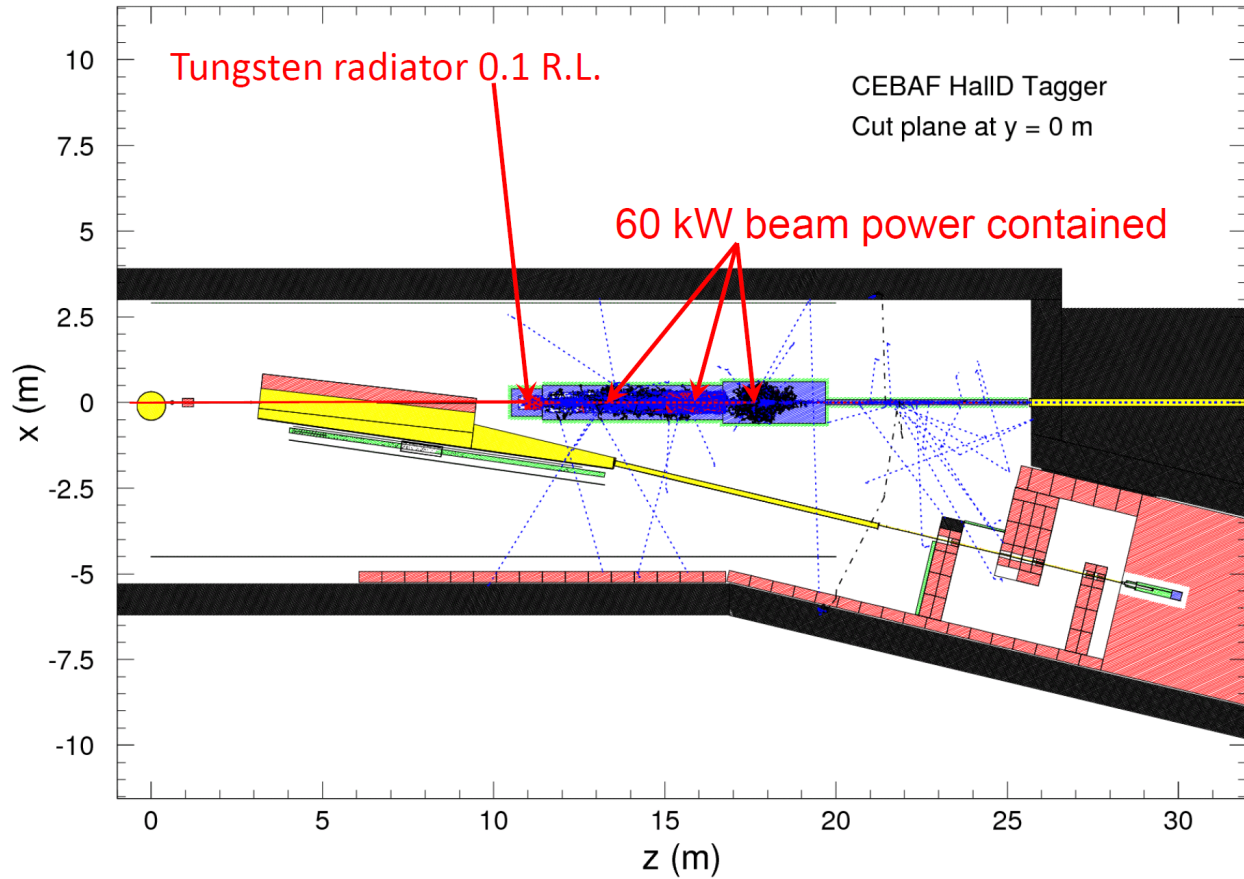


Figure 6: A plane cut of the Tagger vault model built using the GEANT3 package, showing the CPS assembly and the simulation of 2000 beam electrons at 12 GeV.

sign was opportunistic as it used the standard copper beam dump device and standard iron shielding blocks available at that time. The design required dump accessibility, so it was not possible to make the shielding hermetic, and heavy labyrinth walls were needed. Using a Tungsten alloy with a density about 2.5 times higher than Iron, all linear dimensions can be made correspondingly smaller. Another factor was a certain degree of conservatism required for a permanent design, which can be avoided in the design dedicated for a limited-period experiment.

One of the special features of the new concept design is the difficulty of reaching its innards once operations have started, because of the high levels of induced radioactivity inside. Thus, special attention should be devoted to the reliability of all inner elements of the CPS.

## 6. Implementation Features and Cost Estimate

We do not see principal obstacles to implementation of the CPS concept in the experiment.

The new dump core may have characteristics close to the one installed already, such that the dump cooling system can be re-used (maximum 60 kW cooling power).

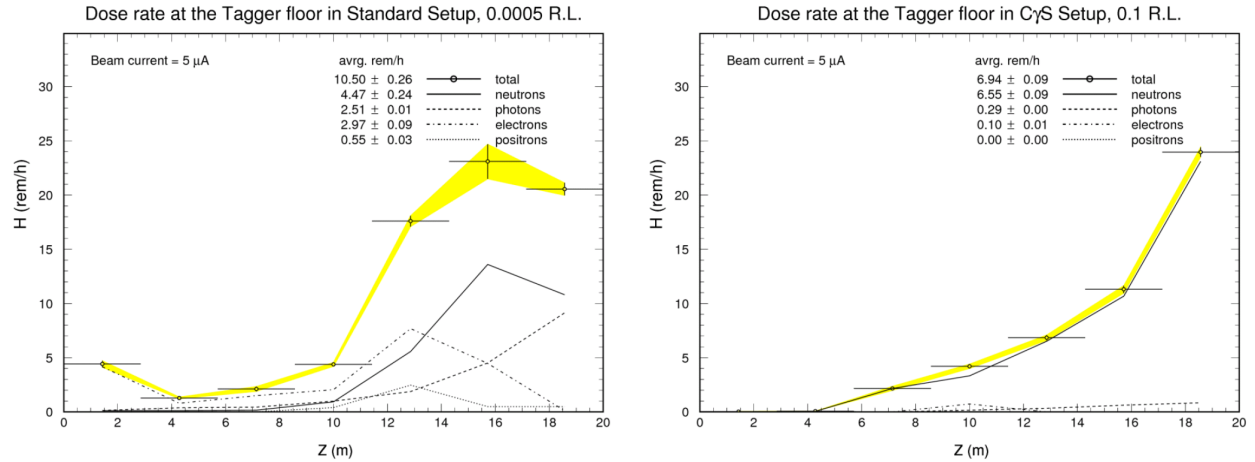


Figure 7: The plots show a comparison of dose rate estimates in the Tagger Area in the two conditions: (left panel) nominal Hall D operation with the standard amorphous radiator at 0.0005 R.L., - with (right panel) radiator at 0.1 R.L., used as part of the Compact Photon Source setup.

To make long and narrow photon beam collimation we propose to build the core using two symmetric flat plates, left and right, and make matching grooves in them for the beam entry cones, beam line, and the aperture collimator.

Most of the present Tagger Area equipment may remain in place; the CPS will be assembled around the modified gamma line.

The available permanent magnet may be used in the CPS assembly (pending thermal engineering analysis, as there will be a need to have it cooled, dissipating approximately 1.5 kW of power deposited in it). Available identical spare magnet can be installed at the end of the beam line in the Tagger as a protective measure. Alternatively, a new powered magnet could be designed for the CPS, with a comparable field integral (it does not have to be highly precise). In such a case, the present permanent magnet will be moved downstream.

The CPS solution for the new intense high energy gamma source in the Tagger vault will be characterized by the absence of extra prompt irradiation or extra beam line activation for existing structures in the area during and after the operations. The accumulation of radioactivity inside the CPS will be significant, to a large degree preventing access to the inner parts immediately after operations. However, such activation will not present a problem while the CPS stays assembled, due to a very strong self-shielding.

There will be a possibility of switching between the two modes of Hall D operations: a low intensity tagged photon beam, and high intensity photon beam from the CPS.

Disassembly and decommissioning could be postponed until radioactive isotopes decay inside to manageable levels.

Cost would include detailed iterative modeling and simulation to optimize operation parameters, design, engineering and production, plus the choice and cost of bulk shielding material.

Rough cost expectation: within \$0.5 M.

## 7. Conclusions

Compared to the alternative, the proposed CPS solution presents several advantages, including much less disturbance of the available infrastructure at the Tagger Area and better flexibility in achieving high-intensity photon beam delivery to Hall D.

The proposed CPS solution will satisfy proposed  $K_L^0$  beam production parameters

We do not envision big technical or organizational difficulties in the implementation of the conceptual design.

## 8. Acknowledgments

This work is authored by The Southeastern Universities Research Association, Inc. under U.S. DOE Contract No. DEAC05-84150. The U.S. Government retains a non-exclusive, paid-up, irrevocable, world-wide license to publish or reproduce this manuscript for U.S. Government purposes.

## References

- [1] Application Software Group, *GEANT - Detector Description and Simulation Tool*, CERN Program Library Long Writeup W5013, CERN, Geneva, Switzerland (1994).
- [2] B. Wojtsekhowski and G. Niculescu, *Conceptual Design Report: A Compact Photon Source*, JLab Internal Document, Thomas Jefferson National Accelerator Facility, Newport News, VA, USA (June, 2015).
- [3] B. Wojtsekhowski, S. Abrahamyan, and G. Niculescu and the WACS Collaboration, *Polarization Observables in Wide-Angle Compton Scattering at Photon Energies up to 8 GeV*, Proposal PR12-15-003 to Jefferson Lab PAC 43, Thomas Jefferson National Accelerator Facility, Newport News, VA, USA (2015).

## 2.27 Targets for a Neutral Kaon Beam

Christopher Keith

*Thomas Jefferson National Accelerator Facility*

*Newport News, VA 23606, U.S.A.*

### Abstract

A secondary beam of neutral Kaons is under consideration for Hall D at Jefferson Lab to perform spectroscopic studies of hyperons produced by  $K_L^0$  particles scattering from proton and deuteron targets. The proposed physics program would utilize the GlueX detector package currently installed in Hall D. This contribution looks at potential targets for use in the new facility, paying close attention to the existing infrastructure of GlueX and Hall D. Unpolarized cryotargets of liquid hydrogen and deuterium, as well as polarized solid targets of protons and deuterons are examined.

### 1. Introduction

A proposal is currently under consideration to expand Jefferson Lab's program of hadron spectroscopy and develop a secondary  $K_L^0$  beam in experimental Hall D [1]. The Kaon beam will be produced from photoproduction on a beryllium target located about 85 m downstream from the Hall D radiator for Bremsstrahlung photons. Photons escaping the beryllium target will be absorbed by a lead shield, while charged particles will be removed by a sweeper magnet. The  $K_L^0$  flux, collimated into a 6 cm diameter beam, is expected to be of order  $10^4 \text{ s}^{-1}$ , along with a similar rate of high energy neutrons. The existing GlueX detector package and its 1.8 T superconducting solenoid would be utilized for the program.

This contribution examines possible targets for the neutral Kaon beam facility, both unpolarized and polarized hydrogen and deuterium. Emphasis is placed on the former, and in particular on straightforward modifications to the existing GlueX cryotarget that will make it suitable for a large diameter beam of  $K_L^0$ .

### 2. Liquid Hydrogen Target

If possible, the proposed experimental program will utilize the existing GlueX liquid hydrogen cryotarget (Fig. 1), modified to accept a larger diameter target cell. The GlueX target comprises a kapton cell containing liquid hydrogen ( $\text{LH}_2$ ) at a temperature and pressure of about 20 K and 19 psia. The 100 ml cell is filled through a pair of 1.5 m long stainless steel tubes (fill and return) connected to a small vessel where hydrogen gas is condensed from two room temperature storage tanks. Inside the vessel is a large condensation surface for the gas, consisting of numerous copper fins that are cooled by a pulse tube refrigerator (PTR) with a base temperature of 3 K and cooling power of about 20 W at 20 K. A 100 W temperature controller regulates the condenser at 18 K.

The target assembly is contained within an "L"-shaped, stainless steel and aluminum vacuum chamber with a 1 cm thick Rohacell extension surrounding the target cell. The start counter for the GlueX experiment fits snugly over this extension. The vacuum chamber, along with the hydrogen storage tanks, gas handling system, and control electronics, is mounted on a custom-built beam line cart for easy insertion into the Hall D solenoid. A compact I/O

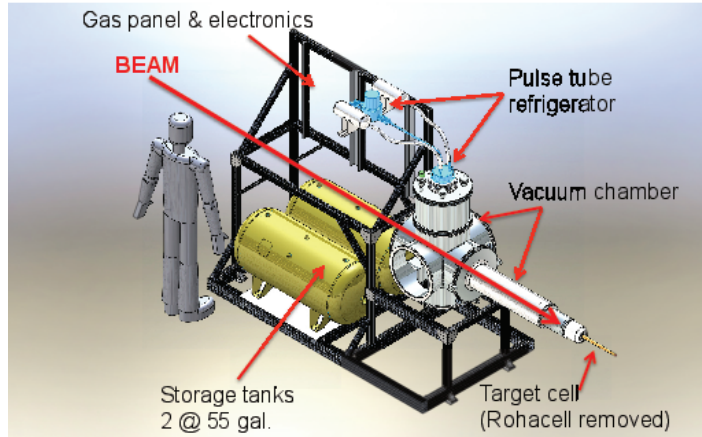


Figure 1: The GlueX liquid hydrogen target.

system monitors and controls the performance of the target, while hardware interlocks on the target temperature and pressure and on the chamber vacuum ensure the system's safety and integrity. The target can be cooled from room temperature and filled with liquid hydrogen in about 5 hours. For empty target runs, the liquid can be boiled from the cell in less than twenty minutes. The cell remains filled with cold hydrogen gas for these runs and can refilled with liquid in about forty minutes.

The GlueX cell (Fig. 2) is closely modeled on those used for experiments in Hall B at Jefferson Lab for more than a decade [2]. It is a horizontal, tapered cylinder about 38 cm long with a mean diameter of 2 cm. A 2 cm diameter reentrant beam window defines the length of  $\text{LH}_2$  in the beam to be about 30 cm. Both entrance and exit windows on the cell are  $75\ \mu\text{m}$  kapton while the cylindrical walls are  $130\ \mu\text{m}$  kapton glued to an aluminum base. In normal operation the cell, the condenser, and the pipes between them are all filled with liquid hydrogen. In this manner the liquid can be subcooled a few degrees below the vapor pressure curve, greatly suppressing the formation of bubbles in the cell. In total, about 0.4 liter of  $\text{LH}_2$  is condensed from the storage tanks, and the system is engineered to safely recover this quantity of hydrogen back into the tanks during a sudden loss of insulating vacuum, with a maximum allowed pressure of 49 psia [3].

A conceptual design for the neutral Kaon beam target is also shown in Fig. 2. The proposed target cell has a diameter of 6 cm and a 40 cm length from entrance to exit windows, corresponding to a volume of about 1.1 liter. The inventory of gas required to operate the target with this cell will be about 1500 STP liter, which can be stored in the existing tanks at about 50 psia. The JLab Target Group will investigate alternative materials and construction techniques to increase the strength of the cell.

The GlueX target system is expected to operate equally well with liquid deuterium ( $\text{LD}_2$ ), which condenses at a slightly higher temperature than hydrogen: 23.3 K versus 20.3 K at atmospheric pressure. Because the expansion ratio of  $\text{LD}_2$  is 13% higher, the storage pressure will about 60 psia. The new target cell will therefore be engineered and constructed to accomodate either  $\text{H}_2$  or  $\text{D}_2$ .



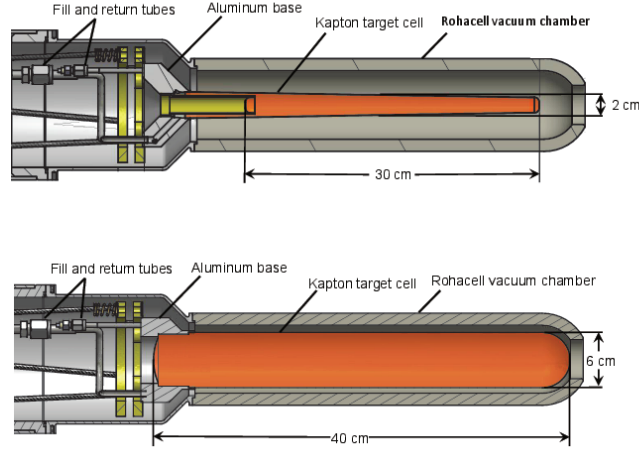


Figure 2: Top: Kapton target cell for the GlueX  $\text{LH}_2$  target. Bottom: Conceptual design for a larger target cell for the proposed  $K_L^0$  beam in Hall D.

### 3. Solid Polarized Target

Dynamically polarized targets were successfully utilized in each of Jefferson Lab's three experimental halls (A, B, and C) during its 6 GeV era [4]. It is natural then to contemplate their use in Hall D as well. We can expect the Hall D solenoid and its accompanying cryogenic facility to play significant roles in the target's design and operation.

To realize dynamic nuclear polarization (DNP), a solid dielectric material is doped with paramagnetic radicals. The unpaired electrons in these radicals are polarized at low temperature and high magnetic field, and microwave-driven spin flip transitions transfer the electron's polarization to nearby nuclei in the material. The nuclear polarization is then transported through the bulk via spin diffusion.

DNP targets generally fall into one of two categories: continuously polarized and frozen spin. In the former case the DNP process is maintained continuously throughout the scattering experiment, while frozen spin targets are polarized intermittently, and the scattering data is acquired while the polarization slowly decays. Continuously polarized targets require a highly uniform polarizing magnet of 2.5–5 T whose geometry limits the acceptance of scattered particles. A similar magnet is also required to polarize a frozen spin target, but the target sample can then be removed from the high field and maintained by a much less massive "holding" magnet during data acquisition, provided it is cooled to a temperature of 50 mK or less. For this reason frozen spin targets are limited to particle beams no greater than about  $10^8 \text{ s}^{-1}$ , while continuously polarized targets have operated up to  $\sim 10^{12} \text{ s}^{-1}$ . Because of its high resistance to radiation damage, irradiated ammonia ( $\text{NH}_3$  or  $\text{ND}_3$ ) continuously polarized at 1 K and 5 T is the usual choice for electron beams up to 140 nA. Chemically doped butanol ( $\text{C}_4\text{H}_{10}\text{O}$ ) has become the material of choice for frozen spin targets, thanks to its ease of production and handling, and its lack of polarizable background nuclei other than hydrogen. Protons in either ammonia or butanol can be dynamically polarized in excess of 90%. Deuterated ammonia can be polarized to about 60%, and deuterated butanol to

80–90%.

At the expected  $K_L^0$  rate of the proposal, either type of polarized target is suitable. However, the 1.8 T field of the Hall D solenoid is too weak and too inhomogeneous (0.25 T/m) to act as an effective polarizing magnet for DNP. It would serve as an excellent holding magnet for a frozen spin target though. Polarization decay times up to 4000 hours were observed with the FROST target in Hall B using a 0.5 T holding field [5]. From these results we anticipate relaxation times exceeding 10,000 hours at 1.8 T. The target would be polarized outside the Hall D solenoid using a warm-bore magnet similar to the one used for the FROST target and moved to the GlueX solenoid for data acquisition. A small transfer coil would be incorporated inside the target cryostat to maintain the polarization while the target is moving.

The size of the polarized target sample will be critical. For best results, the polarizing field should be uniform to about 100 ppm over the sample volume. The cost of a magnet suitable for a 6 cm sample diameter will be significant, so smaller diameters should be considered. Approximately 2 mW/g of microwave power is necessary for DNP at 2.5 T. Thus the sample volume will also determine the refrigeration capacity of a frozen spin target. Frozen butanol consisting of 1–2 mm beads has a density of 1.1 g/cm<sup>3</sup>, a packing fraction of about 0.6, and a dilution factor of 0.135. A target sample 2 cm in diameter and 23 cm long would provide a similar proton luminosity as the 30 cm long LH<sub>2</sub> target. Dynamic polarization of the 50 g sample would require about 0.1 W of microwave power at 2.5 T and 0.3 K. A <sup>3</sup>He-<sup>4</sup>He dilution refrigerator similar to FROST's would be suitable for this application, operating at a <sup>3</sup>He circulation rate of 30 mmol/s during polarization and 1–2 mmol/s during frozen spin mode.

A frozen spin target consumes liquid helium at a rate of a few liters per hour to operate the dilution refrigerator. The Hall D cryogenic plant may not be able to provide this volume of LHe to a polarized target and maintain the GlueX solenoid at the same time. In this case the polarized target will require a separate source of LHe, and should be designed to economize <sup>4</sup>He consumption. Alternatively, one may consider a so-called “cryogen-free” dilution refrigerator (CFDR), where the circulating <sup>3</sup>He is condensed by a small cryocooler such as the PTR utilized for the GlueX cryotarget [6]. Unfortunately, present day CFDRs cannot provide the cooling power necessary to polarize a 50 g target sample. In its place, we can consider a hybrid system using two pulse tubes (Fig. 3). Together these can condense <sup>3</sup>He at a rate sufficient for frozen spin operation and simultaneously condense 5–10 l/day of <sup>4</sup>He into a 50 liter reservoir within the target cryostat. Once sufficient liquid is accumulated, it would support an increased <sup>3</sup>He circulation rate long enough to polarize the sample, about 8 hours. The <sup>4</sup>He level in the reservoir would naturally decrease during this time but recover during the week or more of frozen spin operation.

#### 4. Summary

Possible targets for a neutral Kaon beam in Hall D have been examined. It is found that the existing GlueX cryotarget can be modified to accept liquid hydrogen or deuterium cell diameters up to 6 cm, with some R&D required to increase the working pressure of the current GlueX cells. For polarized target experiments a frozen spin target of butanol is indicated. It will be more difficult to realize a 6 cm diameter sample in this case, due to the

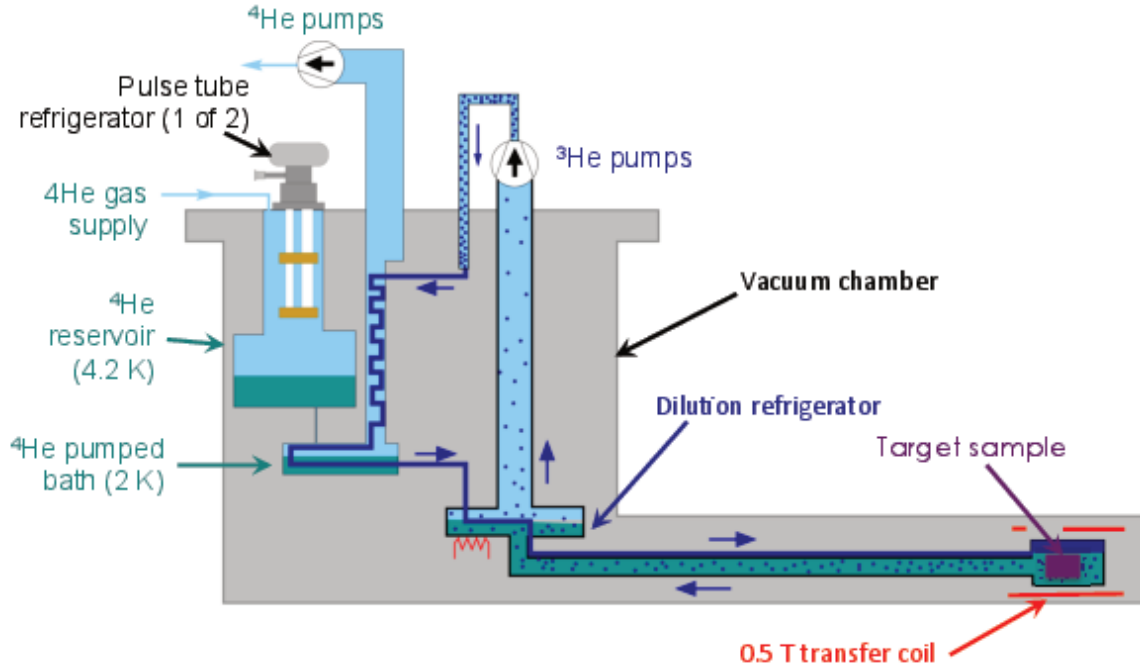


Figure 3: Schematic drawing of a hybrid cryogen-free frozen spin target. See text for details.

magnetic field and cooling power requirements necessary for dynamic polarization. Instead a 23 cm long sample with 2 cm diameter is considered.

## 5. Acknowledgments

This material is based upon work supported by the U.S. Department of Energy, Office of Science, Office of Nuclear Physics under contract DE-AC05-06OR23177.

## References

- [1] M.J. Amarian *et al.*, *Physics Opportunities with a Secondary  $K_L^0$  Beam at JLab*, Proposal for JLab PAC44 (in preparation).
- [2] B.A. Mecking *et al.*, Nucl. Instr. and Meth. A **503**, 513 (2003).
- [3] D. Meekins, TGT-CALC-401-007: *Hall D Cryogenic Target: General calculations for relief of the  $LH_2$  target.*
- [4] C.D. Keith, in Proceedings of PSTP 2015, PoS (PSTP 2015) 013.
- [5] C.D. Keith *et al.*, Nucl. Instr. and Meth. A **684**, 27 (2010).
- [6] K. Uhlig and W. Hehn, Cryogenics, **37**, 279 (1997).

### 3 List of Participants of KL2016 Workshop

- Mohammad (Saif) Ahmad, GWU <msahmad@gwu.edu>
- Michael Albrow, FNAL <albrow@fnal.gov>
- Moskov Amaryan, ODU <mamaryan@odu.edu>
- Frank (Ted) Barnes, DOE-NP <ted.barnes@science.doe.gov>
- William J. Briscoe, GWU <briscoe@gwu.edu>
- Daniel Carman, JLab <carman@jlab.org>
- Shloka Chandavar, Ohio U. <cshloka@jlab.org>
- Eugene Chudakov, JLab <gen@jlab.org>
- Pavel Degtyarenko, JLab <pavel@jlab.org>
- Michael Döring, GWU <doring@gwu.edu>
- Robert Edwards, JLab <edwards@jlab.org>
- Ishara Fernando, Hampton U. <ishara@jlab.org>
- Igor Filikhin, NCCU <ifilikhin@nccu.edu>
- Alessandra Filippi, I.N.F.N. Torino <filippi@to.infn.it>
- José L. Goity, Hampton U./JLab <goity@jlab.org>
- Helmut Haberkzettel, GWU <helmut@gwu.edu>
- Avetik Hayrapetyan, JLU Giessen <Avetik.Hayrapetyan@uni-giessen.de>
- Charles Hyde, ODU <chyde@odu.edu>
- Hiroyuki Kamano, RCNP, Osaka U. <kamano@rcnp.osaka-u.ac.jp>
- Christopher Keith, JLab <ckeith@jlab.org>
- Roman Kezerashvili, NY City College of Tech., CUNY <rkezerashvili@citytech.cuny.edu>
- Franz Klein, GWU <fklein@jlab.org>
- Michael Kohl, Hampton U. <kohlm@jlab.org>
- Valery Kubarovsky, JLab <vpk@jlab.org>
- Ilya Larin, ODU <ilarin@jlab.org>
- Haiyun Lu, U. of Iowa <hlu@jlab.org>

- David Mack, JLab <mack@jlab.org>
- Maxim Mai, HISKP Bonn U. <mai@hiskp.uni-bonn.de>
- D. (Mark) Manley, KSU <manley@kent.edu>
- Vincent Mathieu, IU <mathieuv@indiana.edu>
- Georgie Mbianda Njenchu, ODU <gmbia001@odu.edu>
- Robert McKeown, JLab <bmck@jlab.org>
- Curtis Meyer, CMU <cmeyer@cmu.edu>
- Victor Mokeev, JLab <mokeev@jlab.org>
- Hugh Montgomery, JLab <mont@jlab.org>
- Fred Myhrer, USC <myhrer@sc.edu>
- Kanzo Nakayama, UGa <nakayama@uga.edu>
- James Napolitano, Temple U. <napolj@temple.edu>
- Hiroyuki Noumi, RCNP, Osaka U. <noumi@rcnp.osaka-u.ac.jp>
- Yongseok Oh, Kyungpook Nat. U. <yohphy@knu.ac.kr>
- Hiroaki Ohnishi, RIKEN/RCNP Osaka U. <h-ohnishi@riken.jp>
- Eulogio Oset, U. de Valencia <eulogio.oset@ific.uv.es>
- Emilie Passemar, IU/JLab <epassema@indiana.edu>
- Eugene Pasyuk, JLab <pasyuk@jlab.org>
- Michael Pennington, JLab <michaelp@jlab.org>
- Angels Ramos, U. of Barcelona <ramos@ecm.ub.edu>
- David Richards, JLab <dgr@jlab.org>
- James Ritman, FZJ <j.ritman@fz-juelich.de>
- Torri Roark, ODU <troar001@odu.edu>
- Patrizia Rossi, JLab <rossi@jlab.org>
- Elena Santopinto, I.N.F.N. Genova <elena.santopinto@ge.infn.it>
- Reinhard Schumacher, CMU <schumacher@cmu.edu>
- Elton Smith, JLab <elton@jlab.org>

- Alexander Somov, JLab <somov@jlab.org>
- Justin Stevens, JLab <jrsteven@jlab.org>
- Igor Strakovsky, GWU <igor@gwu.edu>
- Adam Szczepaniak, IU/JLab <aszczepa@indiana.edu>
- Simon Taylor, JLab <staylor@jlab.org>
- Dominik Werthmueller, Glasgow U. <dominik.werthmueller@glasgow.ac.uk>
- Bogdan Wojtsekhowski, JLab <bogdanw@jlab.org>
- Veronique Ziegler, JLab <ziegler@jlab.org>
- Bingsong Zou, ITP/CAS <zoubs@itp.ac.cn>